The low-pressure partial-melting behaviour of natural boron-bearing metapelites from the Mt Stafford area, central Australia.

by
Esmé Marelien Spicer

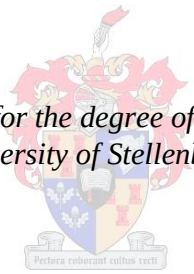

Dissertation presented for the degree of Doctor of Science at the University of Stellenbosch

Promoter: Prof. Gary Stevens
Faculty of Science
Department of Geology

December 2011

Declaration

By submitting this thesis/dissertation electronically, I declare that the entirety of the work contained therein is my own, original work, that I am the sole author thereof (save to the extent explicitly otherwise stated), that reproduction and publication thereof by Stellenbosch University will not infringe any third party rights and that I have not previously in its entirety or in part submitted it for obtaining any qualification.

December 2011

Abstract

This study has examined the 3 kbar partial melting behaviour of 4 metapelites collected from the highest grade rocks occurring below the anatectic zone of the Mt Stafford area, Arunta Inlier, central Australia. In this area, metasediments are interpreted to have undergone partial melting within the andalusite stability field, possibly as a result of a lowering of the metapelite solidus by the presence of boron in the rocks. Two of the samples were two mica metapelites (MTS70 and MTS71) that both contained significant quantities of tourmaline and were thus boron enriched. The other two samples were biotite metapelites. One of these rocks contains only a trace of tourmaline (MTS8) and the other is tourmaline free (MTS7). Despite expectations that muscovite in the two mica samples would break down via a subsolidus reaction, muscovite was stable to above 750 °C due to the incorporation of Ti, phengitic and possibly F components into its structure. Between 750 and 800 °C, muscovite melted out completely via a coupled muscovite + biotite fluid-absent incongruent reaction. In the most mica-rich sample this reaction produced ~ 60 % melt at 800 °C. In the biotite metapelites, biotite melting began at a temperature below 800 °C and was accompanied by very modest melt production at this low temperature. In contrast to the two mica metapelites, the main pulse of melt production in these samples occurred at a temperature between 850 and 950 °C. In both these samples biotite + melt coexistence persisted for a temperature range in excess of 150 °C, and in MTS8, biotite was still in the run products at 950 °C. The very refractory nature of these evolved biotite compositions is most likely a consequence of both the presence of a Ti buffering phase in the assemblage (ilmenite) and the essentially plagioclase-free nature of the starting compositions. Under the fluid-absent conditions of this study tourmaline is clearly a reactant in the partial melting process, but does not appear to shift the fluid-absent incongruent melting reactions markedly. Neither quartz, nor andalusite was completely consumed in the melting reactions, indicating the metastable persistence of andalusite to higher than the wet solidus temperatures. The assemblages do not change much with increasing temperature and mimic the field relationships.

The fluid-absent melting experiments indicated that the main pulse of melting occurred between 850 and 950 °C, significantly higher than indicated by the field evidence of 600 to 675 °C, therefor disequilibrium in the experiments can not be ruled out. The presence of a fluid during partial melting at Mt Stafford provides therefor an explanation of the low temperatures at which melting occurred.

Opsomming

Die 3 Mpa vloeistof-vrye gedeeltelike smelting van 4 metapeliete, gekollekteer van die hoogste graad rotse net onder die anatektiese sone van die Mt Stafford area, Arunta inlêer, sentraal Australië, is bestudeer. Die metapeliete van hierdie area word geinterpreteer dat hulle gedeeltelike smelting in die andalusiet stabiliteitsveld ondergaan het, moontlik as ‘n resultaat van die verlaging van die metapeliet solidus as gevolg van die teenwoordigheid van boor. Twee van die monsters bestudeer was twee-mika metapeliete (MTS70 en MTS71) met beduidende hoeveelhede toermalyn en is dus boor-verryk. Die ander twee monsters was biotiet metapeliete, waarvan een spoorhoeveelhede toermalyn (MTS8) bevat het en die ander toermalyn vry was (MTS7). Ten spyte van verwagtinge dat muskoviet in die twee mika monsters sou afbreek via ‘n subsolidus reaksie, was dit stabiel tot bo 750 °C as gevolg van die vervanging van Ti, fengitiese en moontlik F komponente in die muskoviet struktuur. Tussen 750 en 800 °C het muskoviet heeltemal gesmelt deur die vloeistof-vrye gekoppelde muskoviet+biotiet reaksie. In die monster met die meeste mika het hierdie reaksie ~ 60 % gesmelt by 800 °C. In die biotiet metapeliete het die biotiet smelt reaksie begin by ‘n temperatuur onder 800 °C en lae hoeveelhede smelt is by hierdie lae temperature geproduseer. In kontras met die twee-mika metapeliete het die hoof puls van smeltproduksie in hierdie monsters plaasgevind tussen 850 en 950 °C. In beide hierdie monsters het biotiet+smelt bestaan oor ‘n wye temperatuur reeks van 150 °C. Biotiet was steeds ongesmelt in MTS8 by 950 °C. Die hoë refraktoriese natuur van hierdie biotiet samestellings is hoogs waarskynlik ‘n gevolg

van die teenwoordigheid van ‘n Ti-bufferende fase (ilmenite) en die afwesigheid van plagioklaas in die begin samestellings. Toermalyn is duidelik ‘n reaktant in hierdie vloeistof-vrye gedeeltelike smelting studie, maar dra nie beduidend by tot die verlaging van die inkongruente smeltingsreaksies nie. Nie kwarts of andalusiet het heeltemal gesmelt oor die temperatuurreeks nie, wat aandui dat die andalusiet stabiel is by temperature hoër as die nat solidus. Die mineraalverspreidings verander nie veel met verhoging in temperatuur nie en mimiek dus die veld verwantskappe. Die vloeistof-vrye smeltings eksperimente het aangedui dat die hoofpuls van smelting tussen 850 en 950 °C geskied het, wat aansienlik hoër is soos aangedui uit die veldgetuienis van 600 tot 675 °C, dus is die moontlikheid van disekwilibrium gedurende die eksperimente ‘n moontlikheid. Die moontlikheid dat vloeistof teenwoordig was tydens die smeltproses by Mt Stafford verskaf dus ‘n oplossing vir die lae temperature wat tydens smelting bereik is.

Acknowledgements

The author wishes to thank the many people who assisted and contributed to the production of this dissertation. She wishes to express her sincere appreciation to the following persons and institutions:

1. My husband, for his love and support.
2. My Parents, for their love and support.
3. Friends, for their support and encouragement.
4. Prof Gary Stevens, through sharing his knowledge and expertise, for helping me become a better scientist.
5. Prof Ian Buick, for his valuable input on the Mt Stafford rocks throughout the thesis.
6. The Australian Research Council (IREX Grant and Senior Research Fellowship to ISB) and the National Research Foundation of South Africa (funding to GS and ongoing PhD bursary to EMS) for providing funding for this study.
7. Mr Neil Steenkamp at the SEM facility at the University of Stellenbosch and John Terlet at the Centre for Electron Microanalysis and Microscopy of Southern Australia, Adelaide, for providing assistance with microanalysis.
8. Prof Roger Gibson is gratefully acknowledged for providing the sample material and information on sample localities.
9. Richards Bay Minerals, for giving me the time to complete this thesis. In particular for the support of Jan Louw and Johan Jacobs.
10. David London, for providing a very thorough review of this work for the publication in Contributions to Mineralogy and Petrology.
11. Prof Jeff Moyen, Prof Giles Droop and Prof Dirk van Reenen, for their valuable input during the examination process.

Table of contents

List of figures

between Zones 2a and 2b. The boundary between Zones 2b and 2c is defined by the first appearance of sillimanite partially pseudomorphing andalusite (White *et al*., 2003).

Fig. 1.3, p27: The P-T conditions observed in the field at Mt Stafford superimposed onto Fig 1.1 (yellow shaded zone). Zone 1 - 2 boundary conditions (position of the solid vertical line in the yellow zone) are inferred to be 620 ºC, 2.3 - 2.8 kbar and Zone 2c - 3 boundary conditions are inferred to be midway between 650 – 680 ºC, 2.8 - 3.3 kbar (solid line at ~670 ºC). The position of the solidus (position of the dotted vertical line) is located on the Zone 2a – 2b boundary, but unconstrained (Greenfield *et al.*, 1996).

Fig. 2.1, p33: Reaction (1) = Metapelite solidus (Thompson, 1982); reaction (2) the most commonly cited aluminium silicate triple point (Holdaway, 1971); reaction (3) = the muscovite subsolidus reactions from Thompson (1982) and reaction (4) = Huang & Wyllie (1974); reaction (5) = Biotite melting reactions from Vielzeuf & Holloway (1988) and Le Breton & Thompson (1988); reaction (6) = Vielzeuf & Montel (1994); reaction (7) = the synthetic biotite gneiss from Patiño-Douce & Beard (1995) and reaction (8) = the synthetic quartz amphibolite from Patiño-Douce & Beard (1995).

Fig. 2.2, p44: P-T pseudosections from White et al. (2003) showing alternative subsolidus mineral assemblage relationships for the typical aluminous metapelite composition. (a) P-T pseudosection for conditions of fluid in excess. Also shown are the 2 sigma error bars on the andalusite - sillimanite reaction. The inset shows calculated aluminosilicate mode contours for part of the diagram. (b) Semiquantitative P-T pseudosection showing the mineral relationships relative to a wet solidus depressed to lower temperatures because of the presence of boron. The position of the solidus is not calculated but is shifted to lower temperatures manually. Also shown are the 2 sigma error bars on the andalusite - sillimanite reaction. The grey arrow shows the position of a field gradient in P-T that is consistent with the petrographic observations assuming sillimanite replaces andalusite at the calculated reaction. (c) P-T

pseudosection calculated assuming the metastable persistence of andalusite to temperatures above the calculated andalusite - sillimanite reaction. (d) Semiquantitative P-T pseudosection showing the mineral relationships relative to a wet solidus depressed to lower temperatures and the metastable persistence of andalusite. The grey arrow shows the position of a field gradient in P-T that is consistent with the petrographic observations assuming andalusite metastably persists beyond its calculated stability.

Fig. 2.3, p46: Calculated P-T pseudosection from White *et al*. (2003) for the supersolidus part of the aluminous metapelite. Because of the need to fix water contents in the bulk rock at the solidus, the water-absent subsolidus fields are inappropriate for interpreting the pre-melting prograde evolution. The pseudosection also shows calculated molar mode contours in percent for several minerals and silicate melt. Insert (a) shows detail of the mode changes that occur within the area indicated by the box. The quartz-bearing aluminous metapelites have a relatively simple evolution at temperatures above the breakdown of biotite and develop an assemblage dominated by cordierite, K-feldspar and silicate melt in upper Zone 3 and Zone 4.

Fig. 3.1, p50: Area map of the Arunta Region, Mt Stafford, indicating the sample locations of the 4 starting materials. MTS70 and 71 are located on the border of zone 1 and 2 and MTS7 and 8 are located close to the metapelite solidus in zone 2.

Fig. 3.2, p52: Backscattered scanning electron images of the starting materials used in this study: MTS7 (A), MTS8 (B), MTS70 (C) and MTS71 (D).

Fig. 3.3, p56: The starting compositions used in this study compared with those of previous studies. PJ Gr. ‘63 Pettijohn (1963), V&H ‘88 Vielzeuf & Holloway (1988), PDBa ‘96 and PDBb ‘96 Patińo-Douce & Beard (1996), PDB ‘95 Patińo-Douce & Beard (1995), PDJ ’91 Patińo-Douce & Johnson (1991), ST. Pel. ‘97 and ST. Gr. ’97 Stevens *et al*. (1997), WH R.S. ‘69 Whetten *et al*. (1969), V&M Gr.‘94 Vielzeuf & Montel (1994), SH ‘56 Shaw (1956) the

and the two mica metapelites (B). The data for the experimental biotite includes compositions produced across the range of temperatures where biotite was stable.

Fig. 5.5, p100: Projection of new feldspar compositions on the Ab-Or-An plane. The projection of the 300 MPa feldspar solvus at 750–1000 °C is from Fuhrman & Lindsley (1988).

Fig. 5.6, p102: Y site Al plotted against Fe + Mn + Mg + Ti for the residual (old) and new recrystallised (new) tourmaline present in the run products from MTS71 at 850 °C.

Fig. 5.7A-C, p103: Plots of Al^{VI} vs. Ti (A), Ti vs Fe + Mg + Mn (B) and Si + Al^{VI} vs. Ti + Al^{IV} (C) for muscovite in both the starting materials (open symbols) and run products (shaded symbols) from the two mica metapelites at 750 ˚C.

Fig. 5.8 A-C, p107: A) ASI vs. SiO_2 (wt%) in the glasses. B) A plot of ASI variation as a function of temperature in the glasses. The arrows represent calculated ASI values, based on the formulae proposed by Acosta-Vigil and London (2003), for melts at 800 ˚C with 3.8wt% dissolved H_2O and coexisting with cordierite (Crd) and tourmaline (Tur). C) Normative Qtz-Ab-Or plots for the glasses produced in this study. The glasses in MTS7 and MTS70 show compositional evolution away from Ab and towards Qtz, with increasing temperature. These are indicated with arrows and are consistent with the presence of quartz in most of the high temperature experiments, as well as the preferential partitioning of plagioclase, in the case of MTS7, and Na-bearing tourmaline, in the case of MTS70, into the first melts.

Fig. 5.9, p116: Back scattered SEM image of typical Al-Si oxides or sillimanite-mullite needles in the run product from MTS70, one of the tourmaline bearing samples.

Fig. 5.10A, B, p120: Phase proportions in the run products expressed as a function of temperature. A) Melt proportions relative to those of the principal reactant minerals in the four samples. The unshaded area represents cordierite. B) A comparison of the melt proportion variations as a function of temperature in the four samples. This highlights the relatively low temperature melt production in the two mica metapelites, the pulse of melt production from the biotite

metapelites between 850 and 900 ˚C, and the control of melt fraction at very high temperature by bulk rock water content.

Fig. 6.1, p129: The melting reactions from the muscovite metapelites MTS70, 71 (reaction 9 in red) and biotite metapelites MTS7 and 8 (reaction 10 in red) overlayed onto Fig 2.1. Reaction (1) = Metapelite solidus (Thompson, 1982); reaction (2) the most commonly cited aluminium silicate triple point (Holdaway, 1971); reaction (3) = the muscovite subsolidus reactions from Thompson (1982) and reaction (4) = Huang & Wyllie (1974); reaction (5) = Biotite melting reactions from Vielzeuf & Holloway (1988) and Le Breton & Thompson (1988); reaction (6) = Vielzeuf & Montel (1994); reaction (7) = the synthetic biotite gneiss from Patiño-Douce & Beard (1995) and reaction (8) = the synthetic quartz amphibolite from Patiño-Douce & Beard (1995).

Fig. 6.2, p131: Calculated B_2O_3 concentrations in the glasses from MTS70 and MTS71 expressed as a function of temperature.

Fig. 6.3, p134: The melting reactions from the muscovite metapelites MTS70, 71 (reaction 12) and biotite metapelites MTS7 and 8 (reaction 13) superimposed onto Fig 1.3. Greenfield *et al.*, (1996) found that the position of the solidus (position of the dotted vertical line in the yellow zone) is located on the Zone 2a – 2b boundary, but unconstrained at between 600 and 675 ºC.

List of tables

Table 4.5e, p75: Mn-Zn silicates (Rhodonite = 3 Oxygens and Willemite 4 = Oxygens). Minerals were analysed with 20 kV, 3.92 nA beam current and 13 mm working distance.

Table 4.6a, p76: Precision and accuracy statistics of SEM-EDS quantitative analysis on albite (8 Oxygens). Minerals were analysed with 20 kV, 3.92 nA beam current and 13 mm working distance.

Table 4.6b, p77: Precision and accuracy statistics of SEM-EDS quantitative analysis on almandine and pyrope garnets (12 Oxygens). Minerals were analysed with 20 kV, 3.92 nA beam current and 13mm working distance.

Table 4.6c, p79: Precision and accuracy statistics of SEM-EDS quantitative analysis on Cr-diopside, clino- and orthopyroxenes (6 Oxygens). Minerals were analysed with 20 kV, 3.92 nA beam current and 13 mm working distance.

Table 5.1, p87: Summary of experimental conditions and results

Table 5.2, p93: Average compositions ($n \geq 5$) for the minerals observed in the run products. The elements Na, Mg, Al, Si, K, Ca, Ti, Mn and Fe were analysed for in each case, but only values >0 were included in the tables. Fe^{3+} values were calculated according to the method of Droop (1987). The following number of oxygens, in brackets, was used to calculate the cations for each mineral group: cordierite (18 O), feldspar (8 O), tourmaline (49 O), spinel (4 O), andalusite/sillimanite (5 O), and muscovite and biotite (22 O).

Table 5.3, p106: Average glass compositions. Standard deviations and analytical conditions are discussed in the text. Cation formulae calculated to 10(O).

Table 5.4a, p109: Biotite/Glass partition coefficients

Table 5.4b, p110: Felspar/Glass partition coefficients

Table 5.4c, p111: Cordierite/Glass partition coefficients

Table 5.4d, p112: Mt Stafford MTS70 biotite/muscovite partition coefficients

Chapter 1: Introduction

Crustal anatexis is a fundamental geological process that has enabled the chemical differentiation of the crust. Present-day tectonic processes drive crustal anatexis in a variety of settings and the process is ongoing and cyclic through the earth's history. In metasedimentary rocks the factors that control anatexis, such as composition of the protolith, water availability and metamorphic pressure-temperature gradient are broadly understood, through both field and experimental studies. The breakdown of hydrous minerals via incongruent fluid-absent melting reactions, is accepted to be the main melt-producing process that operates in the crust (e.g. Thompson, 1982; Vielzeuf & Holloway, 1988; Brown, 1994; Brown *et al*., 1995; Gardien *et al*., 1995; White *et al*., 2003). Substantial amounts of melt can be produced via this process in crustal rocks at high temperatures (Thompson, 1982; Grant, 1985; Wickham, 1987; Sawyer, 1987; Vielzeuf & Holloway, 1988; Powell & Downes, 1990; Vernon *et al*., 1990; Harte *et al*., 1991; Hand & Dirks, 1992; Brown, 1994; Brown *et al*., 1995; Carrington & Harley, 1995; Gardien *et al*., 1995; Fitzsimons, 1996; Greenfield *et al*., 1996; Carson *et al*., 1997; Greenfield *et al*., 1998; Sawyer *et al*., 1999; Spear *et al*., 1999; Sawyer, 2001; White & Powell, 2002; White *et al*., 2003). Both muscovite and biotite melting reactions occur with rising temperature in metapelites (Thompson, 1982; Brown, 1994; Spear *et al*., 1999; White *et al*., 2003). In contrast, muscovite breakdown commonly occurs at subsolidus conditions in low-pressure granulites (Vernon *et al*., 1990; Brown, 1994; Brown *et al*., 1995; White *et al*., 2003) and melting occurs through a series of biotite breakdown reactions only. Despite the smaller number of melting reactions that occur in this setting, the rocks may develop substantial amounts of melt (Greenfield *et al*., 1996; White *et al*., 2003) as the low pressure melts have a relatively low water content in comparison with their higher pressure counterparts (Holtz & Johannes, 1994; White *et al*., 2003). In high-*T*, low-*P* terranes, where such melting reactions occur in regional metamorphosed rocks with a discrete source of heat, the evidence of melting is preserved due to a pronounced lateral thermal gradient outward from a high-grade core (Laramie Complex (Grant & Frost, 1990), Mt Stafford (Vernon *et al*., 1990;

Greenfield *et al*., 1996; White *et al*., 2003) and Cooma (Vernon, 1982; Ellis & Obata, 1992)). Such rocks have commonly been referred to as regional aureoles, but the discrete source of heat is not always exposed at the surface (White *et al*., 1974). The bulk of this study has been published and is referenced (Spicer *et al*., 2003; Buick *et al*., 2006).

1.1 Fluid-absent partial melting

In attempting to understand low pressure partial melting of metasediments, a substantial body of useful research exists, that relates to phase stabilities and melt chemistry during the water-saturated melting behaviour of metasedimentary rocks at low pressures (2 MPa) (Icenhower & London, 1997; Wolf & London, 1997; Acosta-Vigil & London, 2003; Evensen & London, 2003). However, most experimental studies of fluid-absent partial melting in natural metapelitic rocks have focussed on intermediate to higher pressure conditions of anatexis (5 MPa or above); for example, Storre (1972), Vielzeuf & Holloway (1988), Le Breton & Thompson (1988), Carrington & Harley (1995), Stevens *et al*. (1997), Pickering & Johnston (1998). This general lack of relevant fluid-absent experimentation hampers the interpretation of the anatectic evolution of metapelites in low-pressure, high-temperature metamorphic terranes, such as may develop during unusually low-pressure regional metamorphism (Mt Stafford area, Arunta Inlier, central Australia, Greenfield *et al*., 1998) and, as contact metamorphic aureoles around large, high-temperature intrusions (for example, the Bushveld Complex, South Africa, Wallmach *et al*., 1995; the Laramie anorthosite, USA, Frost *et al*., 2002; the Mt Stafford area, central Australia, Buick *et al*. 2006).

The phase relations relevant to low-pressure partial fluid-absent and -present melting of metapelites are summarised in Figure 1.1. A crucial issue is the points of convergence (Figure 1.1 intersections 9 and 10) between the wet metapelite solidus (Thompson, 1982; Huang & Wyllie, 1974) (Figure 1.1 reaction 1), the subsolidus dehydration reactions for muscovite and biotite (Figure 1.1 reactions 6 and

3), and the fluid-present (Figure 1.1 reactions 4 and 7) and fluid-absent (Figure 1.1 reactions 5 and 8) incongruent melting reactions for these minerals. For muscovite, this point has been calculated to lie close to 6 kbar and 640 ºC for the system KASH (Holland & Powell, 2002) (Figure 1.1 reaction 6a, point 11). The addition of Na to the system (KNASH) shifts this point to approximately 4 kbar and 640 ºC (Holland & Powell, 2001) (Fig. 1.1 reaction 9, point 9). This predicts that in rocks evolving along P-T trajectories at lower pressures than 4 kbar, no muscovite melting will occur and muscovite will break down by pre-anatectic subsolidus processes. Thus, muscovite melting should be unlikely in many low P, high T metamorphic terrains, despite the fact that in some cases this has been inferred from petrographic and field relations. Thus, partial melting in low-pressure, high-temperature terranes, may differ significantly in character from that in more normal regional metamorphic P-T trajectories for the following reasons:

1. In low-pressure areas (regionally metamorphosed rocks do not normally access this P-T space), muscovite and possibly biotite, may partially or completely breakdown via subsolidus dehydration reactions, as opposed to the more conventional fluid-absent incongruent melting reactions encountered at higher pressure (above 5 kbar). This raises the possibility that, where the fluid from muscovite subsolidus devolatilization is retained, biotite fluid-present, or indeed, haplogranitic wet-melting may occur with further heating. The alternative to the above mentioned scenario is that fluid produced via the subsolidus dehydration reaction is lost and less or no melting occurs.
2. In low-pressure, high-temperature metamorphism, the prograde P-T evolution commonly traverses the andalusite-sillimanite phase transition and incongruent partial melting has been inferred to have begun in the andalusite stability field (Vernon *et al*., 1990; Greenfield *et al*., 1998). Despite the fact that the wet haplogranitic + Al_2SiO_5 (Johannes & Holtz, 1996) solidus just intersects the andalusite phase boundary, the accepted position of the wet metapelite solidus (Thompson, 1982, Kerrick, 1990) relative to the Al_2SiO_5 phase boundaries

(Holdaway, 1971) suggests that inconguent melting of metasediments in this area would require that the temperature of the solidus be lowered by some mechanism (Fig. 1.1).

Since muscovite does not readily seem to melt in the muscovite stability field at these pressures, other alternatives that might be considered are the presence of boron and/or fluorine in fluids that might lower the temperature of the solidus (Chorlton & Martin, 1978; Kerrick & Speer, 1988; London *et al*., 1996). A possible mechanism that might allow muscovite to melt under such unusually low-temperature conditions might be fluxing by boron, which may shift the solidus to lower temperatures (Fig. 1.1). As boron is an element typically concentrated in pelagic shales, this process, if viable, may be of general petrologic importance. Experiments in synthetic haplogranitic systems indicate that addition of 5 to 17 wt% B_2O_3, in the fluid phase, lowers the water saturated solidus by between 60 to 130 ºC, at 1 MPa (Chorlton & Martin, 1978); Pichavant, 1981). In contrast, Benard *et al*. (1985) examined phase relationships in tourmaline-bearing leucogranites and found that the presence of tourmaline only lowered the H_2O-saturated solidus temperature by 5 to 20 ºC. In these experiments, tourmaline is a demonstrated liquidus phase and at 1 kbar, persists up to 795 ºC. Wolf & London (1997) and London (1999) concluded that in metapelites that contain tourmaline as the principal source of boron, the inception of anatexis would promote reactions that will consume tourmaline, liberate boron to the melt and conserve ferromagnesian components in residual biotite, spinel, or cordierite, or garnet at higher pressures. At 750 ºC, 2 MPa, fO_2 Ni-NiO, and aH_2O = 1, a given fraction of peraluminous melt can dissolve boron to approximately 20 wt% equivalent of tourmaline (to generate 2 wt% B_2O_3 in the melt). In combination with the earlier studies in haplogranitic systems this suggests that the water-saturated metapelite solidus may be shifted by up to 60 ºC by the inclusion of tourmaline in the system. This would generally not allow muscovite melting in the andalusite stability field (Fig. 1.1).

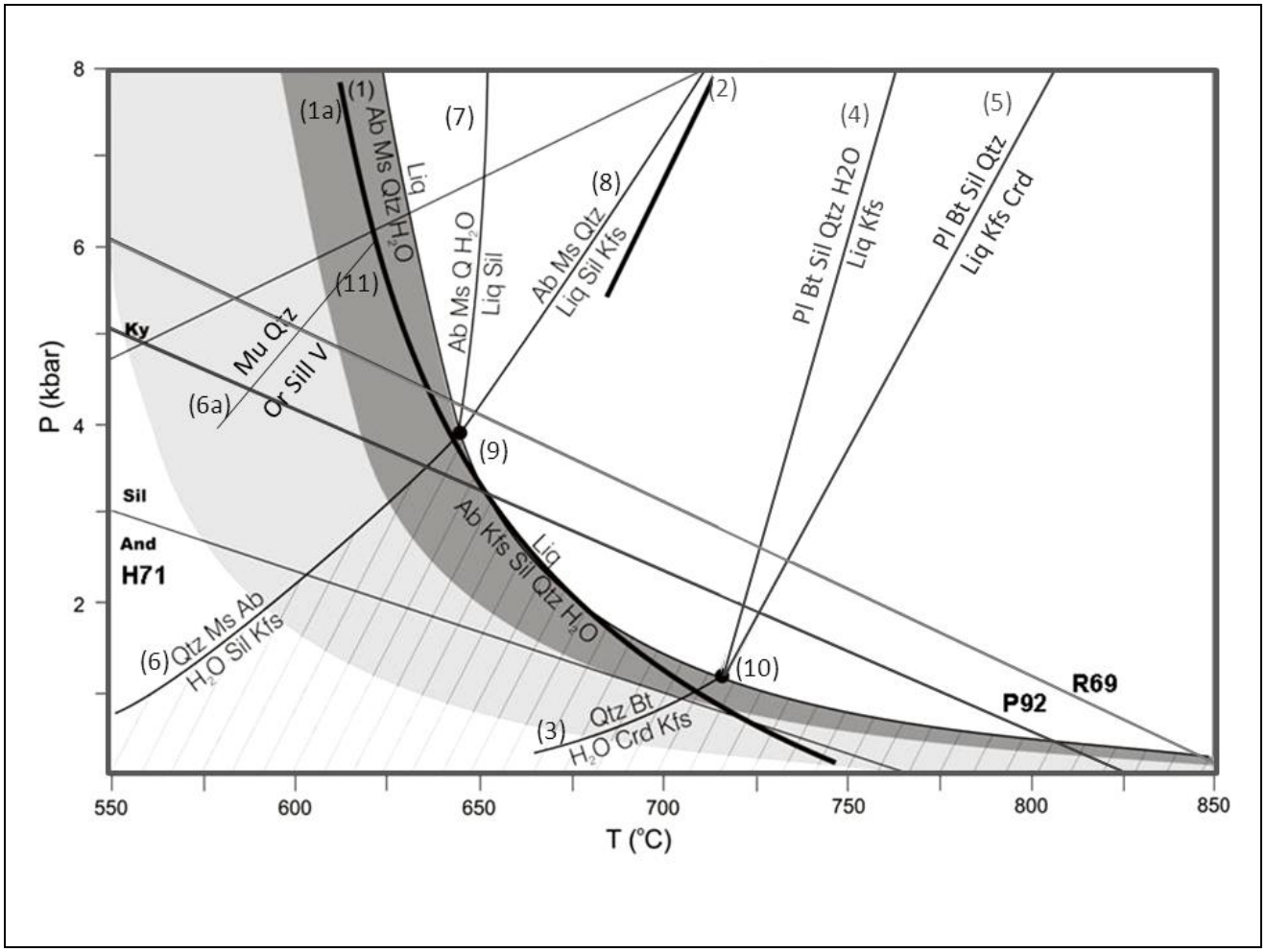

Fig. 1.1: Selected sub-solidus dehydration reactions and melting reactions relevant to the partial melting experiments. Reaction (1) and (1a) = metapelite wet solidi as constrained by Thompson (1982). Reaction (2) = muscovite dehydration melting as extrapolated from the experiments of Storre & Karotke (1972). Reaction (3) biotite fluid-absent melting = extrapolated from the biotite dehydration melting as extrapolated from data (reactions 4 and 5) of LeBreton & Thompson (1988); Reactions (6), (6a), (7) and (8) are KNASH sub-solidus and melting reactions = theoretical calculations of Holland & Powell (2001); Points of convergence (9) = muscovite, quartz and albite melting reactions intersecting with the wet metapelite solidus, (10) = biotite melting reactions intersecting with the wet metapelite solidus and (11) = muscovite and quartz melting reactions intersecting with the wet metapelite solidus; Al_2SiO_5 phase boundaries H71 = Holdaway (1971) and R69 = Richardson et al., (1969) and P92 = Pattison (1992); biotite wet melting = estimated position between dehydration melting reactions for muscovite and biotite. Light shading = maximum shift of the haplogranitic (quartz + K-feldspar + albite) wet solidus resulting from the addition of up to 17 wt% B_2O_3 in the fluid, modelled on the behaviour of the system at 1 kbar, as documented by Chorlton & Martin (1978) and Pichavant (1981). Heavy shading = likely shift in the wet granite solidus in natural rocks where B_2O_3 concentrations in the melt are buffered by equilibria involving tourmaline, modelled on the observations of Wolf & London (1997) and London (1999). Cross-hatching = the area below the solidus that andalusite is stable.

1.2 Uncertainty in the position of the Al_2SiO_5 triple point and phase boundaries

A wealth of experimental data exists on the position of the andalusite-sillimanite equilibrium boundary (Holm & Kleppa, 1966; Weill, 1966; Holdaway, 1971; Salje, 1986; Pattison & Harte, 1985, 1988; Kerrick & Spear, 1988; Kerrick, 1990; Pattison & Tracy, 1991; Pattison, 2001; Friedrich *et al*., 2004). The triple point can be located in P-T space somewhere in the interval between 3.8 kbar, 500 ºC (Holdaway, 1971; Holdaway & Mukhopadhyay, 1993) and 4.5 kbar, 550 ºC (Kerrick, 1990; Bohlen *et al*., 1991; Pattison, 1992; Pattison, 2001). Reasons for discrepancies between experimental results are numerous and include the presence of minor elements Mn and Fe^{3+} (Okrusch & Evans, 1970; Winter & Ghose, 1979; Grambling & Williams, 1985), the hydroxide components (Wilkins & Sabine, 1973; Beran & Gotzinger, 1987; Beran *et al*., 1989, 1993; Bell *et al*., 2004; Wieczorek *et al*., 2004) and mostly the structural state (Doukhan & Christie, 1982; Doukhan *et al*., 1985; Kerrick, 1986; Salje, 1986) of these minerals. Pattison (2001) argued that the effect of Fe and Mn on the position of the triple point is modest though. Of importance are the large discrepancies that exist between the experimental study of Richardson et al. (1969), who used fibrolitic sillimanite and that of the more generally accepted study of Holdaway (1971), who used prismatic sillimanite. Due to the discrepancies between experimental results, many investigators turned to field studies.

The metastable persistence of aluminosilicate minerals outside their stability range is well documented in a number of field studies (Heitanen, 1956; Hollister, 1969; Greenwood, 1976; Grambling, 1981; Wenk, 1983; Holland & Powell, 1985; Vernon, 1982, 1987; Evans & Berti, 1986; Kerrick, 1988; Pattison, 1992; Garcia-Casco & Torres-Roldan, 1996; Whitney, 2002; Stahle *et al*., 2004; Cesare *et al*., 2002, 2003; Droop & Moazzen, 2007) and does not necessarily fall in the same location as is presented by Holdaway (1971) in Fig 1.1 and in the same relation to the wet granite solidus of Thompson (1982). Most of these field studies placed the andalusite-sillimanite equilibrium

in positions between the Holdaway (1971) and Richardson *et al*. (1969) curve. Several of these studies of metapelitic andalusite-sillimanite phase equilibria in low-pressure settings (relavant to andalusite + melt stability) rejected the Holdaway (1971) curve because it was impossible to reconcile the andalusite stability field with other phase equilibrium constraints (Vernon, 1982; Vernon *et al*., 1990; Pattison & Tracy, 1991; Pattison, 1992; Johnson & Vernon, 1995), but Pattison (1992) provided a calculated position midway between the Holdaway (1971) and Richardson *et al*. (1969) positions. This allows for an andalusite + haplogranitic melt stability field below 3 kbar, without the need of F, B, Li or excess Al components in the melt (Clarke *et al*., 2005). For the purpose of this study the Holdaway (1971) curve is accepted.

1.3 The Mt Stafford metapelites, central Australia

Details of the Mt Stafford metamorphism are presented in Chapter 2, this section is only a general introduction to the study area. At Mt Stafford, in the Anmatjira–Reynolds Range area of the Proterozoic Arunta Inlier of central Australia, andalusite-bearing metasedimentary gneisses show a rapid change in metamorphic grade over a 10 km wide low-P/high-T regional aureole (Collins & Vernon, 1991; Cartwright *et al*., 1996; Greenfield *et al*. 1996; Greenfield *et al*., 1998; White *et al*., 2003). Field evidence exists in a sequence of metasedimentary rocks metamorphosed from greenschist to granulite facies conditions, that the rocks underwent partial anatexis and migmatization in the andalusite stability field at high temperature and low pressure conditions. A series of metamorphic and deformation events, which will be discussed in more detail in Chapter 2, resulted in a low-*P*/high-*T* regional aureole, containing migmatites (Collins & Vernon, 1991), which has been divided into five zones (Greenfield *et al*., 1996), ranging from greenschist (Zone 1) to granulite facies (Zones 4 and 5) over a distance of 10 km (Fig 1.2 a and b). Results provided by the mineral equilibria studies of White *et al*. (2003) at Mt Stafford indicate a pressure increase accompanying the

temperature rise from Zone 1 to Zone 5. Thus the field gradient across the area is positively sloped in P–T. Although the absolute thermal source for the Mt Stafford metamorphism is not positively identified, previous workers in the area (Vernon *et al.*, 1990; Greenfield *et al*., 1996, 1998), inferred either a localized but largely hidden intrusive source for the heat or have proposed the source as radiogenic heating. Furthermore, the intrusion of a granite body (the northern granite) into partially molten migmatites in Zone 5 indicates that magmatism occurred in the area during peak metamorphism. If the heat source for the metamorphism is localized, such as an igneous intrusion, then a non-linear temperature gradient would result (White *et al*., 2003). Although the outcrop area of the northern granite is too small to be responsible for the metamorphism at Mt Stafford, it may extend under the sequence or have extended over it. Alternatively, the granite itself may be a product of another larger thermal anomaly that underlies Mt Stafford (White *et al*., 2003). Anatectic migmatite features occur in all but the lowermost of five metamorphic zones, which grade from greenschist through amphibolite to granulite. Thus, in these metasediments melting appears to have occurred at relatively low temperature, in the amphibolite zone, at pressures low enough to stabilize andalusite. The position of the solidus is not constrained, but is accepted to be in the region of P = 2.3 – 2.8 kbar and T = 600 to 675 °C (Greenfield *et al*. 1996, 1998; White *et al*., 2003).

Water-present conditions will lower the solidus temperature of any silicate rock, and potential melt fluxing will result, due to the influence of boron or detrital tourmaline breakdown, has been discussed as possibly accounting for muscovite melting at temperatures low enough to allow anatexis in the andalusite stability field (Greenfield *et al*., 1996, 1998). However, the overall distribution of tourmaline and the distribution of boron-bearing fluids in the terrane are unconstrained, and Greenfield (1997) suggested that melting both before and after the crossing of the andalusite to sillimanite reaction was possible in different parts of the terrane.

White *et al*. (2003) agreed with these findings, stating that all mineral assemblages, including andalusite, were stabilised to higher temperatures. The stability of the mineral assemblages is probably due to the presence of minor elements. Substantial uncertainties on the andalusite - sillimanite reaction have been found by White *et al*. (2003) and the presence of minor elements, such as ferric iron, in aluminosilicates, may shift the equilibria in P–T space. The muscovite + quartz breakdown reaction may occur in the andalusite field at pressures below about 2.5 kbar within the upper andalusite - sillimanite error limit. Below this pressure andalusite is the stable polymorph produced where the mode of aluminosilicate increases. Given the observation of metastable persistence of andalusite into the sillimanite stability field from several studies (Vernon *et al*., 1990; Greenfield *et al*., 1996), it is possible that sillimanite did not grow in these rocks until temperatures at which the kinetic barriers to this reaction had been overcome and/or the mode of aluminosilicate began to increase. If sillimanite is not produced at the andalusite - sillimanite reaction, mineral equilibria relationships involving aluminosilicate are the metastable andalusite-bearing ones. This will have an effect on the position of the resultant, metastable aluminosilicate-bearing assemblage fields and on the slope and position of the metastable andalusite to sillimanite transition.

a)

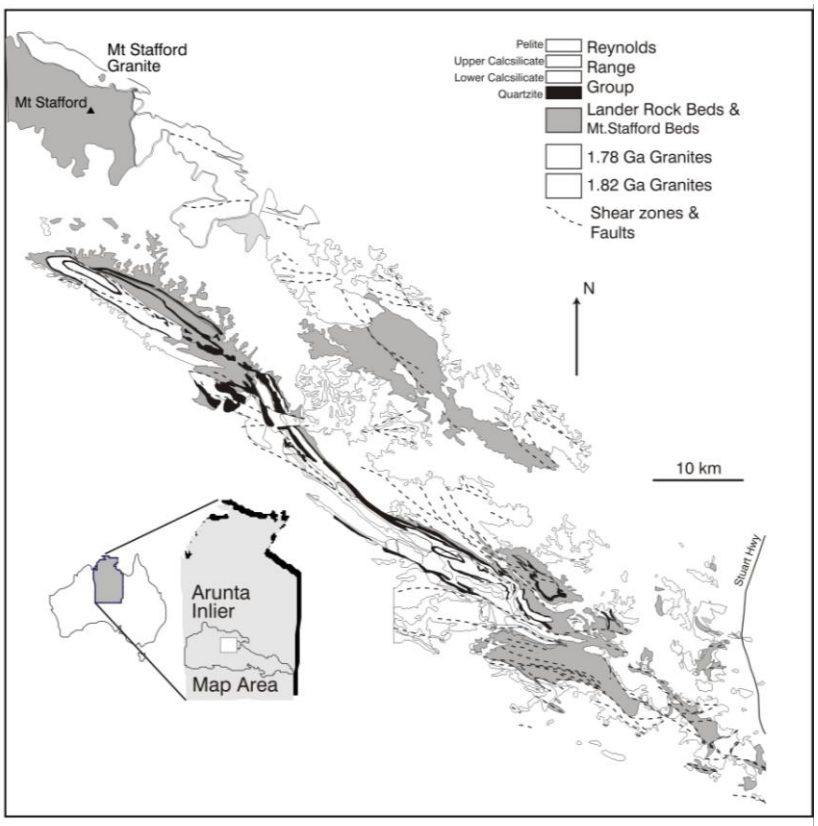

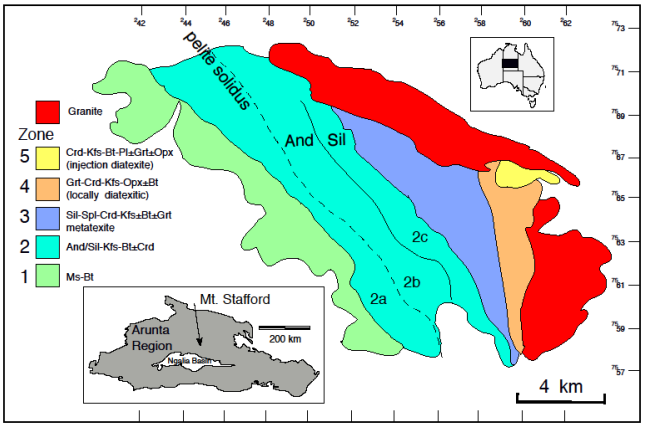

b)

Fig. 1.2: Mt Stafford area, Arunta Inlier, central Australia. (a) The larger Reynolds Range area, Arunta Inlier (Cartwright *et al*., 1996). (b) Predominant rock types and zones of the Mt Stafford, Arunta Inlier (Cartwright *et al*., 1996). Greenfield *et al*. (1996) subdivided Zone 2 into Zones 2a, 2b and 2c. The first appearance of felsic segregations marks the boundary between Zones 2a and 2b. The boundary between Zones 2b and 2c is defined by the first appearance of sillimanite partially pseudomorphing andalusite (White *et al*., 2003).

The inferred wet solidus in the pseudosection calculations of White *et al.* (2003) occurs at temperatures well above the calculated andalusite to sillimanite transition, even when the substantial uncertainties of this reaction are taken into account. The amount the solidus can be shifted to lower temperatures is limited by the need to have muscovite breakdown occur under subsolidus conditions. Thus it was found by White *et al*. (2003) that the solidus at Mt Stafford cannot be shifted to lower temperatures by much more than about 25 °C. Overall, the metastable persistence of andalusite, probably the depression of the solidus and the overstepping of the sillimanite reaction are all required to match the observed subsolidus mineral assemblage development. The P-T conditions of the study area are plotted onto Fig 1.1 and presented in Fig 1.3.

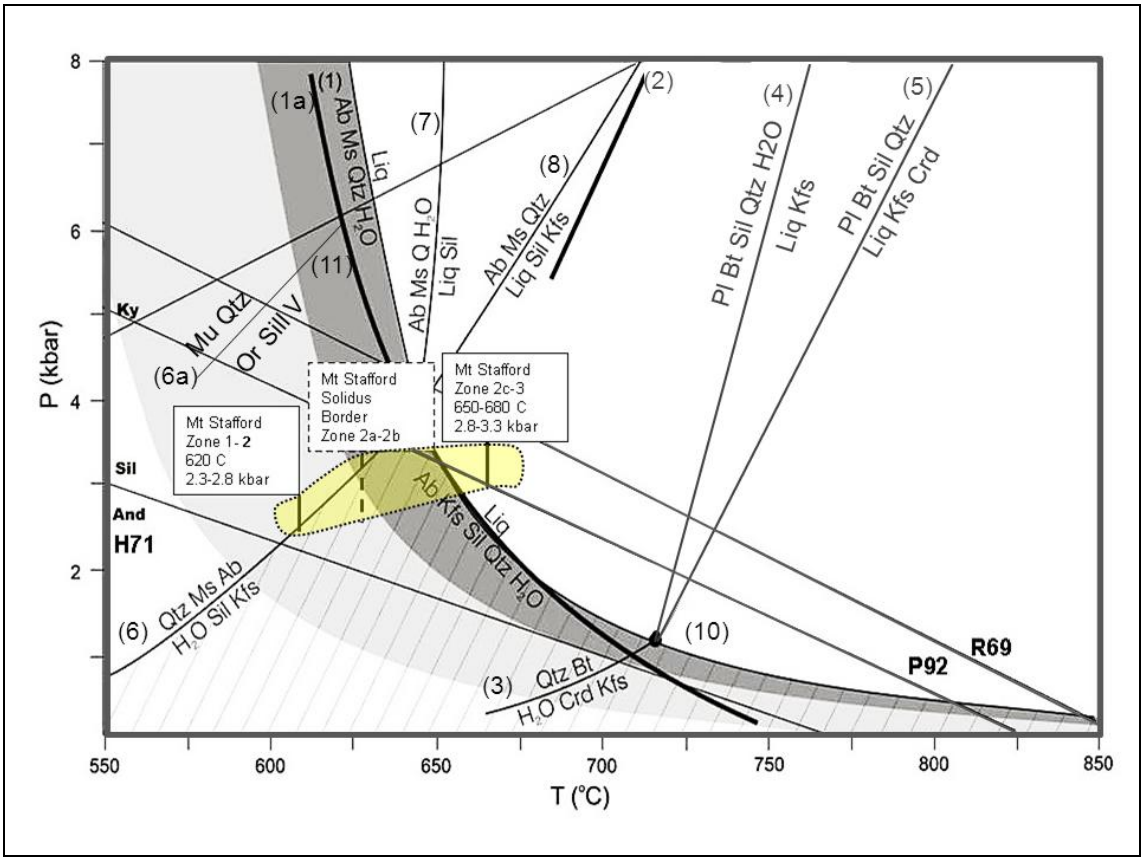

Fig. 1.3: The P-T conditions observed in the field at Mt Stafford superimposed onto Fig 1.1 (yellow shaded zone). Zone 1 - 2 boundary conditions (position of the solid vertical line in the yellow zone) are inferred to be 620 ºC, 2.3 - 2.8 kbar and Zone 2c - 3 boundary conditions are inferred to be midway between 650 – 680 ºC, 2.8 - 3.3 kbar (solid line at ~670 ºC). The position of the solidus (position of the dotted vertical line) is located on the Zone 2a – 2b boundary, but unconstrained (Greenfield *et al.*, 1996).

1.4 Aims of the study

The rocks in the Mt Stafford region underwent partial anatexis and migmatization in the andalusite stability field at relatively low temperature (600 to 675 °C) and low pressure (< 5 kbar) conditions, which is contradictory to the accepted andalusite-sillimanite boundary of Holdaway (1971). If the Holdaway (1971) curve is accepted, melting in the andalusite stability field is impossible due to the relative positions of the wet granite solidus and the muscovite dehydration equilibria in quartz saturated rocks.

The general aim of this study is to better understand the complex interplay between bulk rock geochemistry, mineralogy and melting at Mt Stafford, which is of global relevance to our understanding of the relationships between metamorphism, geochemistry and partial melting. The following three aims have been selected as focus areas:

1. To use an experimental approach to build on the previous field and phase relationship research in the Mt Stafford region and to demonstrate that fluid-absent melting of natural metapelites can occur at low pressure over a range of temperatures under specified circumstances,
2. To counter the general lack of experimental knowledge in low pressure fluid-absent partial melting terranes; and
3. To investigate the phase relationships of the micas and the possible metastability of andalusite in the Mt Stafford metasediments that has been used to explain the occurrence of andalusite in leucosomes.

Chapter 2: Previous studies

2.1 Previous experimental studies on biotite and muscovite fluid-absent melting

The phase relationships, mineral and melt chemistry during low-pressure (200 MPa) water-saturated melting of metasedimentary rocks has been the subject of a number of recent studies (Wolf & London 1997; Icenhower & London 1997; Acosta-Vigil & London 2003; Evensen & London 2003). However, most experimental studies of fluid-absent partial melting in natural metapelitic rocks have focussed on intermediate to higher pressure conditions of anatexis (500 MPa or above); as mentioned in the introduction, Storre (1972); Vielzeuf & Holloway (1988); Le Breton & Thompson (1988); Carrington & Harley (1995); Stevens *et al*. (1997); Pickering & Johnston (1998). Some of the starting material compositions used in these studies is close to the composition of the Mt Stafford metapelites and their findings will be discussed in more detail in the following paragraphs.

Melting of metapelite starting materials under fluid-absent conditions was investigated by Vielzeuf & Holloway (1988) and very useful information was obtained on the behaviour of biotite and muscovite during these experiments. The experiments were performed at 7, 10, and 12 kbar and at temperatures ranging from 750 to 1250 °C. The experimental observations in this study lead to the following conclusions:

1) In the fluid-absent melting of metapelites, S-type granitic melts produced below 850 °C are primarialy the result of muscovite incongruent melting and are water-rich;

2) These melts are generated in small amounts (<10 %) in most common metapelites by reactions that begin at 750 °C at pressures of 7 kbar;

3) At 7 and 10 kbar, the breakdown of the biotite + sillimanite + plagioclase + quartz assemblage produces a large amount of melt within the narrow temperature range of 850 to 875 °C.

Since Mt Stafford metapelites contain biotite and muscovite in the pre-anatectic assemblage, it is important to note that Vielzeuf & Holloway (1988) found that the biotite reaction can be extended to lower pressures since (i) As a consequence of the pressure dependence of water solubility in silicate melts, any given source rock will produce more melt, by a given fluid-absent reaction, at lower pressure. At a given pressure, higher-temperature reactions can produce more melt from a given source rock (Clemens & Vielzeuf (1987), (ii) the reaction Bt + Als + Pl + Q = L + Gt + Kf has a large dP/dT slope, and, (iii) the reaction intersects the wet granite solidus at low pressure ~ 1 kbar and 720 ºC. In contrast, the observation on muscovite melting cannot be reliably extrapolated to lower pressure because of the likely intersection with the wet granite solidus. The muscovite dehydration reaction has a low dP/dT slope before it intersects the wet granite solidus at low temperatures and because the biotite and muscovite melting reactions have such contrasting P-T slopes they will therefore be discussed separately.

The biotite dehydration-melting experiments of Patińo Douce & Beard (1995), additional to the research of Vielzeuf & Holloway (1988), which are relevant to low P, add to the understanding of biotite behaviour during fluid-absent melting (Fig 2.1). They reported from dehydration-melting experiments (3000 - 15000 MPa) of a gneiss and amphibolite that there is no significant difference between the vapour-absent solidi of biotite- and hornblende-bearing quartz-saturated rocks of comparable Mg# (Mg number). The vapour-absent melting and crystallization experiments were performed on two bulk compositions that model metamorphic rocks containing a single hydrous phase: a biotite gneiss [37% bio (Mg# 55), 34% qtz, 27% plg (An_{38}), 2% ilm] and a quartz amphibolite [54% hbl (Mg# 60), 24 % qtz, 20 % plg (An_{38}), 2 % ilm]. Experiments were performed at 3 and 5 kbar in internally heated pressure vessels (IHPV), and at 7, 10, 12·5 and 15 kbar in piston cylinder apparatus (PC), from the vapour-absent solidi to (at least) the temperature at which the hydrous mineral disappeared. Dehydration-melting begins at similar temperatures in both bulk

compositions, ranging from T ~ 850 °C at P = 3 kbar *T* ~ 930 °C at P = 15 kbar. The hydrous mineral disappears ~ 50 °C above the solidus in both systems, except in IHPV experiments at $f(O_2)$ above Ni–NiO, in which biotite stability extends up to atleast 80 °C above the solidus. Although the solidi of both types of rock are similar, melt productivity is considerably greater in the biotite gneiss than in the quartz amphibolite. Crustal melting at T < 900 °C will generate similar melt fractions (up to 20 %, depending on P) from both types of lithologies. However, if temperatures can rise to 950 °C or more during anatexis, then biotite gneisses can generate 2 - 3 times more silicic melt than quartz amphibolites. The melts generated by both starting materials at T < 1000 °C are felsic and consistently peraluminous. In both systems, variations in melt productivity with P are controlled by three competing factors: (1) the positive d P/dT slopes of the solidi, (2) decreasing H_2O activity with increasing *P* at constant H_2O content, and (3) Na_2O activity, which increases with *P* concomitantly with breakdown of plagioclase. The biotite gneiss produces strongly peraluminous granitic melts (SiO_2 > 70 wt%) and residual assemblages of quartz norite (P > 12.5 kbar) or garnet pyroxenite (*P*>12.5 kbar). The quartz amphibolite produces strongly peraluminous granodioritic melts (SiO_2 > 70 wt%) that coexist with clinopyroxene + orthopyroxene + plagioclase + quartz ± (at P > 10 kbar) garnet. The results of coupled melting and crystallization experiments on the quartz amphibolite suggest that strongly peraluminous granitoid rocks (e.g. cordierite-bearing and two-mica granites) can be derived from melting of Al-poor protoliths (Patińo Douce & Beard, 1995).

Vielzeuf & Montel (1994) performed a range of fluid-absent experiments on quartz-rich aluminous metagreywackes between 100 and 2000 Mpa (Fig. 2.1). Ca-poor Al-metagreywackes represent fertile rocks at commonly attainable temperatures (i.e. 800 - 900 °C), below 700 Mpa and 30 - 60 % of melt can be produced towards the higher temperatures. The multivariant field of the complex reaction Bt + Pl + Qtz = Grt/Crd/Spl + Opx + Kfs + melt limited by the Opx-in and Bt-out curves, is located

between 810 – 860 °C at 100 MPa, 800 – 850 °C at 200 MPa, 810 – 860 °C at 300 MPa, 820 – 880 °C at 500 MPa, 860 – 930 °C at 800 MPa, 890 – 990 °C at 1000 MPa, and at a temperature lower than 1000 °C at 1500 and 1700 MPa. The melting of biotite + plagioclase + quartz produced melt + orthopyroxene + cordierite or spinel at 100, 200 and 300 MPa, and melt + orthopyroxene + garnet from 500 to 1700 MPa (+ Qtz, Pl, FeTi Oxide at all pressures). K-feldspar was found as a product of the reaction in some cases and we observed that the residual plagioclase was always strongly enriched in orthoclase component. Available experimental constraints indicate that extensive melting of pelites takes place at a significantly lower temperature (850 °C ± 20) than in Al-metagreywackes (950 °C ± 30), at 1000 MPa. The common observation from these experiments that biotite is no longer stable in aluminous paragneisses, while it still coexists commonly with orthopyroxene, garnet, plagioclase and quartz, provides rather tight temperature constraints for granulitic metamorphism (Vielzeuf & Montel, 1994).

Thin layers of gneisses, composed of orthopyroxene, garnet, plagioclase, and quartz (± biotite), interbedded within sillimanite-bearing paragneisses are quite common in granulite terrains (Vielzeuf & Montel, 1988) (Fig 2.1). They may result from partial melting of metagreywackes and correspond to recrystallized mixtures of crystal (+ trapped melt) left behind after removal of a major proportion of melt (Vielzeuf & Montel, 1994). Patińo Douce & Beard (1996) presented results of dehydration melting experiments (3 - 15 kbar, 810 - 950 °C, fO_2 < QFM and > Ni-NiO) on two Fe-rich mixtures of metagreywackes, which differ only in their biotite compositions (Mg# = 23, 0.4), where Mg# = (100*Mg/Mg+Fe). Dehydration melting of metagreywackes of constant modal composition generates a wide range of melt fractions, melt compositions and residual assemblages, through the combined effects of pressure, Fe/Mg ratio and fO_2. These important biotite melting reactions discussed in the above paragraphs are summarised in Fig 2.1.

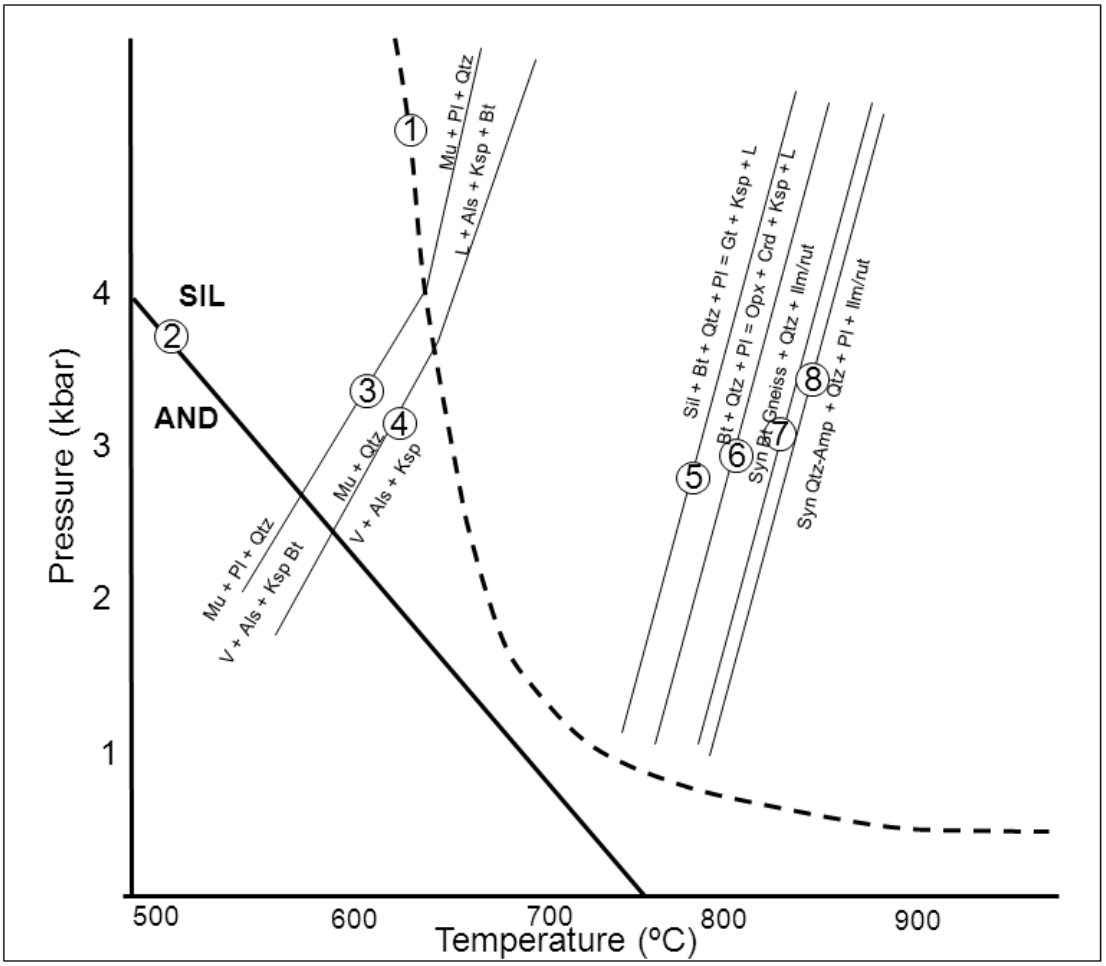

Fig. 2.1: Reaction (1) = Metapelite solidus (Thompson, 1982); reaction (2) the most commonly cited aluminium silicate triple point (Holdaway, 1971); reaction (3) = the muscovite subsolidus reactions from Thompson (1982) and reaction (4) = Huang & Wyllie (1974); reaction (5) = Biotite melting reactions from Vielzeuf & Holloway (1988) and Le Breton & Thompson (1988); reaction (6) = Vielzeuf & Montel (1994); reaction (7) = the synthetic biotite gneiss from Patiño-Douce & Beard (1995) and reaction (8) = the synthetic quartz amphibolite from Patiño-Douce & Beard (1995).

Experimental muscovite subsolidus (pre-anatectic) breakdown and general melting behaviour are discussed in the following sections. H_2O-saturated experiments by Icenhower & London (1995) on synthetic metapelite compositions (muscovite + quartz + albite and muscovite + quartz + albite + biotite + aluminum silicate + cordierite) performed over the temperature interval of 600 - 750 °C at 200 MPa (H_2O) revealed that partial fusion commences at 625 °C along the metastable extension of the reaction muscovite + quartz + albite + H_2O = melt + aluminum silicate to 200 MPa to below the

intersection of reactions albite + orthoclase + quartz + H_2O = L and muscovite + quartz = orthoclase + aluminiumsilicate + H_2O. Biotite is stable over the entire temperature interval, although it reacts progressively to hercynite + melt at the high end of the temperature range. In the absence of quartz, muscovite that survives initial melting breaks down to corundum + orthoclase between 700 and 725 °C. Minor corundum and aluminum silicate are present at 650 °C, whereas corundum with a large Fe + Ti component is present at and above 700 °C. Finally, corundum and hercynite exist with orthoclase-rich feldspar and remaining biotite at 750 °C. Both muscovite and its equivalent orthoclase + corundum assemblage contribute substantial excess Al to melt, bringing the value of the Aluminium Saturation Index (Zen, 1986) or A/CNK (A/CNK (Clarke, 1981) = molar [(Al_2O_3/(CaO + Na_2O + K_2O)] of melt to 1.4.

Brearley & Rubie (1990) have examined in detail the effect of H_2O on the textures produced and mechanisms observed during the breakdown of muscovite + quartz under experimental disequilibrium conditions and revealed some interesting disequilibrium behaviour of muscovite which might be of relevance to this study. Under H_2O-saturated conditions (1 wt % H_2O added) muscovite reacts completely at 757 °C and 1 kbar to a metastable assemblage of peraluminous melt + mullite + biotite, a reaction which delays the formation of the stable equilibrium assemblage K feldspar + sillimanite + biotite. In contrast, muscovite in the H_2O-undersaturated experiments breaks down by the stable dehydration reaction producing K feldspar + sillimanite + biotite and by metastable melting reactions in the same sample. The composition of the metastable melt is controlled by a number of kinetic factors which change as a function of time and reaction progress. Early melts are highly siliceous and sodic due to the rapid dissolution of quartz relative to muscovite, coupled with the incongruent melting of the paragonite component of muscovite and crystallization of biotite. The delayed nucleation of mullite results in Al supersaturation of the melt, which inhibits the rate of the melting reaction. Once mullite nucleates the degree of Al melt supersaturation is decreased and the rate of

muscovite dissolution increases. After complete reaction of muscovite, the melt chemistry continues to change as Si diffuses into the pseudomorphs formed by muscovite breakdown from adjacent quartz. Even after 5 months at 757 °C large compositional gradients in Si and Al still persist within the melt. Metastable melting can occur initially, catalysed by traces of grain boundary fluid or by fluid released from the dehydration of muscovite. Once melting starts any fluid is strongly partitioned into the melt phase, reducing μH_2O and under these conditions further melting is inhibited and the stable dehydration reaction will continue (Brearley & Rubie, 1990). If the H_2O produced during muscovite dehydration is released and diffused through the rock and the wet metapelite solidus is overstepped as often happens in contact metamorphic terranes, biotite fluid-present melting may result and the normal subsolidus reactions consuming quartz and feldspar do not occur (Buick *et al*., 2004). Examination of examples of natural muscovite reacted under disequilibrium conditions in xenolithic and contact metamorphic rocks at low pressures suggests that metastable melting is an important process under certain geological conditions, such as in contact metamorphic terranes (for example, the Bushveld Complex, South Africa, Wallmach *et al*., 1995; the Laramie anorthosite, USA, Frost *et al*., 2002). It is possible that it is widespread in contact metamorphic rocks, but the textures indicative of metastable melting reactions are obscured during the extended cooling histories of such rocks (Brearley & Rubie, 1990).

Mullite (Mul) formation after high-T muscovite (Ms) breakdown has been noted and studied by Rodriguez-Navarro *et al.* (2003) in phyllosilicate-rich bricks. At $T \geq 900$ °C Ms de-hydroxylation is followed by partial melting that triggers the nucleation and growth of acicular mullite crystals. An analytical electron microscopy study reveals that the Mul is a 3:2-type with a $^{[6]}(Al_{1.686}Ti_{0.031}Fe_{0.159}Mg_{0.134})^{[4]}(Al_{2.360}Si_{1.649})O_{9.82}$ formula and an O atom vacancy of $x = 0.18$. This is consistent with X-ray diffraction results [i.e., unit-cell parameters: $a = 7.553(7)$, $b = 7.694(7)$, and $c = 2.881(1)$ Å, $V = 167.45$ Å^3]. The initial stage of the process resulting in Mul growth followed the

balanced reaction Ms → 0.275Mul + 0.667Melt + 0.244K_2O + 0.01Na_2O + 0.125H_2O, yielding an alkali-poor peraluminous melt. H_2O with K (and Na), which are lost along the (001) planes of de-hydroxylated Ms, play a significant role as melting agents. Devineau *et al*. (2006) investigated the thermal decomposition of muscovite in natural granite powders heated to 1175 °C for durations from 5 min to 68 h, at 1 bar, paying special attention to the early stages of decomposition. This study shows that muscovite is completely transformed after 5 min. Muscovite pseudomorphs consist of glass, mullite, and Al-rich oxides. For short durations (5 and 40 min), the Al-rich phase was identified by XRD, electron diffraction, and TEM microanalysis as γ-Al_2O_3 containing 4 – 8 wt% FeO (total Fe), probably a few weight percents of MgO, and possibly up to 10 wt% SiO_2.

2.2 Previous experimental studies on the role of boron during melting

The experimental studies that investigate boron as a melt fluxing agent are discussed below because boron has been proposed by Greenfield *et al*. (1996) as a possible agent to lower the position of the wet granite solidus into the andalusite stability field at Mt Stafford. Some researchers addressed the problem of boron fluxing in either granitic or metapelitic starting compositions. These studies, together with tourmaline stability experiments, are summarized in the following paragraphs to give insight into the influence of boron on the melting reactions. Tourmaline stability experiments were discussed because tourmaline is the main carrier mineral for boron in medium-grade metasediments.

The study of Pichavant (1981) investigated the effect of boron on a H_2O saturated haplogranite at 1 kbar and found that the solidus temperature of the Q – Or - Ab composition is lowered by 60 °C when 5 wt% B_2O_3 is added and by more than 130 °C when 17 wt% B_2O_3 is added (Fig 2.1). This study is relavant to the experimental work presented in this study as it sparked the suggestions of boron fluxing at Mt Stafford to facilitate melting in the andalusite stability field. In the Mt Stafford area, boron fluxing of melting reactions has been proposed as a mechanism to induce partial melting at

unusually low temperatures (Greenfield *et al*., 1998). Adding components, allowing for the formation of the more stable boron-bearing mineral tourmaline, instead of the oxide B_2O_3, changes the picture.

The study of Benard *et al.* (1985) examined the phase relations of tourmaline leucogranites and the significance of tourmaline in silicic magmas. They found that the presence of tourmaline slightly lowers the (H_2O saturated) solidus temperature from 5 to 20 °C compared to the tourmaline-free solidus. Tourmaline is the last major phase to disappear for both leucogranites studied and is a demonstrated liquidus phase for both. The tourmalines are always richer in Mg than the melt is, but Fe and Mg are not especially partitioned between crystallizing tourmaline and melt. Melt compositions do not depart significantly from the minima and eutectic points in the reference synthetic experimental granitic systems. Their data show that the phase relations for granitic systems are not significantly changed when the boron content of the melt is fixed by tourmaline saturation. In such compositions, tourmaline possesses a large region of stability as a function of temperature between 1 to 3 kbar.

Wolf & London (1997) and London (1999) concluded that in metapelites that may contain tourmaline as the principal source of boron, the inception of anatexis would promote reactions that will consume tourmaline, liberate boron to the melt and conserve ferromagnesian components in residual biotite, spinel, or cordierite, or garnet at higher pressures. In typical metapelites, the ASI of melts will be near 1.3 if equilibrium between melt and muscovite, aluminosilicate, spinel, etc. is attained. At their experimental conditions (750 °C, 200 MPa, fO_2 Ni-NiO, $a(H_2O) = 1$) a given fraction of peraluminous melt can dissolve boron to approximately 20 wt% equivalent of tourmaline (to generate 2 wt% B_2O_3). Truly aluminous metapelites are poor sources of large volumes of melt because their bulk compositions lie far from the Na-rich minimum composition (Patińo-Douce & Johnson (1991), London (1995), Icenhower & London (1995). It is possible, therefore, that the productions of very

small melt volumes, coupled with the decomposition of muscovite (London (1995), London & Icenhower (1995) could generate magmas that are saturated with respect to tourmaline early in their history. Quartzofeldspathic rocks, however, are capable of generating large enough quantities of melt that they would expect all tourmaline to be consumed during anatexis. Thus, most common melt compositions may acquire boron and not be tourmaline saturated. Tourmaline in quartzofeldspathic granulites is a rare occurrence (Grew, 1996) and may indicate that these rocks have not melted.

The work by Chorlton & Martin (1978) indicated that the addition of 5 – 10 wt% boron to a water-saturated synthetic (prepared by the gel method) granitic system lowers the solidus at 1 kbar by 125 °C; the liquidus seems similarly affected. The more recent work discussed above on more realistic natural compositions indicates that these findings are also not applicable to the present study as in the natural rocks tourmaline provides a stable resevour for a substantial portion of the boron in the system.

2.3 Field and petrogenetic studies applicable to Mt Stafford

This section cover in detail what was not dealt with in Chapter 1, section 1.3. A substantial amount of research on field relationships (Clarke *et al*., 1990; Collins & Vernon, 1991; Collins & Williams, 1995; Greenfield *et al*., 1996) at Mt Stafford has been summarized in detail by White *et al*. (2003). The following paragraphs (refer to Chapter 1, Fig 1.2 a,b) represent a summary of this work, as well as of petrogenetic work (Figs 2.2 and 2.3) of White *et al*. (2003) on the Al-rich metapelites at Mt Stafford. Peak metamorphism at Mt Stafford occurred during a pre-1820 Ma $D_1 - M_1$ event (Collins & Williams, 1995), which was divided into D_{1a} and D_{1b} by Vernon *et al*. (1990). The area preserves only limited effects of a $D_2 - M_2$ event that pervasively recrystallized rocks in the Mt Weldon area further east (Clarke *et al*., 1990). The results of U – Pb dating of zircon from syn-tectonic granitoids were used to infer that the $D_2 - M_2$ event was short lived and occurred between *c*. 1780 and 1770 Ma

(Collins & Williams, 1995). However, the results of recent U – Th – Pb dating of zircons and monazites from granulite-facies metasediments have been used to argue that $D_2 - M_2$ occurred at *c*. 1600 Ma (Vry *et al*., 1996; Williams *et al*., 1996). At Mt Stafford, the $D_1 - M_1$ event resulted in a low-P/high-T regional aureole (Collins & Vernon, 1991), which has been divided into five zones (Greenfield *et al*., 1996), ranging from greenschist (Zone 1) to granulite facies (Zones 4 and 5) over a distance of 10 km (White *et al.* 2003). The zones have been described by previous workers and a summary is givien in the paragraphs below.

Zone 1:

The rocks of Zone 1, also called the muscovite zone by Vernon *et al*. (1990), are dominantly interbedded metagreywackes and metapelitic schists. These rocks are dominated by muscovite, biotite and quartz with minor chlorite, tourmaline and ilmenite. Andalusite, rich in quartz inclusions, occurs in some aluminous Zone 1 rocks. Cordierite is present in poorly outcropping massive metasiltstones that are inferred to be the protolith for the cordierite granofels.

Boundary zone 1-2:

The boundary between Zones 1 and 2 is marked by the appearance of dark spots in some metasedimentary rocks that are inferred to represent cordierite porphyroblasts that have since been pseudomorphed by symplectites of biotite, andalusite and quartz (Vernon *et al*., 1990). The subsolidus evolution of the metapelites primarily involves the breakdown of muscovite and the appearance of cordierite, K-feldspar and andalusite porphyroblasts. The appearance of cordierite and K-feldspar, a marked increase in the mode of aluminosilicate, and the disappearance of muscovite, occur at almost the same place in the sequence, the boundary between Zones 1 and 2. Thus, it is likely that the Zone 1–Zone 2 boundaries occurs close to the intersection between the subsolidus trivariant

field, in which coexisting muscovite and quartz break down, and the trivariant field in which subsolidus cordierite is first produced (White *et al*., 2003).

Zone 2:

Zone 2 rocks are distinguished by the appearance of andalusite porphyroblasts and K-feldspar in metapelite and metagreywackes, and commonly contain the assemblage aluminosilicate, cordierite, K-feldspar, biotite and quartz in metapelite and metagreywacke. The initial leucosome is concentrated in patches around the large aluminosilicate porphyroblasts in the form of millimetre- to centimetre-wide moats. Hence, this melting relationship is restricted to, or at least concentrated around, the isolated aluminosilicate porphyroblasts. A poorly layered cordierite-rich rock termed 'cordierite granofels' by Greenfield *et al*. (1996) becomes common in Zone 2. The cordierite granofels may contain up to 60 % cordierite at this grade. Greenfield *et al*. (1996) subdivided Zone 2 into Zones 2a, 2b and 2c. The first appearance of felsic segregations marks the boundary between Zones 2a and 2b. These leucocratic segregations contain microcline with idioblastic faces within large optically continuous quartz grains, and were interpreted by Greenfield *et al*. (1996, 1998) to represent the development of partial melt from crossing the wet solidus. The boundary between Zones 2b and 2c is defined by the first appearance of sillimanite partially pseudomorphing andalusite (White *et al*., 2003).

Zone 3:

The low-temperature boundary of Zone 3 is defined by a marked decrease in the mode of biotite. The appearance of spinel + cordierite-bearing symplectites that mantle aluminosilicate porphyroblasts in Zone 3 was interpreted by Greenfield *et al*. (1996, 1998) to represent the local complete consumption of biotite and the stabilizing of coexisting spinel + quartz. Some metapelite samples, especially those rich in aluminosilicate, lack biotite in Zone 3. The cordierite granofels commonly becomes aluminosilicate-absent in Zone 3. However, where present, the aluminosilicate porphyroblasts are also

mantled by cordierite + spinel-bearing symplectites (White *et al*., 2003). Garnet-bearing assemblages become common in metapsammite and less aluminous metapelite near the high-temperature end of Zone 3. Garnet commonly overgrows prograde biotite.

Boundary Zones 3-4:

The boundary between Zones 3 and 4 is marked by the appearance of orthopyroxene in metapsammitic rocks. Orthopyroxene may also occur in the cordierite granofels, but is absent from most samples. In metapelitic rocks, inferred peak metamorphic assemblages involving cordierite, spinel, K-feldspar and quartz, with or without minor biotite, are most common. The assemblages sillimanite, cordierite, spinel, K-feldspar and quartz, and cordierite, spinel, garnet, K-feldspar and quartz, both with or without minor biotite are also developed. However, the distribution of minerals in many samples is patchy, and several assemblages may be developed in a single rock on a millimetre to centimetre scale (White *et al*., 2003). Centimetre-scale leucocratic segregations occur on a decimetre scale in upper Zone 3 and Zone 4. The segregations are generally K-feldspar- and quartz-rich and may additionally contain cordierite, biotite and garnet, depending on metamorphic grade. The most common types contain prismatic K-feldspar grains with crystal faces against interstitial pools of optically continuous quartz. Less commonly the K-feldspar – quartz relationships are reversed, with idioblastic quartz in optically continuous K-feldspar. Equant cordierite grains are also common in leucosomes and are also enclosed by optically continuous pools of quartz or K-feldspar.

Zone 4:

Garnet-bearing leucosomes are restricted to Zone 4, where they also preserve idioblastic faces against optically continuous quartz or K-feldspar. The idioblastic nature of K-feldspar and cordierite in the leucosomes and the large bodies of optically continuous host minerals is consistent with their growth in the presence of melt, and in some examples their crystallization from melt (Sawyer, 1999).

However, what proportion of each grain crystallized from melt, as opposed to having a sub-solidus or peritectic origin, is unclear (White *et al*., 2003).

Zone 5

Zone 5 consists of granulite facies metapelites containing cordierite, K-feldspar, biotite, plagioclase with or without minor abundances of garnet and orthopyroxene. The intrusion of the northern granite body into partially molten migmatites in Zone 5 indicates that magmatism occurred in the area during peak metamorphism. Although the outcropping area of the northern granite is too small to be responsible for the metamorphism at Mt Stafford, it may extend under the sequence or have extended over it. Alternatively, the granite itself may be a product of another larger thermal anomaly that underlies Mt Stafford (White *et al*., 2003).

Aluminosilicate relationships

The location of the andalusite to sillimanite transition at Mt Stafford occurs at higher grade than the inferred crossing of the wet solidus (Fig 2.2), which is inconsistent with most experimental and thermodynamic data (White *et al*., 2003). The source of this may lie in the position of the andalusite to sillimanite reaction relative to where this transition is first observed in the sequence and/or in the location of the calculated solidus. Andalusite may persist with sillimanite into Zone 4 conditions, whether by metastable persistence or by metastable growth, depending on increasing or decreasing modes of andalusite. These modes are shown in Fig 2.2a for the P-T region in question. They are close to constant or decreasing until the muscovite+quartz breakdown reaction is reached where a small jump in mode is predicted. Above the reaction the modes decrease with rising temperatures. Substantial uncertainties, 2 sigma errors calculated by THERMOCALC, on the andalusite - sillimanite reaction are presented in Fig 2.2a and b. Minor elements (Fe and Mn) may also shift the equilibria. The muscovite + quartz breakdown reaction may occur in the andalusite field at pressure below about 2.5 kbar for the upper andalusite - sillimanite error limit. Below this pressure andalusite

is the stable polymorph produced where the mode of aluminosilicate increases. It is possible that sillimanite did not grow in these rocks until temperatures at which the kinetic barriers to this reaction had been overcome. If sillimanite was not produced at the andalusite - sillimanite reaction, these mineral equilibria relationships are the metastable andalusite-bearing ones, which will have an effect on the position and slope of the aluminosilicate-bearing fields. Fig 2.2c shows the subsolidus mineral equilibria relationships calculated with andalusite metastably persisting. The wet solidus still occurs at temperatures well above the andalusite-sillimanite transition, even with uncertainties and the presence of boron or fluorine (suggested by Greenfield (1997) to lower the position of the solidus (boron/fluorine depression of the solidus shown in Fig 2.2b and d). The solidus cannot be shifted to lower temperatures by much more than 25 ºC. Therefore, both the metastable persistence of andalusite and the depression of the solidus are required to match the observed mineral assemblages.

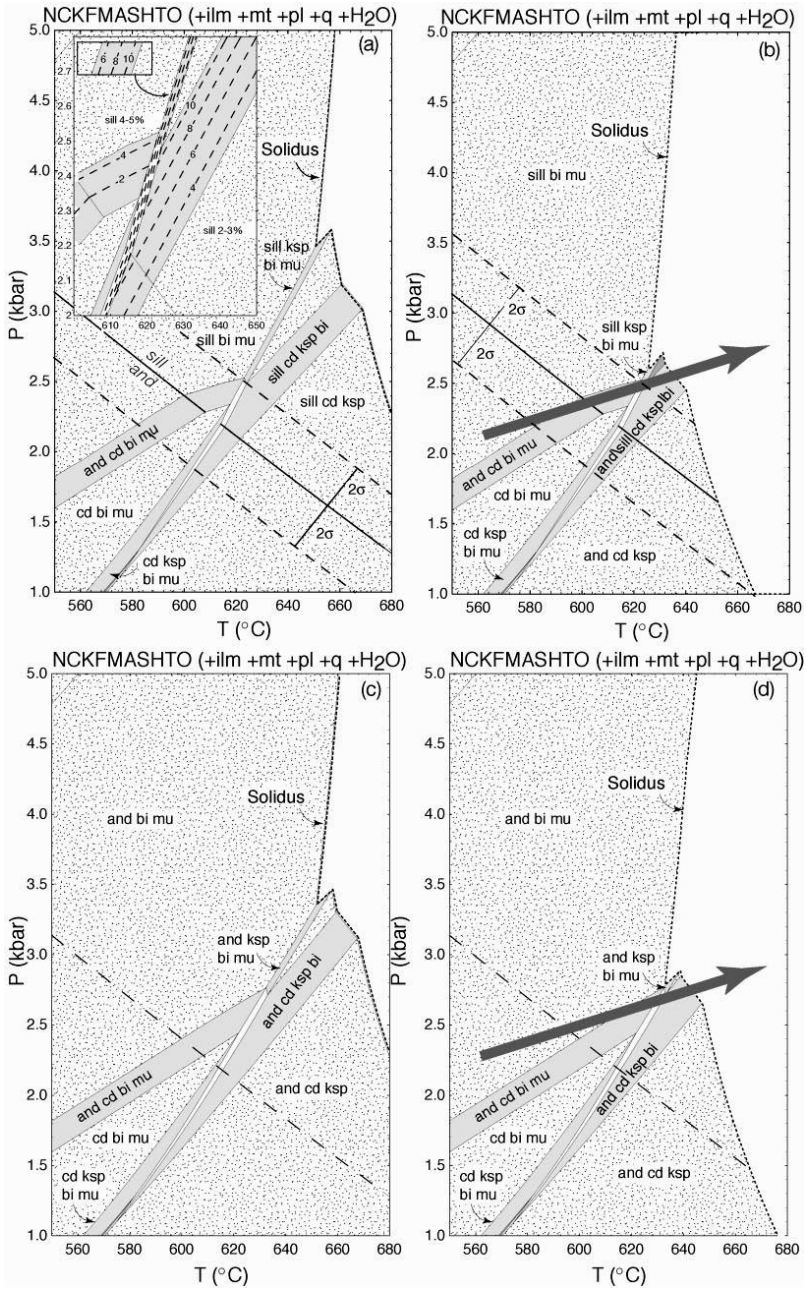

Fig. 2.2: P-T pseudosections from White et al. (2003) showing alternative subsolidus mineral assemblage relationships for the typical aluminous metapelite composition. (a) P-T pseudosection for conditions of fluid in excess. Also shown are the 2 sigma error bars on the andalusite - sillimanite reaction. The inset shows calculated aluminosilicate mode contours for part of the diagram. (b) Semiquantitative P-T pseudosection showing the mineral relationships relative to a wet solidus depressed to lower temperatures because of the presence of boron. The position of the solidus is not calculated but is shifted to lower temperatures manually. Also shown are the 2 sigma error bars on the andalusite - sillimanite reaction. The grey arrow shows the position of a field gradient in P-T that is consistent with the petrographic observations assuming sillimanite replaces andalusite at the calculated reaction. (c) P-T pseudosection calculated assuming the metastable persistence of andalusite to temperatures above the calculated andalusite - sillimanite reaction. (d) Semiquantitative P-T pseudosection showing the mineral relationships relative to a wet solidus depressed to lower temperatures and the metastable persistence of andalusite. The grey arrow shows the position of a field gradient in P-T that is consistent with the petrographic observations assuming andalusite metastably persists beyond its calculated stability.

Melt production:

White *et al*. (2003) (Fig 2.3) summarised that melt production was dominated by a series of multivariant biotite breakdown reactions, not the univariant reactions suggested by previous studies. Although the three main metasedimentary rock types produced similar amounts of melt at the highest grades, their melt production histories differed markedly as a function of temperature. Aluminous metapelites produced more melt at lower temperatures (Zones 2 and 3), whereas metapsammite and cordierite granofels experienced an additional major melt-producing step at higher temperatures (upper Zone 3 and Zone 4). This melting step involved the breakdown of biotite to produce garnet, K-feldspar and melt, and in some rocks the production of orthopyroxene. Melt production in Zone 4 exceeded 25 mol %, resulting in the formation of in situ diatexites. Complex relationships involving aluminosilicate porphyroblasts resulted in the breakdown of biotite and aluminosilicate being drawn out over a wide temperature range, from subsolidus conditions to temperatures close to 750 ºC. Initially, much of the melting developed around the aluminosilicate porphyroblasts during the breakdown of coexisting biotite, aluminosilicate and quartz. However, much of the rock was chemically isolated from the porphyroblasts and could not react to produce melt. As temperatures rose, the presence of the large isolated aluminosilicate porphyroblasts controlled the spatial development of quartz-absent, spinel-present compositional domains, the formation of spinel being governed by the silica-undersaturated breakdown of coexisting biotite and aluminosilicate.

Fig 2.3 (White *et al*., 2003) is a pseudosection representing the phase relations in an aluminous metapelite above the solidus, where the rock becomes fluid-absent. Further melting relies on the breakdown of hydrous minerals and the supersolidus calculations involve a fixed water content for the rock. The water content is fixed at <1 % modal water in the rock at the solidus, between where it is intersected by the subsolidus muscovite breakdown reaction and the subsolidus biotite and sillimanite breakdown reaction (P = 3.2 kbar, T = 640 ºC) (White *et al*., 2003). Because of the small

modal water content immediately below the solidus, little melt is produced at the solidus. With rising temperature biotite and sillimanite modes rapidly decrease as cordierite and melt content increase. The melting is concentrated around aluminosilicate porphyroblasts, reflecting pre-existing textures, from field relationships. The large aluminosilicate porphyroblasts may partition the bulk-rock composition into high- and low-alumina domains. In the high-alumina domains, the aluminosilicate:biotite ratio was such that biotite was consumed before aluminosilicate, but in the low-alumina domains, biotite (sufficiently isolated) would persist to higher temperatures. At temperatures above the breakdown of coexisting sillimanite, biotite and quartz, little change in the mineral assemblage occurs and the assemblage cordierite – sillimanite - K-feldspar - quartz and melt is stable.

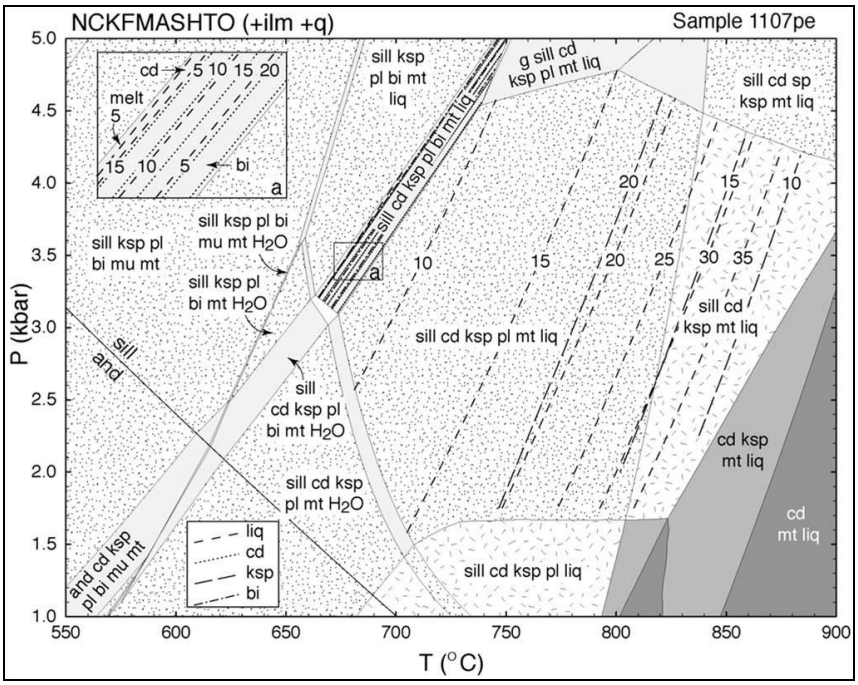

Fig. 2.3: Calculated P-T pseudosection from White *et al*. (2003) for the supersolidus part of the aluminous metapelite. Because of the need to fix water contents in the bulk rock at the solidus, the water-absent subsolidus fields are inappropriate for interpreting the pre-melting prograde evolution. The pseudosection also shows calculated molar mode contours in percent for several minerals and silicate melt. Insert (a) shows detail of the mode changes that occur within the area indicated by the box. The quartz-bearing aluminous metapelites have a relatively simple evolution at temperatures above the breakdown of biotite and develop an assemblage dominated by cordierite, K-feldspar and silicate melt in upper Zone 3 and Zone 4.

2.4 Summary

A substantial amount of experimental and field work has been discussed on fluid-absent melting behaviour of rocks containing micas. The exact mechanism and conditions of anatexis at Mt Stafford at low pressures and temperatures are estimates of field observations and pseudosection calculations. Appropriate experimental studies of biotite and muscovite behaviour under fluid-absent, low pressure and temperature conditions in the absence of plagioclase have not been conducted previously and current interpretations rely on an extrapolation of higher pressure work to the conditions proposed for Mt Stafford anatexis. The Mt Stafford rocks provide an ideal source to fill the gap in experimental work at low pressures, since muscovite is present in the Zone 1 rocks close to the solidus, biotite is present in the Zone 2 rocks. Biotite and muscovite combinations exist together on the boundary of Zones 1 and 2, therefore providing the two-mica scenario at low pressure conditions close to the solidus. The melting behaviour of tourmaline can also be studied as it is present from Zone 1 to Zone 2 areas. Additionally, andalusite has been used by previous studies to infer the conditions of anatexis, present as pre- and post-anatectic phase, at Mt Stafford. This study provides the ideal opportunity to study andalusite and tourmaline behaviour under low pressure, low to high temperature conditions within a natural assemblage of minerals in a constrained environment.

Chapter 3: Starting materials and experimental design

3.1 Equipment

The experimental petrology laboratory at the University of Stellenbosch is the only facility of this kind in Africa. The laboratory consists of two small volume, Holloway design internally heated gas vessels designed for maximum pressure temperature conditions of 10 000 bar and 1000 °C; a bank of conventional, water pressurised cold-seal vessels; and, two non-end-loaded piston cylinder apparati equipped with 18.75, 12.5 and 10 mm diameter pressure vessels. All the experiments conducted as part of this study used the internally heated, small-volume Holloway type gas vessel, using high-purity argon as the pressure medium. The 5Ω furnace used had a hot spot of approximately 2 cm. When loaded with the 10 mm internal diameter silica glass tubes used as sample carriers, the temperature variation within the hot spot was less than 5 °C, with the vessel mounted horizontally. Up to 4 capsules between 12 and 15 mm long were loaded into the glass tube side-by-side and two type-K Inconel sheathed thermocouples situated at either end of the capsules monitored the temperature gradient over the sample volume. The small space left around the thermocouple and sample capsules were packed tightly with refractory Si wool to keep gas circulation to a minimum, therby further reducing the temperature gradient across the sample volume. Additionally, small degrees of vessel tilt were applied to keep the temperature gradient through the sample volume as low as possible during experiments. Temperature measurement of the primary thermocouple and control of the furnace was achieved using a Temperature Controls® multi-function solid-state temperature controller with integral ice point acting through a 1kw thyristor unit. The temperature of the second control thermocouple was measured using a similar device. Temperatures were readily maintained to within 1 °C of the set point for the duration of an experiment. Confining pressures were monitored via a Heise® bourdon tube gauge and pressure was stable to ± 0.1 MPa during the course of each

experiment. Experiments were conducted over the pressure-temperature range 2.9 to 3.2 MPa and 750 to 1000 ºC.

Samples were ground for up to two hours with a mechanical mortar and pestle in an attempt to produce an average grain size of 5 µm in the powders. Despite the long grinding time, the existence of minerals of high hardness, as well as the lubricating effect of the substantial amount of mica in the samples, ensured that some larger (20 – 50 µm) particles of hard minerals were always present, although the average grain size was in the order of 10 µm. Sample powders were dried at 200 ºC overnight and kept under vacuum in a desiccator prior to loading into gold capsules. The capsules (12 mm long by 5 mm outside diameter) were constructed from 0.25 mm thick high-purity annealed gold plate. Approximately 100 - 200 mg of sample powder, stored under vacuum over a desiccant, was sealed into the capsules using an arc welder. The capsules were then weighed and vacuum tested in a water bath for leaks. On completion of the experiments, the run products were removed from the capsules and mounted in epoxy resin, polished and carbon coated for Scanning Electron Microscopy.

3.2 Starting materials

The Mt Stafford rocks provide an ideal source to fill the gap in experimental work on fluid-absent of plagioclase deficient metapelite melting at low pressures. Muscovite is present in the Zone 1 rocks and biotite is present in the Zone 2 rocks. Biotite and muscovite combinations exist together on the border of the Zone 1 and 2 rocks, therefore providing the two-mica scenario for this experimental study. Tourmaline's melting behaviour can also be studied as it is present in the pegmatitic zones in higher Zone 2 areas. Additionally, andalusite has been used to infer the conditions of anatexis, and is present as pre- and post-anatectic phase, at Mt Stafford. The starting materials were selected keeping these factors in mind.

The four starting compositions (Fig 3.1) were chosen to reflect a range of metapelitic compositions from outcrops interpreted to represent the highest-grade pre-anatectic rocks available from the Mt Stafford area. Compositions MTS7 and MTS8 were chosen to present the andalusite-bearing metapelities and metapsammites from below the solidus and border of Zone 2a and 2b (Fig 3.1). MTS70 and MTS71 were chosen to present metapelites with elevated boron contents due to the high abundance of tourmaline in these samples. The samples were chosen to study the position of the solidus at Mt Stafford, andalusite stability near the solidus as well as the influence of elevated boron contents on the position of the solidus.

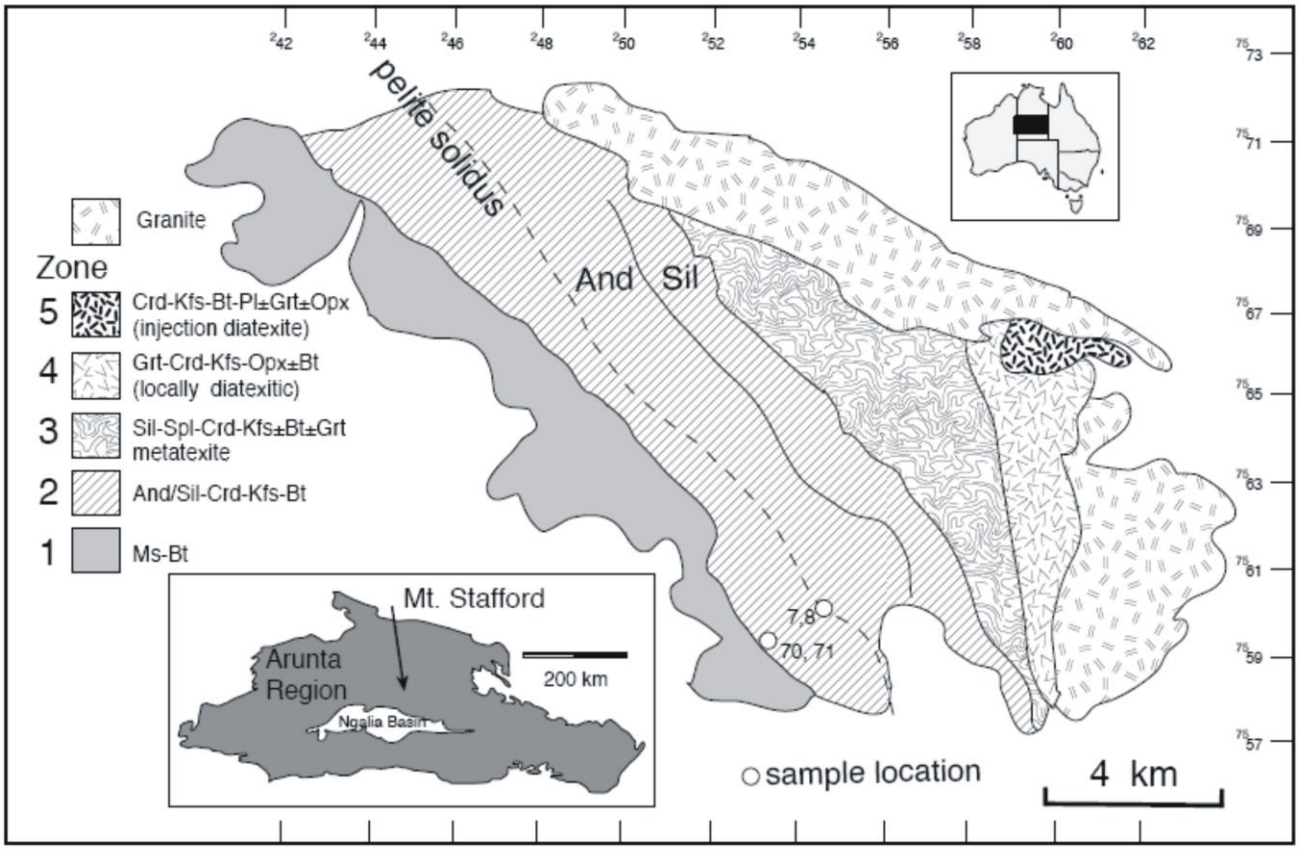

Fig. 3.1: Area map of the Arunta Region, Mt Stafford, indicating the sample locations of the 4 starting materials. MTS70 and 71 are located on the border of zone 1 and 2 and MTS7 and 8 are located close to the metapelite solidus in zone 2.

MTS7 and MTS8 are biotite metapelites from Mt Stafford metamorphic zone 2c (Greenfield *et al.*, 1998) (Fig 3.2). The mineral assemblage in MTS7 and MTS8 is biotite, K-feldspar, quartz cordierite and minor plagioclase, with accessory tourmaline (in MTS8). MTS70 and MTS71 are tourmaline-bearing two mica metapelites. These rocks contain no plagioclase feldspar and consist primarily of quartz, muscovite, biotite and tourmaline. MTS71 additionally contains minor K-feldspar. Table 3.1 summarizes the major element bulk-rock geochemistry of the starting materials and Table 3.2a summarizes the average mineral chemistry of each sample (all analyses and standard deviations are listed in Appendix 1), as well as the mineral proportions (Table 3.2b), as constrained by least-squares mixing calculations using the bulk-rock and mineral compositions. The output of the least-squares mixing calculations was restricted to the phases observed during SEM analysis of the starting materials and the results were cross-checked with image analysis on the backscattered SEM images. The plagioclase-poor nature of the samples is a characteristic feature of metapelites from Mt. Stafford (Greenfield *et al.*, 1996).

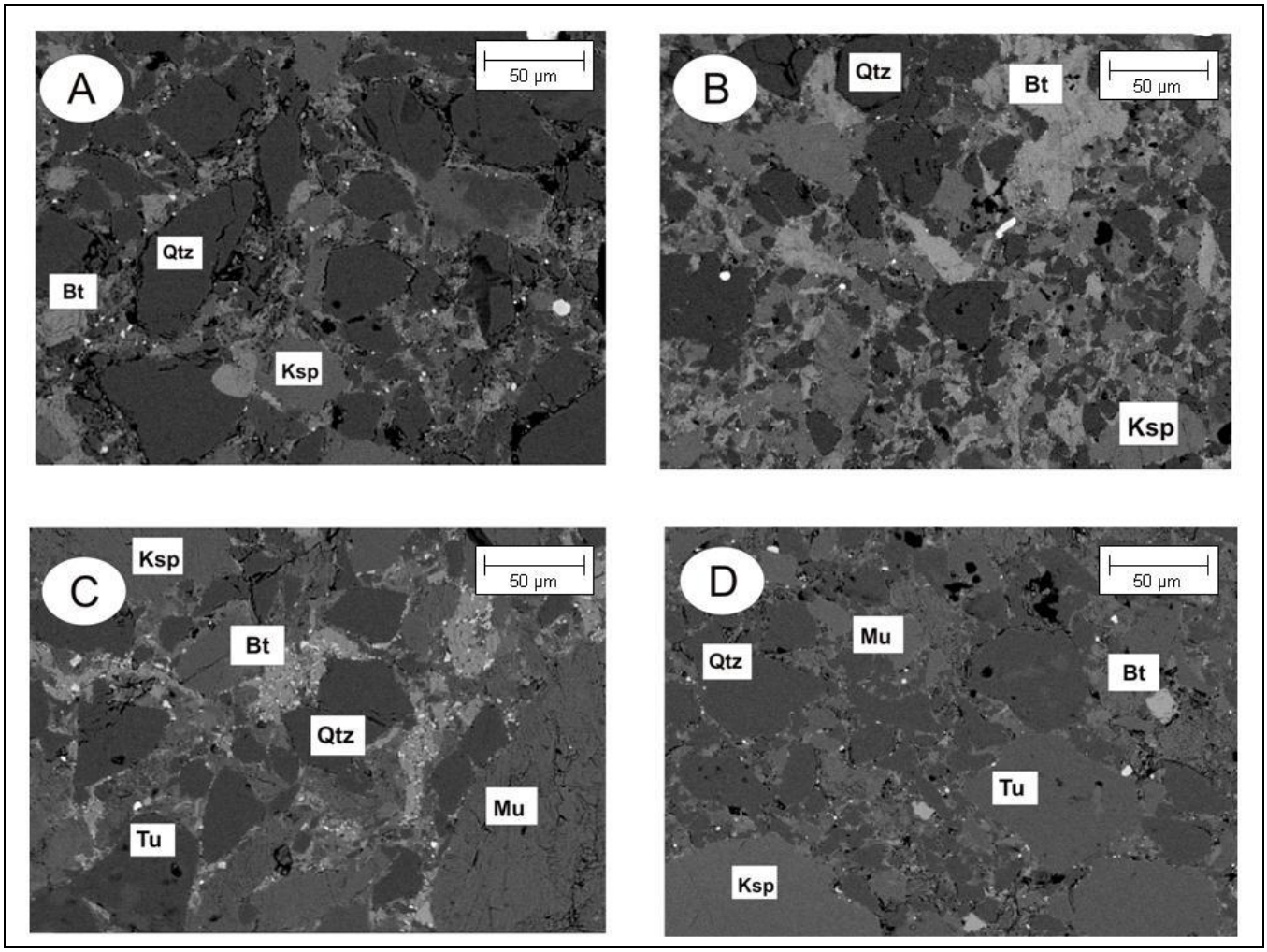

Fig. 3.2: Backscattered scanning electron images of the starting materials used in this study: MTS7 (A), MTS8 (B), MTS70 (C) and MTS71 (D).

Table 3.1: Major element composition of the starting materials, analysed by XRF.

Description	Biotite metapelites		Muscovite metapelites	
Sample	**MTS7**	**MTS8**	**MTS70**	**MTS71**
SiO_2	71.87	64.15	65.69	76.65
TiO_2	0.58	0.67	0.68	0.46
Al_2O_3	15.35	19.99	17.58	12.91
Fe_2O_3T	5.22	6.03	6.38	3.77
MnO	0.04	0.04	0.12	0.04
MgO	1.60	2.04	1.39	1.05
CaO	0.21	0.22	0.35	0.41
Na_2O	1.30	1.63	1.06	0.89
K_2O	4.26	6.04	4.98	2.20
P_20_5	0.13	0.15	0.31	0.33
H_2O-	0.15	0.11	0.06	0.06
LOI	0.50	0.54	1.71	0.92
Total	101.20	101.60	100.30	99.70
Mg #	41.26	43.69	33.42	38.93
ASI	2.16	2.08	2.26	2.82

Table 3.2a: Average mineral compositions in the starting materials. H_2O, and B_2O_3 values for tourmaline (49 Oxygens), muscovite (22 Oxygens) and biotite (22 Oxygens) are calculated according to the respective mineral stoichiometry.

K-feldspar				Plagioclase		Cordierite		
Sample	**MTS7**	**MTS8**	**MTS71**	**MTS7**	**MTS8**	**Sample**	**MTS7**	**MTS8**
SiO_2	63.32	64.38	64.04	63.33	65.75	**SiO_2**	47.12	45.70
TiO_2	0.03	0.03	0.00	0.00	0.00	**TiO_2**	0.10	0.05
Al_2O_3	18.35	18.41	18.03	23.13	20.54	**Al_2O_3**	32.92	33.60
FeO	0.05	0.20	0.18	0.13	0.22	**FeO**	7.56	5.91
MgO	0.01	0.04	0.00	0.00	0.00	**MgO**	8.43	9.54
CaO	0.01	0.00	0.00	3.24	1.97	**CaO**	0.02	0.04
Na_2O	1.15	1.13	2.20	10.18	11.26	**Na_2O**	0.09	0.06
K_2O	14.17	14.25	14.62	0.30	0.62	**K_2O**	0.44	0.17
Total	97.09	98.45	99.07	100.31	100.36	**Total**	96.83	95.14
Si	2.99	3.00	2.99	2.80	2.90	**Si**	4.94	4.83
Ti	0.00	0.00	0.00	0.00	0.00	**Ti**	0.01	0.00
Al/Al IV	1.02	1.01	0.99	1.20	1.07	**Al**	4.06	4.18
Fe tot	0.00	0.01	0.01	0.00	0.01	**Fe tot**	0.66	0.52
Mn			0.00	0.00	0.00	**Mn**	0.00	0.00
Mg	0.00	0.00	0.00	0.00	0.00	**Mg**	1.32	1.50
Ca	0.00	0.00	0.00	0.15	0.09	**Ca**	0.00	0.00
Na	0.11	0.10	0.20	0.87	0.96	**Na**	0.02	0.01
K	0.85	0.85	0.87	0.02	0.03	**K**	0.06	0.02
Cat Total	4.98	4.97	5.05	5.05	5.06	**Mg#**	66.52	74.21
Ab	11.01	10.73	10.05	77.37	83.93	**Cat Total**	11.06	11.09
An	0.04	0.02	0.00	16.06	3.69			
Or	88.96	89.25	86.30	1.77	3.66			

Table 3.2a Continued

	Biotite				Muscovite		Tourmaline		
Sample	**MTS7**	**MTS8**	**MTS70**	**MTS71**	**MTS70**	**MTS71**	**Sample**	**MTS70**	**MTS71**
SiO_2	33.99	34.55	34.44	33.99	47.69	47.73	**SiO_2**	35.78	36.63
TiO_2	2.40	2.47	1.96	2.06	0.58	0.68	**TiO_2**	0.80	0.81
Al_2O_3	18.85	19.31	17.55	16.97	34.15	34.03	**Al_2O_3**	31.89	32.59
FeO	21.12	20.51	25.91	25.86	1.97	2.26	**B_2O_3(c)**	10.41	10.58
MnO	0.09	0.15	0.60	0.38	0.05	0.05	**FeO**	10.86	10.13
MgO	7.69	7.81	4.08	3.71	0.85	0.76	**MnO**	0.16	0.06
CaO	0.05	0.03	0.05	0.13	0.01	0.03	**MgO**	4.05	4.17
Na_2O	0.10	0.12	0.06	0.09	0.39	0.31	**CaO**	0.20	0.16
K_2O	8.90	9.20	8.75	8.29	10.07	10.22	**Na_2O**	2.16	2.21
F	0.25	0.22	1.00	0.82	0.38	0.44	**K_2O**	0.05	0.04
Cl	0.00	0.01	0.02	0.02	0.01	0.02	**H_2O(c)**	3.59	3.65
H_2O(c)	3.70	3.76	3.25	3.26	4.35	4.33	**Total**	99.94	101.03
F	0.11	0.09	0.42	0.35	0.16	0.18	**Mg#**	40.06	42.45
Total	97.02	98.03	97.24	95.22	100.34	100.68	**Si**	5.97	6.02
Mg#	39.34	40.43	21.95	20.36	43.30	38.06	**Ti**	0.10	0.10
Si	5.34	5.36	5.54	5.58	6.31	6.31	**Al/Al iv**	0.04	0.00
Ti	0.28	0.29	0.24	0.25	0.06	0.07	**AlZ**	6.00	6.00
Al/Al iv	2.66	2.64	2.46	2.42	1.69	1.69	**AlY**	0.24	0.30
Al vi	0.84	0.89	0.87	0.86	3.63	3.62	**Fe2+**	1.52	1.39
Fe2+	2.78	2.66	3.49	3.55	0.22	0.23	**Mn2+**	0.02	0.01
Mn2+	0.01	0.02	0.08	0.05	0.01	0.00	**Mg**	1.01	1.02
Mg	1.80	1.81	0.98	0.91	0.17	0.15	**Ca**	0.04	0.03
Ca	0.01	0.00	0.01	0.02	0.00	0.00	**Na**	0.70	0.70
Na	0.03	0.03	0.02	0.03	0.10	0.08	**K**	0.01	0.01
K	1.79	1.82	1.79	1.74	1.70	1.72	**OH**	4.00	4.00
F	0.12	0.11	0.51	0.43	0.16	0.18	**Cation Total**	22.64	22.59
Cl	0.00	0.00	0.01	0.01	0.00	0.00	**X**	0.74	0.74
OH	3.87	3.89	3.49	3.57	3.84	3.82	**Y**	2.89	2.82
Cation Total	19.54	19.52	19.47	19.41	17.88	17.87	**Z**	6.00	6.00
Oct	5.71	5.66	5.65	5.62	4.08	4.07	**(OH,F)**	4.00	4.00
Int	1.83	1.86	1.82	1.79	1.80	1.80			
Fe+Mg	4.58	4.46	4.46	4.46	0.39	0.37			
Ti+Alvi	1.12	1.17	1.10	1.11	3.68	3.69			
Alvi+Si	6.18	6.24	6.40	6.44	9.93	9.93			
Ti+Aliv	2.94	2.93	2.70	2.68	1.75	1.76			
Fe+Mg+Mn	4.59	4.48	4.54	4.51	0.39	0.37			

Table 3.2b: Phase proportions for the starting materials calculated by a least squares mixing routine using the data in tables 1 and 2a. r^2 = the sum of the squared residuals. H_2O, BO_3 and F contents in the whole rock were calculated from the modes and mineral composition data in table 3.2.

Sample	**MTS70**	**MTS71**	**MTS7**	**MTS8**
r^2	**0.199**	**0.207**	**0.753**	**0.327**
Qtz	0.39	0.58	0.37	0.28
Bt	0.16	0.03	0.22	0.30
Ksp		0.01	0.19	0.24
Tu	0.17	0.23	-	-
Mu	0.29	0.14	-	-
Crd	-	-	0.08	0.01
And	-	-	0.07	0.13
Plag	-	-	0.05	0.04
BO_3 (wt%)	0.02	0.03	-	-
H_2O (wt%)	1.67	0.64	0.85	1.16
F (wt%)	1.19	0.04	0.03	0.03

K-feldspar from samples MST7 and MST8 is microcline ($Or_{77-93}An_{0-1}Ab_{6-22}$). Tourmaline is a schorl-dravite-elbaite solid solution, and is zoned from relatively elbaite-rich cores to more dravite-schorl-rich margins. The average tourmaline Mg# is 39 in MTS70 and 42 in MTS71. Biotite in sample MST7 has a Mg# of 39, MST8 has Mg# of 40, MTS70 has Mg# of 21 and MTS71 has Mg# of 20 with 3 - 3.8 wt% H_2O. The TiO_2 content in biotite is, on average, 2.06 wt% for MTS71, 1.96 wt% for MTS70, 2.46 wt% for MTS8 and 2.40 wt% for MTS7. Muscovite in samples MST70 and MST71 has approximately 4 wt% H_2O and has a Mg# of 43 and 38 respectively. Muscovite in sample MTS70 has a phengitic component (Fe + Mg) of 0.39 cations pfu and MTS71 of 0.40 cations pfu (corresponding to 2.82 and 3.03 wt% FeO + MgO respectively).

The major element compositions of the starting materials are similar to those used in numerous previous studies (refer to the caption of Fig. 3.3), and are particularly similar to the average shale composition defined by Shaw (1956). The main differences between this study and other previous studies, as discussed in Chapter 1 and 2, is the lack of plagioclase in the Mt Stafford starting materials and the experiments in this study were performed at lower pressures. Despite this broad compositional similarity, compositions MTS7 and MTS70 are enriched in Si relative to previously used compositions (Fig. 3.3). All four compositions are also relatively enriched in Al_2O_3 and an "alkali feldspar" component, relative to the range of compositions defined by previous studies, but relatively poor in the "ferromagnesian" component (Fig.3.3). As the compositions used in this study are virtually plagioclase-free, the feldspar component reflects the K_2O-rich nature of the rocks. All four compositions are reasonably strongly peraluminous, but have lower A/CNK values than some compositions used in some previous studies. The calculated modal mineralogy of the starting materials, combined with the mineral compositions in the starting materials was used to calculate the water content of the starting mixtures (Table 3.2b). Both groups of samples contain a H_2O-rich and –poor example. In the two mica metapelite starting mixtures (MTS70 and MTS71), MTS70 contains

1.67 wt% H_2O; in contrast, the more quartz-rich, mica-poor MTS71 contains only 0.64 wt% H_2O. Similarly, in the biotite metapelite compositions MTS8 is relatively H_2O-rich (1.16 wt%), while the more quartz-rich MTS7 contains 0.85 wt% H_2O. MTS70 and 71 contains 0.02 and 0.03 wt% BO_3 respectively, based on calculated values from modal tourmaline.

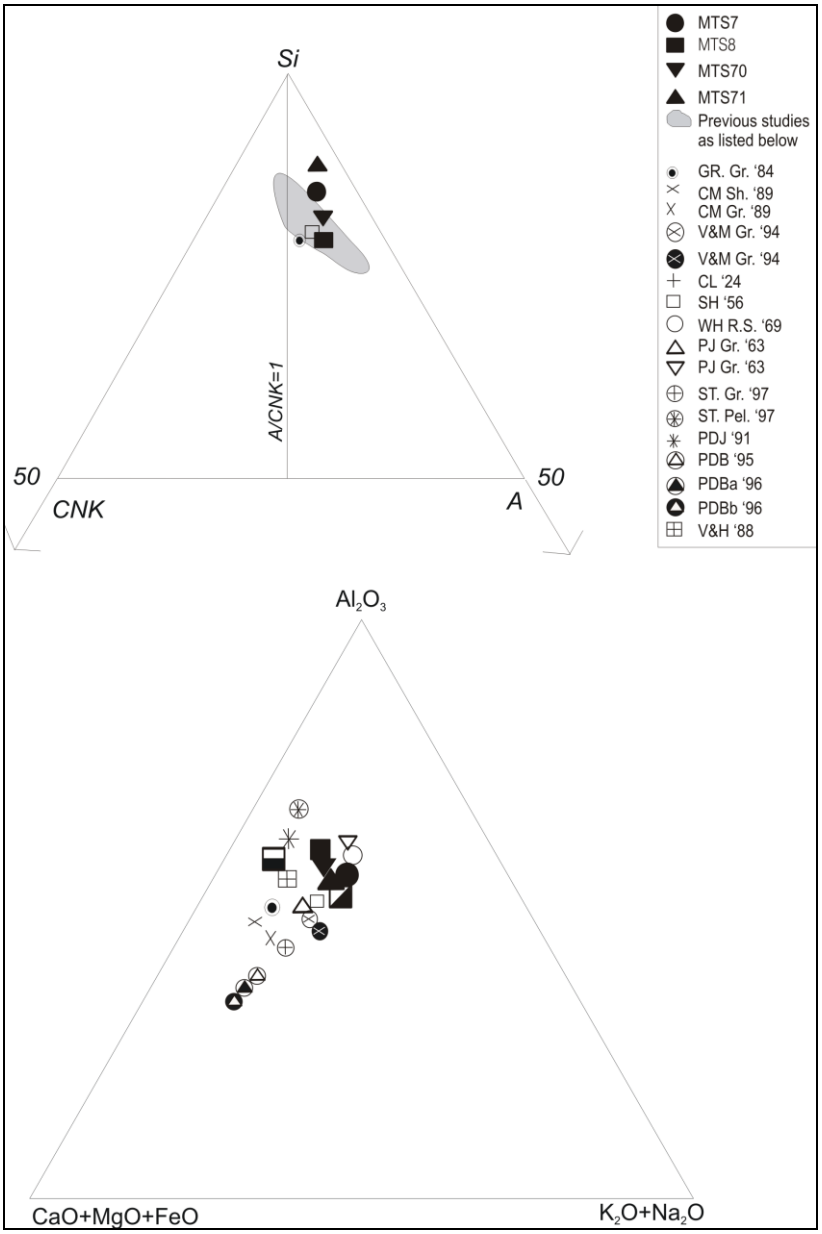

Fig. 3.3: The starting compositions used in this study compared with those of previous studies. PJ Gr. '63 Pettijohn (1963), V&H '88 Vielzeuf & Holloway (1988), PDBa '96 and PDBb '96 Patińo-Douce & Beard (1996), PDB '95 Patińo-Douce & Beard (1995), PDJ '91 Patińo-Douce & Johnson (1991), ST. Pel. '97 and ST. Gr. '97 Stevens *et al*. (1997), WH R.S. '69 Whetten *et al*. (1969), V&M Gr.'94 Vielzeuf & Montel (1994), SH '56 Shaw (1956) the average shale, CL '24 Clarke (1924), GR. Gr. '84 Gromet *et al*. (1984), CM Sh. '89 and CM Gr. '89 Gromet *et al*. (1984).

Chapter 4: Analytical techniques

The starting materials, minerals and experimental run products were characterised and analysed by X-ray Fluorescence (XRF), Electron Microprobe Analysis (EMPA) and Scanning electron microscope Energy Dispersive Spectrometry (SEM-EDS) analysis. In all cases the analyses were performed by the candidate. The precision, accuracy and application of these techniques are discussed in detail in this chapter. The SEM-EDS methodology sections that follow are valuable to all geoscientists that require mineral analysis at high spatial resolution from major to minor elemental concentrations.

4.1 Bulk and phase analysis of the starting materials

The starting materials were analysed by XRF on a Philips® 1404 wavelength dispersive spectrometer at the Stellenbosch University. Major elements (Na, Mg, Al, Si, P, K, Ca, Ti, Fe and Mn) were analysed on fused glass beads with operating conditions of 50 mA and 50 kV and a Rh X-Ray tube. Matrix effects in the samples were corrected for by applying theoretical alpha factors and measured line overlap factors to the raw intensities measured (Tertian & Claisse, 1982; Willis, 2004).

Geological standard reference materials from various sources (for example NIST and SARM) were used for calibration of major and trace element analytical procedures (Tertian & Claisse, 1982; Willis, 2004). Statistical data on the precision and accuracy of the XRF technique is presented in Table 4.1.

Table 4.1: Major element XRF precision and accuracy data

Major element analyses by XRF, statistical factors of calibration lines

Element	Al2O3	CaO	Cr2O3	Fe2O3	K2O	MgO	MnO	Na2O	NiO	P2O5	SiO2	TiO2
*CSE (Kcps)	0.016	0.020	0.002	0.007	0.014	0.003	0.002	0.007	0.001	0.002	0.035	0.006
*K	0.140	0.101	0.000	0.027	0.086	0.052	0.041	0.165	0.031	0.044	0.020	0.093

Stability of spectrometer, test on 1 sample, repeated 10 times without drift correction applied

Sample	Al2O3	CaO	Cr2O3	Fe2O3	K2O	MgO	MnO	Na2O	*NiO*	P2O5	SiO2	TiO2
Average	0.553	0.650	0.017	3.814	0.096	0.481	0.332	4.094	*BD*	0.011	41.345	0.018
STDEV	0.009	0.013	0.004	0.008	0.004	0.020	0.007	0.069	*BD*	0.003	0.079	0.006

Major element analyses, standard reference materials analysed as Unknowns

Standard Analysed												
Standard	**SiO2**	**TiO2**	**Al2O3**	**Cr2O3**	**Fe2O3T**	**MnO**	**NiO**	**MgO**	**CaO**	**Na2O**	**K2O**	**P205**
JG-1	72.77	0.24	14.23	0.002	2.12	0.06	0.000	0.75	0.56	3.35	3.94	0.10
JB-1	52.35	1.28	14.56	0.068	8.94	0.16	0.017	7.61	9.30	2.79	1.35	0.26
BHVO-1	49.69	2.73	13.67	0.041	12.39	0.18	0.017	7.04	11.43	2.16	0.48	0.26
NIM-N	52.70	0.18	16.59	0.000	9.07	0.19	0.014	7.35	11.53	2.46	0.20	0.00
Standard Published Values												
JG-1	72.30	0.26	14.20	0.001	2.14	0.06	0.001	0.74	2.18	3.39	3.97	0.10
JB-1	52.17	1.34	14.53	0.047	8.97	0.16	0.014	7.73	9.29	2.79	1.43	0.26
BHVO-1	49.94	2.71	13.80	0.029	12.23	0.17	0.012	7.23	11.40	2.26	0.52	0.27
NIM-N	52.64	0.20	16.50	0.003	8.91	0.18	0.012	7.50	11.50	2.46	0.25	0.03
Relative % differences												
Standard	**SiO2**	**TiO2**	**Al2O3**	**Cr2O3**	**Fe2O3T**	**MnO**	**NiO**	**MgO**	**CaO**	**Na2O**	**K2O**	**P205**
JG-1	0.65	8.46	0.20	233.33	0.84	6.35	100.00	1.62	74.22	1.18	0.76	2.06
JB-1	0.34	4.55	0.17	44.68	0.30	1.88	21.43	1.50	0.08	0.14	5.80	0.38
BHVO-1	0.50	0.55	0.96	41.87	1.28	5.95	40.50	2.64	0.22	4.42	7.31	4.03
NIM-N	0.10	10.50	0.52	100.00	1.84	2.78	16.67	1.95	0.22	0.16	19.20	100.00

Definitions

CSE = Counting statistical error, depending on counting time on backgrounds and peaks

K = indicates the goodness of the regression line, taking into account the number of standards and the difference between the input chemistry of standard library and the calculated value from the calibration line. Must approach 0

BD = Below Detection limits

Mineral compositions in the starting materials, were determined by electron microprobe analysis at the Centre for Electron Microscopy and Microstructural Analysis (CEMMSA, University of Adelaide) using a Cameca® SX51 Microprobe. Analytical conditions were a take off angle of 40 °, an acceleration voltage of 15.0 kV, probe current of 10 nA and the smallest possible spot size. A suite of natural mineral and glass standards were used for calibration. The crystal selection available on the Wavelength Dispersive X-ray Spectrometers allows the collection of X-rays over the elemental range Boron (Z = 5) to Uranium (Z = 92). The Cameca SX51 was configured typically with:

- Four multi-crystal Wavelength Dispersive X-ray Spectrometers (two with two crystals) with resolution of a few eV.
- Energy Dispersive X-ray Detector coupled to a Moran PC based Analyser which is operated at liquid nitrogen temperatures with resolution of approximately 140 eV.

The configuration for the wavelength spectrometers was: Spectrometer 1: PET crystal, Spectrometer 2: PET crystal, Spectrometer 3: LIF crystal, Spectrometer 4: TAP crystal. The elements were analysed in the following order on each spectrometer: Spectrometer 1: K, Ti; Spectrometer 2: Ca; Spectrometer 3: Mn, Fe; Spectrometer 4: Na, Mg, Al, Si; Number of oxygens: 24 and Number of H_2O: 0.Standards used for the calibration of each element were K: ast_33: Obsidian for elements Na, K, Al, Fe, silicate glass; Ti: TiO_2; Ca: Wolly: Wollastonite 34.12% Ca; Mn: Rhodochrosite; Fe: Fe_2O_3; Na: ast_33: Obsidian for elements Na, K, Al, Fe, silicate glass; Mg: MgO; Al: ast_2: Almandine Garnet Fe_3 Al_2 Si_3 O_{12}; Si: ast_2: Almandine Garnet Fe_3 Al_2 Si_3 $O_{12.}$ Mineral abbreviations follow Kretz (1983) apart from the following: Fe-Ts = Fe Tschermakite component of muscovite.

4.2 Analysis of the experimental run products by SEM-EDS

The quantification of the compositions of minerals and glasses at high spatial resolution is important for mineralogy, petrology, applied mineralogy, but even more so in experimental petrology due to very small crystal sizes. Scanning Electron Microscopes are used for a very wide range of applications, of which quantitative mineral analysis is not very common. EDS is well recognised as a semi-quantitative mineral analytical tool. For example, as discussed by Harding (2002), when coupled to an EDS system, they are invaluable to identify possible mineral assemblages (Harding, 2002), to get a quick idea of the elemental composition of phases and to perform a semi-quantitative analysis. The degree of sophistication of computer-aided scanning electron microscopy/energy dispersive X-ray spectrometry (SEM-EDS) microanalysis has advanced to the point where it is

possible with a single command to automatically perform sequential qualitative analysis (peak identification) and semi-quantitative analysis (Newbury, 2005).

Electron Microprobe Analysis (EMPA) is the traditional micro-analysis method to analyse minerals, accurately and quantitatively, from the major elements (> 0.1 to 100 wt%) down to trace element level (5 ppm to 0.1 wt%). The EMPA could not be used in this study though as the analysis area is limited to 5 µm. The Scanning Electron Microscope, coupled with a liquid nitrogen cooled SiLi or Peltier cooled energy dispersive detector (SEM-EDS) and BSE imaging, was preferred for this study as the technique offers crucial high resolution imaging advantages, indispensable to experimental petrology, as well as the opportunity to use a lower energy beam, which reduces the volume from which characteristic X-rays are generated, making it possible to analyse small crystals in the run products. The small volumes of minerals and glasses (Fig 5.1 in Chapter 5), produced as products in experiment near the solidus in many appropriate source compositions, often necessitate the use of a more high resolution micro-beam technique with backscattered imaging capabilities instead to site the analysis point. With this technique the experimental run products, as small as 1 µm, could be identified and analysed with certainty.

The composition, of which Na, K, Al and Si plays an important role, of glasses provides a basis for characterization and prediction of the physical and chemical properties needed to describe igneous geological processes. It is difficult to constrain the composition of glasses as they often contain the light elements B, Na, Si and K (Luth, 1967; Eggler & Holloway, 1977; Burnham, 1979; Nielsen & Sigurdsson, 1981; Clemens & Vielzeuf, 1987; London *et al*., 1988) in significant abundances, which are notoriously difficult to analyze accurately in non-crystalline solids or glasses (Lineweaver, 1962; Varshneya *et al.*, 1966; Borom & Hanneman 1967; Vassamillet & Caldwell, 1969; Kushiro, 1972; Goodhew & Gulley, 1974; Goodhew, 1975; Watkins *et al*., 1978; Spray & Rae, 1995). It has been

shown via SIMS analysis that electron-beam irradiation causes permanent damage to hydrous, silica-rich glasses, and even under optimum EMPA conditions (low beam energy and defocused beam diameter) it causes damage to the glass as manifested by a marked depletion in alkali ions at the surface of an irradiated sample (Humphreys *et al*., 2006). The light elements migrate and rearrange during micro-beam analysis since glass materials do not have fixed structures or order, but a looser arrangement of atoms, supporting migration during the heating of the glass during analysis. Migration depth depends on species diffusivity and the degree of heating caused by the electron beam, and therefore increases with increasing electron beam current. In addition to the elemental migration, fluorescent yield decreases inversely with atomic number, therefore further problems arise to excite enough X-rays from the light elements with non-aggressive micro-beams. There is therefore a fine line between providing enough energy to excite these light elements and providing too much causing severe migration of elements (Morgan & London, 1996). For comparatively immobile components, such as Si and Al, count rates increase with prolonged beam exposure, a phenomenon termed "grow-in" (Morgan & London, 1996). Analysts tend not to correct for Al and Si "grow-in", which, because of the abundance of these elements in typical rhyolitic glasses, represents a potentially large source of error. Na loss and the grow-in of Al and Si are of particular concern when EMPA or SEM-EDS is used to estimate the H_2O contents of silicate glasses (Devine *et al*., 1995). The work of Morgan & London (1996) demonstrates that the migratory behavior of Na also depends on the H_2O content of glass, in addition to the anhydrous bulk composition. This results in a problem that cannot easily be dealt with by using appropriate standards or a single correction routine. Over the course of a typical investigation of partial melting temperatures, melt major element composition and water content will change. The implication of this effect is that the Na and H_2O values in the unknown will continually change and the calibration procedure will not be a perfect match throughout the range of compositions.

Different combinations of beam current, spot size (defocused beams), and counting times are used to analyze hydrous glasses. In this instance defocused beams are not utilized due to the small areas of glass in experimental run products.Thus to accurately quantify melt compositions near the solidus it is important to be able to perform a spot analysis. Various corrections have been applied to Na analyses by EMPA that are quite large, often exceeding 10-15 %. When coupled with the poor statistical accuracy accompanying low count rates (even at 5-10 nA incident currents) and the short counting times commonly used, such corrections lend considerable uncertainty to the compositions obtained. Although the electron beam in EMPA is generally more stable (Fournelle, 2006), due to its higher beam energy and probe current of 10 nA, it is also more aggressive. The lower energy of the SEM electron beam (1-3 nA), compared to EMPA (10 nA) has a smaller excitation volume for characteristic X-rays that causes less light element migration (Morgan & London, 1996). The traditional SEM-EDS technique has been further refined for glass analysis by using a freezing stage to minimize element migration. Vassamillet & Caldwell (1969) have shown that for potassium and sodium the diffusion rate increases with increasing initial specimen temperature. It should follow, therefore, that by reducing the specimen temperature sufficiently the diffusion process should cease. The initial concentration can then be measured at a temperature where diffusion is negligible. The severe loss of sodium counts during microprobe analysis of silicate glasses can therefore be corrected for or avoided. The migration of sodium due to heating under the electron beam can be arrested by cooling the sample to -90 °C during analysis. A routine of estimating the sodium concentration has therefore been developed by Nielsen & Sigurdsson (1981) where an empirical technique estimates the initial sodium concentration from the rate of decay in sodium counts during continuous electron bombardment of the sample.

In practice, both EMPA and SEM-EDS methods require either knowledge of the approximate composition of the sample or repeated analysis with the first pass used to approximate the sample

composition for the selection of appropriate standard glass materials. Standardization on glasses with compositions similar to those of the unknowns (using identical beam conditions and counting parameters) can provide good analytical results because the effects of element mobility in the standard tend to cancel those in the unknown, but do not provide the ultimate solution for changing H_2O and Na contents over the P-T interval of the experiments. By applying experimental and analytical results from the glasses quantitatively, new insights into rock-forming and synthetic processes can be made with confidence.

4.2.1 Standard Reference Materials

The SEM-EDS technique has been refined in this study and involved the use of natural mineral reference materials. The reference materials were obtained from Astimex, a commercial supplier of polished metallic element, rare earth elements; mineral and synthetic compound standards suitable for electron microprobe and scanning electron microscope X-ray analysis (Obsidian, Albite, Almandine, Pyrope, Sanidine, Plagioclase, Diopside, Spodumene, Rhodonite, Biotite, Chlorite). All naturally occurring stable elements are represented, with the exception of the noble gases. Additional in-house mineral reference materials were obtained from the University of Cape Town (jjg1424-cpx, jjg1424-opx, mon-32grt, rom-33grt, mon-34grt and jjg1424grt) as cross-checks for some mineral groups. Their compositions have been constrained by EMPA. The obsidian glass standard contains 0.8 wt% water, not a perfect comparison as it is slightly less than the experimental glasses, so the effect of Na-migration would not be as strong as in some of the more H_2O-rich glasses produced in these experiments. The glasses produced in this study range from 7 to 10 wt% H_2O for muscovite fluid-absent melting near the solidus at mid-crustal pressures and 4 wt% for biotite melting, despite the fluid-absent nature of the experiments. The glasses produced in the higher temperature experiments correspond better with the 2 wt% H_2O glass standard.

4.2.2 Analytical procedure

The minerals and glasses were analyzed on a LEO 1430 VP scanning electron microscope, fitted with an ultra-thin Be window, a Backscattered 1.33 eV Centaurus detector and Oxford Inca Energy Dispersive Spectrometry software. A freezing stage that cools the samples to -194 ^{o}C (Liquid Nitrogen temperatures) to counteract migration of the light elements was fitted for the analysis of the glass. The samples were all carbon coated and the inter-element (matrix) effects were corrected for by means of a set of fundamental parameters built into the Inca software package which incorporates XPP matrix correction (similar to ZAF), spectrum processing by top hat filtering and least squares fitting and automatic correction for coating elements. Complex EDS spectra were analyzed by means of spectral deconvolution. The SEM-EDS analytical beam conditions for analysis of crystalline phases were 20 kV accelerating voltage, a faraday cup specimen current of -3.92 ± 0.2 nA, a working distance of 13 ± 0.01 mm and a counting time of 50 seconds. These beam conditions were chosen because in combination they ensured minimum X-ray counts of 5000 cts for the light and minor elements. These conditions were used to analyse mineral standard reference materials and it is important to note that these conditions were adhered to for the analysis of the unknown minerals. Three problems were addressed with this SEM-EDS technique, the possible beam instability, a more sophisticated calibration procedure for mineral anlaysis and special conditions for glass analysis.

4.2.2.1 Beam stabilizing procedure

A stable source of electrons, or X-rays in the case of other analytical techniques, is one of the most important factors in obtaining reliable results or all non-normalised calibration-based analytical techniques. The main assumption for a good calibration is that a specific amount of emitted X-rays, commonly known as total intensity or X-ray counts, can be related to a specific concentration in a standard reference material. This calibration curve is then applied to unknown samples, assuming the

primary source conditions are constant. If the excitation source is fluctuating it is impossible to have a reliable calibration curve.

To get to these stable conditions required for a reliable calibration in the LEO SEM, a number of measures were put in place. The stage of the microscope was fitted with a specimen current monitor, but as the beam interacts with different materials in different ways, the specimen current monitor could not be used to control the beam without the help of a Faraday cup. Consequently, a Faraday cup was constructed and mounted on the stage alongside the sample. By monitoring beam current through the Faraday cup, the beam energy of the SEM was modulated with adjustments to the spotsize and the total number of electrons per unit of time thereby kept stable. During the analysis of the standard reference materials and the unknown samples, the specimen current, as measured by the Faraday cup, was kept relatively constant to 3.9 nA ± 0.1.

It is very important that the vacuum conditions in the SEM sample chamber are stable before the electron beam is switched on. The vacuum stabilization can take from 15 minutes to an hour depending on the thickness of resin-mounted samples or other gas emiting material introduced into the chamber. When the vacuum is stable, the electron beam can be switched on and stabilized for 5 minutes. It has to be optimized on a Co metal standard to correct for detector drift and it is appropriate to repeat this after sample changes. This optimization procedure is built into the INCA software before measurements can commence. Measurements on the Faraday cup can start after the beam has stabilized for approximately 5 minutes under constant vacuum and the detector has been obtimized on the Co metal standard. Once the correct beam current used for the standard reference materials has been obtained, the faraday cup is used every 5-10 minutes, or when known wt% totals decrease or increase during analysis, to monitor beam fluctuation. This procedure is repeated for

every new sample loaded into the SEM. This procedure produces constant count rates and therefore accurate concentrations of elements and true totals can be obtained.

4.2.2.2 General standardization procedure

When used in a semi-quantitative way, standardization typically involves a comparison between spectra from a range of materials, built into the EDS software acquisition package, and unknown spectra to get quick semi-quantitative answers. The problem with this “check” technique for mineral analysis is that it typically required normalization of the results to 100 wt%, mostly because of the slight instability of the low energy scanning electron microscope beam, and due to the lack of proper calibration procedures. Often the actual algorithms employed in commercial software for each stage of the analysis are not provided nor are any inherent limitations in applying such "black box" software described to enable the analyst to estimate the performance (Newbury, 2005). Mineral compositions can thus be slightly shifted from their true values due to the constant sum effect as well as through the use of standards that do not ideally match the matrix of the unknown phase that generally consist of pure metals, oxides or simple compounds of the element of interest.

Quantitative analysis of the experimental run products with SEM-EDS involves a more detailed calibration procedure. The compositions of standard reference minerals and glass were entered in the Oxford Inca software EDS micro-analysis package, along with the built-in virtual standards. When analysing minerals these standard reference minerals are selected for calibration instead of the virtual (“black box”) standards. The identification of the elements responsible for the characteristic peaks in the EDS spectrum is obviously the first critical step in performing a robust analysis. The characteristic X-ray line used for each element can be selected, but the software package proposes the

strongest line by default for standardisation. In case of severe overlapping X-ray lines this needs to be kept in mind and a different X-ray line might be more appropriate.

The garnet and pyroxene 'in-house' reference minerals were not used as standards, but purely for testing purposes. Each element in each mineral of interest was standardised on an element in a mineral of similar composition or group. Table 4.2 contains the details of calibrations for the major rock forming silicate and sulphide minerals. Various options are available to calculate oxygen, but in general oxygen is calculated by stoichiometric addition for the silicate minerals, since it is bound in stoichiometric proportions. Sulphur was treated as an unknown element and a calibration was prepared in similar fashion as for the other elements in sulphides.

Table 4.2: EDS calibration procedures for sulphide, Mn-Silicate, Mica, Pyroxene, Glass, Garnet and Feldspar mineral groups.

Sulphides			Mn-Zn Silicate		Biotite		Pyroxene	
Element	**Reference Mineral**	**Internal Line**	**Element**	**Reference Mineral**	**Element**	**Reference Mineral**	**Element**	**Reference Mineral**
S	Pentlandite	-	**Mg**	Diopside	**Na**	Albite	**Na**	Jadeite
Fe	Marcasite	-	**Al**	Biotite	**Mg**	Pyrope	**Mg**	Diopside
Co	Pentlandite	-	**Si**	Spodumene	**Al**	Pyrope	**Al**	Cr-Diopside
Ni	Pentlandite	-	**Ca**	Diopside	**Si**	Pyrope	**Si**	Jadeite
Cu	Chalcopyrite	-	**Mn**	Rhodonite	**Cl**	Tugtupite	**Ca**	Diopside
Zn	Sphalerite	-	**Fe**	Almandine	**K**	Sanidine	**Cr**	Cr-Diopside
Mo	-	Mo	**Zn**	Willemite	**Ca**	Plagioclase AN65	**Mn**	Cr-Diopside
Pb	-	PbF2			**Ti**	Biotite	**Fe**	Cr-Diopside
					Cr	Cr Diopside	**Ni**	Olivine
					Mn	Pyrope		
					Fe	Almandine		

Table 4.2 Continued

Glass Analysis		Garnet		Feldspar		Chlorite	
Element	**Reference Material**	**Element**	**Reference Mineral**	**Element**	**Reference Mineral**	**Element**	**Reference Mineral**
Na	Albite	**Mg**	Pyrope	**Na**	Albite	Mg	olivine
K	Sanidine	**Al**	Almandine	**Al**	Plagioclase AN65	Al	Pyrope
Al	Plagioclase AN65	**Si**	Pyrope	**Si**	Albite	Si	Pyrope
Si	Quartz	**Ca**	Pyrope	**K**	Sanidine	Ca	Plagioclase AN65
Ca	Plagioclase AN65	**Ti**	Pyrope	**Ca**	Plagioclase AN65	Cr	Cr Diopside
Ti	Biotite	**Cr**	Cr Diopside	**Fe**	Biotite	Fe	Almandine
Fe	Biotite	**Mn**	Pyrope	**Ba**	Sanidine	Ni	Olivine
Mn	Biotite	**Fe**	Almandine				
Mg	Plagioclase AN65	**Ni**	Olivine				

Some basic principles apply when selecting suitable standards for micro-beam mineral analysis. The concentration of the relevant element in the standard needs to be higher than the unknown element, and for elements present in concentrations above 5 wt% of the oxide the concentration in the standard should ideally be close to that of the unknown. This ensures that the spectral deconvolution procedure will not be extrapolated towards higher concentrations and the unknown element's peak shape will fit with ease under the standard element. This requirement dictates the use of different standards for different elements in the case of most minerals and glasses. The calibration mineral from which the elements are selected for calibration is matched as close as possible to the composition of the unknown mineral and elements are calibrated within the same group of minerals, for example feldspars are used when analysing unknown feldspars. This ensures that the density of the minerals compare and subsequently the excitation volumes and background heights under each element.

When standard minerals from exactly similar groups are not available, element calibrations among silicates, glasses or oxides work well, but metals and sulphides can not be used to calibrate for silicates and vice versa. Luckily for the SEM-EDS analyst the elements in minerals occur in

stoichiometric proportions that can be used to double check the calibration methods. All the cation totals for the reference materials and unknown minerals have been calculated as double check.

4.2.2.3 Glass-specific analysis procedure

The influence of machine parameters on glass analysis has been tested to constrain the best analytical setup to suit the experimental glasses produced in this study. Even though the typical EMPA defocused beam method is very commonly used for other studies where large melt volumes are available, it could not be used for these samples since melt volumes close to the solidus are very low and need a technique with high spatial resolution. As mentioned in the introduction to this chapter, it is wise to get a feel for the anhydrous composition of the glasses before deciding on an analytical setup.

Firstly various analysing times were investigated for both SEM-EDS (Table 4.3) and EMPA techniques to constrain light element and Na-loss. Secondly three SEM setups (Table 4.4) were investigated for silicate glass analysis. Firstly, higher energy beam conditions were selected, 30 kV accelerating voltage, 13mm working distance, a Faraday cup specimen current of -5.3 nA, calculating to a beam energy of $1.59E^{-04}$ kW to emphasize effect of Na-loss in the obsidian standard and to simulate electron probe-like conditions of analysis. Secondly, the normal SEM-EDS analytical beam conditions for analysis of crystalline phases were investigated, which are 20 kV accelerating voltage, a Faraday cup specimen current of -3.92 nA, a working distance of 13mm, calculating to a total beam energy of $7.84E^{-05}$ kW. The third setup incorporated the normal beam setup, but was used in conjunction with the freezing stage to counteract migration of the light elements.

Table 4.3: Selected SEM-EDS and EMPA analysing times

50 seconds	**Na**	**Al**	**Si**	**K**	**Ca**	**ASI**	**Cl**	**Fe**
ns-obs-1	1.99	6.86	35.01	4.29	0.48	1.22	0.39	1.37
ns-obs-2	1.96	6.82	34.98	4.33	0.46	1.22	0.39	1.46
ns-obs-3	1.99	6.91	35.27	4.31	0.48	1.23	0.37	1.31
ns-obs-4	1.96	6.88	35.10	4.29	0.43	1.24	0.37	1.31
ns-obs-5	1.98	6.93	35.12	4.27	0.48	1.24	0.33	1.31
Average	1.98	6.88	35.09	4.29	0.47	1.23	0.37	1.35
STDEV	0.02	0.05	0.11	0.02	0.02	0.01	0.03	0.06
Obs Standard	**3.01**	**6.94**	**34.56**	**4.18**	**0.54**	**1.02**	**0.36**	**1.34**
%Relative Error	**52.39**	**0.88**	**1.52**	**2.66**	**15.38**	**16.74**	**2.81**	**0.84**
Abs Error	1.03	0.06	0.53	0.11	0.07	0.21	0.01	0.01
25 Seconds	**Na**	**Al**	**Si**	**K**	**Ca**	**ASI**	**Cl**	**Fe**
25-1	2.69	6.82	34.66	4.26	0.54	1.06	0.30	0.94
25-2	2.62	6.92	34.62	4.21	0.46	1.10	0.34	0.91
25-3	2.62	6.95	34.88	4.22	0.44	1.11	0.37	0.94
25-4	2.61	6.83	35.00	4.17	0.50	1.09	0.38	1.03
25-5	2.61	6.87	34.93	4.33	0.49	1.08	0.38	1.08
Average	2.63	6.88	34.82	4.24	0.49	1.09	0.36	0.98
STDEV	0.03	0.06	0.17	0.06	0.04	0.02	0.03	0.07
Obs Standard	**3.01**	**6.94**	**34.56**	**4.18**	**0.54**	**1.02**	**0.36**	**1.34**
%Relative Error	**14.36**	**0.86**	**0.74**	**1.37**	**10.82**	**5.68**	**1.40**	**36.67**
Abs Error	0.38	0.06	0.26	0.06	0.05	0.06	0.00	0.36
10 Seconds	**Na**	**Al**	**Si**	**K**	**Ca**	**ASI**	**Cl**	**Fe**
10-1	2.70	6.97	35.19	4.32	0.58	1.07	0.33	0.99
10-2	2.86	6.78	35.09	4.27	0.51	1.02	0.35	0.91
10-3	2.84	6.95	35.08	4.36	0.51	1.04	0.36	1.05
10-4	2.88	6.80	35.30	4.11	0.45	1.04	0.31	1.07
10-5	2.90	6.99	35.37	4.11	0.35	1.08	0.32	1.12
Average	2.83	6.90	35.21	4.23	0.48	1.05	0.33	1.03
STDEV	0.08	0.10	0.13	0.12	0.09	0.02	0.02	0.08
Obs Standard	**3.01**	**6.94**	**34.56**	**4.18**	**0.54**	**1.02**	**0.36**	**1.34**
%Relative Error	**6.19**	**0.62**	**1.83**	**1.23**	**12.56**	**2.51**	**7.58**	**30.20**
Abs Error	0.18	0.04	0.65	0.05	0.06	0.03	0.03	0.31
5 Seconds	**Na**	**Al**	**Si**	**K**	**Ca**	**ASI**	**Cl**	**Fe**
5-1	2.90	7.06	35.38	4.14	0.48	1.07	0.00	0.86
5-2	2.98	6.83	34.99	4.29	0.49	1.01	0.36	1.06
5-3	3.15	6.88	35.47	4.17	0.54	0.99	0.29	1.09
5-4	3.08	6.69	35.22	4.18	0.58	0.97	0.31	0.96
5-5	3.18	7.36	35.65	4.35	0.40	1.05	0.35	0.78
Average	3.06	6.96	35.34	4.23	0.50	1.02	0.26	0.95
STDEV	0.12	0.26	0.25	0.09	0.07	0.04	0.15	0.13
Obs Standard	**3.01**	**6.94**	**34.56**	**4.18**	**0.54**	**1.02**	**0.36**	**1.34**
%Relative Error	**1.57**	**0.35**	**2.21**	**1.09**	**8.35**	**0.53**	**36.40**	**41.38**
Abs Error	0.05	0.02	0.78	0.05	0.04	0.01	0.10	0.39

Table 4.4: Three combinations of analytical setups, firstly a higher beam energy setup to show enhanced light element losses, secondly a normal beam energy setup for mineral analysis and thirdly the normal beam energy setup in conjunction with a freezing stage to constrain light element losses.

Higher strength Setup: 30kV, -5.3nA Specimen current, 13mm working distance

Spectrum	Na	Al	Si	Cl	K	Ca	Fe	O	Total	ASI
hb-obs1	1.42	6.41	32.68	0.35	3.60	0.47	1.29	44.85	91.05	1.44
hb obs2	1.41	6.42	32.47	0.32	3.55	0.44	1.29	44.59	90.49	1.46
hb obs3	1.42	6.45	32.45	0.32	3.52	0.46	1.28	44.75	90.84	1.47
hb-obs4	1.39	6.45	32.58	0.34	3.62	0.43	1.29	44.74	90.84	1.46
hb-obs5	1.45	6.50	32.69	0.34	3.60	0.42	1.34	44.94	91.28	1.45
Average	1.42	6.44	32.57	0.33	3.58	0.44	1.30	44.77	90.90	1.45
STDEV	0.02	0.03	0.11	0.01	0.04	0.02	0.02	0.13	0.29	0.50
Standard Value	**3.01**	**6.94**	**34.56**	**0.36**	**4.18**	**0.54**	**1.34**	**48.63**	**100.58**	**1.02**
Abs error	1.59	0.50	1.99	0.03	0.60	0.10	0.04	3.86	9.68	0.43
%Relative Error	112.42	7.71	6.10	7.72	16.81	21.95	3.17	8.61	10.65	29.62

Normal Setup: -3.92 nA, 20 kV, 13mm working distance

Spectrum	Na	Al	Si	Cl	K	Ca	Fe	O	Total	ASI
ns-obs-1	1.99	6.86	35.01	0.39	4.29	0.48	1.37	48.14	98.51	1.22
ns-obs-2	1.96	6.82	34.98	0.39	4.33	0.46	1.46	48.09	98.49	1.22
ns-obs-3	1.99	6.91	35.27	0.37	4.31	0.48	1.31	48.47	99.12	1.23
ns-obs-4	1.96	6.88	35.10	0.37	4.29	0.43	1.31	48.21	98.54	1.24
ns-obs-5	1.98	6.93	35.12	0.33	4.27	0.48	1.31	48.30	98.72	1.24
Average	1.98	6.88	35.09	0.37	4.29	0.47	1.35	48.24	98.67	1.23
STDEV	0.02	0.05	0.11	0.03	0.02	0.02	0.06	0.15	0.26	0.01
Standard Value	**3.01**	**6.94**	**34.56**	**0.36**	**4.18**	**0.54**	**1.34**	**48.63**	**100.58**	1.02
Abs Error	1.03	0.06	0.53	0.01	0.11	0.07	0.01	0.39	1.91	0.21
%Relative Error	52.39	0.88	1.52	2.81	2.66	15.38	0.84	0.81	1.93	16.74

Freezing stage used in conjunction with the normal analytical setup

Sample	Na	Al	Si	Cl	K	Ca	Fe	O	Total	ASI
Obs-1	3.01	6.83	34.78	0.31	4.39	0.44	1.33	48.21	99.30	0.99
Obs-2	3.04	6.78	34.61	0.31	4.32	0.45	1.37	47.97	98.84	0.99
Obs-3	3.06	6.79	34.79	0.30	4.38	0.50	1.32	48.22	99.37	0.98
Obs-4	3.02	6.79	34.67	0.33	4.43	0.44	1.36	48.05	99.08	0.98
Obs-5	3.01	6.79	34.56	0.36	4.37	0.54	1.36	47.96	98.94	0.98
Average	3.03	6.79	34.68	0.32	4.38	0.48	1.35	48.08	99.11	0.99
STDEV	0.02	0.02	0.10	0.03	0.04	0.04	0.02	0.13	0.23	0.01
Standard Value	**3.01**	**6.94**	**34.56**	**0.36**	**4.18**	**0.54**	**1.34**	**48.63**	**100.58**	**1.02**
Abs error	0.02	0.15	0.12	0.04	0.20	0.06	0.01	0.55	1.47	0.03
%Relative Error	0.55	2.14	0.35	12.64	4.54	13.54	0.55	1.14	1.49	3.49

From the data in Table 4.3 it is clear that 5 seconds analysis time causes the least Na loss while still providing acceptable results for the other main elements of interest, such as Al, Si and K. The absolute error on Na is the lowest, 0.05 wt% Na, for the runs completed in 5 seconds. Longer analysis times results in larger absolute errors. The freezing stage in combination with a normal beam setup

(Table 4.4) provides the best analytical conditions with the smallest absolute errors, 0.02 w% Na, for analysing small volumes of Na-rich glasses, typical of the experimental run products in this study.

4.2.3 Accuracy and precision

Tables 4.5 a to e contain accuracy data for the various mineral calibrations and Table 4.6 contains precision data on almandine, pyrope, albite, orthopyroxene and clinopyroxene.

4.2.3.1 Accuracy of silicate mineral analysis

The calibration procedures in Table 4.2 have been applied to a range of silicate reference minerals (Tables 4.5a to e). Various silicates were used to test the calibration and presented as examples of the accuracy capabilities of the technique. The relative % errors of the analysis and reference material values are discussed for each mineral group separately, based on the stoichiometric recalculations to cations and elemental wt %.

The feldspar group analyses (Table 4.5a) all calculated to stoichiometric cation proportions with low relative % errors on the cation values, except for a 7 - 9 % relative error on Fe in plagioclase and sanidine. Fe occurs as a minor element in the plagioclase and sanidine standards (0.37 and 0.18 wt% respectively), but was detected with ease and with relative errors of below 10 %. Na_2O, K_2O and CaO values were well within acceptable error limits, with 0.01 to 3 % relative errors.

Table 4.5a: Feldspar group analyses (8 Oxygens). Minerals were analysed with 20 kV, 3.92 nA beam current and 13 mm working distance.

Mineral	Plagioclase AN65			Sanidine		
Element	Analysis	Reference	% Rel Error	Analysis	Reference	% Rel Error
Na_2O	4.35	4.35	0.02	2.93	3.01	0.64
Al_2O_3	28.54	28.53	0.01	18.51	18.76	0.34
SiO_2	52.13	54.21	0.98	64.06	64.67	0.24
K_2O	0.36	0.41	3.18	12.13	12.11	0.05
CaO	11.79	11.80	0.01	-	-	-
FeO	0.50	0.37	7.37	0.26	0.18	9.09
BaO	-	0.01	-	1.07	1.09	0.46
Total	97.67	100.00	0.59	98.96	99.80	0.21
Si	2.42	2.46	0.39	2.98	2.98	0.00
Ti	0.00	0.00	-	0.00	0.00	-
Al	1.56	1.52	0.60	1.01	1.02	0.10
Fe tot	0.02	0.01	7.94	0.01	0.01	9.32
Ca	0.59	0.57	0.57	0.00	0.00	-
Na	0.39	0.38	0.56	0.26	0.27	0.40
K	0.02	0.02	2.60	0.72	0.71	0.29
Ba	0.00	0.00	50.00	0.02	0.02	0.22
Cat Total	5.00	4.98	0.12	4.99	4.98	0.02

The garnet pyrope analysis (Table 4.5b) calculated to stoichiometric cation proportions with very low relative % errors, except for a 7 % relative error on Cr in pyrope. Cr and Mn occurs as minor elements in the pyrope standard (0.58 and 0.27 wt% respectively), but were detected with very low relative errors. MnO had only 0.09 % relative error for the 0.27 wt% abundance.

Table 4.5b: Garnet group analyses (12 Oxygens). Minerals were analysed with 20 kV, 3.92 nA beam current and 13 mm working distance.

Mineral	Pyrope		
Element	Analysis	Reference	% Rel Error
MgO	19.37	19.33	0.05
Al_2O_3	20.40	21.32	1.11
SiO_2	41.31	41.45	0.08
CaO	4.35	4.65	1.70
TiO_2	1.11	1.16	1.19
Cr_2O_3	0.43	0.58	7.43
MnO	0.27	0.27	0.09
FeO	11.47	11.15	0.70
Total	99.05	99.90	0.21
Si	3.02	2.99	0.25
Ti	0.06	0.06	0.86
Al	1.76	1.81	0.78
Fe tot	0.70	0.67	1.03
Mn	0.02	0.02	0.42
Mg	2.11	2.08	0.37
Ca	0.34	0.36	1.37
Cr	0.02	0.03	7.10
Cat Total	8.03	7.99	0.12

The pyroxene spodumene analysis (Table 4.5c) calculated to stoichiometric cation proportions with extrememly low relative % errors of 0.04 to 0.3 % for all elements. Li cannot be detected by SEM-EDS or EMPA in spodumene, but was included as a calculated element in the stoichiometric calculations to test the other elemental calibrations. 0.04 to 0.48 % relative errors were achieved for the spodumene standard.

Table 4.5c: Pyroxene group analyses (6 Oxygens). Minerals were analysed with 20 kV, 3.92 nA beam current and 13 mm working distance.

Mineral	**Spodumene**		
Element	Analysis	Reference	% Rel Error
Al_2O_3	27.93	27.40	0.48
SiO_2	65.18	64.57	0.24
Li_2O	8.03	8.03	calculated
Total	101.1	100.0	0.28
Al	1.00	0.99	0.20
Si	2.00	2.00	0.04
O	6.00	6.00	0.00
Li	0.99	1.00	calculated
Cation To	3.98	3.99	0.04

The sheet silicates analyses (Table 4.5d) of biotite and chlorite calculated to stoichiometric cation proportions with relative % errors of < 2 % overall. Minor abundances of Cr and Ti were detected with ease and displayed low relative % errors of 0.85 to 1.2 %. The elements Ca and Mn had large relative errors due to detection when not present or no detection when present. These elements were either not present or present as 0.01 wt%.

Table 4.5d: Sheet silicate analyses (22 Oxygens). Minerals were analysed with 20 kV, 3.92 nA beam current and 13 mm working distance.

Mineral	**Biotite**			**Chlorite**		
Element	Analysis	Reference	% Rel Error	Analysis	Reference	% Rel Error
MgO	18.40	19.52	1.48	33.94	33.51	0.32
Al_2O_3	14.84	15.13	0.49	19.18	18.08	1.48
SiO_2	37.00	38.72	1.14	30.64	30.04	0.50
K_2O	10.13	9.91	0.55	-	-	-
CaO	-	0.10	-	0.00	0.03	50.00
TiO_2	1.77	1.77	0.04	-	-	-
Cr_2O_3	-	-	-	1.06	0.98	1.87
MnO	0.21	0.04	33.81	-	-	-
FeO	10.59	10.72	0.31	3.45	3.31	1.00
Total	93.21	95.91	0.71	88.49	85.95	0.73
Si	5.58	5.63	0.20	4.50	4.53	0.17
Ti	0.20	0.19	0.89	0.00	0.00	-
Al	2.64	2.59	0.45	3.31	3.21	0.81
Fe tot	1.34	1.30	0.62	0.42	0.42	0.33
Mn	0.03	0.00	34.31	0.00	0.00	-
Mg	4.14	4.23	0.54	7.42	7.53	0.35
Ca	0.00	0.02	50.00	0.00	0.00	50.00
Na	0.00	0.00	-	0.00	0.00	-
K	1.95	1.84	1.49	0.00	0.00	-
Cr	0.00	0.00	-	0.12	0.12	1.20
Cat Total	15.87	15.80	0.11	15.66	15.69	0.05

Mn-Zn silicates rhodonite and willemite (Table 4.5e) calculated to stoichiometric cation proportions with relative % errors < 2 % for all elements except Fe in rhodonite with a 7 % relative error. High and low abundances of Mn were detected with ease and calculated to stochiometry.

Table 4.5e: Mn-Zn silicates (Rhodonite = 3 Oxygens and Willemite 4 = Oxygens). Minerals were analysed with 20 kV, 3.92 nA beam current and 13 mm working distance.

Mineral	**Rhodonite**			**Willemite**		
Element	Analysis	Reference	% Rel Error	Analysis	Reference	% Rel Error
SiO_2	47.39	45.98	0.75	27.75	28.09	0.31
CaO	6.07	6.40	1.33	-	-	-
MnO	37.66	37.66	0.00	5.20	4.82	1.87
FeO	2.05	1.55	6.98	-	-	-
ZnO	7.39	7.51	0.40	68.93	66.89	0.75
Total	101.56	99.10	0.61	102.49	99.80	0.66
Si	1.01	1.00	0.25	1.00	1.02	0.57
Fe tot	0.04	0.03	6.49	0.00	0.00	-
Mn	0.68	0.70	0.50	0.16	0.15	1.61
Zn	0.12	0.12	0.90	1.84	1.80	0.49
Cat Total	1.99	2.00	0.13	3.00	2.98	0.19

4.2.3.2 Precision of silicate mineral analysis

The precision of SEM-EDS analysis was tested on albite, almandine, orthopyroxene, clinopyroxene and three pyrope mineral standards (Table 4.6). Absolute differences and relative % errors between the standard reference values and the mineral analysis were calculated for the wt% and cation proportions. Standard deviations were calculated for each of these mineral analysis (n = 10).

The albite repeat analyses achieved 0.05 to 5 % relative errors, with standard deviations of 0.03 to 0.28 wt%. K_2O had the highest relative error and SiO_2 the highest standard deviation. Na_2O, often the problematic element due to migration away from the irradiated area, had a relative error of 0.6 % and a standard deviation of only 0.13 wt%. The cation proportions are all stoichiometric with relative errors of < 5 %.

Table 4.6a: Precision and accuracy statistics of SEM-EDS quantitative analysis on albite (8 Oxygens). Minerals were analysed with 20 kV, 3.92 nA beam current and 13 mm working distance.

Feldspar Albite	Average (n=10)	Albite Reference	Difference	%Rel Error (MPD)	Stdev (n=10)
Na_2O	11.30	11.58	0.28	0.60	0.13
Al_2O_3	19.20	19.53	0.33	0.42	0.13
SiO_2	68.66	68.52	0.14	0.05	0.28
K_2O	0.18	0.22	0.04	5.07	0.03
CaO	0.11	0.13	0.02	3.12	0.05
Total	99.35	100.00	0.65	0.16	0.34
Si	3.01	2.99	0.02	0.13	0.00
Al	0.99	1.00	0.01	0.34	0.01
Ca	0.01	0.01	0.00	3.05	0.00
Na	0.96	0.98	0.02	0.52	0.01
K	0.01	0.01	0.00	4.99	0.00
Cat Total	4.98	5.00	0.02	0.10	0.01

The relative errors range from 0.03 to 1.96 %, with standard deviations of 0.04 0.32 wt %, for the almandine repeats. The largest relative error (1.96 %) was observed for MnO. The cation proportions are all stoichiometric. The pyrope garnets (mon-32grt, rom-33grt, mon-34grt and jjg1424grt) all had relative errors of < 5 % with the largest standard deviation 0.63 wt % on mon-32grt. The jj1424grt

showed the largest, 8.34 %, relative error on 0.32 wt% MnO. Minor amounts of Cr, Ti and Mn were detected with ease and the relative errors on these minor elements were all below 10 %.

Table 4.6b: Precision and accuracy statistics of SEM-EDS quantitative analysis on almandine and pyrope garnets (12 Oxygens). Minerals were analysed with 20 kV, 3.92 nA beam current and 13mm working distance.

Garnet		**Almandine**					**Mon-32**			
Element	Average (n=10)	Almandine Reference	Difference	%Rel Error	Stdev (n=10)	Average (n=10)	MON32-grt Reference	Difference	%Rel error	Stdev
MgO	10.49	10.70	0.21	0.50	0.09	18.02	18.72	0.70	0.95	0.16
Al_2O_3	21.83	22.05	0.22	0.25	0.06	21.10	21.92	0.82	0.96	0.18
SiO_2	39.18	39.19	0.01	0.003	0.15	41.39	41.72	0.33	0.20	0.28
CaO	4.23	4.20	0.03	0.19	0.04	5.07	4.54	0.53	2.78	0.06
TiO_2	-	-	-	-	-	1.35	1.10	0.25	5.11	0.06
Cr_2O_3	-	-	-	-	-	0.35	0.27	0.08	6.70	0.04
MnO	0.64	0.59	0.05	1.96	0.04	0.36	0.31	0.05	4.00	0.06
FeO	23.53	23.27	0.26	0.27	0.18	13.20	11.58	1.62	3.27	0.10
Total	99.95	100.00	0.05	0.01	0.32	100.84	100.17	0.67	0.17	0.63
Si	2.99	2.98	0.01	0.06	0.01	2.99	3.00	0.01	0.09	0.00
Ti	-	-	-	-	-	0.07	0.06	0.01	5.21	0.00
Al	1.94	1.96	0.01	0.18	0.00	1.78	1.84	0.06	0.85	0.01
Fe tot	1.50	1.48	0.02	0.34	0.01	0.80	0.70	0.10	3.38	0.01
Mn	0.04	0.04	0.00	2.03	0.00	0.02	0.02	0.00	4.11	0.00
Mg	1.19	1.21	0.02	0.43	0.01	1.94	2.01	0.07	0.84	0.01
Ca	0.35	0.34	0.00	0.26	0.00	0.39	0.35	0.04	2.88	0.00
Cr	-	-	-	-	-	0.02	0.02	0.00	6.80	0.00
Cat Total	8.01	8.01	0.00	0.00	0.00	8.01	7.99	0.03	0.08	0.00

Table 4.6b continued

Garnet		**Garnet Mon-34**					**Garnet Jjg1424**			
Element	Average (n=10)	MON34-grt Reference	Difference	%Rel error (MPD)	Stdev	Average (n=10)	JJG1424-grt Reference	Difference	%Rel error (MPD)	Stdev
MgO	19.40	20.15	0.75	0.94	0.11	19.87	20.47	0.60	0.74	0.20
Al_2O_3	20.99	21.92	0.93	1.08	0.15	23.08	23.31	0.23	0.25	0.21
SiO_2	41.89	41.95	0.06	0.03	0.20	42.38	42.32	0.06	0.04	0.30
CaO	4.98	4.64	0.34	1.75	0.02	5.08	4.65	0.43	2.22	0.18
TiO_2	1.28	1.13	0.15	3.07	0.06	0.12	0.09	0.03	6.98	0.03
Cr_2O_3	0.94	0.79	0.15	4.20	0.03	1.03	1.06	0.03	0.72	0.05
MnO	0.28	0.24	0.04	3.60	0.06	0.45	0.32	0.13	8.34	0.06
FeO	10.46	9.85	0.61	1.51	0.13	8.52	7.91	0.61	1.87	0.14
Total	100.22	100.25	0.03	0.01	0.52	100.54	100.13	0.41	0.10	0.59
Si	3.01	2.98	0.02	0.20	0.01	3.00	2.99	0.01	0.05	0.01
Ti	0.07	0.06	0.01	3.31	0.00	0.01	0.00	0.00	6.99	0.00
Al	1.76	1.82	0.06	0.85	0.01	1.91	1.92	0.02	0.24	0.01
Fe tot	0.63	0.59	0.04	1.74	0.01	0.50	0.47	0.04	1.88	0.01
Mn	0.02	0.01	0.00	3.83	0.00	0.03	0.02	0.01	8.35	0.00
Mg	2.08	2.14	0.06	0.71	0.01	2.10	2.16	0.06	0.73	0.01
Ca	0.38	0.35	0.03	1.98	0.00	0.39	0.35	0.03	2.23	0.01
Cr	0.05	0.04	0.01	4.44	0.00	0.06	0.06	0.00	0.71	0.00
Cat Total	7.99	8.00	0.01	0.02	0.00	7.98	7.98	0.00	0.01	0.00

Table 4.6b continued

Garnet			**Rom-33**		
Element	Average (n=10)	ROM33-grt Reference	Difference	%Rel error	Stdev
MgO	18.16	18.48	0.32	0.43	0.18
Al_2O_3	21.49	21.75	0.26	0.30	0.17
SiO_2	41.74	41.63	0.11	0.06	0.20
CaO	4.77	4.62	0.15	0.82	0.07
TiO_2	1.26	1.17	0.09	1.92	0.05
Cr_2O_3	0.13	0.13	0.00	0.00	0.02
MnO	0.37	0.34	0.03	2.01	0.05
FeO	12.73	12.21	0.52	1.05	0.08
Total	100.65	100.34	0.31	0.08	0.59
Si	3.00	3.00	0.01	0.05	0.01
Ti	0.07	0.06	0.01	3.05	0.00
Al	1.81	1.83	0.02	0.32	0.01
Fe tot	0.77	0.74	0.03	1.03	0.01
Mn	0.02	0.02	0.00	1.99	0.00
Mg	1.95	1.98	0.04	0.45	0.01
Ca	0.37	0.36	0.01	0.80	0.00
Cr	0.01	0.01	0.00	0.02	0.00
Cat Total	7.99	7.99	0.00	0.00	0.01

The ortho- and clinopyroxene analyses (samples jjg1424-cpx, jjg1424-opx) had relative errors of < 10 % for most elements. Al_2O_3 had a 17.6 % relative error for jjg1424-cpx and a 13.96 % relative error for jjg1424-opx, which might be due to difficulties with subtracting the background between the Mg and Si peaks. MnO had a 19.52 % relative error in jjg1424 opx, but the abundance is low (0.08 wt %). Minor abundances of Ti, Cr and Mn were very accurately detected in the jjg1424 cpx pyroxene with relative errors of 3.02, 3.56 and 9.8 % respectively. The largest standard deviation, 0.67 wt%, was observed on the total oxide values for these pyroxenes. NiO, present in trace amounts of 0.002 wt%, were detected with a relative error of 16.67 %. Despite the large relative errors for some elements, the cation proportions were stoichiometric. The Cr-diopside analyses had low relative errors, the highest 5.44 % on 0.1 wt% TiO_2. Standard deviations range from 0.02 to 0.56 wt% and all cation proportions are stoichiometric.

Table 4.6c: Precision and accuracy statistics of SEM-EDS quantitative analysis on Cr-diopside, clino- and orthopyroxenes (6 Oxygens). Minerals were analysed with 20 kV, 3.92 nA beam current and 13 mm working distance.

Pyroxene		**Cr-Diopside**			
Element	Average (n=10)	Cr-Diopside Reference	Difference	%Rel error	Stdev
Na_2O	0.47	0.44	0.03	1.83	0.02
MgO	16.62	17.17	0.55	0.81	0.10
SiO_2	54.36	54.59	0.23	0.11	0.35
CaO	25.95	25.50	0.45	0.44	0.14
TiO_2	0.08	0.10	0.02	5.44	0.02
Cr_2O_3	0.55	0.50	0.05	2.28	0.03
FeO	1.44	1.39	0.05	0.82	0.04
Total	99.66	99.69	0.03	0.01	0.56
Si	1.98	1.99	0.00	0.06	0.00
Ti	0.002	0.003	0.00	5.39	0.00
Fe tot	0.04	0.04	0.00	0.87	0.00
Mg	0.90	0.93	0.03	0.76	0.00
Ca	1.02	1.00	0.02	0.49	0.00
Na	0.05	0.05	0.00	1.88	0.00
Cr	0.02	0.01	0.00	2.33	0.00
Cat Total	4.03	4.03	0.00	0.01	0.00

Table 4.6c continued

Pyroxene		**Jjg1424-Cpx**					**Jjg1424-Opx**			
Element	Average (n=10)	JJG1424-cpx Reference	Difference	%Rel error	Stdev	Average (n=10)	JJG1424-opx Reference	Difference	%Rel error	Stdev
Na_2O	1.72	1.55	0.17	2.53	0.06	0.18	0.16	0.02	3.46	0.02
MgO	15.95	16.61	0.66	1.02	0.15	34.92	35.71	0.79	0.56	0.27
Al_2O_3	1.43	2.99	1.56	17.62	0.02	0.66	1.18	0.52	13.96	0.02
SiO_2	55.25	54.57	0.68	0.31	0.36	58.64	57.57	1.07	0.46	0.45
CaO	22.78	21.54	1.24	1.40	0.17	0.24	0.30	0.06	5.62	0.03
TiO_2	0.22	0.25	0.03	3.02	0.02	0.07	0.11	0.04	9.81	0.03
Cr_2O_3	0.70	0.81	0.11	3.56	0.04	0.19	0.21	0.02	3.13	0.02
MnO	0.08	0.06	0.02	8.10	0.05	0.18	0.08	0.10	19.52	0.07
FeO	1.73	1.64	0.09	1.27	0.06	5.25	4.91	0.34	1.65	0.10
NiO	0.004	0.002	0.002	16.67	0.00	-	-	-	-	-
Total	99.86	100.02	0.16	0.04	0.68	100.34	100.07	0.27	0.07	0.67
Si	1.99	1.96	0.03	0.44	0.00	2.00	1.97	0.03	0.42	0.00
Ti	0.01	0.01	0.00	2.89	0.00	0.00	0.00	0.00	9.85	0.00
Al	0.06	0.13	0.06	17.51	0.00	0.03	0.05	0.02	14.00	0.00
Fe tot	0.05	0.05	0.00	1.40	0.00	0.15	0.14	0.01	1.61	0.00
Mn	0.003	0.002	0.00	8.23	0.00	0.01	0.00	0.00	19.49	0.00
Mg	0.86	0.89	0.03	0.89	0.00	1.78	1.82	0.04	0.60	0.00
Ca	0.88	0.83	0.05	1.53	0.00	0.01	0.01	0.00	5.66	0.00
Na	0.19	0.17	0.02	2.66	0.01	0.02	0.02	0.00	3.42	0.00
Cr	0.02	0.02	0.00	3.43	0.00	0.00	0.01	0.00	3.17	0.00
Ni	0.00	0.00	0.00	-	0.00	-	-	-	-	-
Cat Total	4.06	4.05	0.01	0.06	0.00	3.99	4.01	0.02	0.12	0.00

The above data sets have not just been used to test precision, but also to plot a graph (Fig 4.1) of wt% element agains % relative error to investigate correlations between the abundance of elements and

their corresponding % relative errors. Most analyses have relative errors of < 5 wt%. There is a general indirect relationship found in all the minerals that indicate that the largest relative errors (5 to 10 wt%) are found within the very low abundance or minor element (< 1 wt%) ranges, for example 0.27 wt% Cr_2O_3 in mon32-grt have a slightly larger relative error of 6.7 %.

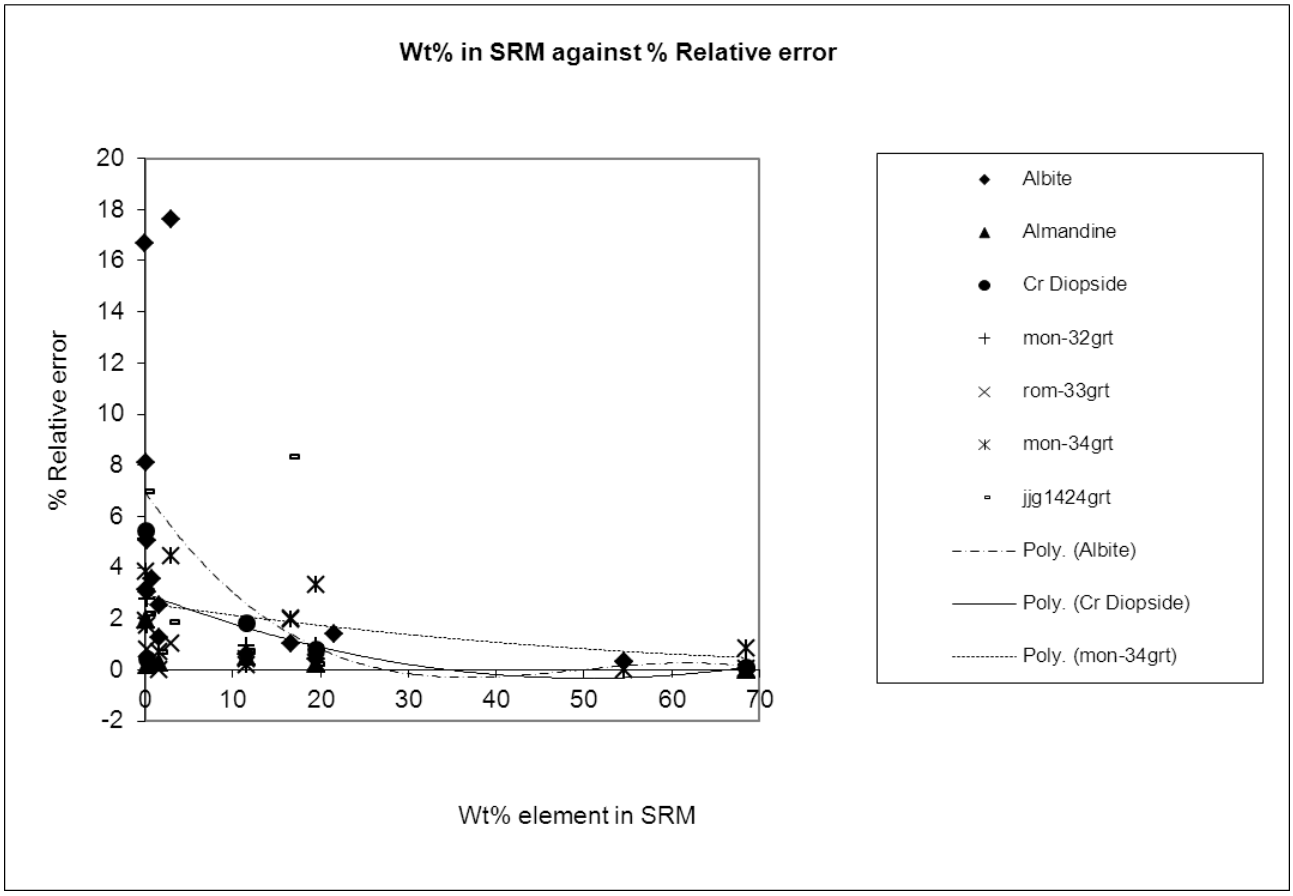

Fig. 4.1: A general plot of wt% element in the standard reference material (SRM), for most of the minerals in the accuracy and precision section, plotted against the % relative error between the SRM value and average value for that group of analyses. Trend lines indicate an indirect relationship between the two parameters in all the mineral types.

4.2.3.3 Accuracy and precision of glass analysis

The appropriate analysis time and optimum beam and physical conditions were investigated on the obsidian glass standard which, as mentioned before, is not the best fit to compare to water-rich low temperature melts. Small volumes of glass are often encountered in experimental petrology samples

and can be accurately analysed with SEM-EDS. They are problematic with EMPA since the spotsize does not allow high resolution work of < 5 µm. The migration of light elements, especially Na, away from the beam during EMPA analysis can be constrained with the use of the less energetic SEM-EDS beam setup, but still needs to be use in conjunction with a cryo-stage for quantitative results (Fig 4.3).

Analysis time

Table 4.3 and Fig 4.2 demonstrate the influence of analysis time on the light elements, particularly Na concentration. Real time analyses of between 5 and 10 seconds will produce the most reliable Na values, whereas 25 to 50 seconds analysis time will result in severe Na losses of up to 2.5 wt% Na. The relative % errors for Na, Ca, Si, K and Al analyses all improved with short analysis times to below 10 %. Cl and Fe had lower relative % errors with the 50 seconds analysis time.

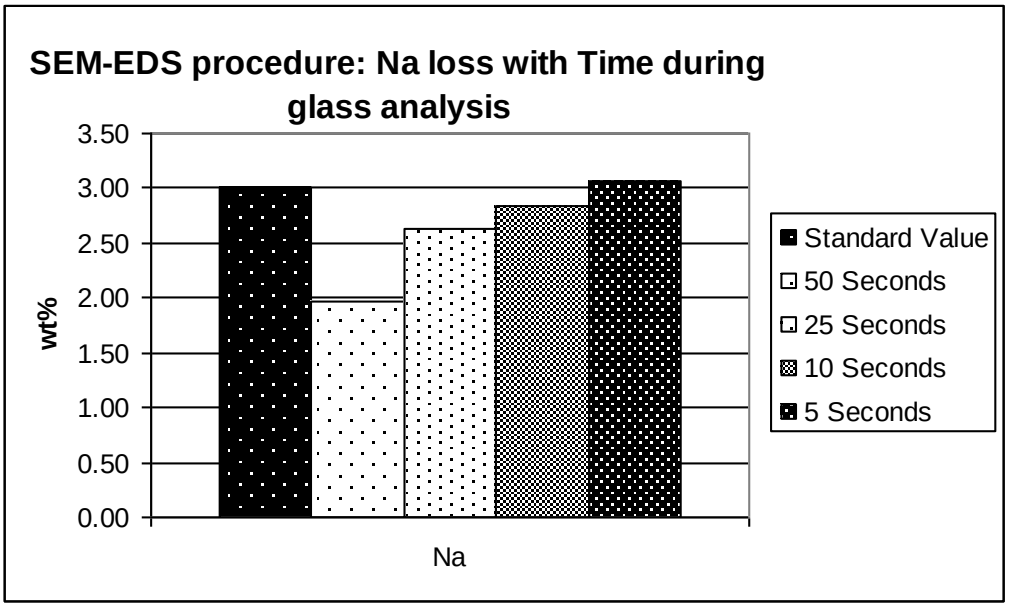

Fig. 4.2: Demonstration of the very crucial influence of SEM-EDS analysis time on the Na abundance. Real times of between 5 and 10 seconds will produce the most reliable Na values in glasses and other materials of similar compositions.

Beam conditions:

The results of the three analytical beam setups performed on the obsidian glass standard are summarized in Table 4.4. Three setups were used, a high energy beam setup of 5.3 nA, the normal beam setup of 3.9 nA, which was chosen due to sufficient X-ray counts of 4000 cts for the light and trace elements, and the normal beam setup used in conjunction with the freezing stage to cool the glass down to -180 °C to inhibit element migration. Averages were calculated from n = 5 and standard deviations are very low for these analyses. From Table 4.4 it is clear that the analyses of Na become more accurate, by increasing up to 1.5 wt% Na, moving from the high energy beam setup, where the Na loss is high (112.42 % relative error), to the normal setup, with little Na loss (52.39 % relative error), and finally the normal setup used with the freezing stage which reduced the relative error to 0.02 wt% Na. Fig 4.3 reflects the absolute errors on these three setups for all the elements.

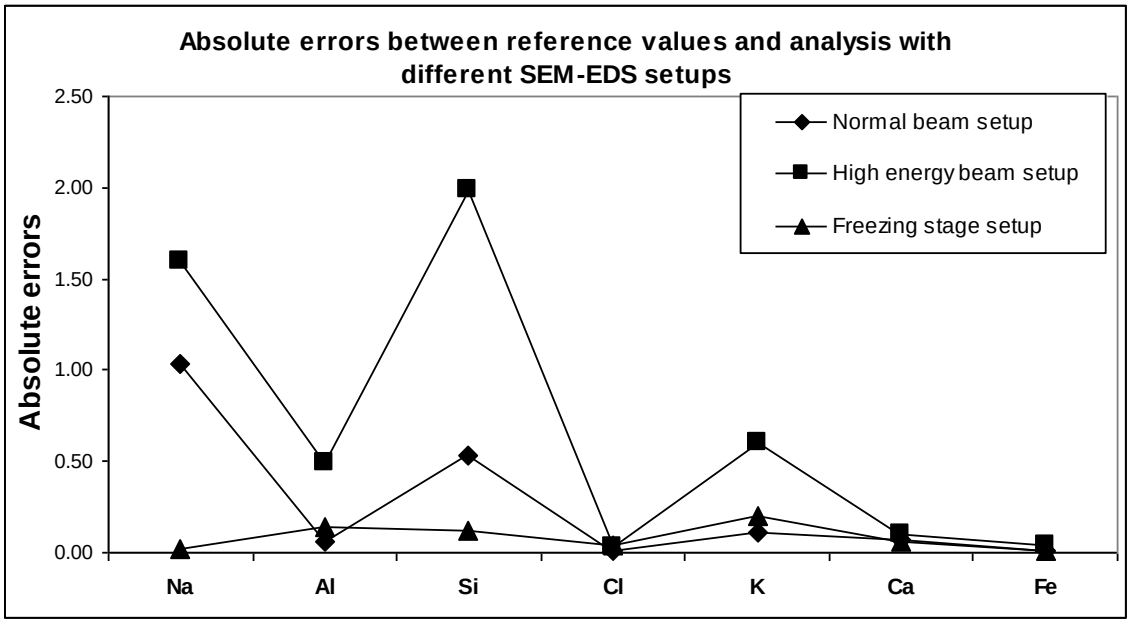

Fig. 4.3: The errors and the degree to which the analytical setup for glasses can influence the outcome of the results. It is clear that errors decrease from the high energy beam setup to the normal setup and is at their lowest for most of the elements when the freezing stage is used in conjunction with the normal setup. The elements most influenced by a stronger beam setup are Na, Si and K, but these errors decrease in each case with the use of the freezing stage.

4.2.4 Discussion of experimental phase analysis by SEM-EDS

The information presented above illustrates that the SEM-EDS technique can be used with confidence to determine the composition of a range of minerals and glasses quantitatively. The advantages and disadvantages for both SEM-EDS and the conventional EMPA techniques are listed below for consideration before attempting quantitative mineral analysis with SEM-EDS.

4.2.4.1 Mineral Analysis

The disadvantages of SEM-EDS technique

Elements present in concentrations below 0.5 wt% are less accurate when analysed by SEM-EDS, compared to conventional EMPA analysis. The SEM-EDS method is not accurate to abundances below 0.08 wt%. The SEM-EDS analyses are more affected by coating thickness and irregularities due to the lower energy of the electron beam. Care needs to be taken to obtain similar coating thicknesses when coating standard reference materials and unknown samples. The resolution and deconvolution of X-ray lines are not as good as with WDS systems, for example the Al content could not be accurately determined in the ortho- and clinopyroxenes due to poor discrimination between background and peaks. Counting times for minor transition elements Fe, Mn and Cr might have to be longer, for example 100 seconds instead of 50 seconds, to improve the precision and accuracy of the analyses.

The advantages of the SEM-EDS technique

Relative % errors of below 10 % (Fig 4.1) can be achieved for major and minor elements in most minerals. Precision is achievable as long as the electron beam is regularly monitored by the Faraday cup and specimen current monitor. It is a quick method, 50 seconds real time, compared to 1-15 min with EMPA to obtain accurate results. Na and K can be reliably determined with the SEM-EDS in

glasses and feldspar minerals, due to the less aggressive beam setup. It is an inexpensive method compared to EMPA with no moving parts that need recalibration and expensive maintenance. Due to the high resolution capabilities SEM-EDS has better spatial resolution for identifying and analysing small phases or areas. Energy Dispersive Spectrometry detectors do not have analysing crystals and therefore no fluorescence takes place due to analysing crystals, therefore less inter-element effects. The calibration procedure is relatively easy since inter-element effects are corrected in the software package in a fundamental parameters procedure.

4.2.4.2 Glass Analysis

The data for the glass analysis section show that when attempting silicate glass analysis with SEM-EDS, the analytical conditions need to be carefully planned to prevent Na, and to a lesser extent all light element, loss. Short analysis times of 5 to 10 seconds and a defocused beam are crucial if no cryogenic stage is available. Since a defocused beam is not always practical because of very small analysis areas (> 5 µm) of glass, it is more practical to use a less aggressive, but focused SEM beam in combination with a freezing stage. The SEM beam conditions must be carefully monitored with a Faraday cup after every five to ten analyses to produce analysis with true wt% totals. The combination of a less aggressive, controlled beam with a cold (~ -180 ºC) glass will give the most accurate results, leading to improved assumptions of the origin of these silicate glasses. In the absence of a freezing stage, the SEM-EDS system can be used for glass analysis with a defocused beam, Faraday cup and low beam energy, but accuracy will be less than with the complete setup. When EMPA analysis is the only available technique, a defocused beam in combination with short analysis times and correction procedures is the alternative micro-beam technique, but only volumes larger than 5 µm can be safely analysed and calibration procedures are complicated and very careful standard – unknown matching is required to correct for Na loss.

Chapter 5: Experimental Results

The fine grain-size of most products of experimental studies makes their identification by standard optical techniques difficult in comparison with natural rocks and minerals, because such diagnostic features as colour, extinctions angles, and optical sign cannot be readily determined. Another difficulty is, of course, the limited amount of material available in the quenching experiment, which makes the production of thin sections troublesome. The experimental run products in this study were rapidly quenched in their gold capsules, tested for leaks and carefully opened. After opening they were mounted in resin and polished. Special care was taken during polishing since the experimental amounts were limited and glassy material polishes down quickly. Reflected light was used to determine if the polished surface was smooth enough for micro-analysis. The polished sections were carbon coated for high resolution backscattered electron imaging with the Scanning Electron microscope, phase identification and analysis.

5.1 Phase proportions estimations

Image analysis using the software analySIS® and backscattered electron images of the run products was used to calculate phase proportions in the run products. Phase analysis is a quantitative area analysis for individual grey-value phases. Pre-requisite for this is that several grey-value areas are defined and assigned to a colour. The result is a sheet containing the respective areas of each phase in mm^2 and volume %. Care needs to be taken to take representative BS images of the run products at the lowest magnification possible to include all phases. The reproducibility of the image analyses depends strongly on the choice of BS images used for a sample. In this study, sets of at least 3 images, considered to be representative, were taken for each run product at different locations and the average of the image analysis results from these was adopted as a reliable measure of phase proportions in the run products. Problems surfaced when cordierite was less abundant in the melt and

could not be distinguished from melt by the image analysis program. The same problem occurred when calculating andalusite in the lower temperature runs.

Due to the above-mentioned problems with image analysis, the phase proportions were determined for all the runs by a combination of image analysis and a least squares mixing program. The starting material composition and experimental phase compositions (wt %) were used for these calculations and the phases identified in each run were used as guide to calculate their abundances. Care was taken to constrain the r^2 values to between 0.01 and 0.7.

5.2 Identifying the solidus

The experimental conditions, as well as the phases produced are listed in Table 5.1. Melting of the charges at conditions slightly above the solidus was identified by the occurrence of thin films of glass between mineral phases (Fig.5.1.A, 5.1.B, 5.1.C, 5.1 D) as well as peritectic K-feldspars.

Table 5.1: Summary of experimental conditions and results

P (kbar)	T (°C)	Duration (h)	Reactants Phases present	Products Phases present	Accessory Phases
MTS 7				**Biotite Metapelite**	
3.2	1000	120	Q,And	Gl, Spl, Cord	Ilm
3.2	950	108	Q	Gl, Spl, Cord	Ilm
3.2	900	144	Q, Biot, Ksp, And, Cord	Gl, Spl, Ksp, Biot, Cord	Ilm
3.2	850	228	Q, Biot, Ksp, And, Cord	Gl, Spl, Ksp, Biot, Cord	Ilm
3.0	800	180	Q, Biot, Ksp, And, Cord	Gl, Spl	Ilm
2.9	750	372	Q, Biot, Ksp, And, Plag, Cord		Ilm
MTS 8				**Biotite Metapelite**	
3.2	1000	120	Q, Ksp	Gl, Spl, Cord	Zr, Ap
3.2	950	108	Ksp, Q, Biot	Gl, Spl, Cord	Ilm, Zr, Ap
3.2	900	144	Ksp, Q, Biot, And, Cord	Gl, Spl, Biot, Ksp, Cord	Ilm, Zr, Ap, Mon
3.2	850	228	Ksp, Q, Biot, And, Cord	Gl, Spl, Biot, Ksp, Cord	Ilm, Zr, Ap, Mon
3.0	800	180	Ksp, Q, Biot, And, Plag, Cord	Gl, Spl	Ilm, Zr, Ap, Mon, Tu
2.9	750	372	Ksp, Q, Biot, And, Plag, Cord		Ilm, Zr, Ap, Mon, Tu
MTS 70				**Muscovite-Biotite Metapelite**	
3.2	1000	120		Gl, Spl, Cord, Sill/Mul	Ilm
3.2	950	108	Q	Gl, Spl, Cord, Sill/Mul	Ilm
3.2	900	144	Q	Gl, Spl, Cord, Sill/Mul	Ilm
3.2	850	228	Q, Biot	Gl, Spl, Cord, Sill/Mul	Ilm
3.0	800	180	Q, Biot, Tu	Gl, Spl, Cord, Sill/Mul, Tu, Biot	Ilm, Ap
2.9	750	372	Q, Biot, Mu, Tu		Ilm, Ap
MTS 71				**Muscovite-Biotite Metapelite**	
3.2	1000	120	Q	Gl, Spl, Cord, Sill/Mul	Ilm, Zr
3.2	950	108	Q	Gl, Spl, Cord, Sill/Mul	Ilm
3.2	900	144	Q	Gl, Spl, Cord, Sill/Mul	Ilm
3.2	850	228	Q, Tu	Gl, Spl, Cord, Sill/Mul, Tu	Ilm
3.0	800	180	Q, Tu, Biot	Gl, Spl, Cord, Tu, Biot	IlmAp
2.9	750	372	Q, Tu, Biot, Mu		Ilm, Ap

In all cases, the first appearance of melt coincided with the appearance of new anhydrous phases, and no new mineral phases were identified in the subsolidus experiments, indicating that melting occurred through an incongruent reaction. Melting in the charges coincided with clear textural changes and, on opening the capsules, samples that had melted were observed to be hard and brittle with a glassy sheen. These samples were easily polished.

In contrast, samples that had not melted had recrystallised sufficiently to form competent aggregates that could be mounted in resin, but that were easily fractured and were difficult to polish.

5.3 Solidus positions in the biotite vs two mica samples

All samples had begun to melt by 800 ºC, but not by 750 ºC. Thus, the solidus for each composition is located between 750 and 800 ºC. However, the degree of melting, as reflected by the melt proportion in the charges at 800 ºC, was significantly different to suggest likely significant differences in the solidus temperatures, within the interval 750 to 800 ºC. The two mica samples (MTS70 and MTS71) lost muscovite and melted substantially (Fig 5.1.A and 5.1.B). In contrast, the biotite metapelites (MTS7 and MTS8) (Fig 5.1.C and 5.1.D), melted very little in the 800 ºC experiment, suggesting that, as has been documented in previous studies at higher pressures (for example, Gardien *et al.*, 1995), muscovite incongruent melting occurs at lower temperatures (i.e. in this case, closer to 750 ºC) than that of biotite.

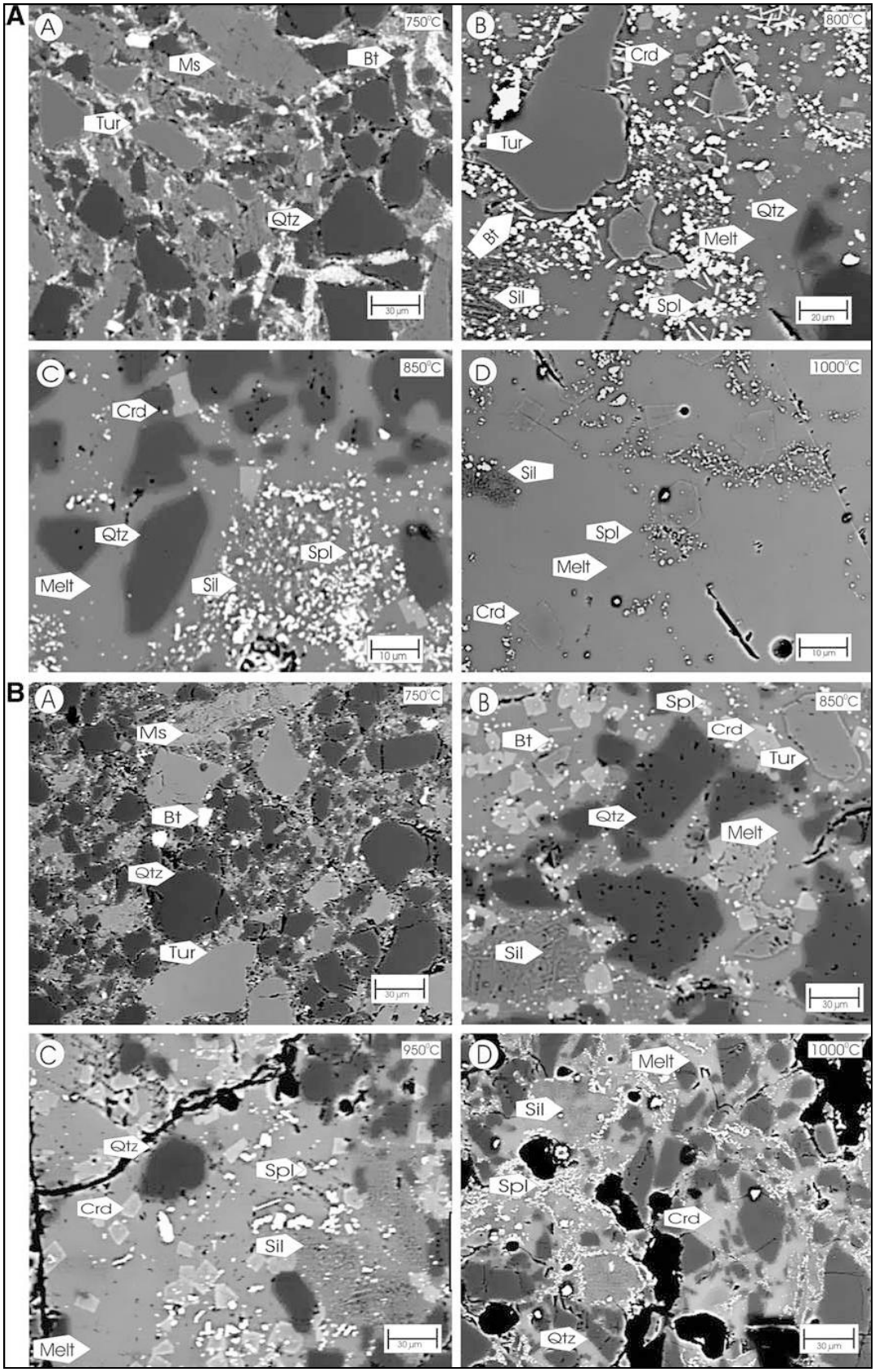

Fig. 5.1: Back scattered SEM images of typical phase relationships in the run products from all experiments. A) MTS70, B) MTS71

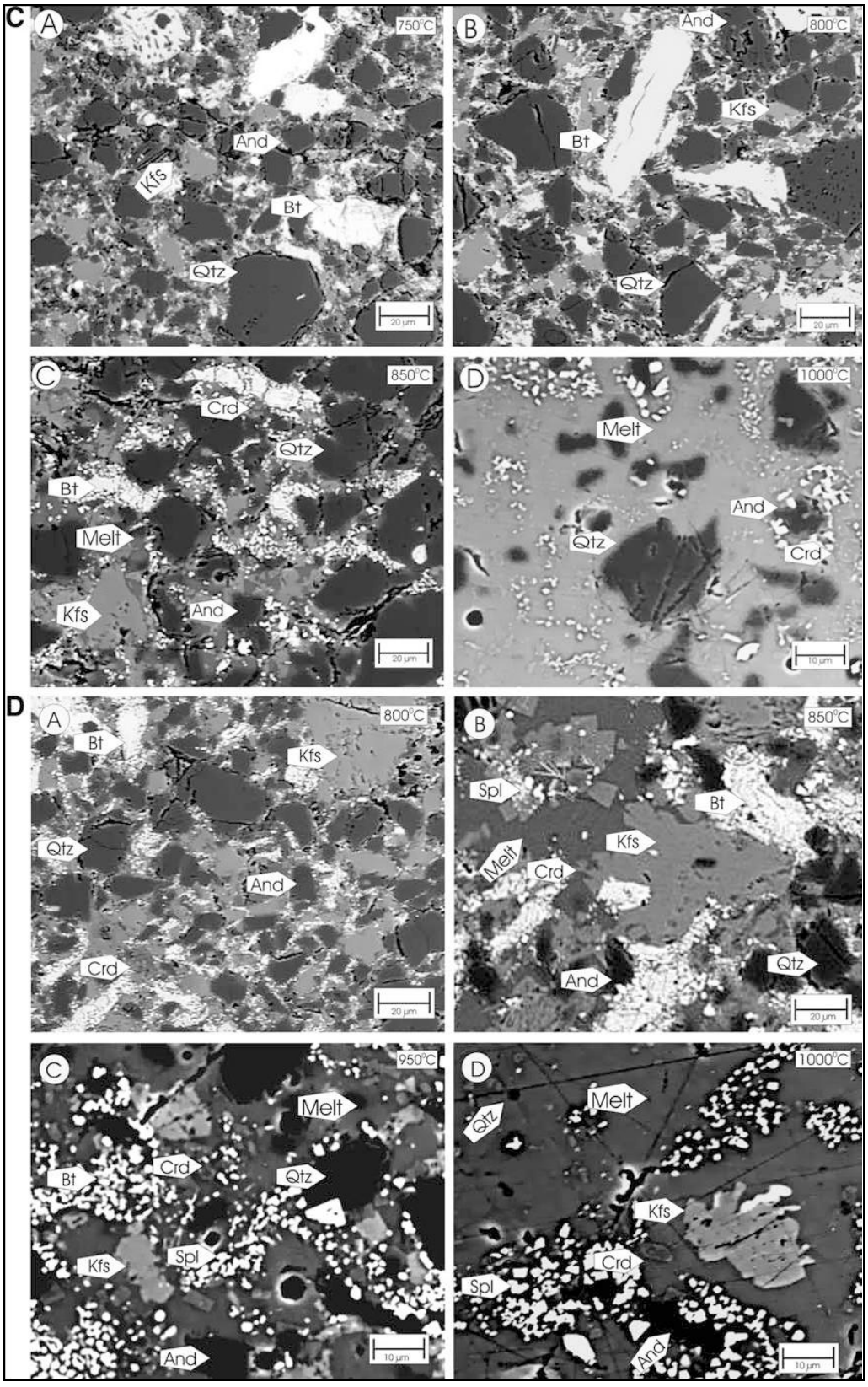

Fig. 5.1 continued: Back scattered SEM images of typical phase relationships in the run products from all experiments. C) MTS7 and D) MTS8

5.4 Phase relations in the run products

Quartz was present in all the run products as a residual phase that occurred in decreasing proportions with increasing temperature, except for the highest temperature experiment on MTS70 where quartz was completely consumed. In the two mica samples (MTS70 and MTS71) (Fig 5.1.A and 5.1.B) phase changes within the melting interval, but below 850 ºC, can be interpreted to reflect quartz, biotite, muscovite and tourmaline melting to produce melt, euhedral spinel, sillimanite/mullite, cordierite and new, euhedral biotite (Table 5.2). In MTS70 biotite disappeared between 850 and 900 ºC, whereas, in MTS71 biotite was completely consumed by 850 ºC.

Tourmaline disappeared from the MTS70 assemblage between 800 and 850 °C. Euhedral, recrystallized tourmaline crystals were present in MTS71 at 850 ºC (Fig 5.1.A and 5.1.B), but were absent from the 900 ºC run products. At temperatures above muscovite stability, cordierite, spinel and melt are produced at the expense of biotite and tourmaline, and at temperatures above biotite and tourmaline stability, melt proportions increase as a function of temperature relative to spinel, cordierite and sillimanite/mullite, which are present to 1000 ºC. In some of the experiments at temperature above 900 ºC, the newly formed aluminium silicate phase could be confirmed to be sillimanite rather than mullite on the basis of Al:Si ratio. In experiments close to the solidus, the crystal sizes were small (< 2 µm), and melt contamination made accurate determination of the Al:Si ratio difficult. Despite this, there were clear indications that in some cases the Al:Si ratio was higher than ideal sillimanite, and that the product could possibly be mullite. However, corundum mixed (analytically) with small amounts of melt contamination could also produce high Al:Si ratios (MTS71), but the presence of K_2O in the analysis would indicate this scenario.. Transmission electron microscopy or electron backscattered diffraction coupled to a SEM might be useful to identify such small crystals, but the small amounts of run products produced did not allow such investigations to be carried out.

In the biotite-bearing samples (MTS7 and MTS8), phase changes close to the solidus are consistent with quartz, biotite, and andalusite melting to produce melt, euhedral cordierite, spinel and K-feldspar (Fig. 5.1.C and 5.1.D). In MTS7, biotite and K-feldspar were exhausted between 950 and 1000 ºC (Fig. 5.1.C.), and in MTS8 biotite was exhausted between 900 and 950 ºC, but K-feldspar persisted up to 1000 ºC (Fig.5.1.D). Andalusite was never completely consumed by the melting reactions in both samples. At temperatures above biotite stability, melt, cordierite and spinel proportions increase, at the expense of K-feldspar, quartz and andalusite, as a function of temperature.

5.5 Phase compositions

Table 5.2 contains average compositions (n = 5 with standard deviations for each element as listed in Chapter 4) for the minerals observed in the run products. The elements Na, Mg, Al, Si, K, Ca, Ti, Mn and Fe were analysed for in each case, but only values > detection limits were reported. Those values below detection limits were set to 0. The typical detection limits for SEM-EDS technique, as discussed in Chapter 4, are 0.05 wt %. Fe^{3+} values were calculated according to the method of Droop (1987).

Table 5.2: Average compositions (n ≥ 5) for the minerals observed in the run products. The elements Na, Mg, Al, Si, K, Ca, Ti, Mn and Fe were analysed for in each case, but only values >0 were included in the tables. Fe^{3+} values were calculated according to the method of Droop (1987). The following number of oxygens, in brackets, was used to calculate the cations for each mineral group: cordierite (18 O), feldspar (8 O), tourmaline (49 O), spinel (4 O), andalusite/sillimanite (5 O), and muscovite and biotite (22 O).

Cordierite	**MTS7**		**MTS8**		**MTS70**					**MTS71**				
Temp (°C)	1000	950	1000	950	1000	950	900	850	800	1000	950	900	850	800
Na_2O	0.39	0.46	0.78	0.53	0.57	0.29	0.62	0.51	0.41	0.55	0.53	0.56	0.59	0.84
MgO	9.05	9.48	8.81	8.81	8.50	9.43	8.42	6.57	8.03	8.22	8.25	7.12	7.27	3.95
Al_2O_3	32.24	33.45	31.34	32.60	33.24	33.33	32.63	31.71	32.66	32.73	32.39	32.29	32.64	28.77
SiO_2	49.28	48.43	49.40	48.74	47.94	48.75	48.26	47.92	48.20	48.29	49.29	48.47	48.07	51.77
K_2O	1.00	0.16	1.74	1.22	0.45	0.62	0.84	0.83	0.49	0.79	0.38	0.29	0.37	1.28
CaO	0.00	0.04	0.01	0.00	0.02	0.05	0.04	0.11	0.09	0.01	0.07	0.00	0.07	0.18
TiO_2	0.00	0.00	0.08	0.28	0.00	0.00	0.02	0.07	0.00	0.13	0.00	0.09	0.00	0.77
MnO	0.11	0.00	0.20	0.19	0.25	0.27	0.39	0.49	0.51	0.14	0.09	0.09	0.10	0.16
FeO	7.14	7.45	6.76	6.92	7.99	6.97	7.55	11.22	8.70	8.43	8.45	9.86	10.05	12.15
Total	99.21	99.47	99.11	99.28	98.95	99.71	98.76	99.43	99.09	99.29	99.46	98.77	99.15	99.86
Si	5.04	4.93	5.08	4.99	4.93	4.95	4.97	4.99	4.97	4.96	5.04	5.02	4.97	5.37
Ti	0.00	0.00	0.01	0.02	0.00	0.00	0.00	0.01	0.00	0.01	0.00	0.01	0.00	0.06
Al	3.88	4.01	3.79	3.93	4.02	3.98	3.96	3.89	3.96	3.96	3.90	3.94	3.97	3.51
Fe tot	0.61	0.63	0.58	0.59	0.69	0.59	0.65	0.98	0.75	0.72	0.72	0.85	0.87	1.05
Mn	0.01	0.00	0.02	0.02	0.02	0.02	0.03	0.04	0.04	0.01	0.01	0.01	0.01	0.01
Mg	1.38	1.44	1.35	1.34	1.30	1.43	1.29	1.02	1.23	1.26	1.26	1.10	1.12	0.61
Ca	0.00	0.00	0.00	0.00	0.00	0.01	0.00	0.01	0.01	0.00	0.01	0.00	0.01	0.02
Na	0.08	0.09	0.16	0.10	0.11	0.06	0.12	0.10	0.08	0.11	0.11	0.11	0.12	0.17
K	0.13	0.02	0.23	0.16	0.06	0.08	0.11	0.11	0.06	0.10	0.05	0.04	0.05	0.17
Mg#	69.30	69.40	69.88	69.44	65.48	70.68	66.55	51.06	62.18	63.49	63.49	56.30	56.31	36.70
Cat Total (incl Na+K)	11.12	11.12	11.21	11.15	11.14	11.12	11.15	11.16	11.12	11.15	11.09	11.08	11.12	10.98
Cat Total (excl Na+K)	10.91	11.01	10.82	10.89	10.97	10.98	10.92	10.94	10.97	10.93	10.93	10.92	10.95	10.64

Biotite	**MTS7**				**MTS8**				**MTS70**			**MTS71**	
Temp (°C)	850	800	750	950	900	850	800	750	850	800	750	800	750
Na_2O	0.59	0.95	0.82	0.75	0.53	0.61	0.76	0.68	0.46	0.34	0.49	0.40	0.79
MgO	9.03	8.51	7.50	11.29	12.14	8.60	10.10	9.24	10.98	10.67	4.99	4.80	5.25
Al_2O_3	17.69	17.76	17.66	15.81	15.67	17.59	18.05	18.02	17.55	15.99	17.81	18.37	19.27
SiO_2	35.66	36.67	35.99	39.91	40.50	35.76	37.70	36.66	38.86	38.15	37.88	38.87	40.95
K_2O	9.29	9.16	9.21	8.93	9.04	9.43	9.19	9.32	9.33	9.93	9.47	9.76	9.06
TiO_2	2.19	2.33	2.79	4.09	3.50	2.21	2.56	2.68	1.92	3.26	1.85	3.10	1.96
MnO	0.06	0.07	0.29	0.06	0.05	0.21	0.06	0.16	0.17	0.22	0.46	0.02	0.26
FeO	20.81	20.95	22.18	15.04	13.95	21.26	18.31	19.44	16.79	17.51	23.38	20.45	18.07
Total	95.32	96.39	96.43	95.88	95.38	95.66	96.72	96.21	96.05	96.07	96.33	95.79	95.61
Si	5.47	5.55	5.50	5.86	5.94	5.49	5.60	5.52	5.75	5.71	5.79	5.87	6.06
Ti	0.25	0.27	0.32	0.45	0.39	0.25	0.29	0.30	0.21	0.37	0.21	0.35	0.22
Al	3.20	3.17	3.18	2.73	2.71	3.18	3.16	3.20	3.06	2.82	3.21	3.26	3.36
Fe tot	2.67	2.65	2.83	1.85	1.71	2.73	2.27	2.45	2.08	2.19	2.99	2.58	2.24
Mn	0.01	0.01	0.04	0.01	0.01	0.03	0.01	0.02	0.02	0.03	0.06	0.00	0.03
Mg	2.07	1.92	1.71	2.47	2.65	1.97	2.24	2.08	2.42	2.38	1.14	1.08	1.16
Na	0.17	0.28	0.24	0.21	0.15	0.18	0.22	0.20	0.13	0.10	0.15	0.12	0.23
K	1.82	1.77	1.80	1.67	1.69	1.85	1.74	1.79	1.76	1.90	1.85	1.88	1.71
Mg#	43.61	42.00	37.59	57.22	60.81	41.90	49.58	45.88	53.83	52.07	27.55	29.52	34.13
Cat Total	15.67	15.62	15.61	15.26	15.24	15.68	15.51	15.56	15.45	15.50	15.38	15.14	15.00
Al iv	2.53	2.45	2.50	2.14	2.06	2.51	2.40	2.48	2.25	2.29	2.21	2.13	1.94
Al vi	0.67	0.72	0.67	0.59	0.64	0.67	0.75	0.72	0.81	0.54	1.00	1.13	1.42
Fe+Mg	4.74	4.57	4.54	4.32	4.36	4.70	4.51	4.53	4.50	4.58	4.12	3.66	3.40
Ti+Alvi	0.93	0.99	0.99	1.05	1.03	0.92	1.04	1.03	1.03	0.90	1.21	1.48	1.64
Alvi+Si	6.15	6.27	6.17	6.46	6.58	6.16	6.35	6.25	6.57	6.25	6.79	7.00	7.48
Ti+Aliv	2.78	2.71	2.82	2.59	2.45	2.77	2.69	2.78	2.46	2.65	2.42	2.49	2.16
Fe+Mg+Mn	4.75	4.58	4.58	4.33	4.37	4.72	4.52	4.55	4.52	4.60	4.18	3.66	3.43

Table 5.2 continued

Spl	MTS7	MTS8		MTS70		MTS71
Temp (^{o}C)	1000	1000	1000	950	800	950
Na_2O	0.70	1.17	0.84	0.65	0.81	1.14
MgO	6.71	9.40	6.35	7.11	3.65	1.95
Al_2O_3	51.91	55.48	52.99	51.71	46.58	44.14
SiO_2	1.91	1.66	1.37	1.38	1.77	1.35
K_2O	0.12	0.13	0.05	0.10	0.14	0.05
CaO	0.02	0.00	0.01	0.05	0.03	0.03
TiO_2	0.56	0.36	0.52	0.38	4.48	0.80
MnO	0.15	0.21	0.39	0.48	0.69	0.16
Fe_2O_3	8.98	8.74	9.19	10.87	6.36	17.64
FeO	29.86	23.72	29.24	28.38	35.67	34.52
Total	100.91	100.87	100.94	101.10	100.18	101.77
Si	0.05	0.05	0.08	0.04	0.05	0.04
Ti	0.01	0.01	0.01	0.01	0.10	0.02
Al	1.76	1.82	1.76	1.76	1.63	1.62
Fe tot	0.91	0.74	0.88	0.92	1.03	1.31
Mn	0.00	0.00	0.01	0.01	0.02	0.00
Mg	0.29	0.39	0.27	0.31	0.16	0.09
Ca	0.00	0.00	0.00	0.00	0.00	0.00
Na	0.04	0.06	0.05	0.04	0.05	0.07
K	0.00	0.00	0.01	0.00	0.01	0.00
Mg#	23.97	34.66	23.15	24.93	13.60	6.46
Cat Total	3.07	3.07	3.06	3.09	3.05	3.16
Fe II	0.84	0.67	0.83	0.83	0.98	1.15
Fe III	0.07	0.07	0.06	0.09	0.05	0.16

Mu	MTS70	MTS71
Temp (^{o}C)	750	750
Na_2O	0.79	0.69
MgO	0.33	0.00
Al_2O_3	31.58	31.63
SiO_2	48.07	48.58
K_2O	10.97	11.04
TiO_2	0.60	0.51
MnO	0.08	0.08
FeO	2.08	2.24
Total	94.51	94.77
Si	6.49	6.54
Ti	0.06	0.05
Al	5.02	5.01
Fe tot	0.23	0.25
Mn	0.01	0.01
Mg	0.07	0.00
Na	0.21	0.18
K	1.89	1.90
Mg#	22.26	0.00
Cat Total	13.98	13.94

Ilm	MTS7					MTS8			MTS70	MTS71
Temp (^{o}C)	1000	950	850	800	750	950	900	850	750	950	750
Na_2O	0.45	0.42	0.39	0.58	0.48	0.49	0.76	0.74	0.37	0.42	0.53
MgO	2.51	0.50	1.09	0.86	0.98	2.49	2.99	1.50	0.50	1.70	0.42
Al_2O_3	0.79	1.26	0.50	0.52	0.51	1.04	1.53	0.32	0.34	0.79	0.64
SiO_2	0.64	3.08	0.85	0.51	0.68	1.70	3.24	0.59	0.83	0.91	1.38
K_2O	0.09	0.26	0.09	0.00	0.05	0.21	0.31	0.13	0.17	0.06	0.20
CaO	0.03	0.05	0.11	0.09	0.10	0.00	0.00	0.07	0.06	0.00	0.08
TiO_2	46.84	53.34	51.40	64.74	58.07	43.79	41.35	65.74	62.89	50.07	50.66
MnO	0.19	0.15	0.57	0.66	0.62	0.45	0.13	0.73	0.64	0.82	0.22
Fe Total	48.20	40.75	45.07	31.66	38.36	49.83	49.67	29.76	34.39	45.64	45.92
FeO	36.24	40.75	42.51	31.66	37.08	44.42	43.49	29.76	34.39	40.23	43.09
Fe_2O_3	11.97	0.00	2.56	0.00	1.28	5.41	6.18	0.00	0.00	5.41	2.83
Total	99.74	99.81	100.08	99.62	99.85	100.00	99.98	99.59	100.18	100.40	100.07
Si	0.03	0.06	0.02	0.01	0.02	0.04	0.08	0.02	0.02	0.03	0.03
Ti	0.89	0.77	0.97	1.14	1.05	0.84	0.79	1.15	1.11	0.88	0.95
Al	0.03	0.04	0.01	0.01	0.01	0.03	0.05	0.01	0.01	0.03	0.02
Fe tot	1.01	1.23	0.94	0.62	0.78	1.06	1.05	0.58	0.68	1.02	0.96
Mn	0.00	0.00	0.01	0.01	0.01	0.01	0.00	0.01	0.01	0.02	0.00
Mg	0.09	0.02	0.04	0.03	0.04	0.09	0.11	0.05	0.02	0.08	0.02
Ca	0.00	0.00	0.00	0.00	0.00	0.00	0.00	0.00	0.00	0.00	0.00
Na	0.02	0.02	0.02	0.03	0.02	0.02	0.04	0.02	0.02	0.03	0.03
K	0.00	0.01	0.00	0.00	0.00	0.01	0.01	0.00	0.01	0.01	0.01
Mg#	8.05	1.41	4.17	4.64	4.40	8.18	9.69	7.78	2.51	7.66	1.62
Cat Total	2.08	2.16	2.02	1.86	1.94	2.12	2.13	1.84	1.87	2.09	2.02
Fe II	0.93	1.07	0.92	-	0.92	0.95	0.92	-	-	0.93	0.94
Fe III	0.08	0.16	0.02	-	0.02	0.12	0.13	-	-	0.09	0.02
X_{Hem}	1.02	1.25	0.94	-	0.94	1.08	1.07	-	-	1.02	0.96

Table 5.2 continued

Ksp	MTS7					MTS8			
		recr							
Temp (°C)	850	850	800	750	1000	850	recr 850	800	750
Na_2O	2.48	2.27	2.28	2.52	1.49	2.62	2.81	2.40	2.04
Al_2O_3	18.78	17.64	17.03	16.64	16.74	17.95	19.10	17.37	17.06
SiO_2	63.88	64.97	66.07	66.09	65.08	65.14	64.51	64.21	65.90
K_2O	13.18	13.84	13.81	13.92	15.04	13.40	13.56	12.94	14.28
CaO	0.14	0.03	0.00	0.00	0.00	0.00	0.15	0.00	0.00
TiO_2	0.23	0.18	0.00	0.02	0.16	0.15	0.17	0.43	0.00
FeO	0.29	0.59	0.38	0.17	0.10	0.29	0.38	2.04	0.12
Total	98.97	99.53	99.56	99.37	98.61	99.55	100.68	99.38	99.41
Si	2.96	2.94	3.04	3.05	3.04	3.00	2.95	2.99	3.04
Ti	0.01	0.01	0.00	0.00	0.01	0.01	0.01	0.02	0.00
Al	1.03	1.05	0.92	0.91	0.92	0.97	1.03	0.95	0.93
Fe tot	0.01	0.01	0.01	0.01	0.00	0.01	0.01	0.08	0.00
Ca	0.01	0.01	0.00	0.00	0.00	0.00	0.01	0.00	0.00
Na	0.22	0.24	0.20	0.23	0.13	0.23	0.25	0.22	0.18
K	0.78	0.77	0.81	0.82	0.90	0.79	0.79	0.77	0.84
Cat Total	5.02	5.03	5.00	5.01	5.01	5.01	5.05	5.01	5.00

Pl	MTS7	MTS8
Temp (°C)	750	800
Na_2O	11.21	10.12
Al_2O_3	20.44	22.99
SiO_2	65.44	62.95
K_2O	0.62	0.30
CaO	1.96	3.22
TiO_2	0.00	0.00
FeO	0.22	0.13
Total	99.88	99.71
Si	2.90	2.80
Ti	0.00	0.00
Al	1.07	1.20
Fe tot	0.01	0.00
Ca	0.09	0.15
Na	0.96	0.87
K	0.03	0.02
Cat Total	5.06	5.05

Tu	MTS71			MTS70			MTS8		
Temp (°C)	850 o	850 n	800	750	800	750	750	800L	800D
Na_2O	2.60	2.86	3.17	3.14	3.42	2.94	2.72	3.52	2.57
MgO	2.85	4.31	3.00	3.71	4.17	3.81	4.13	2.07	3.91
Al_2O_3	31.65	31.45	30.07	29.85	29.86	30.29	32.18	29.72	31.86
SiO_2	35.74	35.88	37.04	36.79	38.07	37.78	37.82	37.68	37.86
K_2O	0.12	0.07	0.12	0.07	0.06	0.12	0.07	0.08	0.08
CaO	0.17	0.18	0.05	0.13	0.10	0.18	0.34	0.04	0.17
TiO_2	1.00	0.95	0.87	0.97	0.85	0.81	0.79	0.26	0.36
MnO	0.10	0.09	0.09	0.11	0.10	0.09	0.00	0.22	0.07
FeO	11.42	10.10	11.49	11.17	9.50	10.79	8.73	12.58	9.15
Total	85.66	85.90	85.90	85.92	86.11	86.90	86.78	86.16	86.03
Si	6.01	5.99	6.02	5.96	6.07	6.01	6.18	6.05	6.05
Ti	0.13	0.12	0.11	0.12	0.10	0.12	0.10	0.11	0.11
Al	6.27	6.18	6.27	6.21	6.21	6.23	6.19	6.22	6.21
Fe tot	1.61	1.41	1.62	1.55	1.29	1.49	1.19	1.43	1.39
Mn	0.01	0.01	0.01	0.02	0.01	0.01	0.00	0.01	0.01
Mg	0.72	1.07	0.69	0.92	1.00	0.88	1.00	0.90	0.94
Ca	0.03	0.03	0.01	0.04	0.04	0.03	0.06	0.04	0.04
Na	0.85	0.93	0.94	0.94	0.93	0.92	0.79	0.90	0.90
K	0.03	0.02	0.02	0.01	0.02	0.02	0.01	0.02	0.02
Mg#	15.41	21.59	14.90	18.65	21.89	18.49	22.86	19.36	20.25
Cat Total	15.65	15.76	15.70	15.78	15.68	15.71	15.53	15.68	15.68
Na+K+Ca (X)	0.91	0.97	0.97	1.00	0.99	0.97	0.87	0.96	0.96
Al (Z)	6.00	6.00	6.00	6.00	6.00	6.00	6.00	6.00	6.00
Al (Y)	0.27	0.18	0.27	0.21	0.21	0.23	0.19	0.22	0.21

5.6 Spinel and Ilmenite

The oxide minerals produced in these experiments, especially in the low temperature runs, were difficult to analyse due to small crystal sizes and possibly melt inclusions. Consequently, some listed analyses include minor amounts of Si, Na and K that are interpreted to reflect contamination from the

surrounding glass (Table 5.2), and in other cases, reasonably good quality, and representative data could not be obtained due to this problem. Despite these difficulties, the available data indicate that the spinel compositions produced are complex solid solutions between spinel series and magnetite series end-members, consisting predominantly of spinel, hercynite and magnetite, with very minor concentrations of ulvöspinel and, in some cases, maghemite. The spinel compositions vary slightly across the experimental range, but are typically similar to Mag_8 Spl_{30} Hc_{62}. The Mg# (100*Mg/Mg+Fe) of spinel lies between that of the coexisting melts (Table 5.3) and cordierite (Table 5.2).

Ilmenite compositions are Mn-poor and, at relatively low temperatures, are close to ideal ilmenite composition (Table 5.2). The limited data available suggest that at temperatures of 950 and 1000 ˚C, ilmenite includes a small but significant hematite component. X_{Hem} ($0.5Fe^{3+}$ /Ti + $0.5Fe^{3+}$ + Fe^{2+}) values are typically between 0.94 and 0.96, in newly formed ilmenite from experiments close to the solidus, and between 1.02 and 1.25 in the highest temperature experiments. The Fe^{3+} concentrations in spinel and ilmenite are sensitive indicators of oxygen fugacity in the capsules (Ghiorso & Sack, 1991). This is important, as hydrogen diffusion out of the capsules into the pure argon pressure medium can be problematic in raising fO_2 and decreasing the amount of water available to enter the melt. In experiments on Fe-bearing starting compositions, the occurrence of this process is usually signified by the development of a redox gradient in the capsule, with a more oxidised rim zone signified by a rind of magnetite bearing melt developed against the capsule, (e.g. see discussion in Stevens *et al.*, 1997). The relatively low magnetite and hematite component concentration in respectively the spinel and ilmenite produced in these experiments, as well as the lack of a zonation of the charges with respect to oxide mineral distribution, argues against this process having had a significant effect on the redox state of these experiments. This is probably a function of the relatively thick walls of the gold capsules used, as well as the relatively low pressure of the experiments,

compared to others where the problem was noted and needed to be countered by the use of fO_2 buffering techniques (e.g. Stevens *et al.*, 1997).

5.7 Cordierite

Cordierite compositions are listed in Table 5.2. In general, the cordierite cation totals calculate to slightly above the ideal of 11, for the formulae based on 18 oxygen, despite very careful standardization procedures. However, if Na and K are excluded from the analysis, cordierite cation totals calculate to 11 or slightly below, and Si:Al ratios are close to ideal. Na and K may not be chemically bonded in cordierite, but can occur in channel-ways of the mineral structure where they are charge balanced by the presence of OH^- and other volatile groups accommodated in the same structures (Vry *et al.*, 1990). This suggests that relatively high Na and K values measured for the cordierite in this study reflect the presence of channel-way Na and K. Contamination by melt inclusions, or surrounding melt is unlikely as then most Na- and K-rich compositions should also be characterised by high Si:Al ratios, and this is not the case. No major element zonation was detected in cordierite from any of the runs. Mg partitions strongly into cordierite relative to coexisting spinel and melt, and cordierite Mg# generally increases as a function of temperature in all compositions (Fig. 5.2).

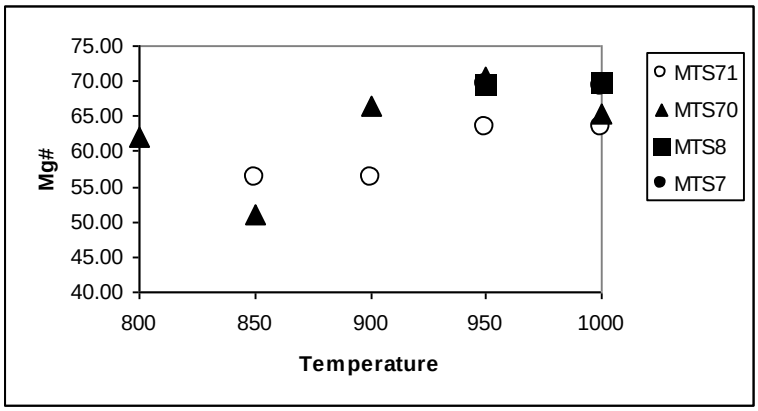

Fig. 5.2: Cordierite Mg# variation as a function of temperature. The data plotted represent newly crystallised cordierite.

5.8 Biotite

The Mg# of biotite generally increases towards higher temperatures (Fig. 5.3). On plots of Al^{VI} vs Ti and Si + Al^{VI} vs Ti + Al^{IV}, which may be used to show composition trends associated with the incorporation of Ti into the biotite structure via the respective substitutions $2Al^{VI}$= Ti + (Fe,Mg) and Ti + Al^{IV} = Si + Al^{VI}, the data for both the starting biotite compositions and those produced in the experiments, demonstrate a trend more consistent with the latter substitution (Fig 6a and b). Biotite in the run products from samples MTS7 and MTS8 has lower Al^{VI} + Ti relative to the remainder of the O-site occupants than the starting composition biotite from these rocks. This is interpreted to reflect an adjustment of the biotite to less aluminous compositions in these relatively muscovite-free rocks during partial melting. In contrast, the presence of muscovite and tourmaline in the two-mica samples appears to buffer Al^{VI} in biotite to higher values over a similar temperature interval.

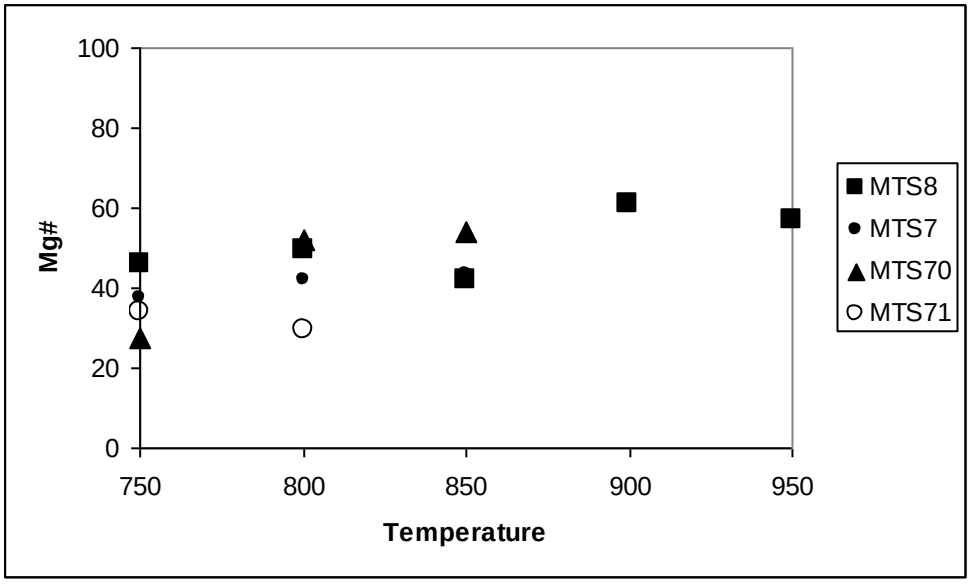

Fig. 5.3: Biotite Mg# variation as a function of temperature. The data plotted represent newly crystallised biotite.

A

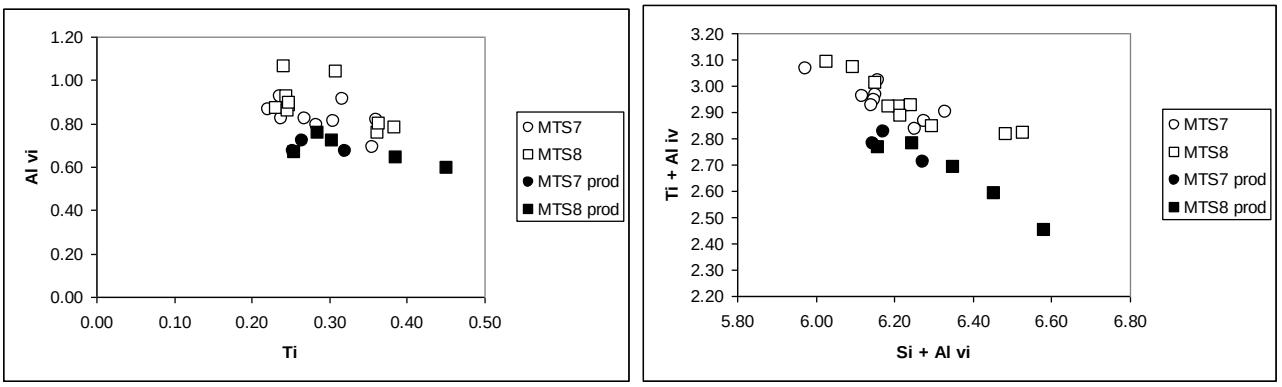

B

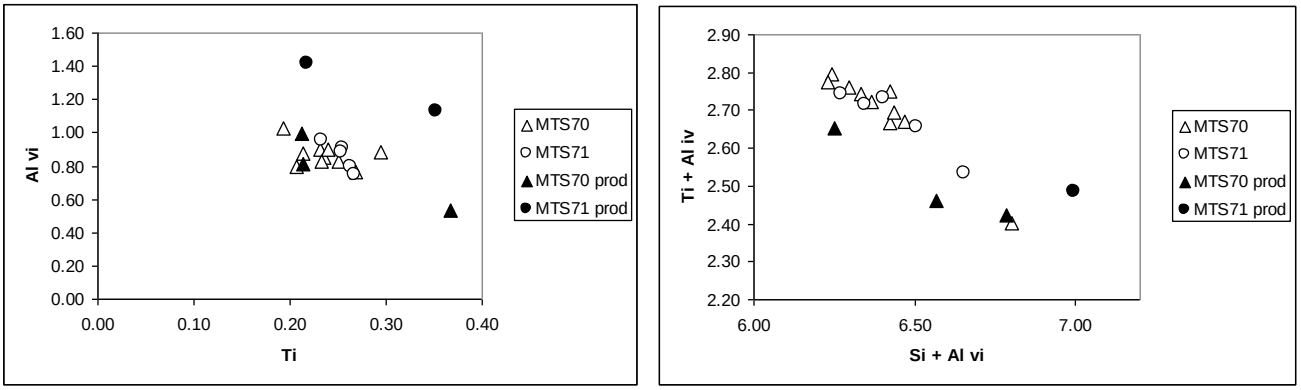

Fig. 5.4A and B: Plots of Al^{VI} vs. Ti and Si + Al^{VI} vs. Ti + Al^{IV} for biotite in both the starting materials (open symbols) and run products (shaded symbols), for the biotite metapelites (A) and the two mica metapelites (B). The data for the experimental biotite includes compositions produced across the range of temperatures where biotite was stable.

5.9 K-feldspar

In all the K-feldspar-bearing run products some relict K-feldspar exists that shows no compositional shift from the starting compositions. This is consistent with the documented very slow rates of diffusional adjustment of feldspar compositions (Spear *et al*., 1991). However, in lower temperature, partially melted runs from the biotite-bearing compositions some new K-feldspar exists as a product of the melting reactions. The new K-feldspar is Na (and to a much lesser degree Ca) enriched and K depleted relative to that in the starting material. This possibly represents a shift towards a high temperature ternary feldspar composition (Fig. 5.5). The occurrence of the new Na enriched feldspar

might also be a function of the presence of trace amounts of plagioclase which have been detected in the biotite-bearing starting materials. No plagioclase has been detected in the muscovite-biotite-bearing starting materials. At temperatures above about 660 °C complete solid solution exists between $NaAlSi_3O_8$ and $KAlSi_3O_8$. At lower temperatures solid solutions intermediate between K-feldspar and albite are unstable and might coexist together during slow crystallization. Plagioclase may completely dissolve in the melt phase if the protolith is low in Ca and Na. In protoliths containing more Ca and Na (e.g. metamorphic plagioclase), plagioclase reacts. Johannes (1989) showed that partial melting of plagioclase (An_{60}) in the system Qz-Ab-An-H_2O at 200 MPa (2 kbar) and 850 °C produces new plagioclase crystals $An_{82–85}$ as well as a more sodic plagioclase component in the melt. It is suggested that new plagioclases resulting from melting reactions in the Earth's crust will be in local equilibrium because the reactions occur with rising temperature (White, 2004; Carrington & Watt, 1995).

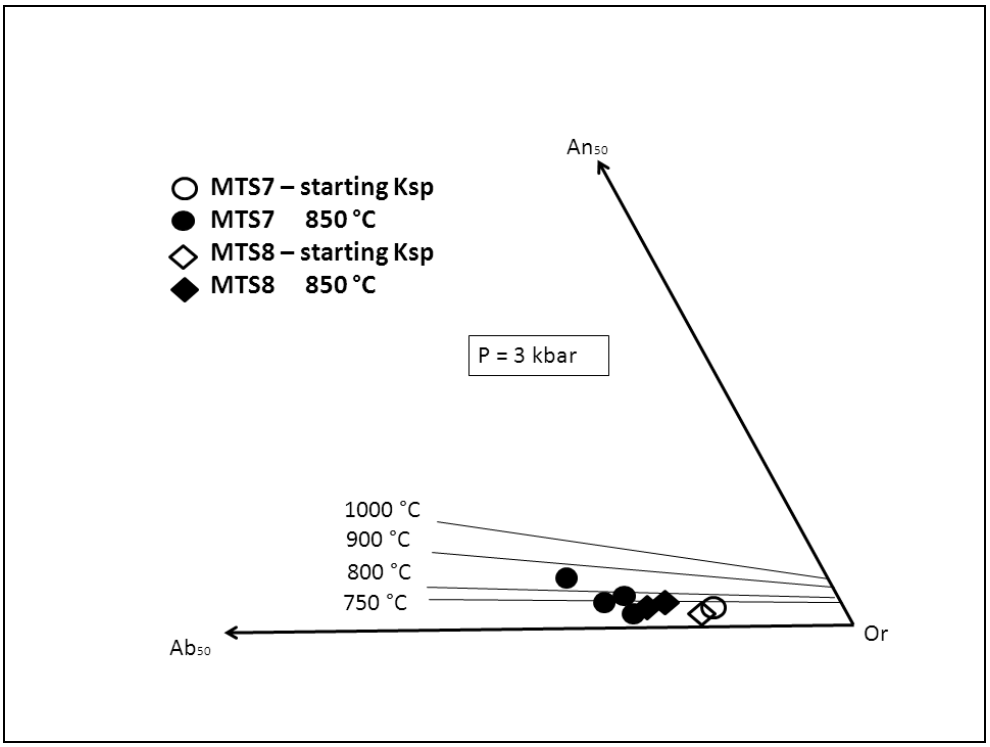

Fig. 5.5: Projection of new feldspar compositions on the Ab-Or-An plane. The projection of the 300 MPa feldspar solvus at 750–1000 °C is from Fuhrman & Lindsley (1988).

5.10 Tourmaline

All the new tourmalines analysed fall within the schorl-dravite-elbaite series, with very little or no vacancy in the X-site (Na + K + Ca) (Table 5.2). The occurrence of a substantial vacancy in the Y-site (Table 5.2) suggests the presence of Li in the run product tourmaline. However, the assumption that the amount of Li substitution should be balanced by the same amount of Al substitution in the Y-site does not hold in all the cases as the vacancy in the Y-site is not always equal to the amount of Al in the Y-site. The starting tourmaline was chemically zoned. Zones that appeared lighter in BSE SEM images (higher average Z) were depleted in Al (present in the Y site), but were enriched in the Fe+Mn+Mg+Ti components (Fig. 5.6). Newly crystallized tourmaline identified in the run products is significantly less compositionally variable than tourmaline in the starting materials, with compositions that cluster closer to a pure dravite-schorl solid solution (Fig. 5.6).

It is common for black schorl, rich in Fe and relatively poor in Al, to crystallize during the first, such as the early-pegmatitic, stages of tourmaline crystallization. As the melting reaction proceeds the tourmaline composition will change accordingly (Sperlich *et al*., 1996; Henry *et al.*, 1999; Akizuki *et al*., 2001; Roda-Robles *et al*., 2004).The chemical zonation is typical of complex geological history which is reflected in multi-staged tourmaline growth, with cores that represent detrital fragments surrounded by metamorphic overgrowths (Henry & Dutrow, 1996, 2001).

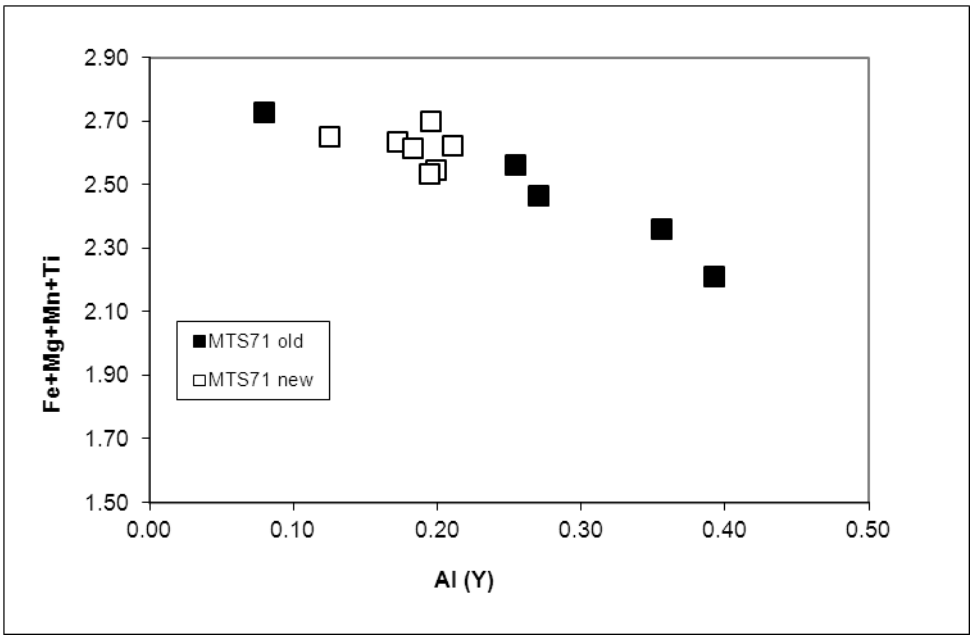

Fig. 5.6: Y site Al plotted against Fe + Mn + Mg + Ti for the residual (old) and new recrystallised (new) tourmaline present in the run products from MTS71 at 850 °C.

5.11 Muscovite

Muscovite is present in the run products in only the 750 ºC runs of samples MST70 and MST71. In both experiments it has shifted composition significantly from that of the starting material, to have lower Mg#, lower total phengitic component and higher Si contents (6.31 to 6.49 and 6.51 cations pfu) (Table 5.2). The Ti concentrations at 750 ºC remain similar to those in the starting materials. Ti incorporation into the muscovite structure may be linked to tschermak ($Ti+Al^{IV} = Si+Al^{VI}$) or phengite ((Fe, Mg, Mn) + Ti = Al^{VI}) component substitutions (Guidotti et al., 1994a; Guidotti & Sassi, 1989). On plots of Ti vs Al^{VI} and Ti + Al^{IV} vs Si + Al^{VI} (Fig. 5.7A,B), that may be used to reflect mineral composition trends indicative of Ti incorporation via the phengitic and tschermakitic substitution respectively, the 750 ºC product muscovite defines similar trends to those in the starting materials for both the mentioned substitution reactions. In both samples, Ti concentrations show no systematic correlation, or very little, with Al^{VI}, despite a clear depletion in the phengitic component in the run product muscovite. In contrast, both samples demonstrate a clear trend consistent with $Ti+Al^{iv}$ depletion and $Si+Al^{vi}$ enrichment towards higher temperatures via the coupled tschermakitic

substitution reaction (Fig.5.7C). On this diagram the compositional shift away from the starting muscovite in both samples is also clear.

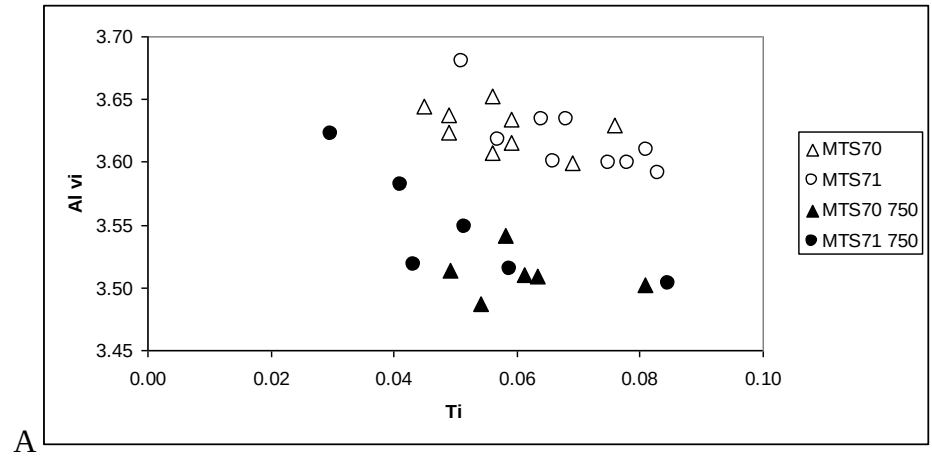

A

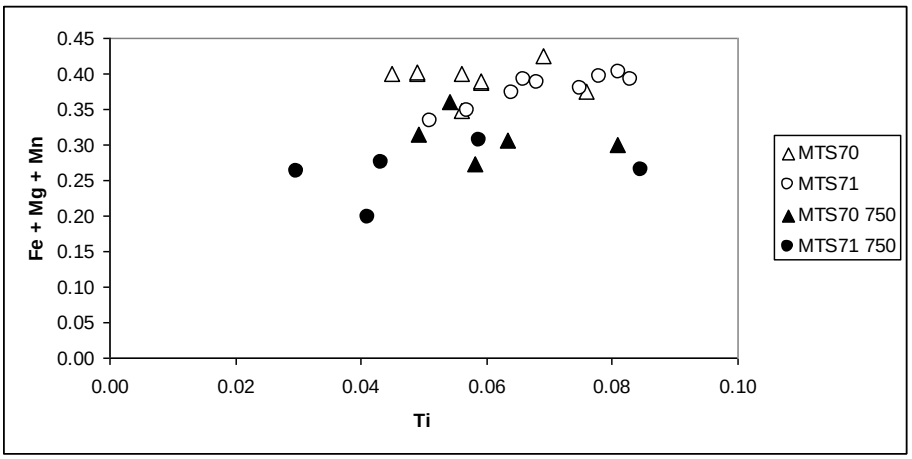

B

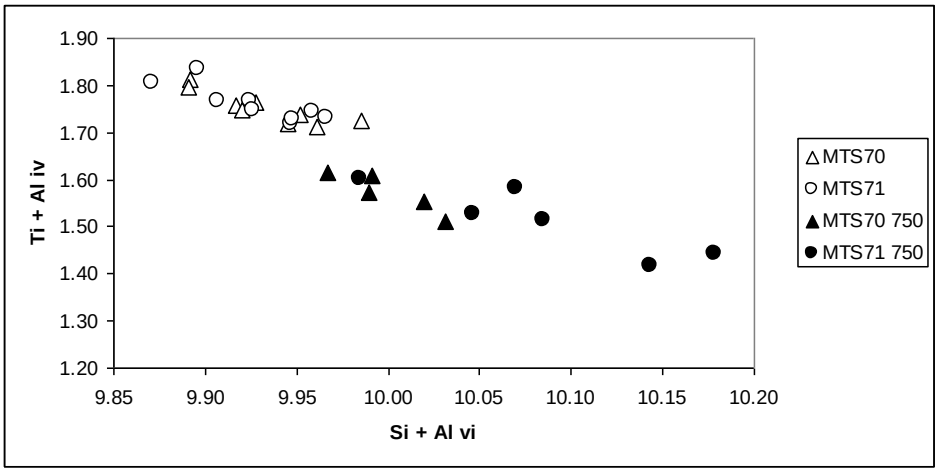

C

Fig. 5.7A-C: Plots of Al^{VI} vs. Ti (A), Ti vs Fe + Mg + Mn (B) and Si + Al^{VI} vs. Ti + Al^{IV} (C) for muscovite in both the starting materials (open symbols) and run products (shaded symbols) from the two mica metapelites at 750 ˚C.

5.12 Melt

Glass compositions from all experiments that produced analysable glass volumes are listed in Table 5.3. Average glass compositions are normalized to 100 wt% for ease of comparison; however, the listed totals are those of the original un-normalized analyses. The analytical conditions and typical standard deviations are discussed in Chapter 4. Compositional variation within the melts was investigated by multiple analyses on glass from different parts of the charge. Significant compositional variation was not detected and the compositions listed represent averages of several analyses that are considered to be typical. The standard deviations (wt%) for each element in these analyses are typically: Na_2O 0.1-0.3, MgO 0.1-0.3, Al_2O_3 0.4-0.6, SiO_2 0.3-1.1, K_2O 0.2-0.8, CaO 0.1, TiO_2 0. 1, MnO_2 0.1, FeO 0.1-0.3. Norms have been calculated with the program Magma, which uses oxide weight percentages, water content and P-T conditions, and ASI values were calculated using an Excel spreadsheet. All the glass compositions are peraluminous and leucocratic, with SiO_2 concentrations of > 70 wt% (Fig. 5.8A-C) and normative Hy contents typically in the range of 2 to 5 wt%. All the glasses have relatively low normative Ab concentrations as a consequence of the plagioclase-poor nature of the Mt Stafford starting materials. In the biotite-only samples, which contain a small plagioclase fraction in the starting material, the glass compositions evolve from relatively Na_2O-rich close to the solidus (e.g. 3.6 wt% Na_2O at 850 ºC in MTS7), to Na_2O-poor compositions at high temperatures and high melt volumes (e.g. 1.8 wt% Na_2O at 1000 ºC in MTS7). In contrast, the plagioclase-free two mica samples produced glasses with low Na_2O concentrations throughout the melting range. The glass compositions produced from these samples are generally more peraluminous than those produced from the biotite-bearing starting materials (Fig. 5.8A-C).

Aluminium Saturation Index (ASI = A/CNK (Clarke, 1981) = molar [$(Al_2O_3/(CaO+Na_2O+K_2O)$]) has recently been shown to be a sensitive function of H_2O concentration, as well as coexisting aluminous mineral assemblage, in haplogranitic melts at 700 to 800 ºC, and 200 MPa (Acosta-Vigil

& London, 2003). Mass balance calculations, based on calculated phase proportions, as discussed below, and ideal H_2O concentrations in biotite, indicate maximum H_2O concentrations in the melt at 800 ºC, of 3.4 to 3.8 wt%. In the case of the biotite-only samples the melt is in equilibrium with cordierite, and in the case of the biotite- and muscovite-bearing metapelites, the melt is in equilibrium with tourmaline and cordierite.

The data of Acosta-Vigil & London (2003) suggest that with this H_2O content at 800 ºC, the melts produced in this study should have a maximum ASI of 1.15 and 1.29, in the biotite-only and biotite- and muscovite-bearing metapelite respectively. These values agree reasonably well with the calculated ASI values for the 800 ºC experiments (Fig. 5.8A-C) and possibly account for the higher ASI values in the tourmaline-bearing samples across the entire melting range.

Table 5.3: Average glass compositions. Standard deviations and analytical conditions are discussed in the text. Cation formulae calculated to 10(O).

Biotite-only metapelites										
Sample			**MTS7**					**MTS8**		
Temp °C	**1000**	**950**	**900**	**850**	**800**	**1000**	**950**	**900**	**850**	**800**
n	**5**	**3**	**3**	**4**	**3**	**3**	**4**	**3**	**3**	**2**
Na_2O	1.70	1.28	2.17	2.34	3.53	1.82	1.98	2.20	2.47	2.30
MgO	0.05	0.13	0.09	0.00	0.78	0.05	0.00	0.14	0.12	0.11
Al_2O_3	10.74	10.24	11.37	11.85	16.23	11.86	10.99	11.29	12.47	13.25
SiO_2	74.38	76.92	72.79	73.84	71.02	71.88	74.45	72.13	70.77	72.70
K_2O	6.75	5.01	6.94	6.28	4.05	7.96	7.23	7.00	6.62	6.69
CaO	0.07	0.06	0.12	0.21	0.76	0.05	0.09	0.09	0.16	0.23
TiO_2	0.42	0.32	0.33	0.19	0.11	0.43	0.33	0.38	0.10	0.37
MnO	0.07	0.02	0.08	0.06	0.03	0.05	0.03	0.02	0.04	0.04
FeO	2.07	2.33	1.35	1.49	2.01	1.92	1.42	1.29	1.65	1.69
Total	96.24	96.32	95.25	96.27	98.52	96.01	96.51	94.55	94.39	97.38
Si	4.22	4.30	4.18	4.18	3.93	4.13	4.21	4.17	4.11	4.09
Ti	0.02	0.01	0.01	0.01	0.00	0.02	0.01	0.02	0.00	0.02
Al	0.72	0.67	0.77	0.79	1.06	0.80	0.73	0.77	0.85	0.88
Fe tot	0.10	0.11	0.06	0.07	0.09	0.09	0.07	0.06	0.08	0.08
Mn	0.00	0.00	0.00	0.00	0.00	0.00	0.00	0.00	0.00	0.00
Mg	0.00	0.01	0.01	0.00	0.06	0.00	0.00	0.01	0.01	0.01
Ca	0.00	0.00	0.01	0.01	0.05	0.00	0.01	0.01	0.01	0.01
Na	0.19	0.14	0.24	0.26	0.38	0.20	0.22	0.25	0.28	0.25
K	0.49	0.36	0.51	0.45	0.29	0.58	0.52	0.52	0.49	0.48
Mg#	4.15	8.75	10.49	0.57	40.99	4.54	0.00	16.36	11.19	10.15
Cat Total	5.74	5.60	5.80	5.77	5.86	5.84	5.77	5.81	5.84	5.82
ASI	1.05	1.06	1.01	1.07	1.25	1.01	0.98	0.99	1.08	1.16

Muscovite-Biotite metapelites									
Sample			**MTS70**				**MTS71**		
Temp °C	**1000**	**950**	**900**	**850**	**800**	**1000**	**950**	**850**	**800**
n	**4**	**4**	**5**	**3**	**5**	**3**	**5**	**4**	**2**
Na_2O	1.11	1.11	1.08	1.18	1.23	2.14	1.76	1.49	1.03
MgO	0.50	0.21	0.18	0.00	0.00	0.63	0.08	0.00	0.12
Al_2O_3	11.91	11.04	11.22	11.43	11.38	13.21	11.68	11.70	13.99
SiO_2	73.92	72.40	72.18	71.93	71.89	66.74	71.27	67.14	65.91
K_2O	5.93	6.62	6.89	6.95	7.69	5.64	4.87	6.17	6.26
CaO	0.13	0.18	0.15	0.14	0.09	0.56	0.44	0.41	0.27
TiO_2	0.69	0.36	0.46	0.26	0.29	0.67	0.38	0.23	0.71
MnO	0.15	0.11	0.08	0.08	0.10	0.09	0.11	0.05	0.05
FeO	3.49	1.80	1.74	1.70	1.46	4.25	2.89	2.50	2.81
Total	97.81	93.84	93.99	93.66	94.12	93.94	93.49	89.69	91.14
Si	4.14	4.20	4.19	4.19	4.18	3.96	4.15	4.11	3.98
Ti	0.03	0.02	0.02	0.01	0.01	0.03	0.02	0.01	0.03
Al	0.78	0.75	0.77	0.78	0.78	0.92	0.80	0.84	1.00
Fe tot	0.16	0.09	0.08	0.08	0.07	0.21	0.14	0.13	0.14
Mn	0.01	0.01	0.00	0.00	0.01	0.00	0.01	0.00	0.00
Mg	0.04	0.02	0.02	0.00	0.00	0.06	0.01	0.00	0.01
Ca	0.01	0.01	0.01	0.01	0.01	0.04	0.03	0.03	0.02
Na	0.12	0.13	0.12	0.13	0.14	0.25	0.20	0.18	0.12
K	0.42	0.49	0.51	0.52	0.57	0.43	0.36	0.48	0.48
Mg#	20.20	17.12	15.71	0.00	0.00	20.92	4.51	0.00	6.81
Cat Total	5.71	5.71	5.72	5.73	5.77	5.89	5.71	5.78	5.79
ASI	1.41	1.18	1.18	1.18	1.25	1.24	1.30	1.18	1.34

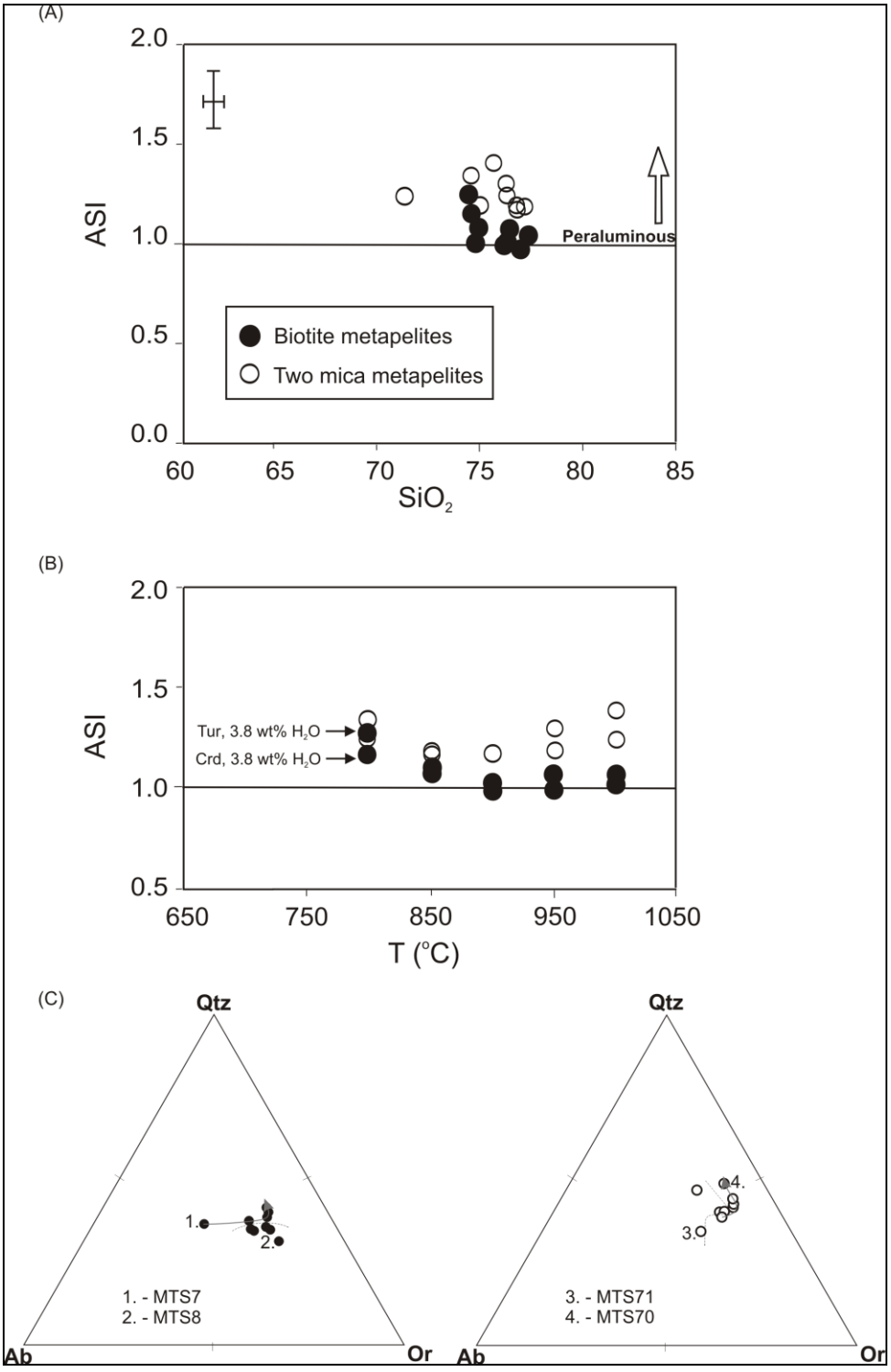

Fig. 5.8 A-C: A) ASI vs. SiO_2 (wt%) in the glasses. B) A plot of ASI variation as a function of temperature in the glasses. The arrows represent calculated ASI values, based on the formulae proposed by Acosta-Vigil and London (2003), for melts at 800 ˚C with 3.8wt% dissolved H_2O and coexisting with cordierite (Crd) and tourmaline (Tur). C) Normative Qtz-Ab-Or plots for the glasses produced in this study. The glasses in MTS7 and MTS70 show compositional evolution away from Ab and towards Qtz, with increasing temperature. These are indicated with arrows and are consistent with the presence of quartz in most of the high temperature experiments, as well as the preferential partitioning of plagioclase, in the case of MTS7, and Na-bearing tourmaline, in the case of MTS70, into the first melts.

5.13 Evaluation of equilibrium

If we revisit Fig 1.2 in Chapter 1 the typical subsolidus muscovite breakdown (Mu + Qtz = Ksp + Sill + H_2O) occurs at a temperature between 650 °C (at 4 kbar), followed by wet biotite melting (Bt + H_2O + Ksp + Sill = Melt + Spl + Crd) in experiments at appropriately high temperatures (725 to 750 °C). The muscovites and biotites in the Mt Stafford two mica samples seem to be thermally stable when compared to the above scenario.

To confirm equilibrium has been achieved in the experiments existing SEM-EDS data sets for all the starting materials and the 750 ºC experimental run were used to determine minor and trace element partitioning between coexisting biotite-melt, cordierite-melt, feldspar-melt and muscovite-melt pairs. Sample MTS70 was used for biotite-muscovite partition coefficients due to the abundance of biotite and muscovite in this sample and in the experimental run products. These data can give insight on mineral-melt partitioning in the experiments and can be compared to an experimental (water-present, 600-750 °C, 2 kbar) partitioning study in synthetic aluminous gneisses and metapelites containing muscovite-quartz-albite-biotite-aluminum silicate-cordierite assemblages of Icenhower and London (1995) and data from the natural Macusani peraliminous partial melts, Peru (London et al., 1988; 1989; Pichavant et al., 1987, 1988). Empirical partition coefficients are displayed as the weight concentration of the element of interest in biotite, feldspar, cordierite or muscovite divided by its concentration in glass, biotite or muscovite. These are according to recommendations by Beattie et al. (1993) and are denoted as $D(M)^{Bt/gl}$, $D(M)^{Bt/Mu}$ or $D(M)^{Mu/gl}$, where M = element of interest. Partition coefficients determined in this study are listed in Table 5.4a, b, c and d. Mineral composition data from Table 5.2 was used for these calculations. Due to the small crystal sizes, EMP analysis (Appendix 4) were the only method used to obtain minor and trace element data from these muscovite-biotite pairs. The crystals were too small for LA-ICP-MS analysis for analysis of the ultra-trace elements. As discussed previously, the system is saturated in Ti-, Si- and Al- oxides, as these

minerals under investigation occur with quartz, Al-silicates and ilmenite. Micas were not zoned and care was taken to avoid obvious cleavages to obtain the best results.

Table 5.4a: Biotite/Glass partition coefficients

Biotite/Glass	mts7	mts7	mts8	mts8	mts8	mts70	mts70	mts71	Icenhower& London 1995	Pichavant et al. 1988
Temperature	850	800	900	850	800	850	800	800	650	650
D(Na)bt/gl	0.3	0.3	0.2	0.2	0.3	0.4	0.3	0.4	0.11-0.23	
D(Al)bt/gl	1.5	1.1	1.4	1.4	1.4	1.5	1.4	1.3	1.3-1.4	
D(Si)bt/gl	0.5	0.5	0.6	0.5	0.5	0.5	0.5	0.6	0.55-0.60	
D(K)bt/gl	1.5	2.3	1.3	1.4	1.4	1.3	1.3	1.6	1.69-2.5	
D(Ti)bt/gl	10.2	3.1	37.0	13.8	10.9	13.6	35.4	11.6	4-27.33	80.75
D(Fe)bt/gl	320.4	708.7	632.3	520.1	417.8	199.2	172.4	448.8	16.8-23.6	39.91
D(Mg)bt/gl	1877.2	10.9	85.6	73.9	94.3			41.6	37.6-133	210

$D(M)^{bt/gl}$ show very good correspondence in general with data from the synthetic metapelite experimental study of Icenhower and London (1995) and the natural peraluminous volcanic partial rhyolites from Macusani, Peru (London et al., 1988; 1989; Pichavant et al., 1987, 1988) (Table 5.4a). From the $D(M)^{bt/gl}$ it is clear that Ti, Mg and Fe partition very strongly into the biotite over the melt phase, which is confirmed by the Icenhower and London (1995) study. $D(Ti)^{bt/gl}$ = 4-27.33 (Icenhower and London, 1995) and 80.75 (Macusani volcanics) and ranges between 3 and 36.07 in this study. The exact values do not agree with other studies and are dependent on bulk compositions between the four starting materials. They increase with increasing temperature for all four Mt Stafford starting compositions. $D(Mg)^{bt/gl}$ = 10-94.28 (the value of 1877 in this study is due to the very low Mg contents in the glass and is probably not a good indication of the true partition coefficient) for Mt Stafford, Icenhower and London (1995) reported $D(Mg)^{bt/gl}$ = 37.6-133 and the $D(Mg)^{bt/gl}$ for Macusani = 210. $D(Fe)^{bt/gl}$ = 199.16-708.71 reported in this study (16.8-23.6 was reported by Icenhower and London (1995) and Macusani $D(Fe)^{bt/gl}$ = 39.91) does not compare to the other studies.

D(Al)bt/gl = 1.09-1.54 and D(K)bt/gl = 1.29-2.26 indicate that Al and K partitions preferentially into biotite over glass. Values are consistent, with no trend observed with a rise in temperature. Similar values of $D(Al)^{bt/gl}$ = 1.3-1.4 and $D(K)^{bt/gl}$ = 1.69-2.5 were reported by Icenhower and London (1995). The $D(Na)^{bt/gl}$ is 0.25-0.39 and the $D(Si)^{bt/gl}$ is 0.48-0.59 and both Na and Si partition rather into glass than biotite and correspond to the values of Icenhower and London (1995) of $D(Na)^{bt/gl}$ = 0.11-0.23 and a $D(Si)^{bt/gl}$ = 0.55-0.60.

Table 5.4b: Felspar/Glass partition coefficients

Ksp/Glass	MTS7	MTS7	MTS7	MTS8	MTS8	MTS8	MTS8
Temperature	850	850recr	800	1000	850	850recr	800
D(Na)ksp/gl	1.06	0.97	0.65	0.82	1.06	1.14	1.04
D(Al)ksp/gl	1.59	1.49	1.05	1.41	1.44	1.53	1.31
D(Si)ksp/gl	0.87	0.88	0.89	0.91	0.92	0.91	0.88
D(K)ksp/gl	2.10	2.20	2.20	1.89	2.03	2.05	1.94
D(Ca)ksp/gl	0.64	0.14	0.00	0.00	0.00	0.93	0.00
D(Ti)ksp/gl	1.19	0.96	0.00	0.36	1.43	0.48	-
D(Fe)ksp/gl	0.19	0.39	0.25	0.05	0.17	0.23	1.21

The partition coefficients between feldspar and glass (Table 5.4b) indicate that Al and K partition into feldspar rather than glass. The $D(Al)^{fsp/gl}$ is 1.05-1.59 and no real trend is observed with increasing temperature. The $D(K)^{fsp/gl}$ is 1.89-2.2 and no trend is observed with increasing temperature. Na partitions more readily into feldspar than glass in some cases, but the values are mostly close to 1 with $D(Na)^{fsp/gl}$ = 0.65-1.07 which means that Na does not partition preferentially into one phase or another. A slight increase in D with temperature is observed for all the starting materials. The $D(Si)^{fsp/gl}$ is 0.88-0.92 and Si partitions preferentially into glass over feldspar and no real variation is observed. The $D(Fe)^{fsp/gl}$ is 0.05-0.29 and Fe partitions strongly into glass over feldspar. The $D(Ti)^{fsp/gl}$ is quite variable as it is close to detection limits in feldspar and glass.

Table 5.4c: Cordierite/Glass partition coefficients

Cordierite/Glass	MTS7	MTS7	MTS8	MTS8	MTS70	MTS70	MTS70	MTS70	MTS70	MTS71	MTS71	MTS71	MTS71
Temperature	1000	950	1000	950	1000	950	900	850	800	1000	950	850	800
D(Na)crd/gl	0.2	0.4	0.4	0.3	0.5	0.3	0.6	0.4	0.3	0.3	0.3	0.4	0.8
D(Al)crd/gl	3.0	3.3	2.6	3.0	2.8	3.0	2.9	2.8	2.9	2.5	2.8	2.8	2.1
D(Si)crd/gl	0.7	0.6	0.7	0.7	0.6	0.7	0.7	0.7	0.7	0.7	0.7	0.7	0.8
D(K)crd/gl	0.1	0.0	0.2	0.2	0.1	0.1	0.1	0.1	0.1	0.1	0.1	0.1	0.2
D(Ca)crd/gl	0.0	0.6	0.2	0.0	0.2	0.3	0.3	0.8	1.0	0.0	0.2	0.2	0.7
D(Ti)crd/gl	0.0	0.0	0.2	0.8	0.0	0.0	0.0	0.3	0.0	0.2	0.0	0.0	1.1
D(Mn)crd/gl	1.7	0.0	3.6	7.1	1.7	2.5	4.8	5.8	5.0	1.5	0.8	2.1	3.5
D(Fe)crd/gl	3.5	3.2	3.5	4.9	2.3	3.9	4.3	6.6	6.0	2.0	2.9	4.0	4.3
D(Mg)crd/gl	180.4	75.6	171.7	-	17.2	45.1	46.2	-	-	13.0	107.4	-	34.3

The partition coefficients between cordierite and glass (Table 5.4c) indicate that Mg partitions preferentially into cordierite rather than into glass with a $D(Mg)^{crd/gl}$ of 13-180. The Mg values are dependent on bulk rock composition and are close to detection limits in the glass, therefore the $D(Mg)^{crd/gl}$ will always be very large. The data do not show significant trends with increasing temperature. The $D(Fe)^{crd/gl}$ is 2.3-6.6 and shows a consistent decrease for both MTS70 and MTS71 with increasing temperature. This trend has also been observed by Guidotti (1977) and the partitioning of Mg and Fe from cordierite into the glass phase plays an important role in the $D(Ti)^{biot/mu}$, even more so than the $D(Mg/Fe)^{mu/bt}$. Al partitions preferentially into cordierite rather than into glass with a $D(Al)^{crd/gl}$ of 2.1-3.3 and no trends were observed with an increase in temperature. The $D(Mn)^{crd/gl}$ is quite variable due to the close proximity of Mn abundances to the detection limits, but Mn partitions into cordierite rather than glass. Na, Si, K, Ca and Ti strongly partition rather into glass than cordierite.

Table 5.4d: Mt Stafford MTS70 biotite/muscovite partition coefficients

Sample D(M)bt/mu	Mt Stafford starting material n=5		Mt Stafford: 750 C, 3.2 kbar n=10	
	Average	Stdev	Average	Stdev
D F	1.80	0.94	1.79	0.52
D Cl	3.16	2.70	2.81	1.91
D Si	0.78	0.02	0.80	0.08
D Ti	3.08	0.16	3.47	0.58
D Al	0.52	0.02	0.56	0.05
D Fe	11.81	1.13	11.80	3.07
D Mn	5.50	1.30	9.50	6.97
D Mg	5.29	0.38	5.45	1.50
D Ca	31.89		6.33	0.50
D Na	0.20	0.10	0.80	0.44
D K	0.79	0.09	0.76	0.18
D Cr	1.03	0.47	0.98	0.20

Table 5.4e: Biotite/muscovite partion coefficients from previous experimental studies on metapelites or peraluminous granites.

Study	**Experimental Studies**						
Conditions	Metapelite synthetic mix 490-680 C, 7-12kbar		650, 2 kbar	700, 2kbar	650 C, 2 kbar	**Avg**	**Std Dev**
D(M)bt/mu	Yang&Rivers 2000 Greenschist	Yang&Rivers 2000 Amphibolite	Icenhower& London 1995 Granite	Icenhower& London 1995 Granite	Pichavant et al 1988 Two-mica Al Silicate volcanics		
D F			1.30	1.60		**1.45**	**0.21**
D Cl							
D Si							
D Ti			3.30	5.90	12.00	**7.07**	**4.47**
D Al							
D Fe			4.50	7.80	19.70	**10.67**	**8.00**
D Mn	20.62	24.18	5.00	3.60	2.80	**11.24**	**10.30**
D Mg			3.50	5.80	52.50	**20.60**	**27.65**
D Ca							
D Na	0.48	0.28				**0.38**	**0.14**
D K							
D Cr	0.95	2.53				**1.74**	**1.12**

Table 5.4f: Biotite/muscovite partion coefficients from previous studies on natural metapelites or peraluminous granites compared to Mt Stafford MTS70.

Study	Natural Rock data					Mt Stafford MTS70	
Conditions	Sillimanite zone	Pegmatite	Granitoids	Avg	Std Dev	Aluminous metapelite	750 C, 3.2 kbar
D(M)bt/mu	Dahl et al 1993	Shearer et al 1986	Neiva et al 1987			Mt Stafford MTS70 starting material	Mt Stafford MTS70
D F		2.00	1.70	**1.85**	**0.21**	1.80	1.79
D Cl						3.16	2.81
D Si						0.78	0.80
D Ti	2.90		5.60	**4.25**	**1.91**	3.08	3.47
D Al						0.52	0.56
D Fe	14.00		17.00	**15.50**	**2.12**	11.81	11.80
D Mn	16.96			**16.96**	**-**	5.50	9.50
D Mg			9.50	**9.50**	**-**	5.29	5.45
D Ca						31.89	6.33
D Na	0.20			**0.20**	**-**	0.20	0.80
D K						0.79	0.76
D Cr	1.00			**1.00**	**-**	1.03	0.98

The standard deviation values of the partition coefficients for Biotite/Muscovite over the range of other studies are very large, making the averages of little real collective value. This indicates that there are relatively few pulished trace element partitioning studies for biotite-muscovite pairs in metamorphic systems to compare to this study. Most of these data sets have also been obtained from bulk analysis of mineral separates unlike this study.

The Mt Stafford MTS70 starting material partition coefficients between biotite and muscovite of F (1.8±0.94), Ti (3.08±0.16), Fe (11.81±1.13), Mn (5.5±1.3), Mg (5.29±0.38), Na (0.2±0.1) and Cr (1.03±0.47) corresponds well with the other studies (Table 5.4d, e, f) on peraluminous systems. Similar corresponding results is seen in the MTS70 750 ºC, 3.2 kbar experimental run product

partition coefficients between biotite and muscovite of F (1.79±0.52), Ti (3.47±0.58), Fe (11.80±3.07), Mn (9.50±6.97), Mg (6.33±2.36), Na (0.80±0.44) and Cr (0.98±0.2). F, Cl, Ti, Fe, Mn and Mg partition into biotite rather than muscovite, but Si, Al, Na, K and Cr partitions into muscovite rather than biotite. The trends and absolute values agree with biotite-muscovite partition coefficients determined by Dahl et al. (1993) and Yang and Rivers (2000) (Table 5.4 f).

The $D(F)^{bt/mu}$ obtained in this study are in very good agreement with those of the other studies, in that $D(F)^{bt/mu}$ is independent on temperature and varied insignificantly between 1.80 and 1.79 from the starting material to the higher temperature experimental run at 750 ºC. In the absence of melt, the micas are in equilibrium with respect to $F^- \leftrightarrow OH^-$ exchange. Due to the similarity in slope of F^- and OH^- substitutions in the micas, their partitioning is independent of temperature and composition and they pose the ideal situation to test if equilibrium has been reached (Munoz, 1977). After melting commences F^- is strongly partitioned into the melt phase (Icenhower and London, 1995), but the results discussed are from below the solidus. Cl partition coefficients are often not reported in other studies due to the general low abundances of Cl in the micas. A small change from 3.16 to 2.81 is seen in the $D(Cl)^{bt/mu}$ for Mt Stafford, but it is not clear if this is significant enough to indicate disequilibrium in the experiments as there is no data to compare the results with.

As expected according to Guidotti et al. (1977) and Kwak (1968) the $D(Ti)^{bt/mu}$ increase from 3.08 to 3.47 from the starting material to the higher temperature in MTS70. The partition coefficients of Al, Mg and Mn also increase with increasing temperature. Fe does not show any significant increase in partitioning towards higher temperature. Crystallisation of cordierite (major bulk changes) may influence the partitioning more than the Mg/Fe ratios in biotite or muscovite (Guidotti et al., 1977), but cordierite only started to crystallise with melt in the 800 ºC experiments and could not have had a

larger influence on $D(Ti)^{bt/mu}$ than the expected Ti increase in the micas (Guidotti et al., 1977). $D(Ti)^{biot/mu}$ is strongly controlled by concentration of Mg in muscovite (Yang and Rivers, 2000), which is dependent on metamorphic temperature (Yang and Rivers, 2000; Guidotti et al., 1977) and is reflected in the muscovite trends of this study (Fig 5.7a).

5.14 Sillimanite-(Mullite) phases

Al-Si oxides, commonly known as sillimanite (possibly mullite), were produced in the muscovite-tourmaline bearing samples MTS70 and MTS71. In MTS70 these oxides are present from 800 to 1000 ˚C, in MTS71 from 850 to 1000 ˚C, and are spatially associated with tourmaline and muscovite breakdown (Fig 5.9). Their spatial association with tourmaline can be attributed to a local excess of Al as a result of the tourmaline melting reaction. These Al-Si oxide minerals were difficult to analyse and characterise due to small crystal sizes and possible melt inclusions. Consequently, some listed analyses include minor amounts of Si, Na and K that are interpreted to reflect contamination from the surrounding glass (Table 5.5), and in other cases, reasonably good quality, and representative data could not be obtained due to this problem. Despite these difficulties, the available data indicate that the Al-Si oxide compositions produced are close to the stoichiometry of sillimanite (MTS70 and MTS71) and some corundum (MTS71 850 ºC), with the rare occurrence that barely resembles true mullite. Similar phases were identified by Icenhower and London (1995) in longer runs (4 weeks) and in reverse partial melting experiments on Al-rich greywackes and metapelites, so these phases are not necessarily an indication of disequilibrium conditions. The Al-Si oxide compositions vary slightly across the experimental range, but do not show any consistent trends with increasing temperature. Some melt contamination is evident in most analyses as seen from the small amounts of K, Na and Ca oxides occurring with Al and Si oxides.

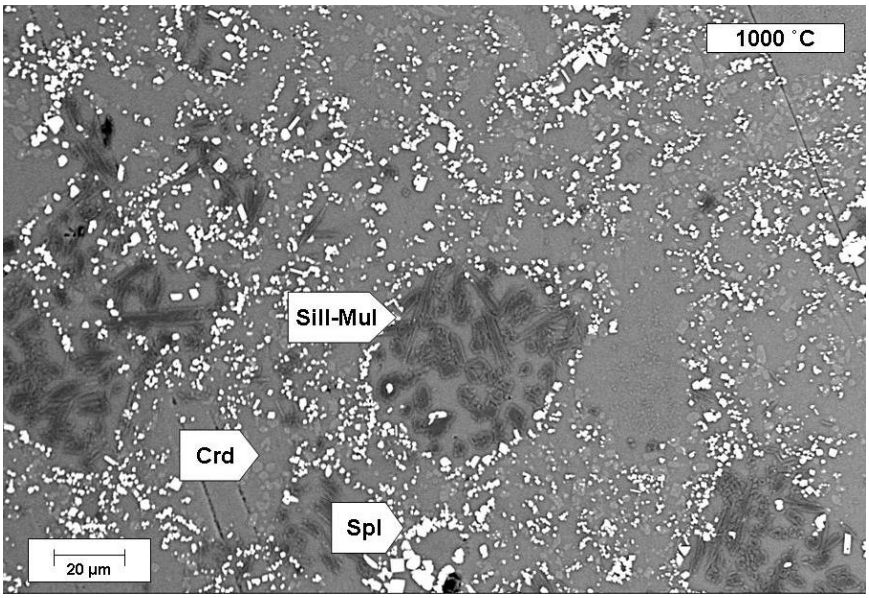

Fig. 5.9: Back scattered SEM image of typical Al-Si oxides or sillimanite-mullite needles in the run product from MTS70, one of the tourmaline bearing samples.

Table 5.5: Sillimanite (possibly Mullite) compositions (5 Oxygens) from MTS70 and MTS71.

Sillimanite-Mullite	MTS70		MTS71	
Temp (°C)	900	800	1000	900
Na_2O	0.41	0.00	0.23	0.00
MgO	0.00	0.00	0.00	0.00
Al_2O_3	63.52	64.55	63.29	68.00
SiO_2	36.45	31.18	36.74	24.80
K_2O	0.00	0.00	0.34	0.00
CaO	0.00	0.00	0.00	0.18
TiO_2	0.00	0.00	0.00	3.18
FeO	0.37	0.42	0.41	1.37
Total	100.76	96.16	101.00	97.53
Si	0.98	0.88	0.99	0.70
Ti	0.00	0.00	0.00	0.07
Al	2.01	2.15	2.00	2.28
Fe tot	0.01	0.01	0.01	0.03
Mn	0.00	0.00	0.00	0.00
Mg	0.00	0.00	0.00	0.00
Ca	0.00	0.00	0.00	0.01
Na	0.02	0.00	0.01	0.00
K	0.00	0.00	0.01	0.00
Cat Total	3.02	3.04	3.02	3.09

5.15 Phase proportions of the biotite vs two-mica metapelites

Phase proportions were determined for all the run products by a combination of image analysis and least squares mixing routine that used the compositions listed in Tables 5.1, 5.2 and 5.3, and that yielded maximum sum of squared residual (r^2) values of 0.7 (MTS71 at 1000 ºC). A spreadsheet was designed to use the oxide wt% to calculate the phase proportions for a least squares mixing routine. The software was prompted to calculate phases that were identified in the run products during SEM investigations. The results are summarized in Table 5.6 and in Figure 5.10 (A, B), and indicate that each sample presents a unique situation, with the melting behaviour being a function of the minerals and mineral proportions presented by the starting material.

Table 5.6: Phase proportions for all the run products as calculated by a least squares mixing routine.

MTS70

Temp °C	**1000**		**950**		**900**		**850**		**800**		**750**
r^2	**0.576**		**0.168**		**0.341**		**0.659**		**0.225**		**0.199**
Melt	80	Melt	72	Melt	69	Melt	66	Melt	59	Qtz	39
Spn	9	Qtz	6	Qtz	6	Qtz	9	Qtz	12	Tu	17
Al_2SiO_5	1	Spn	10	Spn	9	Spn	10	Spn	7	Mu	29
Crd	10	Al_2SiO_5	1	Al_2SiO_5	1	Crd	13	Crd	2	Biot	16
		Crd	10	Crd	14	Biot	1	Tu	16		
								Biot	4		

MTS71

Temp °C	**1000**		**950**		**900**		**850**		**800**		**750**
r^2	**0.7**		**0.596**		**0.358**		**0.215**		**0.486**		**0.135**
Melt	43	Melt	42	Melt	39	Melt	36	Melt	22	Qtz	57
Qtz	38	Qtz	39	Qtz	41	Qtz	44	Qtz	48	Ksp	3
Spl	3	Spl	2	Spl	3	Spl	2	Spl	1	Tu	24
Al_2SiO_5	4	Al_2SiO_5	4	Al_2SiO_5	4	Al_2SiO_5	6	Al_2SiO_5	4	Mu	13
Cord	12	Cord	13	Cord	12	Cord	10	Ksp	3	Biot	4
						Tu	1	Tu	20		
								Biot	2		

MTS7

Temp °C	**1000**		**900**		***850***		**800**		**750**
r^2	**0.082**		**0.012**		**0.392**		**0.254**		**0.735**
Melt	74	Melt	49	Melt	8	Melt	3	Qtz	38
Qtz	8	Qtz	22	Qtz	38	Qtz	41	Al_2SiO_5	7
Spl	5	Spl	2	Spl	3	Spl	1	Cord	8
Al_2SiO_5	2	Al_2SiO_5	8	Al_2SiO_5	7	Al_2SiO_5	8	Ksp	19
Cord	10	Cord	1	Cord	10	Cord	9	Plag	5
		Ksp	8	Ksp	15	Ksp	16	Biot	22
		Biot	10	Biot	18	Biot	22		

MTS8

Temp °C	**1000**		**950**		**900**		**850**		**800**		**750**
r^2	**0.650**		**0.253**		**0.490**		**0.234**		**0.143**		**0.349**
Melt	65	Melt	49	Melt	39	Melt	9	Melt	9	Qtz	29
Qtz	5	Qtz	9	Qtz	14	Qtz	27	Qtz	26	Al_2SiO_5	13
Spn	12	Spl	10	Spl	9	Spl	6	Spl	5	Crd	1
Crd	17	Crd	13	Al_2SiO_5	9	Al_2SiO_5	9	Al_2SiO_5	9	Ksp	24
Ksp	2	Ksp	12	Crd	3	Crd	1	Crd	1	Plag	3
		Biot	8	Ksp	20	Ksp	27	Ksp	26	Biot	30
				Biot	6	Biot	21	Plag	3		
								Biot	22		

For example, comparing the melting behaviour of the two muscovite- and biotite-bearing samples (MTS70 and MTS71) with that of the two biotite-bearing samples (MTS7 and MTS8) (Fig. 5.10 A,B) shows that the muscovite-bearing compositions melted more, at lower temperatures, than the muscovite-free samples. This is predictable and broadly consistent with the findings of partial melting

studies on similar compositions at higher pressures (Gardien *et al*., 1995). However, at high temperatures (> 900 ºC), the very quartz-rich nature of MTS71 dictates that melt proportions is lower than in the two muscovite-free samples. Sample MTS70 produced the most melt (79 %), as could be predicted from the mica-rich nature of the starting material (35 % muscovite + biotite). This sample also produced 59 % melt at 800 ºC, compared to 1-13 % melt in all the other samples. The difference in melt proportions between MTS70 and MTS71 at 800 °C are significant. MTS70 contained 26 % muscovite and produced 59 % melt at this temperature. In contrast, MTS71 contained 17 % muscovite and produced only 22 % melt. This difference can be explained in terms of the biotite proportions in the two samples. The MTS71 starting material contained 3 % biotite, and this decreased to 2 % in the 800 ºC run products. In contrast, MTS70 contained 18 % and this proportion had decreased to 4 % in the 800 ºC run products. Biotite of similar composition melted little in the two muscovite-free samples over the same temperature interval, demonstrating the link between muscovite and biotite melting in the two mica samples. Sharp increases in the slope of the melt production curves for samples MTS70 and MTS71 occur in the temperature intervals that coincide with muscovite melting (Fig. 5.10 A,B), but more gradual curves follow the consumption path of biotite in these samples following muscovite breakdown, as well as in the muscovite-free samples (Fig. 5.10). This reflects the wider temperature range of biotite melting brought about by the more divariant character of this reaction. Overall, the patterns of melt proportion variation with temperature demonstrate that, within broadly similar compositions, melt proportion at very high temperatures is largely a function of bulk rock water content (as attributed by the hydrous minerals), but that at temperatures more consistent with natural low-T, low-P metamorphism (750 to 900 °C), it is a function of the nature of the mica assemblage in the samples.

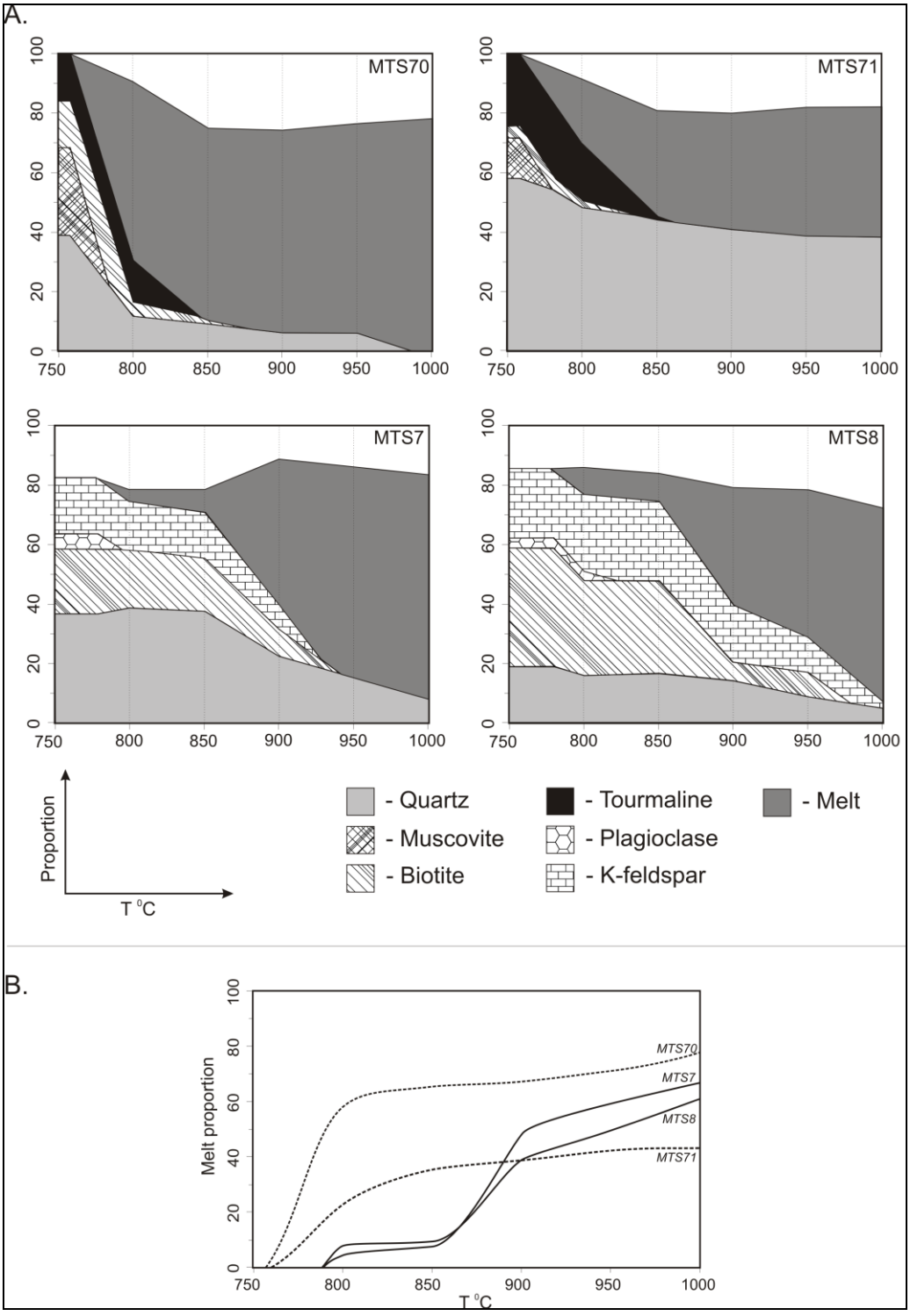

Fig. 5.10A, B: Phase proportions in the run products expressed as a function of temperature. A) Melt proportions relative to those of the principal reactant minerals in the four samples. The unshaded area represents cordierite. B) A comparison of the melt proportion variations as a function of temperature in the four samples. This highlights the relatively low temperature melt production in the two mica metapelites, the pulse of melt production from the biotite metapelites between 850 and 900 ˚C, and the control of melt fraction at very high temperature by bulk rock water content

Chapter 6: Discussion of experimental results

The general lack of relevant fluid-absent experimentation at low pressures (< 5 kbar) led to this study at Mt Stafford, a high temperature low pressure partial melting terrane where melting started at low pressure relatively low temperatures. To better understand the complex interplay between bulk rock geochemistry, mineralogy and possible melting in the andalusite stability field, the initial general aims of this study were:

1. To use an experimental approach to build on the previous field and phase relationship research in the Mt Stafford region and to demonstrate that fluid-absent melting of natural metapelites can occur at low pressure over a range of temperatures under specific circumstances, 2. To counter the general lack of experimental knowledge in high temperature, low pressure fluid-absent partial melting terranes; and 3. To investigate the phase relationships of the micas and the possible metastability of andalusite in the Mt Stafford metasediments that has been used to explain the occurrence of andalusite in leucozome.

In combination, the phase proportion variations and phase relationships in the run products that are detailed in Chapter 5, suggest several interesting results from these experiments. Due to all the interesting findings, the three initial aims are expanded upon in a lot more detail in this chapter. The following headings are thus discussed: (1) equilibrium in the experiments; (2) the high temperature fluid-absent melting of muscovite; (3) the refractory nature of the evolved biotite compositions in the biotite-bearing samples; (4) the lack of an obvious boron related melt fluxing effect near the solidus; (5) the implication of these findings for interpreting low-pressure fluid-absent partial melting in in the “andalusite stability field” in the Mt Stafford area and (6) proposals for future work.

6.1 Equilibrium in the experiments

Due to the high melting temperature of the muscovite and biotite in these rocks, the possibility of disequilibrium has been investigated by evaluating the muscovite – biotite and mineral – melt partition coefficients. The steep positive slope of the muscovite melt reaction makes it nearly temperature independent, allowing extrapolations of low pressure synthetic metapelite studies (such as Icenhower and London, 1995) to those studies at higher pressures (Mt Stafford = 3.2 kbar experiments). Few data sets exist for peraluminous magmas, but Pichavant et al. (1988) reported trace element compositions of biotite, muscovite and glass from the peraluminous Macusani volcanic field, Peru (London et al., 1988; 1989; Pichavant et al., 1987, 1988). Some of these analyses were, however, conducted on mineral separates, and not necessarily involving crystal-glass phases at equilibrium. Walker et al. (1986, 1989) estimated muscovite partition coefficients by dividing average biotite-melt partition coefficients (determined on natural metaluminous compositions) into biotite-muscovite element ratios determined by Shearer et al. (1986) in pegmatites from the Black Hills, South Dakota. It is evident that biotite -melt partitioning data for the major and trace elements of peraluminous systems are not well established and is very much dependent on bulk compositions, but the partitioning data between biotite and melt presented in this study are in good agreement with those of previous studies giving confidence that equilibrium has been obtained during the runs.

Biotite-muscovite pairs in the starting material MTS70 and the 750 °C experiment were compared with literature studies on biotite-muscovite pairs in metapelites. There are relatively few pulished trace element partitioning studies for biotite-muscovite pairs in metamorphic systems (Butler, 1967; Moorbath et al., 1968, Dutrow et al., 1986; Shearer et al., 1986; Hervig and Peacock, 1989, Dahl et al., 1993; Domanik et al., 1993) and most of these data sets have been obtained from bulk analysis of mineral separates, which have commonly proved to be contaminated with micro-inclusions of accessory minerals (Michael, 1988). Very little is known about the dependence of the biotite-

muscovite distribution coefficients on the internal and external factors, so a largely empirical approach has to be adopted when evaluating the data. Finding exact reliable analogues to the data in this study is difficult, but the data agree reasonably well with what has been reported by other studies. There is a remarkable consistency and agreement between the natural, experimental data in Mt Stafford and also amongst the data of the various studies. Overall, minor and trace element distributions for biotite/muscovite pairs should be systematic over a range of increasing temperatures (Yang and Rivers, 2000) and should correlate to bulk compositions (Guidotti et al., 1977; Dahl et al., 1993; Yang and Rivers, 2000) which would indicate equilibrium has been obtained in the experiments. These trends were displayed in accordance with previous studies for the Mt Stafford experiments. Data from Dahl et al. (1993) reveals systematic element distributions across a wide thermal-compositional range that are governed by the crystal structure of the micas and their major element compositions. Increasing trends in $D(Ti)^{bt/mu}$ with temperature is consistent with trends in muscovite Mg compositions and trends observed by Guidotti et al. (1977), Kwak (1968) and Yang and Rivers (2000).

Despite the agreement shown between Mt Stafford partition coefficients and those from the various literature studies, the starting materials muscovite and biotite probably had enough time to equilibrate at 750 ^{o}C during the experiments and so should be in partitioning agreement with other natural high grade rocks. What is important to note is that partitioning in natural rocks does change with the ~ 80 ^{o}C higher temperature stability field that has been observed for the muscovite and biotite in the run products. The large ranges observed in partitioning data from this study and various workers do not give the necessary support that the experiments did reach equilibrium as muscovite in the field at Mt Stafford was observed to have melted at relatively low temperatures. Disequilibrium conditions can not be ruled out completely on the partitioning data presented here.

6.2 The high temperature melting of muscovite

There is a general agreement between the partitioning data of Mt Stafford micas and other studies, but a disagreement with the observed behaviour of muscovite in the field at Mt Stafford. The high temperature melting of muscovite is possibly due to disequilibrium in the experiments, but the composition of muscovite is nevertheless very interesting and needs further discussion. Model system predictions of the melting behaviour of the two muscovite- and biotite-bearing samples involve subsolidus muscovite breakdown (Mu + Qtz = Ksp + Sill + H_2O) at a temperature below 650 °C, followed by wet biotite melting (Bt + H_2O + Ksp + Sill = Melt + Spl + Crd) in experiments at appropriately high temperatures (700 to 750 °C). The melting behaviour of the two natural muscovite- and biotite-bearing rocks at Mt Stafford differs significantly from the above scenario because of the apparent thermal stability of muscovite. In natural rocks, F, Ti, Fe and Mg contents in muscovite (Cipriani *et al*., 1971; Green, 1981; Pichavant *et al*., 1988; Guidotti & Sassi, 1989; Guidotti *et al*., 1994; Vidal *et al*., 2001, Henry *et al*., 2005, Herman & Spandler, 2008, Auzanneau *et al.*, 2009) and Ti contents in biotite (Dalmeyer, 1974; Patińo-Douce & Beard, 1995; Stevens *et al*., 1997; Henri & Guidotti, 2002, Auzanneau *et al.*, 2009) can be correlated with metamorphic grade and are interpreted to enhance the thermal stability of these minerals. Ti concentrations in the micas are considered to reach maximum values when buffered by the presence of a Ti-rich phase. All the starting compositions contained ilmenite, which was also present as an accessory phase in most experiments. In addition to this, the biotite and muscovite in MTS70 and MTS71 contained close to 0.9 and 0.4 wt% F respectively. Thus, the starting micas were buffered to their maximum Ti values appropriate for Mt Stafford metamorphic conditions, and that the run product micas had the opportunity to equilibrate towards maximum possible Ti concentrations as also noted by Guidotti & Sassi (2002). In a similar manner, muscovite would have been buffered to maximum phengitic component concentrations by the coexisting ferromagnesian oxides. In combination, the phengitic component, Ti, and F appear to have stabilised muscovite to above the granite solidus, at 3 MPa, and

allowed for muscovite breakdown via a fluid-absent melting reaction. In MTS71, which contains the starting mineral assemblage Ms+Bt+Kfs+Qtz+Tu, the celadonite content of muscovite would already have been buffered during metamorphism and would therefore not be expected to have changed much during the experiments, but it did as seen in Fig. 5.7 A-C. In the presence of melt, the celadonite content of phengitic muscovite is supposed to be buffered by the presence of Bt+Kfs+Qtz. The celadonite substitution is favoured by increasing P and decreasing T (Guidotti, 1978; Massonne & Schreyer, 1978) and any change in composition would be expected to lower Si, Fe and Mg and increase Al contents. This is not displayed in the experimental run products (Fig. 5.7A-C). Miyashiro & Shino (1985) found that when both Mg-Fe and Tschermak substitution occur in muscovite and some other silicates, a metapelite containing three AFM phases together with muscovite and quartz has at least two independent net-transfer reactions that take place side by side with changing external conditions. The mass balance requirement in the rock is imposed on a linear combination of the two reaction equations, leading to a constraint on the stoichiometric equations among phase components and the progressive compositional changes of muscovite. The maximum possible celadonite content in muscovite under given external conditions is realized in K-feldspar-bearing rocks, and decreases with rising temperature. Besides the fact that ideal muscovite behaves in the model way and natural muscovite achieves greater themal stability through the substitutions of Ti and F (Guidotti & Sassi, 2002), field and petrogenetic evidence from Mt Stafford suggests that most reactions were shifted to higher temperatures (White *et al*., 2003). According to Brearley & Rubie (1990) muscovite in H_2O undersaturated conditions breaks down by the stable dehydration reaction producing K feldspar+sillimanite+biotite and by metastable melting reactions in the same sample. Early melts are highly siliceous and sodic due to the rapid dissolution of quartz relative to muscovite, coupled with the incongruent melting of the paragonite component of muscovite and crystallization of biotite. A delayed nucleation of mullite results in Al supersaturation of the melt, which inhibits the rate of the melting reaction. Once mullite nucleates the degree of Al melt supersaturation is decreased and the

rate of muscovite dissolution increases. After complete reaction of muscovite the melt chemistry continues to change as Si diffuses into the pseudomorphs from adjacent quartz. Even after 5 months at 757 °C large compositional gradients in Si and Al still persist within the melt. Examination of examples of natural muscovite reacted under disequilibrium conditions in xenolithic and contact metamorphic rocks at low pressures suggests that metastable melting is an important process under certain geological conditions. It is possible that it is widespread in contact metamorphic rocks, but the textures indicative of metastable melting reactions are obscured during the extended cooling histories of such rocks (Brearley & Rubie, 1990). Reactions in the metapelites, according to White *et al.* (2003), show that the subsolidus evolution of the metapelites primarily involves the breakdown of muscovite and the appearance of cordierite, K-feldspar and andalusite. Andalusite first appears in Zone 1 rocks, initially restricted to more aluminous compositions. The appearance of cordierite and K-feldspar, a marked increase in the mode of aluminosilicate, and the disappearance of muscovite, occur at almost the same place in the sequence, the boundary between Zones 1 and 2. Thus, it is likely that the Zone 1–Zone 2 boundary occurs close to the intersection between the subsolidus trivariant field, in which coexisting muscovite and quartz break down, and the trivariant field in which subsolidus cordierite is first produced. This intersection moves to different *P–T* conditions with changing bulk-rock composition (White *et al*., 2003).

The decrease in biotite proportions between 750 and 800 °C in the muscovite- and biotite-bearing compositions, as well as the presence of texturally and compositionally distinct new biotite in the run products from these experiments, suggests that the melting reaction at the fluid-absent solidus in the two mica metapelites has the form Mu + Bt_1 + Q + Tu_1 + Ksp = Melt + Bt_2 + Tu_2 + Sil + Crd + Spn which corresponds to work by Garcĩa-Casco *et al.* (1993) on disequilibrium decomposition and breakdown of phengitic muscovite in high P-T gneisses, Betic alpine belt (southern Spain). Muscovite is known for being relatively refractory at low temperatures and several previous studies

have noted that muscovite reaction curves can be easily overstepped (Rubie & Brearley, 1987; Garcĩa-Casco *et al.*, 1993; Scaillet *et al*., 1995, Icenhower and London, 2000). Thus, an alternative interpretation is that muscovite persists metastably to > 750 °C and then breaks down via a disequilibrium reaction, and that the resultant increase in water activity promotes incongruent biotite melting. The observed shift in muscovite compositions in the 750°C, subsolidus experiments, away from the starting muscovite compositions towards higher Si contents, implies muscovite compositions progressed towards a state of equilibrium and possible exchange reactions with biotite and/or ilmenite took place. The alternative explanation that muscovite persists metastably to higher than 750 ^{o}C is not in accordance with the field data that muscovite already disappeared from the rocks at the boundary between zones 1 and 2 as noted by White *et al*. (2003) in the previous paragraph.

The occurrence of sillimanite (possibly mullite) needles in all the runs that contains muscovite might be an indication of disequilibrium conditions as mullite is unstable relative to sillimanite+corundum under those conditions (Holm & Kleppa, 1966; Weill, 1966), but the presence of mullite is not confirmed as the compositions imply sillimanite and minor corundum rather than the disequilibrium phase mullite. The absence of seeds of andalusite (also of K-feldspar in MTS70), the absence of water in the experiments to mimic fluid-absent conditions and the short run times might have suppressed the attainment of equilibrium in these runs in various ways. However, experiments by Icenhower and London (2000) have reported mullite in the run products after reversed experiments and 4 week run times. The presence of mullite is therefore not an indication of disequilibrium.

Besides the possibility of disequilibrium conditions, quantitative estimates by Domanik and Holloway (1996, 2000) show that the phengitic muscovite in calcareous metapelites and natural mineral assemblages are stable, by incorporating phengitic components up to 3.81 pfu Si, to pressures and temperatures of 5.5 - 7.0 GPa and 900 - 1050 ºC. These experiments show that phengite should be stable in metasediments in mature subduction zones to depths of up to 300 km even under

conditions in which $aH_2O \ll 1$ (Domanik & Holloway 2000). Studies by Hoschek (1990), Huang *et al.*, (1973) and Masonne and Schreyer (1987) indicate that at pressures below 3 GPa muscovite melting occurs at T > 700 ºC. The specific nature of these Ti, Fe, Si and Mg substitutions in muscovite remain ambiguous and disputed, but it is clear that, even though insignificant and related to the mineral assemblage into which the muscovite occurs, they do have an effect on muscovite overall solution behaviour (Guidotti & Sassi, 1998a).

Although these studies discussed in the previous paragraphs demonstrated that muscovite can persist to temperatures of 750 ºC, the field evidence from Mt Stafford indicated that the muscovite at Mt Stafford broke down via subsolidus reactions at relatively low temperatures of between 600 and 675 ºC (Greenfield *et al.*, 1996, 1998, White *et al*., 2003) on the border of zone 1 and 2. This disagreement of the field evidence with experimental work may indicate disequilibrium conditions during the experimental work, especially at the low temperatures.

6.3 The refractory nature of the evolved biotite compositions in the biotite-bearing samples

Phase changes close to the solidus in the biotite-bearing samples suggest that the melting reaction defining the fluid-absent solidus in these rocks is Bt + Qtz + Ksp + Al_2SiO_5 (± accessory Pl) = Melt + Spn + Crd. In both samples this reaction started between 750 and 800 ºC. Biotite was exhausted above 900 ºC in MTS7 and above 950 ºC in MTS8, suggesting a biotite melting interval of close to 200 ºC. The only other study (as demonstrated in Fig. 6.1) to demonstrate biotite stability to similar high temperatures (Patińo-Douce & Beard, 1996) also had biotite Ti concentrations buffered by ilmenite coexistence and low plagioclase proportions in the starting material. The early consumption of plagioclase in such compositions changes the nature of the melting reactions from the lower temperature reaction Bt + Qtz + Ksp + Pl + Al_2SiO_5 = Melt + Spl + Crd, to the higher temperature plagioclase-free equivalent. In sample MTS8, Al_2SiO_5 was consumed prior to 950 ºC, to allow biotite to melt via the yet higher temperature reaction Bt + Qtz + Ksp = Melt + Crd. These observations

indicate that in metagreywackes with sufficient feldspar component for feldspar minerals to be present throughout much of the biotite melting range, both Ti buffering by a Ti-rich mineral and high Ksp:Pl ratios in the starting materials, are likely to be important in stabilising biotite to ultra high temperatures. Petrogenetic evidence from Mt Stafford suggests that with rising temperature biotite and sillimanite modes rapidly decrease as cordierite and melt contents increase, which is consistent with the observed mineral assemblage relationships at the Zone 2–Zone 3 boundary. Biotite is calculated to be consumed by the melting reaction at 3.5 kbar and at or before 700 °C (White *et al*., 2003), which does not correlate with the temperature of between 850 and 950 °C at which it was completely consumed in the melting reaction in the experimental run products.

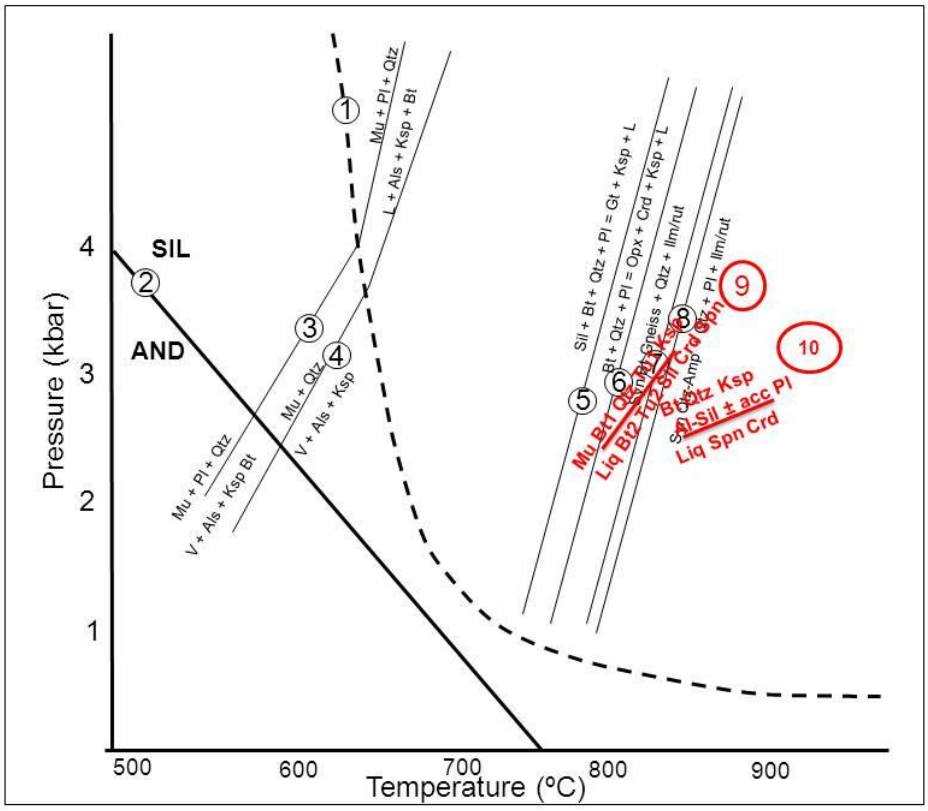

Fig. 6.1: The melting reactions from the muscovite metapelites MTS70, 71 (reaction 9 in red) and biotite metapelites MTS7 and 8 (reaction 10 in red) overlayed onto Fig 2.1. Reaction (1) = Metapelite solidus (Thompson, 1982); reaction (2) the most commonly cited aluminium silicate triple point (Holdaway, 1971); reaction (3) = the muscovite subsolidus reactions from Thompson (1982) and reaction (4) = Huang & Wyllie (1974); reaction (5) = Biotite melting reactions from Vielzeuf & Holloway (1988) and Le Breton & Thompson (1988); reaction (6) = Vielzeuf & Montel (1994); reaction (7) = the synthetic biotite gneiss from Patiño-Douce & Beard (1995) and reaction (8) = the synthetic quartz amphibolite from Patiño-Douce & Beard (1995).

6.4 The lack of an obvious boron related melt fluxing effect near the solidus

In the Mt Stafford area, boron fluxing of melting reactions has been proposed as a mechanism to induce partial melting at unusually low temperatures (Greenfield *et al*., 1998). Since tourmaline occurred in accessory abundances in MTS7 and MTS8 and in major abundances in MTS70 and MTS71, this might be of significance to the field observations by Greenfield *et al.* (1998). This reasoning may be the result of haplogranitic system experiments that have demonstrated a significant lowering of the wet granite solidus (Chapter 1, Fig. 1.2) as a result of minor to moderate boron addition to the system (Chorlton & Martin, 1978; Pichavant, 1981). Studies of tourmaline in natural rocks (London, 1999; Benard *et al*., 1985) suggest that tourmaline is a reasonably refractory phase, even occurring as a liquidus phase in some granites. Tourmaline stability in granitic magmas is strongly determined by ASI (Wolf & London, 1997), with the presence of tourmaline buffering ASI to ~ 1.4 in water saturated near solidus melts at 2 MPa (Acosta-Vigil & London, 2003). The melts produced by muscovite + biotite melting in this study would have been buffered to ASI values ~ 1.2 (Acosta-Vigil & London, 2003), requiring only minor addition to the melt from an aluminous phase (Al_2SiO_5, Tu, Crd) to stabilise tourmaline. This results in relatively low boron concentrations in the near solidus melts, and is consistent with the observation that under the conditions examined here, the presence of high concentrations of boron in the starting materials (as a component in tourmaline) does not flux melting. Indeed, it is difficult to imagine that in equivalent tourmaline-free samples muscovite would have melted at an even higher temperature as there is such a large temperature discrepancy between the experimental and field observations. There was a clear indication from the compositions of tourmaline produced in the experiments relative to that in the starting materials that the elbaitic component had melted preferentially. Boron, as attributed purely by tourmaline, in melt is calculated at ~2.5 % in MTS70 and ~ 6 % in MTS71 at 1000 ˚C. At near solidus temperatures, only ~1 % boron was liberated by tourmaline breakdown in MTS70 and only ~3 % in MTS71. The higher concentration of boron in the starting material of MTS71 has not contributed to a shift in the solidus

to lower temperatures. The modal abundance of muscovite in these two tourmaline-bearing metapelites had more influence on the melting behaviour than boron fluxing.

In these compositions, and under the low-pressure, fluid-absent conditions of these experiments, tourmaline does not appear to therefore markedly lower the solidus. This is demonstrated by the fact that the tourmaline-rich samples melted at a significantly higher temperature than expected (for reasons related to muscovite composition that are described above and possibly disequilibrium conditions during the experiments). Tentative calculations of the B_2O_3 concentrations in the melts (Fig. 6.2), based on the results of the phase proportion calculations presented in Table 5.4 (Chapter 5), suggest that maximum boron concentration in the melts is attained some 100 °C above the solidus, reflecting the relatively restitic character of the tourmaline in these experiments. This suggests that boron influx into a high-grade metasediment, for example as a component in an infiltrating fluid phase, at near solidus conditions would result in tourmaline precipitation, not substantial partial melting.

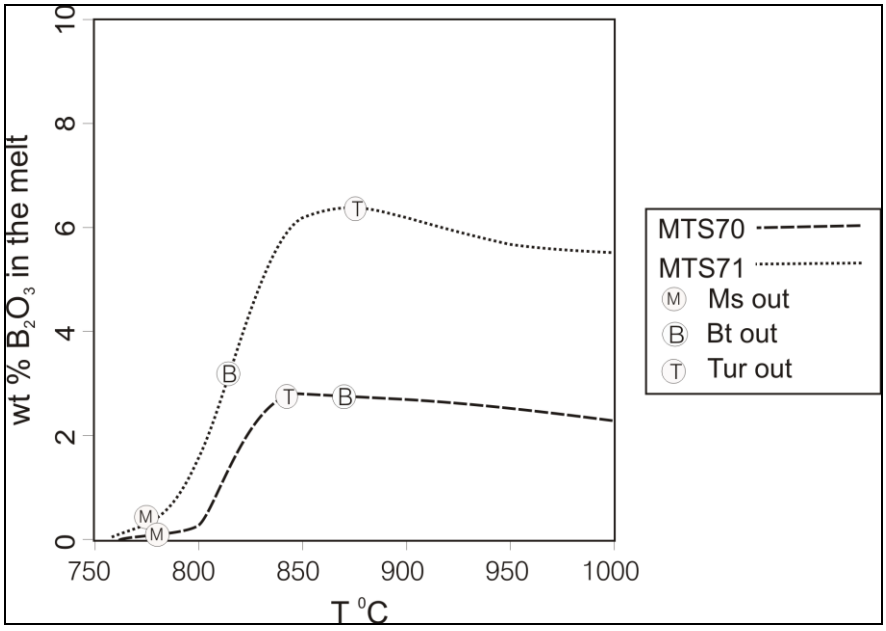

Fig. 6.2: Calculated B_2O_3 concentrations in the glasses from MTS70 and MTS71 expressed as a function of temperature.

6.5 The implication of these findings for interpreting low-pressure partial melting in the andalusite stability field in the Mt Stafford area

It is possible that the andalusite to sillimanite transition preserved at Mt Stafford does not occur at the same conditions as the many calculated or experimentally derived andalusite to sillimanite reactions and the metastable persistence of aluminosilicate minerals outside their stability range is well documented in a number of studies (Richardson *et al.*, 1969; Holdaway, 1971; Pattison & Harte, 1985, 1988; Kerrick & Spear, 1988; Kerrick, 1990; Pattison & Tracy, 1991; Pattison, 1992; Kerrick, 1990; Pattison , 2001; Cesare *et al.*, 2003; Droop & Moazzen, 2007). Field evidence suggests that andalusite may persist, along with sillimanite, in many of the Mt Stafford rocks to Zone 4 conditions (Greenfield *et al*., 1998), which corresponds to approximately 680 ˚C at 3 kbar. Experimental evidence shows that in MTS7 and MTS8, the biotite-bearing metapelites, andalusite was never completely consumed by the melting reactions in both samples, so persisted between 900 and 1000 ˚C at 3.2 kbar. At temperatures above biotite stability, melt, cordierite and spinel proportions increase, at the expense of K-feldspar, quartz and andalusite, as a function of temperature. This finding is consistent with petrogenetic evidence that andalusite modes generally decrease with rising temperature (White *et al*, 2003). The muscovite-bearing metapelites MTS70 and MTS71, with abundant tourmaline, started forming sillimanite phases around 850 ˚C, above the solidus, along with the breakdown of muscovite and tourmaline. Devineau *et al*. (2006) investigated the thermal decomposition of muscovite in natural granite powders heated to 1175 °C for durations from 5 min to 68 h, at 1 bar, paying special attention to the early stages of decomposition. This study showed that muscovite pseudomorphs consist of glass, mullite and Al-rich oxides. An important observation in samples MTS70 and MTS71 are the growth of sillimanite-(mullite) needles in the space where muscovite and tourmaline grains used to be, forming localised circular corona-type textures of cord-spn and sillimanite needles. Al-enriched zones have a stabilizing effect on sillimanite occurrence and the production of an aluminosilicate phase is therefore a result of fluid-absent muscovite and

tourmaline melting in the experiments. The field evidence (Clarke *et al.*, 1990; Collins & Vernon, 1991; Greenfield *et al*., 1996; Collins & Williams, 1995) and calculated pseudosection work of (White *et al*., 2003) underlies the occurrence of metastable andalusite into the high T zones of the Mt Stafford metasediments. As the experimental work of this study proves, andalusite metastably persists to much higher temperatures than expected, which agree relatively, but not exactly with the temperatures observed in the field or the petrogenetic calculations.

6.6 The correlation of the experimental work of this study with experimental, field and petrogenetic studies

The general mineral modes, relationships and assemblages might mimic the work by previous workers at Mt Stafford, but the actual temperatures and solidus positions found in the experimental work do not agree with field ovservations (Clarke *et al.*, 1990; Collins & Vernon, 1991; Greenfield *et al*., 1996; Collins & Williams, 1995) and calculated pseudosection work of (White *et al*., 2003). The experimental melting reactions of the muscovite biotite metapelites (MTS70 and MTS71) and biotite metapelites (MTS7 and MTS8) are overlayed onto Figure 1.3 and presented as reactions (12) and (13) in Figure 6.3. The fluid-absent melting experiments indicated that the main pulse of melting occurred between 850 and 950 °C, significantly higher than indicated by the field evidence of relatively low temperatures of 600 to 675 °C reported by Greenfield *et al.* (1998). From the experiments, the solidus in these samples should be at 3.2 kbar and close to 750 °C for the muscovite metapelites (Figure 6.3 reaction 12) and at 3.2 kbar and close to 800 °C for the biotite metapelites (Figure 6.3 reaction 13), significantly higher than 600 to 675 °C reported by Greenfield *et al.* (1998). Also, as White *et al.* (2003) stated, the amount the solidus can be shifted to even lower temperatures is limited by the need to have muscovite breakdown occur under subsolidus conditions and that the solidus at Mt Stafford cannot be shifted to lower temperatures by much more than about 25 °C. Muscovite in this study did not break down via subsolidus reactions as was expected, but partially reset composition and then

persisted to temperatures of 750 °C before melting was observed, approximately 130 °C above the field observations by Greenfield *et al.* (1996, 1998) and petrogenetic calculations of White *et al.* (2003).

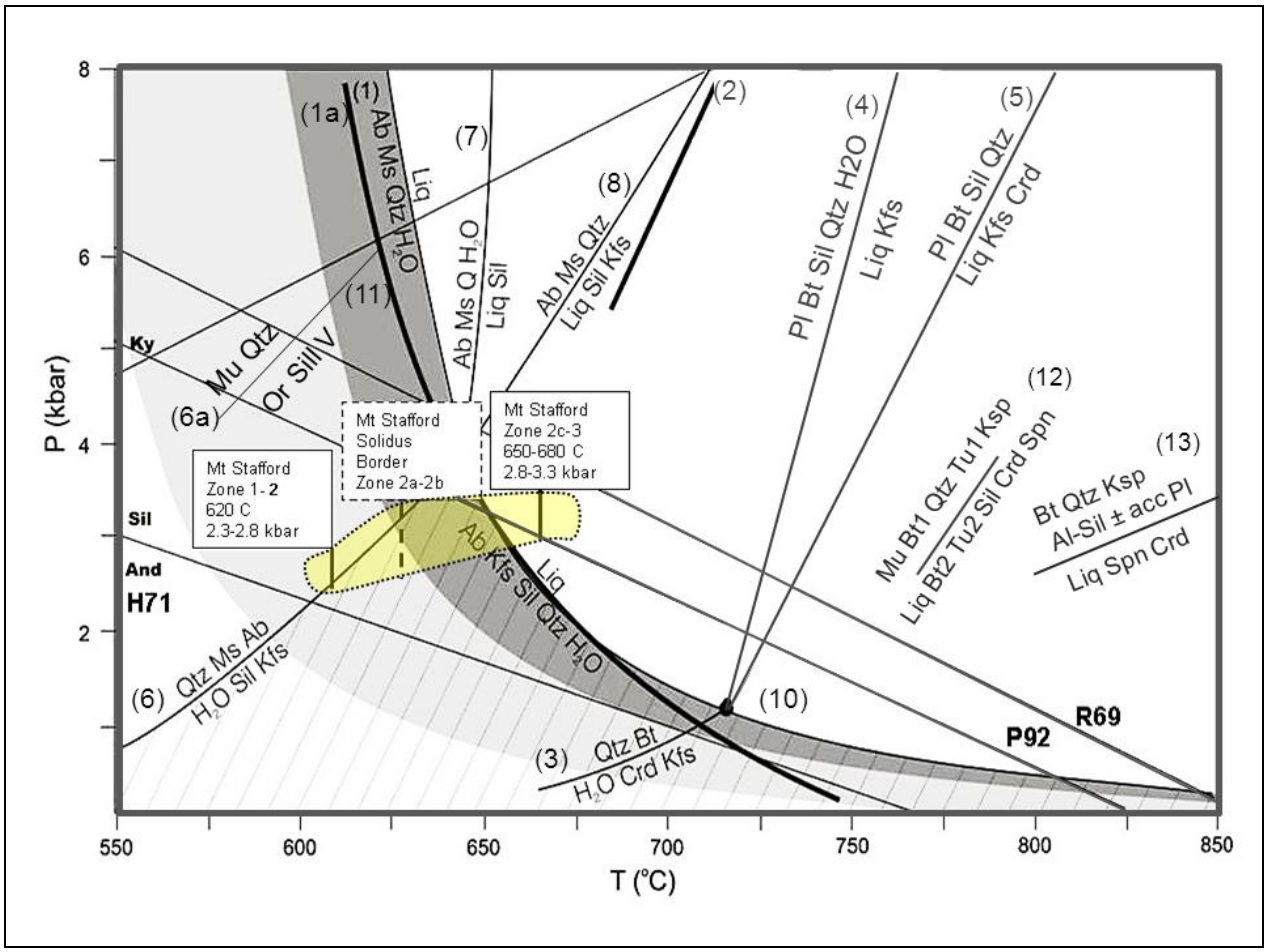

Fig. 6.3: The melting reactions from the muscovite metapelites MTS70, 71 (reaction 12) and biotite metapelites MTS7 and 8 (reaction 13) superimposed onto Fig 1.3. Greenfield *et al.*, (1996) found that the position of the solidus (position of the dotted vertical line in the yellow zone) is located on the Zone 2a – 2b boundary, but unconstrained at between 600 and 675 ºC.

Referring to Figure 2.1, the experimental reactions of the Mt Stafford two mica metapelites MTS70 and MTS71 would have been predicted to lie between reactions (3), (4) the muscovite subsolidus and melting reactions from Thompson (1982) and Huang & Wyllie (1974) at around 3 kbar and 650 to 750 ºC and the biotite melting reactions (5), (6), (7) and (8) from Vielzeuf & Holloway (1988), Le Breton & Thompson (1988), Vielzeuf & Montel (1994), Patiño-Douce & Beard (1995) and Patiño-

Douce & Beard (1995). The experimental reactions of MTS7 and MTS8 would have been predicted to lie close to all the biotite metapelite work of Vielzeuf & Holloway (1988), Le Breton & Thompson (1988), Vielzeuf & Montel (1994), Patiño-Douce & Beard (1995) and Patiño-Douce & Beard (1995) between ~730 and 770 ºC at 3 kbar as the compositions of the samples correspond well with these studies. Neither the two mica metapelites nor biotite metapelites melting reactions occurred in the ranges predicted by literature and in addition do not correspond to field observations, therefore it is very likely that experimental equilibrium was not reached.

6.7 Proposals for future work

Even though the results of these experiments are very interesting, in the absence of reversals and duplicates the stability of the various assemblages observed is only suggested, not proven. Future work to confirm the results presented in this discussion on muscovite and biotite stability would be interesting and neccessary to confirm the solidus and mineral behaviour of muscovite, biotite and andalusite at Mt Stafford. The possibility of disequilibrium vs equilibrium melting and fluid-present vs fluid-absent, rather than the influence of minor components in muscovite and biotite (Ti, Mg, F) on stability, is likely and would have to be confirmed. Follow-up work includes the following:

1. Increased run times to determine if optimum conditions during the experimental runs have been achieved.
2. Repeating experimental runs with the longer run times, across the same P-T conditions, as well as reverse equilibrium experiments to confirm run products and reaction positions.
3. Repeating experimental runs and reversals, as described in points 1 and 2, with H_2O and boric acid present to determine if the low temperatures of the melting interval observed at Mt Stafford by field workers can be duplicated in the experimental runs with the addition of these two components at much lower temperatures.

Chapter 7: Conclusions

The five main findings from this experimental study are expanded upon in the paragraphs below:

1) Phengitic, F-bearing muscovite, in samples MTS70 and MTS71 has melted at a higher than expected temperature of between 750 and 800 ºC. At 750 ºC the muscovites had partially reset to a new composition with no sign of subsolidus breakdown or recrystallization. This suggests that, if disequilibrium conditions are ruled out, a combination of Ti, phengite and F components in the muscovite stabilised it to temperatures above the wet-granite solidus at 3 MPa, enabling muscovite to participate in incongruent fluid-absent melting reactions. In these rocks muscovite appears to melt in a coupled reaction with biotite, allowing for the production of higher melt volumes, at temperatures close to, but much higher than, the wet solidus, in muscovite- and biotite-rich compositions. The muscovite-bearing metapelites MTS70 and MTS71 with abundant tourmaline started breaking down to sillimanite phases around 850 ˚C, above the solidus. The large disagreement in temperature of ~ 100 ˚C between field observations by Greenfield *et al.* (1996, 1998) and petrogenetic calculations by White *et al*. (2003) and the experimental results of this study could indicate that the experiments did not reach equilibrium as muscovite did not have sufficient time during the experiments to melt or break down via subsolidi reactions at the appropriate temperatures. Alternatively to the disequilibrium argument, this study filled the gap in muscovite behaviour under fluid-absent conditions at low pressures and temperatures and focussed the attention on the inaccuracy of metamorphic temperature calculations and estimations from the previous studies. Petrological modeling slightly underestimates the temperature of melting, therefore making direct comparisons speculative.

2) In the similarly Ti-rich, but muscovite-free compositions MTS7 and MTS8, biotite also demonstrates high levels of thermal stability. Biotite persists up to between 900 and 950 ˚C, depending on the starting mineral abundances, which could be due to the tchermakitic stabilizing effect and plagioclase-poor nature of these starting compositions which could stabilize the biotite to

ultrahigh temperatures. Similar studies of the synthetic biotite gneiss from Patiño-Douce & Beard (1995) and the synthetic quartz amphibolite from Patiño-Douce & Beard (1995) also demonstrate the high temperature stability of biotite under similar conditions (Fig. 6.1). The correspondence of the biotite melting temperatures of this study with these two studies strengthens the case against experimental disequilibrium in this study. The temperature mismatch between field observations, petrogenetic calculations and experimental findings are therefore not only apparent from this study, but also from others. The disagreement of ~ 100 ˚C between field observations by Greenfield *et al.* (1996, 1998) and petrogenetic calculations by White *et al*. (2003) and the experimental results of this study indicate that biotite did not melt at the appropriate temperatures of plagioclase-rich source rocks, but it does broaden the experimental knowledge of the temperature constraints of the biotite melting interval for Ti-rich and plagioclase-poor source rocks.

3) This study suggests that boron influx into a high-grade metasediment, without changing water activity, for example as a component in an infiltrating fluid phase; at near solidus conditions would not flux melting and would rather result in tourmaline precipitation. However, as discussed in Chapter 6, B_2O_3 in combination with water in the protolith could significantly lower the solidus in similar starting materials and can explain the low temperatures at which melting was observed by field workers.

4) Neither quartz, nor andalusite was completely consumed in the melting reactions of MTS7 and MTS8, indicating the persistance of andalusite to temperatures significantly higher than those of the wet solidus temperatures and also the proposed andalusite-sillimanite curves proposed by Holdaway (1971), Pattison (1992) or even the highest temperature position of the boundary proposed by Richardson *et al*. (1969). This metastability of andalusite is supported by field evidence (Greenfield *et al.*, 1998) and petrogenetic evidence (White *et al.*, 2003). The mineral assemblages do not change much with increasing temperature and mimic the mineral relationships as reported by the petrogenetic- and fieldwork of White *et al*. (2003) and Greenfield *et al.* (1998) at Mt Stafford. The

observed temperature difference between experimental and field work is approximately 200 ˚C for andalusite stability, double the difference observed for muscovite and biotite reactions from this study and the fieldwork, which indicate that andalusite did persist metastably to very high temperatures.

5) If it is accepted that experimental equilibrium was reached, the fluid-absent melting experiments of this study does not explain the relatively low pressure and temperature fluid-absent partial melting of the biotite and muscovite metapelites proposed by various field workers. The fluid-absent melting experiments indicated that the solidus is around 750 °C in the muscovite metapelites and around 800 °C in the biotite metapelites and the main pulse of melting occurred between 850 and 950 °C, significantly higher by ~ 100 ˚C than indicated by the field evidence of relatively low temperatures of the solidus at 600 to 675 °C reported by Greenfield *et al.* (1998) and confirmed by the petrogenetic work of White *et al.* (2003) with solidus temperatures of 660 to 680 °C at 3 kbar. As mentioned under point 2, petrogenetic modeling underestimates biotite melting temperature relative to experimental studies. It can be confirmed therefore by this study that andalusite were metastable to high temperatures and the presence of a localised fluid influx (probably with B_2O_3) during melting at Mt Stafford can be a plausible explanation of the low temperatures at which melting was observed by field workers. This theory can be confirmed by the proposed future work with H_2O and B_2O_3 added to the starting materials which might confirm the low temperatures of the melting interval observed at Mt Stafford by field workers.

References

A handbook of fusion methods: The preparation of Fused Glass Beads, Retrieved: January, 2008, from http://www.aft-fusion.com/fusionmethods.htm

Acosta-Vigil, A., London, D. (2003) Solubility of excess alumina in hydrous granitic melts in equilibrium with peraluminous minerals at 700-800 ºC and 200 MPa, and applications of the aluminum saturation index. Contributions to Mineralogy and Petrology. 146, 100-119

Akizuki, M., Kuribayashi, T., Nagase, T., Kitakaze, A. (2001) Non-hexagonal liddicoatite-elbaite tourmaline with X-site vacancy. American Mineralogist. 86, 364-369

Auzanneau, E., Schmidt, M.W., Vielzeuf, D., Connolly, J.A.D. (2009) Titanium in phengite: a geobarometer for high temperature eclogites. Contributions to Mineralogy and Petrology, online publication 12 June 2009

Beattie, P., Drake, M., Jones, J., Leeman, W., Longhi, J., McKay, G., Nielsen, R., Palme, H., Shaw, D., Takahashi, E., Watson, B. (1993) Terminology for trace-element partitioning. Geochimica et Cosmochimica Acta. 57, 1605-1606

Benard, F., Moutou, P., Pichavant, M. (1985) Phase relations of tourmaline leucogranites and the significance of tourmaline in silicic magmas. Journal of Geology. 93, 271-291

Beran, D.R., Rossman, G.R., Maldener, J., Endisch, D., Rauch, F. (2004) Hydroxide in kyanite: A quantitative determination of the absolute amount and calibration of the IR spectrum. American Mineralogist. 89, 998-1003

Beran, D.R., Gotzinger, M.A. (1987) The quantitative IR spectroscopic determination of structural OH groups in kyanites. Mineralogy and Petrology. 36, 41-49

Beran, A., Langer, K., Andrut, M. (1993) Singe crystal infrared spectra in the range of hydroxyl fundamental of paragenetic garnet, omphacite, and kyanite in an eclogitic mantle xenolith. Mineralogy and Petrology. 48, 257-268

Boettcher, A.L., Wyllie, P.J. (1969) Melting of granite with excess water to 30 kilobars pressure. Journal of Geology. 76, 235-244

Bohlen, S.R., Montana, Al.L., Kerrick, D.M. (1991) Precise determinations of the equilibria kyanite = sillimanite and kyanite = andalusite, and a revised triple point for Al_2SiO_5 polymorphs. American Mineralogist. 76, 677-680

Borom, M.P., Hanneman, R.E. (1967) Local compositional changes in alkali silicate glasses during electron microprobe analysis. Journal of Applied Physics. 38, 2406-2408

Brearley, A. J., Rubie, D. C. (1990) Effects of H_2O on the Disequilibrium Breakdown of Muscovite+Quartz . Journal of Petrology. 31(4), 925-956

Brown, M. (1994) The generation, segregation, ascent and emplacement of granitic magma: the migmatite-to-crustally-derived granite connection in thickened orogens. Earth-Science Reviews. 36, 83-130

Brown, M., Averkin, Y. A., McLellan, E. L., Sawyer, E. W. (1995) Melt segregation in migmatites. Journal of Geophysical Research. 100, 15655–15679

Burnham, C.W. (1979) The importance of volatile constituents. In H.S. Yoder, Ed., The evolution of the igneous rocks (Fiftieth anniversary perspectives). Princeton University Press, Princeton, New Jersey, pp 439-482

Buick, I.S., Stevens, G., Gibson, G.R.L. (2004) The Role of Water Retention in the Anatexis of Metapelites in the Bushveld Complex Aureole, South Africa: an Experimental Study Journal of Petrology. 45(9), 1777-1797

Buick, I.S, Stevens, G., Hermann, J., Spicer, E. (2006) The behaviour of boron during LP/HT metamorphism of metapelites, Mt. Stafford, central Australia. Geochimica et Cosmochimica Acta. 70 (18), A73-A73

Butler, B.C.M (1967) Chemical study of minerals from the Moine Schists of the Ardnamurchan area, Argyllshire, Scotland. Journal of Petrology. 8, 233-267

Carrington, D.P., Harley, S.L. (1995) Partial melting and phase relations in high-grade metapelites: an experimental petrogenetic grid in the KFMASH system. Contributions to Mineralogy and Petrology. 120, 270-291

Carrington, D. P., Watt, G. R. (1995) A geochemical and experimental study of the role of K-feldspar during water-undersaturated melting of metapelites. Chemical Geology 132, 59-76

Cartwright, I., Buick, I. S., Vry, J. K. (1996) Polyphase metamorphic fluid flow in the Lower Calcsilicate Unit, Reynolds Range, central Australia. Precambrian Research. 77, 211-229

Carson, C. J., Powell, R., Wilson, C. J. L. & Dirks, P. H. G. M. (1997) Partial melting during tectonic exhumation of a granulite terrane; an example from the Larsemann Hills, East Antarctica. Journal of Metamorphic Geology. 15, 105-126

Cesare, B., Gomez-Pugnaire, M.T., Sanchez-Navaz, A., Groberty, B. (2002) Andalusite-sillimanite replacement (Mazarron, SE Spain): A microstructural and TEM study. American Mineralogist. 87, 433-444

Cesare, B., Marchesi, C., Hermann, J., Gomez-Pugnaire, M.T. (2003) Primary melt inclusions in andalusite from anatectic graphitic metapelites: implications for the Al_2SiO_5 triple point. Geology 31, 573-576

Chorlton, L.B., Martin, R.F. (1978) The effect of boron on the granite solidus. Canadian Mineralogist. 16, 239-244

Cipriani, C., Sassi, F.P., Scolari, A. (1971) Metamorphic white micas: Definition of paragenetic field. Schweiz. Mineral. Petrogr. Mitt. 51, 259-302

Clarke, D.B. (1981) The mineralogy of peraluminous granites: a review. Canadian Mineralogist. 19, 3-17

Clarke G. L., Collins W. J., Vernon R. H. (1990) Successive overprinting granulite facies metamorphic events in the Anmatjira Range, central Australia. Journal of Metamorphic Geology. 8, 65-88

Clemens, J.D., Vielzeuf, D. (1987) Constraints on melting and magma production in the crust. Earth and Planetary Science Letters. 86, 287-306

Clemens, J.D., Wall, V.J. (1981) Origin and crystallization of some peraluminous (S-type) granite magmas: Canadian Mineralogist. 1, 111-131

Collins, W.J., Teyssier, C. (1989) Crustal scale ductile fault systems in the Arunta Inlier, central Australia. Tectonophysics. 158, 1-41-4, 49-66

Collins, W. J., Vernon, R. H. (1991) Orogeny associated with anticlockwise *P–T–t* paths: evidence from low-*P*, high-*T* metamorphic terranes in the Arunta Inlier, central Australia. Geology. 19, 835–838

Collins, W. J., Williams, I. S. (1995) SHRIMP ionprobe dating of short-lived Proterozoic tectonic cycles in the northern Arunta Inlier, central Australia. Precambrian Research. 71, 69–89

Dahl, P.S., When, D.C., Feldmann, S.G (1993) The systematics of trace-element partitioning between coexisting muscovite and biotite in metamorphic rocks from the Black Hills, South Dakota, USA. Geochimica et Cosmochimica Acta. 57, 2487-2505

Dalmeyer, R.D. (1974) The Role of Crystal Structure in Controlling the Partitioning of Mg and Fe^{2+} between coexisting Garnet and Biotite. American Mineralogist. 59, 201-203

Devine, J.D., Gardner, J.E., Brack, H.P., Layne, G.D., and Rutherford, MJ. (1995) Comparison of microanalytical methods for estimating H_2O contents of silicic volcanic glasses. American Mineralogist. 80, 319- 328

Devineau, K, Devouard, B., Villieras, F., Faure, F., Devidal, J-L., and Kohler, A. (2006) Evolution of product phase assemblages during thermal decomposition of muscovite under strong disequilibrium conditions. American Mineralogist, 91, 2-3, 413-424

Dingwell, D.B., Pichavant, M., Holtz, F. (1996) Experimental studies of boron in granitic melts. In: Grew ES, Anovitz L (eds) (1996) Boron: mineralogy, petrology, and geochemistry in the

earth's crust (Reviews in Mineralogy vol. 33). Mineralogy Society of America, Washington DC, 331-121

Dolores Pereira Gomez, A., Shaw, D.M. (1997) Behaviour of boron in the generation of an anatectic complex: The Pena Negra complex, central Spain. Lithos. 40, 179-188

Dooley, D. F., Patińo Douce, A. E., 1996. Fluid-absent melting of F-rich phlogopite + rutile + quartz. American Mineralogist. 81, 202-212

Domanik, K.J., Hervig, R.L., Peacock, S.M. (1993) Beryllium and boron in subduction zone minerals: An ion microprobe study. Geochimica et Cosmochimica Acta. 57, 4997-5010

Domanik, K.J., Holloway, J.R. (1996) The stability and composition of phengitic muscovite and associated phases from 5.5 to 11 GPa: Implications for deeply subducted sediments. Geochimica et Cosmochimica Acta. 60, 4133-4150

Domanik, K.J., Holloway, J.R. (2000) Experimental synthesis and phase relations of phengitic muscovite from 6.5 to 11 GPa in a calcareous metapelite from the Dabie Mountains, China. Lithos. 52, 51-77

Doukhan, J.-C., Christie, J.M. (1982) Plastic deformation of sillimanite Al_2SiO_5 single crystals under confining pressure and TEM investigation of the induced defect structure. Bulletin de Mineralogie. 105, 583-589

Doukhan, J.-C., Doukhan, N., Kock, P.S., Christie, J.M. (1985) Transmission electrom microscopy investigation of lattice defects in Al_2SiO_5 polymorhps and plasticity induced polymorphic transformations. Bulletin de Mineralogie. 108, 81-96

Droop, G.T.R. (1987) A general equation for estimating Fe^{3+} concentrations in ferromagnesian silicates and oxides from microprobe analyses, using stoichiometric criteria. Mineralogical Magazine. 51, 431-435

Droop, G.T.R., Moazzen, M. (2007) Contact metamorphism and partial melting of Dalradian pelite and semipelites in the southern sector of the Etive aureole. Scottish Journal of Geology. 43(2), 155-179

Dutrow, B.L., Holdaway, M.J., Hinton, R.W. (1986) Lithium in staurolite and its petrologic significance. Contributions to Mineralogy and Petrology. 94, 496-506

Eggler, D.H., Holloway, J.R. (1977) Partial melting of peridotite in the presence of H_2O and CO_2: Principles and review. Magma Genesis, Oregon Department of Geology and Mineral Industries Bulletin. 96, 15-36

Ellis, D.J., Obata, M. (1992) Migmatite and melt segregation at Cooma, New South Wales. Transactions of the Royal Society of Edinburgh. Earth sciences. 83, 95-106

Evensen, J.M., London, D. (2003) Experimental partitioning of Be, Cs, and other trace elements between cordierite and felsic melt, and the chemical signature of S-type granite. Contributions to Mineralogy and Petrology. 144, 739-757

Fitzsimons, I. C. W. (1996) Metapelitic migmatites from Brattstrand Bluffs, East Antarctica: metamorphism, melting and exhumation of the mid crust. Journal of Petrology. 37, 395–414

Fournelle, J (2006) Silicate Peak Shifts, Spectrometer Peaking Issues and Standard/Specimen Size Discrepancies in EPMA: 3 Bumps in the Road to the Goal of 1% Accuracy. AGU 2006 Conference proceedings

Forbes, W. C. & Flower, M. F. J. (1974) Phase relations of titan-phlogopite, $K_2Mg_4TiAl_2Si_6O_{20}(OH)_4$: a refractory phase in the upper mantle? Earth and Planetary Science Letters. 22, 60-66

Friedrich, A., Kunz, M., Winkler, B., Le Bihan, T. (2004) High-pressure behaviour of sillimanite and kyanite: compressibility, decomposition and indications of a new high-pressure phase. Zeitschrift fur Kristallographie. 219, 324-329

Frost, C.D., Frost, B.R., Bell, J.M., Chamberlain, K.R. (2002) The relationship between A-type granites and residual magmas from anorthosite: evidence from the northern Sherman batholith, Laramie Mountains, Wyoming, USA. Precambrian Research. 119, 45-71

Fuhrman, M.L., Lindsley, D.H. (1988) Ternary-feldspar modelling and thermometry. American Mineralogist. 73, 201-215

Garcĩa-Casco, A., Torres-Roldăn, R.L (1996) Disequilibrium induced by fast decompression in St-Bt-Grt-Ky-Sil-And metapelites from the Betic belt (Southern Spain). Journal of Petrology. 37, 1207-1239

Gardien, V., Thompson, A.B., Grujic, D., Ulmer, P. (1995) Experimental melting of biotite + plagioclase + quartz ± muscovite assemblages and implications for crustal melting. Journal of Geophysical Research. 100, 15581-15591

Ghiorso, M., Sack, R.O. (1991) Thermochemistry of the Oxide Minerals, Reviews in Mineralogy (P.H. Ribbe, ed.), Mineralogical Society of America. 25, 221-264

Goodhew, P.J. (1975) Electron probe microanalysis of glass containing alkali metals. Microstructural Science, 3, 631-641

Goodhew, P.J., Gulley, J.E.C. (1974) The determination of alkali metals in glasses by electron probe microanalysis. Glass Technology, 15, 123-126

Grambling, J.A. (1981) Kyanite, andalusite, sillimanite, and related mineral assemblages in the Truchas Peaks region, New Mexico. American Mineralogist. 66, 702-722

Grambling, J.A., Williams, M.L. (1985) The effect of Fe^{3+} and Mn^{3+} on aluminium silicate phase relations in north-central New Mexico, U.S.A. Journal of Petrology. 26, 324-354

Grant, J.A. (1973) Phase equilibria in high grade metamorphism and partial melting of pelitic rocks. American Journal of Science. 273, 289-317

Grant, J. A. (1985*a*). Phase equilibria in low-pressure partial melting of pelitic rocks. American Journal of Science. 285, 409-435

Grant, J. A. (1985*b*). Phase equilibria in partial melting of pelitic rocks. In: Ashworth, J. R. (ed.) *Migmatites*. Glasgow: Blackie, pp. 86-144

Green, T.H. (1976) Experimental generation of cordierite- or garnet-bearing granitic liquids from a pelitic composition. Geology. 4, 85-88

Greenfield, J.E. (1997) Migmatitic formation at Mt Stafford, central Australia. Ph.D. Thesis, University of Sydney, 231 pp.

Greenfield, J.E., Clarke, G.L., Bland, M., Clark, D.J. (1996) In-situ migmatite and hybrid diatexite at Mt Stafford, central Australia. Journal of Metamorphic Geology. 14, 413-426

Greenfield, J.E., Clarke, G.L., White, W. (1998) A sequence of partial melting reaction at Mt Stafford, central Australia. Journal of Metamorphic Geology.16, 363-378

Greenwood, H.J. (1976) Metamorphism at moderate temperatures and pressure. In: Bailey, D.K.& McDonald, R. (eds) The Evolution of the Crystalline Rocks. London: Academic Press, 187-259

Grew, E.S., Anovitz, L. (eds) (1996) Boron: mineralogy, petrology, and geochemistry in the earth's crust (Reviews in Mineralogy vol. 33). Mineralogical Society of America, Washington DC, pp 331-121

Giudotti, C.V., Cheney, J.T., Guggenheim, S. (1977) Distribution of titanium between coexisting muscovite and biotite in politic schists from northwestern Maine. American Mineralogist. 62, 438-448

Guidotti, C.V. (1978) Compositional variation of muscovite in medium- to high grade metapelites of Northwestern Maine. American Mineralogist. 63, 878-884

Guidotti, C.V., Sassi, F.P., Sassi, R., Blencoe, J.G. (1994a) The effects of ferromagnesian components on the paragonite-muscovite solvus: A semi-quantitative analysis based on chemical data for natural paragonite-muscovite pairs. Journal of Metamorphic Geology. 12, 779-788

Guidotti, C.V., Yates, M.G., Dyar, M.D., Taylor, M.A. (1994b) Petrogenetic implications of Fe^{3+} content of muscovite in pelitic schists. American Mineralogist. 79, 793-795

Guidotti, C.V., Sassi, F.P. (1989) Miscellaneous isomorphous substitutions in Na-K white micas: a review with special emphasis to metamorphic micas. Rend. Fis. Acc. Lincei, s. 9, 9, 57-78

Guidotti, C.V., Sassi, F.P. (2002) Constraints on studies of metamorphic K-Na white micas. In: Reviews in mineralogy and geochemistry. Micas: Crystal chemistry and metamorphic petrology. The mineralogical society of America. 46, 413-448

Hand, M., Dirks, P. H. G. M. (1992) The influence of deformation on the formation of axial-planar leucosomes and the segregation of small melt bodies within the migmatitic Napperby Gneiss, central Australia . Journal of structural geology. 14, (5), 591-604

Harding, D.P. (2002) 'Mineral identification using a scanning electron microscope', Journal of Minerals & Metallurgical Processing. 19(4), 169-177

Harte, B., Pattison, D. R. M., Linklater, C. M. (1991). Field relations and petrography of partially melted pelitic and semi-pelitic rocks. In: Voll, G., Töpel, J., Pattison, D. R. M. & Seifert, F. (eds) Equilibrium and Kinetics in Contact Metamorphism: the Ballachulish Igneous Complex and its Aureole. Berlin: Springer, pp.182-210

Heitanen, A. (1956) Kyanite, andalusite and sillimanite in the schist in Boehls Butte quadrangle, Idaho. American Mineralogist. 41, 1-27

Henry, D.J., Dutrow, B.L. (2001) Compositional zoning and element partitioning in nickeloan tourmaline from a metamorphosed karstbauxite from Samos, Greece. American Mineralogist. 86(10), 1130-1142

Henry, D.J., Guidotti, C.V., Thomson, J.A. (2005) The Ti-saturation surface for low-to-medium pressure metapelitic biotites: implications for geothermometry and Ti-substitution mecanisms. American Mineralogist. 90, 316–328

Henry, D.J., Dutrow, B.L. (1996) Metamorphic Tourmaline. In: E.S. Grew and L.M. Anovitz (Editors), Boron: Mineralogy, Petrology and Geochemistry. Reviews in Mineralogy. 33, 500-555

Henry, D.J., Guidotti, C.V. (2002) Titanium in biotite from metapelitic rocks: Temperature effects, crystal-chemical controls,and petrologic applications. American Mineralogist. 87, 375-382

Henry, D. J., Kirkland, B. L., Kirkland, D. W. (1999) Sector-zoned tourmaline from the cap rock of a salt dome. European Journal of Mineralogy, 11, 263-280

Hensen, B.J., Green, D.H. (1972) Experimental study of the stability of cordierite and garnet in pelitic compositions at high pressures and temperatures, III. Contributions to Mineralogy and Petrology. 38, 151-166

Hermann, J., Spandler, C.J. (2008) Sediment melts at sub-arc depths: an experimental study. Journal of Petrology. 49(4),717–740

Hervig, R.L, Peacock, S.M. (1989) Water and trace elements in coexisting muscovite and biotite from metamorphic rocks. Eos. 70(15), 490

Holdaway, M.J. (1971) Stability of andalusite and the aluminium silicate phase diagram. American Journal of Science. 271, 97-131

Holdaway, M.J., Mukhopadhyay, B. (1993) A re-evaluation of the stability relations of andalusite: thermochemcial data and phase diagram for the aluminium silicates. American Mineralogist. 78, 298-315

Holland, T. J.B, Powell, R. (1985) An internally consistent thermodynamic data set with uncertainties and correlations: 2. Data and results. Journal of Metamorphic Petrology. 3, 343-370

Holland, T.J.B., Powell, R. (2002). An internally consistent thermodynamic data set for phases of petrological interest. Journal of Metamorphic Geology. 16, 309–343 (updated 2002)]

Holland, T.J.B., Powell, R. (2001) Calculation of phase relations involving haplogranite melts using and internally consistent dataset. Journal of Petrology. 42, 673-683

Hollister, L.S. (1969) Metastable paragenetic sequence of andalusite, kyanite, and sillimanite, Kwoiek area, British Columbia. American Journal of Science. 267, 352-370

Holm, J.L., Kleppa, O.J. (1966) The thermodynamic properties of the aluminium silicates. American Mineralogist. 51, 1608-1627

Holtz, F., Johannes, W. (1991) Genesis of peraluminous granites I: Experimental investigation of melt compositions at 3 and 5 MPa and various H_2O activities. Journal of Petrology. 32, 935-958

Holtz, F., Pichavant, M., Barbey, P., Johannes, W. (1992) Effect of H_2O on liquidus phase relations in the haplogranite system at 2 and 5 kbar. American Mineralogist. 77, 1223-1241

Holtz, F., Johannes, W. (1994) Maximum and minimum water contents of granitic melts: implications for chemical and physical properties of ascending magmas. Lithos. 32, 149–159

Hoschek, G. (1990) Melting and subsolidus reactions in the system K_2O-CaO-MgO-Al_2O_3-SiO_2-H_2O. Contributions to Mineralogy and Petrology. 105, 393-402

Huang, W.L., Robertson, J.K, Wyllie, P.J. (1973) Melting relations of muscovite to 30 kb in the system $KAlSi_3O_8$-Al_2O_3-H_2O. Americal Journal of Science. 273, 415-427

Huang, W.L., Wyllie, P.J. (1974) Melting relations of muscovite with quartz and sanidine in the K_2O-Al_2O_3-SiO_2-H_2O system to 30 MPa and an outline of paragonite melting relations. American Journal of Science. 274, 378-395

Huang, W.L., Wyllie, P.J. (1981) Phase relationships of S-type granite with H_2O to 35 MPa: muscovite granite from Harney Peak, South Dakota: J Geophysical Research. 86, 10515-10529

Hülsmans, A., Schmucker, M., Mader, W., Schneider, H. (2000) The transformation of andalusite to mullite + silicate: Part I. Transformation mechanism in [001] A direction. American Mineralogist. 85, 980-986

Humphreys, M. C., Kearns, S. L., Blundy, J. D. (2006) SIMS investigation of electron-beam damage to hydrous, rhyolitic glasses: Implications for melt inclusion analysis**.** American Mineralogist. 91(4), 667-679

Icenhower, J.P., London, D. (1995) An experimental study of element partitioning among biotite, muscovite, and coexisting peraluminous silicic melt at 200 MPa (H_2O). American Mineralogist. 80, 1229-1251

Icenhower, J.P., London, D. (1997) Partitioning of fluorine and chlorine between biotite and granitic melt: experimental calibration at 200 MPa H_2O. Contributions to Mineralogy and Petrology. 127, 17-29

Johannes, W. (1984) Beginning of melting in the granite system Qz-Or-Ab-An-H_2O. Contributions to Mineralogy and Petrology. 86, 264-273

Johannes, W. (1989) Melting of plagioclase - quartz assemblages at 2Kb water pressure. Contributions to Mineralogy and Petrology. 103, 270-276

Johannes, W., Holtz, F. (1996) Petrogenesis and experimental petrology of granitic rocks. Springer. Berlin. 1996. 335 pp

Johnson, S.E., Vernon, R.H. (1995) Stepping stones and pitfalls in the determination of an anticlockwise P-T-t-deformation path: the low-P, high-T Cooma Complex, Australia. Journal of Metamorphic Geology. 13, 165-183

Le Breton, N., Thompson, A.B. (1988) Fluid-absent (dehydration) melting of biotite in metapelites in the early stage of crystal anatexis. Contributions to Mineralogy and Petrology. 99, 226-237

Lineweaver, J.L. (1962) Oxygen outgassing caused by the electron bombardment of glass. Journal of Applied Physics, 34, 1786-1791

Leoni, L., Sartori, F., Tamponi, M., (1998) Compositional variation in K-white micas and chlorites coexisting in Al- saturated metapelites under late diagenetic to low-grade metamorphic

conditions (Internal Liguride Units, Nortern Apennines, Italy). European Journal of Mineralogy. 10, 1321–1339.

Luth, W.C. (1967) Studies in the system $KAlSiO_4$-Mg_2SiO_4-SiO_2-H_2O: I, Inferred phase relations and petrologic application. Journal of Petrology. 8, 372-416

Kerrick, D.M. (1986) Dislocation strain energy in the Al_2SiO_5 polymorphs. Physics and Chemistry of Minerals. 13, 221-226

Kerrick, D.M. (1988) Al_2SiO_5- bearing segregations in the Lepontine Alps, Switzerland: Aluminum mobility in metapelites. Geology. 16, 636-640

Kerrick, D.M. (1990) The Al_2SiO_5 polymorphs. Reviews in Mineralogy, Mineralogical Society of America, Washington D.C.

Kerrick, D.M., Speer, J.A. (1988) The role of minor element solid solution on the andalusite-sillimanite equilibrium in metapelites and peraluminous granitoids. American Journal of Science. 288, 152-192

Kretz, R. (1983) Symbols for rock forming minerals. American Mineralogist. 68, 277-279

Kushiro, I. (1972) Effect of water on the composition of magmas formed at high pressures. Journal of Petrology, 17, 139-193.

Le Breton, N., Thompson, A. B. (1988). Fluid-absent (dehydration) melting of biotite in metapelites in the early stages of crustal anatexis. Contributions to Mineralogy and Petrology .99, 226-237.

London, D. (1987) Internal differentiation of rare-element pegmatites: effects of boron, phosphorus and fluorine. Geochimica Cosmochimica Acta. 51, 403-420

London, D. (1999) Stability of tourmaline in peraluminous granite systems: the boron cycle from anatexis to hydrothermal aureoles. European Journal of Mineralogy. 11, 253-262

London, D., Hervig, R.L., Morgan, G.B. (1988) Melt-vapor solubilities and element partitioning in peraluminous granite-pegmatite systems: experimental results with Macusani glass at 200 MPa. Contributions to Mineralogy and Petrology. 99, 360-373

London, D., Morgan, G.B., Hervig, R.L. (1989) Vapor-undersaturated experiments with Macusani glass + H_2O, at 200 MPa. Contributions to Mineralogy and Petrology. 102, 1-17

Manning, D.A.C., Pichavant, M. (1983) The role of fluorine and boron in the generation of granitic melts. In: Migmatites Melting and Metamorphism (eds Atherton MP, Gribble CD). Shiva publishing Ltd, Nantwich, England. 94-109

Massonne, H.J., Schreyer, W. (1987) Phengite geobarometry based on the limiting assemblage with K-feldspar, phlogopite and quartz. Contributions to Mineralogy and Petrology. 96, 212-224

Michael, P.J. (1988) Partition coefficients for rare earth elements in mafic minerals of high silica rhyolites: The importance of accessory mineral inclusions. Geochimica et Cosmochimica Acta. 52, 275-282

Miyashiro, A., Shido, F. (1985) Tschermak substitution in low- and middle-grade pelitic schists. Journal of Petrology. 26, 449-487

Morgan, $G.B^{VI}$, London, D. (1996) Optimizing the electron microprobe analysis of hydrous alkali aluminosilicate glasses American Mineralogist. 81, 1176-1185

Moorbath, S., Bell, K., Leake, B.E., McKerrow, W.S. (1968) Geochronological studies in Connemara and Murrisk, Western Ireland. In: Radiometric Dating for Geologists. Eds. E.I. Hamilton and R.M. Farquhar. 259-298

Munoz, J.L. (1977) Fluorine-hyroxyl exchange in synthetic muscovite and its application to muscovite-biotite assemblages. American Mineralogist. 62, 304-308

Neiva, A.M.R., Neiva, J.M, Parry, S.J. (1987) Geochemistry of the granitic rocks and their minerals from Serra da Estrela, Central Portugal. Geochimica et Cosmochimica Acta. 51, 439-454

Newbury, D. (2005) Automatic Peak Identification in Scanning Electron Microscopy/Energy Dispersive X-ray (SEM/EDS) Microanalysis: Can You Always Trust the Results? Microscopy and Microanalysis. 11, 545

Nielsen, C.H., Sigurdsson, H. (1981) Quantitative methods for electron microprobe analysis of sodium in natural and synthetic glasses. American Mineralogist, 66, 547-552

Okrusch, M., Evans, B.W. (1970) Minor element in coexisting andalusite and sillimanite. Lithos. 3, 261-268

Patiño Douce, A. E. (1993). Titanium substitution in biotite: an empirical model with applications to thermometry, O_2 and H_2O barometries, and consequences for biotite stability. Chemical Geology. 108, 133–162

Patiño-Douce, A.E., Beard, J.S. (1995) Dehydration-melting of biotite gneiss and quartz amphibolite from 3 to 15 MPa. Journal of Petrology. 36, 707-738

Patiño-Douce, A.E., Beard, J.S. (1996) Effects of P, $f(O_2)$ and Mg/Fe ratio on dehydration melting of model metagreywackes. Journal of Petrology. 37, 999-1024

Patiño-Douce, A.E., Johnson, A.D. (1991) Phase equilibria and melt productivity in the pelitic system: Implication for the origin of peraluminous granitoids and aluminous granulites. Contributions to Mineralogy and Petrology. 107, 202-218

Pattison, D.R.M. (1992) Stability of andalusite and sillimanite and the Al_2SiO_5 triple point: Constraints from the Ballachulish aureole, Scotland. Journal of Geology, 100, 423-446

Pattison, D.R.M (2001) Instability of the Al_2SiO_5 “triple-point” assemblage in muscovite + biotite + quartz-bearing metapelites, with implications. American Mineralogist. 86, 1414-1422

Pattison, D.R.M., Harte, B. (1985) A petrogenic grid for pelites in the Ballachulish and other Scottish thermal aureoles. Journal of the Geological Society of London. 142, 7-28

Pattison, D.R.M., Harte, B. (1988) Evolution of structurally contrasting anatectic migmatites in the 3-kbar Ballachulish aurelole, Scotland. Journal of Metamorphic Geology. 6, 475-494

Pattison, D.R.M., Tracey, R.J. (1991) Phase equilibria and thermobarometry of metapelites. In: D.M. Kerrick, Ed., Contact metamorphism, 26, 105-206. Mineralogical Society of America, Reviews in Mineralogy, Washington , D.C.

Peterson, J. W., Chacko, T., Kuehner, S. M. (1991). The effects of fluorine on the vapor-absent melting of phlogopite + quartz: implications for deep crustal processes. American Mineralogist 76, 470–476

Pichavant, M. (1981) An experimental study of the effect of boron on a water-saturated haplogranite at 1 MPa vapor pressure. Contributions to Mineralogy and Petrology 76, 430-439

Pichavant, M. (1984) The effect of boron on liquidus phase relationships in the system Qz-Ab-Or-H_2O at 1 MPa. EOS. 65, 298

Pichavant, M. (1987) Effect of B and H_2O on liquidus phase relations in the haplogranitic system at 1 kbar. American Mineralogist. 72, 1056-1070

Pichavant, M., Valencia Herrera, J., Boulmier, S., Briqueu, L., Joron, J.L., Juteau, M., Marin, L., Michard, A., Sheppard, S.M.F., Treuil, M., Vernet, M. (1987) The Macusani glasses, SE Peru: Evidence of chemical fractionation in peraluminous magmas. In Geochemical Society Special Publication. 1, 359-373

Pichavant, M., Kontak, D.J., Valencia Herrera, J.V., Clark, A.L.H. (1988) The Miocene-Pliocene Macusani Volcanics, SE Peru: Mineralogy and magmatic evolution of a two-mica aluminosilicate-bearing ignimbrite suite. Contributions to Mineralogy and Petrology. 100, 300–324

Pickering, J.M., Johnston, A.D. (1998) Fluid-absent melting behavior of a two-mica metapelite: Experimental constraints on the origin of the Black Hills granite. Journal of Petrology. 39, 1787-1804

Powell, R., Downes, J. (1990). Garnet porphyroblast-bearing leucosomes in metapelites: mechanisms, phase diagrams, and example from Broken Hill, Australia. In: Ashworth, J. R. & Brown, M.

(eds) High Temperature Metamorphism and Crustal Anatexis. London: Unwin Hyman, pp. 105–123

Preston, R.F., Stevens G., McCarthy, T.S. (2003) Fluid compositions in equilibrium with silica-undersaturated magmas in the system Na_2O-Al_2O_3-SiO_2-H_2O: clues to the composition of fenitizing fluids. Contributions to Mineralogy and Petrology. 144, 559-569

Rapp, R.P., Watson, E.B., Miller, C.F. (1991) Patial melting of amphibolite/eclogite and the origin of archean trondhjemite and tonalite. Precambrian Research. 51, 1-25

Richardson, S.W., Gilbert, M.C., Bell, P.M. (1969) Experimental determination of kyanite-andalusite and andalusite-sillimanite equilibria; the aluminium silicate triple point. American Journal of Science. 267, 259-272

Roda-Robles, E., Pesquera[1], E.A., Gil, P.P., Torres-Ruiz' J., Fontan, F. (2004) Tourmaline from the rare-element Pinilla pegmatite, (Central Iberian Zone, Zamora, Spain): chemical variation and implications for pegmatitic evolution. Contributions to Mineralogy and Petrology. 81 (3-4), 249-263

Rodriguez-Navarro, C., Cultrone, G., Sanchez-Navas, A., Sebastian, E. (2003) TEM study of mullite growth after muscovite breakdown American Mineralogist; 88 (5-6), 713-724

Rutter, M.J., Wyllie, P.J. (1988) Melting of vapour absent tonalite at 10 kb to simulate dehydration melting in the deep crust. Nature. 331:159-160

Salje, E. (1986) Heat capacities and entropies of andalusite and sillimanite: the influence of fibrolitization on the phase diagram of the Al_2SiO_5 polymorphs. American Mineralogist. 71, 1366-1371

Sawyer, E. W. (1987) The role of partial melting and fractional crystallization in determining discordant migmatite leucosome compositions. Journal of Petrology. 28, 445-473

Sawyer, E. W. (2001) Melt segregation in the continental crust: distribution and movement of melt in anatectic rocks. Journal of Metamorphic Geology. 19, 291-309

Scaillet, B., Pichavant, M., Roux (1995) Experimental crystallization of leucogranite magmas. Journal of Petrology. 36, 663-705

Shaw, H. R. (1965) Comments on viscosity, crystal settling, and convection in granitic magmas. American Journal of Science. 263, 120-152

Shaw, D.M. (1956) Geochemistry of pelitic rocks, III. Bulletin of the Geological Society of America. 67, 919-934

Shearer, C.K., Papike, J.J., Simon, S.B., Laul, J.C. (1986) Pegmatite-wallrock interactions, Black Hills, South Dakota: Interaction between pegmatite-derived fluids and quartz-mica schist wallrock. American Mineralogist. 71, 518-539

Spear, F.S., Kohn, M.J., Florence, F.P., Menhard, T. (1991) A model for garnet and plagioclase growth in pelitic schists: implications for thermobarometry and P-T path determinations. Journal of Metamorphic Geology. 8, 683-696

Spear, F. S., Kohn, M. J., Cheney, J. T. (1999) *P–T* paths from anatectic pelites. Contributions to Mineralogy and Petrology. 134, 17-32

Sperlich, R., Giere, R., Frey, M. (1996) Evolution of compositional polarity and zoning in tourmaline during prograde metamorphism of sedimentary rocks in the Swiss central alps. American Mineralogist. 81(9-10), 1222-1236

Spicer, E.M. , Frazenburg, M. (2010) Analysis of experimental geological run products with SEMEDS, implications for high-resolution micro-beam analysis. Conference proceedings. Analitika 2010

Spicer, E.M., Stevens, G., Buick, I.S. (2003) The low-pressure partial-melting behaviour of natural boron-bearing metapelites from the Mt. Stafford area, central Australia. Contributions to Mineralogy and Petrology. 148, 160-179

Spray, J.G., Rae, D.A. (1995) Quantitative electron-microprobe analysis of alkali silicate glasses: A review and user guide. Canadian Mineralogist. 33, 323-332

Stahle, V., Altherr, R., Koch, M., Nasdala, L. (2004) Shock-induced formation of kyanite (Al_2SiO_5) from sillimanite within a dense metamorphic rocks from the Ries crater (Germany). Contributions to Mineralogy and Petrology. 148, 150-159

Stevens, G., Clemens, J.D., Droop, G.T.R. (1997) Melt production during granulite-facies anatexis: experimental data from "primitive" metasedimentary protoliths. Contributions to Mineralogy and Petrology. 128, 352-370

Stewart, A.J., Shaw, R. D., Black, L. P. (1984) The Arunta Inlier: a complex ensialic mobile belt in central Australia. Part 1: Stratigraphy, correlations and origin Australian Journal of Earth Sciences. 31(4), 445-455

Storre, B. (1972) Dry melting of muscovite+quartz in the range P_s = 7 MPa to P_s = 20 MPa. Contributions to Mineralogy and Petrology. 37, 87-89

Storre, B., Karotke, E. (1972) Experimental data on melting reactions of muscovite+quartz in the system K_2O-Al_2O_3-SiO_2-H_2O to 20 kb water pressure. Contributions to Mineralogy and Petrology. 36, 343-345.

Tertian, R., Claisse, F. (1982) 'Principles of quantitative X-ray fluorescence analysis', Heyden & Sons Ltd, London

Thompson, A.B. (1982) Dehydration melting of pelitic rocks and the generation of H_2O-undersaturated granitic liquids. American Journal of Science. 282, 1567-1595

Thompson, A.B., Tracy, R.J. (1979) Model systems for anatexis of pelitic rocks.II. Facies series melting and reaction in the system CaO-$KAlO_2$-$NaAlO_2$-Al_2O_3-SiO_2-H_2O. Contributions to Mineralogy and Petrology. 70, 429-438

Trønnes, R. G., Edgar, A. D., Arima, M. (1985). A high pressure–high temperature study of TiO_2 solubility in Mg-rich phlogopite: implications to phlogopite chemistry. Geochimica et Cosmochimica Acta. 49, 2323-2329

Varshneya, A.K., Cooper, A.R., Cable, M. (1966) Changes in composition

during electron microprobe analysis of K_2O-SrO-SiO_2, glass. Journal of Applied Physics, 37, 2199-2202

Vassamillet, L.F., Caldwell, V.E. (1969) Electron-probe microanalysis of alkali metals in glasses. Journal of Applied Physics, 40, 1637-1640.

Vernon, R. H. (1982) Isobaric cooling of two regional metamorphic complexes related to igneous intrusions in southeastern Australia. Geology. 10, 76–81

Vernon, R.H. (1987) Oriented growth of sillimanite in andalusite, Placitas-Juan Tabo area, New Mexico, U.S.A. Canadian Journal of Earth Science. 24, 580-590

Vernon, R.H., Clarke, G.L., Collins, W.J. (1990) Local, mid-crustal granulite facies metamorphism and melting: an example in the Mount Stafford earea, central Australia. In: High Temperature Metamorphism and Crustal Anatexis (eds Ashworth JR, Brown M). 272-315. Unwin & Hyman, London.

Vidal, O., Parra, T., Trotet, F. (2001) A Thermodynamic model for Fe-Mg Aluminous chlorite using data from phase equilibrium experiments and natural pelitic assemblages in the 100° to 600°C 1 to 25 kb range. American Journal of Science. 301, 557-592

Vielzeuf, D., Clemens, J.D. (1992) The fluid-absent melting of phlogopite+quartz: Experiments and models. American Mineralogist, 77, 1206-1222

Vielzeuf ,D., Holloway, J.R. (1988) Experimental determination of the fluid-absent melting relations in the pelitic system. Contributions to Mineralogy and Petrology. 98, 257-276

Vielzeuf, D., Montel, J.M. (1994) Partial melting of Al-metagreywackes. Part I: Fluid-absent experiments and phase relationships. Contributions to Mineralogy and Petrology. 117, 375-393

Vielzeuf, D., Schmidt, M.W. (2001) Melting relations in hydrous systems revisited: application to metapelites, metagreywackes and metabasalts. Contributions to Mineralogy and Petrology. 141, 251-267

Vry, J.K., Brown, P.E., Valley, J.W. (1990) Cordierite volatile content and the role of CO_2 in high-grade metamorphism. American Mineralogist. 75, 71-88

Walker, R.J., Hanson, G.N., Papike, J.J., O'Neil, J.R., Laul, J.C. (1986) Internal evolution of the Tin Mountain pegmatite, Black Hills, South Dakota. American Mineralogist. 71, 440-459

Walker, R.J., Hanson, G.N., Papike, J.J. (1989) Trace element constraints on pegmatite genesis: Tin Mountain pegmatite, Black Hills, South Dakota. Contributions to Mineralogy and Petrology. 101, 290-300

Wallmach. T., Hatton, C.J., de Waal, S.A. (1995) Retrogressive hydration of calc-silicate xenoliths in the eastern Bushveld Complex: evidence for late magmatic fluid movement. Journal of African Earth Science. 21, 633-646

Watkins, N.D., Sparks, R.S.J., Sigurdsson, H., Huang, T.C., Federman, A., Carey, S., Ninkovich, D. (1978) Volume and extent of the Minoan tephra from Santorini volcano: New evidence from deep-sea sediment cores. Nature, 271, 122-126.

Weill, D.F. (1966) Stability relations in the Al_2O_3-SiO_2 system calculated from solubilities in the Al_2O_3-SiO_2-Na_3AlF_6 system. Geochimica et Cosmochimica Acta. 51, 389-402

Wenk, H.R. (1983) Mullite-sillimanite intergrowth from pelitic inclusions in Bergell tonalite. Neues jahrbuch fur Mineralogie Abhandlungen. 146, 1-14

Whitney, D.L. (2002) Coexisting andalusite, kyanite, and sillimanite: sequential formation of three polymorphs during progressive metamorphism near the Al_2SiO_5 triple point, Sivrihisar, Turkey. American Mineralogist. 84, 405-416

Wickham, S.M. (1987) Crustal anatexis and granite petrogenesis during low-pressure regional metamorphism: the Trois Seigneurs Massif, Pyrenees, France. Journal of Petrology. 28, 127-169

Wieczorek, Al., Libowitzky, E., Beran, Al. (2004) A model for the OH defect incorporation in kyanite based on polarized IR spectroscopic investigations. Schweizerische Mineralogische und Petrographische Mittelungen. 84(3), 333-343

Wilkins, R.W.T., Sabine, W. (1973) Water content of some nominally anhydrous silicates. American Mineralogist. 58, 508-516

Winter, J.K., Ghose, S. (1979) Thermal expansion and high temperature crystal chemistry of the Al2SiO5 polymorphs. American Mineralogist. 64, 573-586

White, R. W., Powell, R., Holland, T. J. B. (2001) Calculation of partial melting equilibria in the system $Na_2O–CaO–K_2O–FeO–MgO–Al_2O_3–SiO_2–H_2O$ (NCKFMASH). Journal of Metamorphic Geology. 19, 139-153

White, R. W., Powell, R. (2002) Melt loss and the preservation of granulite-facies mineral assemblages. Journal of Metamorphic Geology. 20, 621-632

White, R. W., Powell, R., Clarke, G. L. (2002) The interpretation of reaction textures in Fe-rich metapelitic granulites of the Musgrave Block, central Australia: constraints from mineral equilibria calculations in the system $K_2O–FeO–MgO–Al_2O_3–SiO_2–H_2O–TiO_2–Fe_2O_3$. Journal of Metamorphic Geology. 20, 41-55

White, R .W., Powell R., Clarke, G. L. (2003) Prograde metamorphic assemblage evolution during partial melting of metasedimentary rocks at low pressures: migmatites from Mt Stafford, central Australia. Journal of Petrology. 44(11), 1937-1960

White, A.J.R. (2004) Granite melt forming reactions. Ishihara symposium, Geoscience Australia proceedings.

Wickham, S.M. (1989) Problems in the use of granites as indicators of tectonic setting, International Geological Congress, Conference proceedings 1989

Willis, J.P. (2004) Theory and practice of XRF spectrometry, Cape Town: University of Cape Town, [Unpublished course notes].

Wolf, M.B., London, D. (1997) Boron in granitic magmas: stability of tourmaline in equilibrium with biotite and cordierite. Contributions to Mineralogy and Petrology. 130, 12-30

Wolf, M.B., Wyllie, P.J. (1991) Dehydration-melting of solid amphibolite at 10 MPa: textural development, liquid interconnectivity and applications to the segregation of magmas. Mineralogy and Petrology. 44, 151-179

Wolf, M.B., Wyllie, P.J. (1994) Dehydration-melting of amphibolite at 10 MPa: the effects of temperature and time. Contributions to Mineralogy and Petrology. 115, 369-383

Wyllie, P.J. (1977) Crustal anatexis: An experimental review. Tectonophysics. 43, 41-71

Zen, E. (1986) Aluminum enrichment in silicate melts by fractional crystallization: some mineralogic and petrographic constraints. Journal of Petrology. 27,1095-1117

Appendix 1: Starting mineral chemistry

Feldspar	MTS7-1	MTS7-2	MTS7-3	MTS7-4	MTS7-5	Average MTS7	STDEV7	MTS8-1	MTS8-2	MTS8-3	MTS8-4	MTS8-5	Average MTS8	STDEV MTS8
SiO2	63.28	63.14	63.33	63.32	63.52	**63.32**	**0.14**	63.18	64.62	65.18	64.07	64.84	**64.38**	**0.78**
TiO2	0.04	0.08	0.00	0.01	0.02	**0.03**	**0.03**	0.00	0.03	0.00	0.13	0.00	**0.03**	**0.06**
Al2O3	18.10	18.18	18.57	18.52	18.38	**18.35**	**0.21**	18.23	18.67	18.58	18.25	18.33	**18.41**	**0.20**
Fe2O3	0.00	0.13	0.09	0.00	0.03	**0.05**	**0.06**	0.08	0.01	0.07	0.86	0.00	**0.20**	**0.37**
MgO	0.01	0.00	0.01	0.01	0.02	**0.01**	**0.01**	0.01	0.00	0.01	0.19	0.00	**0.04**	**0.08**
CaO	0.00	0.00	0.03	0.00	0.00	**0.01**	**0.01**	0.00	0.00	0.02	0.00	0.00	**0.00**	**0.01**
Na2O	1.32	1.46	1.20	0.89	0.89	**1.15**	**0.26**	0.71	1.07	0.90	1.43	1.53	**1.13**	**0.35**
K2O	13.57	13.71	14.08	14.78	14.73	**14.17**	**0.56**	14.56	14.53	14.54	13.88	13.72	**14.25**	**0.41**
Sum Ox%	96.33	96.70	97.31	97.53	97.60	**97.09**	**0.55**	96.77	98.93	99.30	98.82	98.42	**98.45**	**0.99**
Si	3.00	2.99	2.98	2.99	2.99	**2.99**	**0.01**	3.00	3.00	3.01	2.98	3.01	**3.00**	**0.01**
Ti	0.00	0.00	0.00	0.00	0.00	**0.00**	**0.00**	0.00	0.00	0.00	0.01	0.00	**0.00**	**0.00**
Al/Al IV	1.01	1.02	1.03	1.03	1.02	**1.02**	**0.01**	1.02	1.02	1.01	1.00	1.00	**1.01**	**0.01**
Al VI	0.00	0.00	0.00	0.00	0.00	**0.00**	**0.00**	0.00	0.00	0.00	0.00	0.00	**0.00**	**0.00**
Fe3+	0.00	0.01	0.00	0.00	0.00	**0.00**	**0.00**	0.00	0.00	0.00	0.03	0.00	**0.01**	**0.01**
Mg	0.00	0.00	0.00	0.00	0.00	**0.00**	**0.00**	0.00	0.00	0.00	0.01	0.00	**0.00**	**0.01**
Ca	0.00	0.00	0.00	0.00	0.00	**0.00**	**0.00**	0.00	0.00	0.00	0.00	0.00	**0.00**	**0.00**
Na	0.12	0.13	0.11	0.08	0.08	**0.11**	**0.02**	0.07	0.10	0.08	0.13	0.14	**0.10**	**0.03**
K	0.82	0.83	0.85	0.89	0.89	**0.85**	**0.03**	0.88	0.86	0.86	0.82	0.81	**0.85**	**0.03**
Sum Cat#	4.96	4.98	4.98	4.99	4.98	**4.98**	**0.01**	4.97	4.97	4.96	4.98	4.96	**4.97**	**0.01**
Ab	12.86	13.92	11.46	8.36	8.43	**11.01**	**2.54**	6.93	10.07	8.62	13.52	14.53	**10.73**	**3.22**
An	0.00	0.00	0.17	0.00	0.00	**0.04**	**0.08**	0.00	0.00	0.09	0.00	0.00	**0.02**	**0.04**
Or	87.14	86.08	88.37	91.64	91.57	**88.96**	**2.55**	93.07	89.93	91.29	86.48	85.47	**89.25**	**3.21**

Tourmaline	MTS70-1	MTS70-2	MTS70-3	MTS70-4	Average MTS70	STDEV MTS70	MTS71-1	MTS71-2	MTS71-3	MTS71-4	MTS71-5	Average MTS71	STDEV MTS71
SiO2	35.74	36.21	35.23	35.92	**35.78**	**0.41**	37.52	36.47	36.44	36.43	36.30	**36.63**	**0.50**
TiO2	0.42	0.73	1.21	0.82	**0.80**	**0.33**	0.55	0.41	0.90	1.17	1.00	**0.81**	**0.32**
Al2O3	33.01	31.17	30.87	32.51	**31.89**	**1.03**	33.58	33.03	31.92	32.21	32.19	**32.59**	**0.69**
Al2O3	33.01	31.17	30.87	32.51	**31.89**	**1.03**	33.58	33.03	31.92	32.21	32.19	**32.59**	**0.69**
B2O3(c)	10.42	10.40	10.27	10.54	**10.41**	**0.11**	10.80	10.54	10.47	10.56	10.53	**10.58**	**0.13**
FeO	11.30	11.22	11.73	9.20	**10.86**	**1.13**	10.97	11.19	9.37	9.75	9.36	**10.13**	**0.89**
MnO	0.17	0.09	0.22	0.16	**0.16**	**0.05**	0.05	0.08	0.05	0.02	0.09	**0.06**	**0.03**
MgO	3.12	4.10	3.77	5.21	**4.05**	**0.87**	3.74	3.46	4.46	4.49	4.69	**4.17**	**0.54**
CaO	0.12	0.26	0.22	0.21	**0.20**	**0.06**	0.07	0.00	0.21	0.29	0.25	**0.16**	**0.12**
Na2O	2.05	2.22	2.12	2.23	**2.16**	**0.09**	2.19	2.01	2.28	2.25	2.33	**2.21**	**0.12**
K2O	0.07	0.02	0.03	0.07	**0.05**	**0.03**	0.02	0.07	0.02	0.02	0.05	**0.04**	**0.02**
H2O(c)	3.59	3.59	3.54	3.64	**3.59**	**0.04**	3.73	3.64	3.61	3.65		**3.66**	**0.05**
Sum Ox%	99.99	100.02	99.21	100.53	**99.94**	**0.54**	103.22	100.91	99.73	100.84	100.43	**101.03**	**1.31**
Si	5.96	6.05	5.96	5.92	**5.97**	**0.05**	6.04	6.02	6.05	5.99	5.99	**6.02**	**0.03**
Ti	0.05	0.09	0.16	0.10	**0.10**	**0.04**	0.07	0.05	0.11	0.15	0.12	**0.10**	**0.04**
Al/Al IV	0.04	0.00	0.04	0.08	**0.04**	**0.03**	0.00	0.00	0.00	0.01	0.01	**0.00**	**0.00**
AlZ	6.00	6.00	6.00	6.00	**6.00**	**0.00**	6.00	6.00	6.00	6.00	6.00	**6.00**	**0.00**
AlY	0.45	0.14	0.12	0.24	**0.24**	**0.15**	0.37	0.42	0.24	0.24	0.25	**0.30**	**0.08**
Fe2+	1.58	1.57	1.66	1.27	**1.52**	**0.17**	1.48	1.54	1.30	1.34	1.29	**1.39**	**0.11**
Mn2+	0.02	0.01	0.03	0.02	**0.02**	**0.01**	0.01	0.01	0.01	0.00	0.01	**0.01**	**0.00**
Mg	0.78	1.02	0.95	1.28	**1.01**	**0.21**	0.90	0.85	1.10	1.10	1.15	**1.02**	**0.14**
Ca	0.02	0.05	0.04	0.04	**0.04**	**0.01**	0.01	0.00	0.04	0.05	0.04	**0.03**	**0.02**
Na	0.66	0.72	0.70	0.71	**0.70**	**0.03**	0.68	0.64	0.74	0.72	0.75	**0.70**	**0.04**
K	0.01	0.01	0.01	0.02	**0.01**	**0.01**	0.00	0.02	0.00	0.00	0.01	**0.01**	**0.01**
OH	4.00	4.00	4.00	4.00	**4.00**	**0.00**	4.00	4.00	4.00	4.00	4.00	**4.00**	**0.00**
Sum Cat#	22.58	22.65	22.66	22.68	**22.64**	**0.04**	22.55	22.55	22.59	22.60	22.63	**22.59**	**0.03**
X	0.70	0.77	0.74	0.77	**0.74**	**0.03**	0.70	0.66	0.78	0.77	0.80	**0.74**	**0.06**
Y	2.88	2.83	2.92	2.92	**2.89**	**0.04**	2.82	2.88	2.77	2.83	2.83	**2.82**	**0.04**
Z	6.00	6.00	6.00	6.00	**6.00**	**0.00**	6.00	6.00	6.00	6.00	6.00	**6.00**	**0.00**
(OH,F)	4.00	4.00	4.00	4.00	**4.00**	**0.00**	4.00	4.00	4.00	4.00	4.00	**4.00**	**0.00**
Mg#	32.96	39.44	36.42	50.24	**39.76**	**7.46**	37.83	35.53	45.90	45.09	47.14	**42.30**	**5.24**

Biotite	MTS7-1	MTS7-2	MTS7-3	MTS7-4	MTS7-5	MTS7-6	MTS7-7	MTS7-8	MTS7-9	MTS7-10	Average MTS7	STDEV MTS7
SiO2	33.62	34.13	34.49	32.01	34.35	34.73	34.05	34.11	33.87	34.52	**33.99**	**0.77**
TiO2	2.55	2.03	3.10	2.86	2.30	2.14	1.86	2.41	2.02	2.69	**2.40**	**0.40**
Al2O3	18.57	19.71	19.05	17.46	19.15	19.17	18.65	18.86	18.97	18.89	**18.85**	**0.58**
FeO	21.42	21.65	20.80	21.62	21.15	21.05	21.10	21.44	21.44	19.51	**21.12**	**0.63**
MnO	0.10	0.10	0.06	0.12	0.11	0.08	0.14	0.07	0.07	0.04	**0.09**	**0.03**
MgO	7.31	7.55	7.72	6.70	8.13	8.02	7.74	7.94	7.96	7.82	**7.69**	**0.42**
CaO	0.15	0.14	0.05	0.09	0.00	0.02	0.05	0.02	0.00	0.00	**0.05**	**0.06**
Na2O	0.12	0.13	0.07	0.08	0.14	0.10	0.07	0.10	0.09	0.12	**0.10**	**0.02**
K2O	8.61	8.65	8.90	8.84	9.19	8.67	9.01	9.12	9.27	8.75	**8.90**	**0.24**
F	0.21	0.26	0.39	0.22	0.30	0.49	0.03	0.10	0.30	0.20	**0.25**	**0.13**
Cl	0.00	0.01	0.00	0.00	0.00	0.00	0.00	0.00	0.01	0.01	**0.00**	**0.00**
H2O(c)	3.68	3.73	3.69	3.53	3.73	3.64	3.77	3.79	3.67	3.72	**3.70**	**0.07**
O=F	0.09	0.11	0.16	0.09	0.13	0.20	0.01	0.04	0.13	0.09	**0.11**	**0.06**
O=Cl	0.00	0.00	0.00	0.00	0.00	0.00	0.00	0.00	0.00	0.00	**0.00**	**0.00**
Sum Ox%	96.25	97.96	98.15	93.43	98.44	97.90	96.46	97.91	97.55	96.18	**97.02**	**1.51**
Si	5.34	5.31	5.34	5.29	5.33	5.39	5.39	5.33	5.32	5.42	**5.34**	**0.04**
Ti	0.31	0.24	0.36	0.36	0.27	0.25	0.22	0.28	0.24	0.32	**0.28**	**0.05**
Al/Al IV	2.66	2.69	2.66	2.71	2.68	2.61	2.61	2.68	2.68	2.58	**2.66**	**0.04**
Al VI	0.81	0.93	0.82	0.69	0.82	0.89	0.87	0.80	0.83	0.91	**0.84**	**0.07**
Fe2+	2.84	2.82	2.69	2.99	2.74	2.73	2.79	2.80	2.81	2.56	**2.78**	**0.11**
Mn2+	0.01	0.01	0.01	0.02	0.02	0.01	0.02	0.01	0.01	0.01	**0.01**	**0.00**
Mg	1.73	1.75	1.78	1.65	1.88	1.85	1.83	1.85	1.86	1.83	**1.80**	**0.07**
Ca	0.03	0.02	0.01	0.02	0.00	0.00	0.01	0.00	0.00	0.00	**0.01**	**0.01**
Na	0.04	0.04	0.02	0.03	0.04	0.03	0.02	0.03	0.03	0.04	**0.03**	**0.01**
K	1.74	1.72	1.76	1.86	1.82	1.72	1.82	1.82	1.86	1.75	**1.79**	**0.06**
F	0.11	0.13	0.19	0.11	0.15	0.24	0.02	0.05	0.15	0.10	**0.12**	**0.06**
Cl	0.00	0.00	0.00	0.00	0.00	0.00	0.00	0.00	0.00	0.00	**0.00**	**0.00**
OH	3.89	3.87	3.81	3.89	3.85	3.76	3.98	3.95	3.85	3.90	**3.87**	**0.06**
Sum Cat#	19.51	19.52	19.45	19.60	19.59	19.49	19.57	19.58	19.63	19.41	**19.54**	**0.07**
Mg#	37.80	38.30	39.80	35.60	40.70	40.40	39.50	39.80	39.80	41.70	**39.34**	**1.72**
Oct	5.71	5.74	5.66	5.70	5.73	5.74	5.72	5.73	5.75	5.62	**5.71**	**0.04**
Int	1.80	1.78	1.79	1.90	1.86	1.75	1.85	1.85	1.89	1.79	**1.83**	**0.05**
Fe+Mg	4.57	4.57	4.48	4.64	4.62	4.59	4.62	4.65	4.68	4.39	**4.58**	**0.18**
Ti+Al6	1.12	1.16	1.18	1.04	1.09	1.14	1.09	1.08	1.06	1.23	**1.12**	**0.12**

Biotite	MTS8-1	MTS8-2	MTS8-3	MTS8-4	MTS8-5	MTS8-6	MTS8-7	MTS8-8	MTS8-9	MTS8-10	Average MTS8	STDEV MTS8
SiO2	34.95	34.06	34.52	34.44	35.14	34.50	34.15	34.51	34.58	34.65	**34.55**	**0.32**
TiO2	2.61	3.11	3.12	3.31	2.08	2.14	2.09	1.98	2.13	2.11	**2.47**	**0.52**
Al2O3	19.21	19.12	18.84	19.05	19.97	19.54	19.62	19.28	19.50	19.00	**19.31**	**0.34**
FeO	19.33	21.62	20.73	21.15	19.40	21.02	20.35	20.72	20.79	19.94	**20.51**	**0.75**
MnO	0.08	0.15	0.19	0.17	0.16	0.17	0.17	0.12	0.13	0.17	**0.15**	**0.03**
MgO	6.89	7.52	7.55	7.41	7.80	7.98	7.96	8.44	8.35	8.23	**7.81**	**0.48**
CaO	0.05	0.01	0.06	0.03	0.02	0.04	0.01	0.00	0.02	0.04	**0.03**	**0.02**
Na2O	0.08	0.08	0.18	0.09	0.09	0.10	0.12	0.11	0.18	0.13	**0.12**	**0.04**
K2O	8.93	9.52	9.12	9.44	8.91	9.30	9.27	9.06	9.31	9.10	**9.20**	**0.21**
F	0.19	0.10	0.08	0.22	0.22	0.05	0.44	0.32	0.29	0.31	**0.22**	**0.12**
Cl	0.00	0.01	0.02	0.00	0.01	0.01	0.00	0.00	0.01	0.01	**0.01**	**0.01**
H2O(c)	3.73	3.82	3.82	3.78	3.78	3.86	3.64	3.72	3.76	3.70	**3.76**	**0.07**
O=F	0.08	0.04	0.04	0.09	0.09	0.02	0.19	0.13	0.12	0.13	**0.09**	**0.05**
O=Cl	0.00	0.00	0.00	0.00	0.00	0.00	0.00	0.00	0.00	0.00	**0.00**	**0.00**
Sum Ox%	95.98	99.08	98.19	98.99	97.46	98.68	97.64	98.14	98.91	97.25	**98.03**	**0.97**
Si	5.49	5.27	5.35	5.32	5.43	5.33	5.32	5.35	5.32	5.40	**5.36**	**0.06**
Ti	0.31	0.36	0.36	0.38	0.24	0.25	0.25	0.23	0.25	0.25	**0.29**	**0.06**
Al/Al IV	2.51	2.73	2.65	2.68	2.57	2.67	2.68	2.65	2.68	2.60	**2.64**	**0.06**
Al VI	1.04	0.76	0.80	0.78	1.06	0.89	0.92	0.87	0.86	0.89	**0.89**	**0.10**
Fe2+	2.54	2.80	2.69	2.73	2.51	2.72	2.65	2.69	2.68	2.60	**2.66**	**0.09**
Mn2+	0.01	0.02	0.03	0.02	0.02	0.02	0.02	0.02	0.02	0.02	**0.02**	**0.00**
Mg	1.61	1.73	1.74	1.70	1.80	1.84	1.85	1.95	1.92	1.91	**1.81**	**0.11**
Ca	0.01	0.00	0.01	0.01	0.00	0.01	0.00	0.00	0.00	0.01	**0.00**	**0.00**
Na	0.02	0.02	0.05	0.03	0.03	0.03	0.04	0.03	0.06	0.04	**0.03**	**0.01**
K	1.79	1.88	1.81	1.86	1.76	1.83	1.84	1.79	1.83	1.81	**1.82**	**0.04**
F	0.09	0.05	0.04	0.11	0.11	0.03	0.22	0.16	0.14	0.15	**0.11**	**0.06**
Cl	0.00	0.00	0.01	0.00	0.00	0.00	0.00	0.00	0.00	0.00	**0.00**	**0.00**
OH	3.91	3.95	3.95	3.89	3.89	3.97	3.78	3.84	3.86	3.85	**3.89**	**0.06**
Sum Cat#	19.33	19.58	19.49	19.51	19.41	19.58	19.57	19.57	19.60	19.53	**19.52**	**0.09**
Mg#	38.90	38.30	39.30	38.40	41.70	40.40	41.10	42.10	41.70	42.40	**40.43**	**1.59**
Oct	5.51	5.67	5.62	5.62	5.62	5.71	5.69	5.75	5.72	5.67	**5.66**	**0.07**
Int	1.82	1.90	1.87	1.89	1.78	1.87	1.88	1.82	1.89	1.86	**1.86**	**0.04**
Fe+Mg	4.15	4.53	4.43	4.43	4.30	4.55	4.50	4.63	4.59	4.51	**4.46**	**0.20**
Ti+Al6	1.35	1.12	1.16	1.16	1.30	1.13	1.17	1.10	1.11	1.14	**1.17**	**0.16**

Biotite	MTS70-1	MTS70-2	MTS70-3	MTS70-4	MTS70-5	MTS70-6	MTS70-7	MTS70-8	MTS70-9	MTS70-10	Average MTS70	STDEV MTS70
SiO2	34.34	35.50	36.20	33.24	34.29	33.49	34.35	34.37	34.42	34.21	**34.44**	**0.86**
TiO2	1.76	1.57	2.56	2.17	2.07	1.70	1.91	1.95	1.98	1.94	**1.96**	**0.27**
Al2O3	17.48	16.83	18.49	16.98	17.53	17.59	17.70	17.69	17.46	17.78	**17.55**	**0.45**
FeO	25.82	24.10	26.21	25.93	25.90	27.17	25.90	26.07	25.23	26.78	**25.91**	**0.83**
MnO	0.39	0.58	0.64	0.65	0.57	0.62	0.66	0.64	0.56	0.67	**0.60**	**0.08**
MgO	4.21	3.78	4.48	4.00	4.19	3.97	3.95	4.09	4.04	4.11	**4.08**	**0.19**
CaO	0.11	0.12	0.03	0.07	0.02	0.00	0.06	0.03	0.05	0.02	**0.05**	**0.04**
Na2O	0.06	0.08	0.06	0.07	0.07	0.05	0.05	0.05	0.02	0.05	**0.06**	**0.02**
K2O	8.77	8.19	8.61	8.65	9.11	9.05	8.48	8.96	8.83	8.81	**8.75**	**0.28**
F	0.87	1.07	1.31	1.04	1.42	0.75	0.97	1.03	0.63	0.90	**1.00**	**0.24**
Cl	0.06	0.05	0.01	0.02	0.02	0.03	0.04	0.00	0.00	0.00	**0.02**	**0.02**
H2O(c)	3.29	3.16	3.29	3.14	3.05	3.33	3.25	3.25	3.41	3.32	**3.25**	**0.11**
O=F	0.36	0.45	0.55	0.44	0.60	0.31	0.41	0.43	0.26	0.38	**0.42**	**0.10**
O=Cl	0.01	0.01	0.00	0.00	0.00	0.01	0.01	0.00	0.00	0.00	**0.00**	**0.01**
Sum Ox%	96.76	94.57	101.33	95.52	97.64	97.43	96.91	97.70	96.35	98.20	**97.24**	**1.80**
Si	5.55	5.79	5.54	5.47	5.51	5.43	5.54	5.51	5.57	5.47	**5.54**	**0.10**
Ti	0.21	0.19	0.29	0.27	0.25	0.21	0.23	0.24	0.24	0.23	**0.24**	**0.03**
Al/Al IV	2.45	2.21	2.46	2.53	2.49	2.57	2.46	2.49	2.43	2.53	**2.46**	**0.10**
Al VI	0.88	1.03	0.88	0.77	0.83	0.80	0.90	0.86	0.90	0.82	**0.87**	**0.07**
Fe2+	3.49	3.29	3.36	3.57	3.48	3.69	3.49	3.50	3.41	3.58	**3.49**	**0.11**
Mn2+	0.05	0.08	0.08	0.09	0.08	0.09	0.09	0.09	0.08	0.09	**0.08**	**0.01**
Mg	1.01	0.92	1.02	0.98	1.00	0.96	0.95	0.98	0.97	0.98	**0.98**	**0.03**
Ca	0.02	0.02	0.01	0.01	0.00	0.00	0.01	0.01	0.01	0.00	**0.01**	**0.01**
Na	0.02	0.03	0.02	0.02	0.02	0.02	0.02	0.02	0.01	0.02	**0.02**	**0.01**
K	1.81	1.70	1.68	1.82	1.87	1.87	1.74	1.83	1.82	1.80	**1.79**	**0.06**
F	0.44	0.55	0.64	0.54	0.72	0.38	0.49	0.52	0.32	0.45	**0.51**	**0.12**
Cl	0.02	0.01	0.00	0.01	0.01	0.01	0.01	0.00	0.00	0.00	**0.01**	**0.01**
OH	3.54	3.44	3.36	3.45	3.27	3.61	3.50	3.48	3.68	3.55	**3.49**	**0.12**
Sum Cat#	19.49	19.26	19.34	19.53	19.53	19.62	19.43	19.51	19.44	19.53	**19.47**	**0.10**
Mg#	22.50	21.90	23.40	21.60	22.40	20.70	21.40	21.90	22.20	21.50	**21.95**	**0.74**
Oct	5.64	5.51	5.64	5.68	5.64	5.73	5.66	5.65	5.60	5.71	**5.65**	**0.06**
Int	1.84	1.75	1.70	1.85	1.89	1.89	1.77	1.85	1.84	1.82	**1.82**	**0.06**
Fe+Mg	4.50	4.21	4.38	4.55	4.48	4.65	4.44	4.48	4.39	4.56	**4.46**	**0.14**
Ti+Al6	1.09	1.22	1.18	1.04	1.08	1.00	1.13	1.09	1.14	1.06	**1.10**	**0.10**

Biotite	MTS71-1	MTS71-2	MTS71-3	MTS71-4	MTS71-5	Average MTS71	STDEV MTS71
SiO2	34.59	34.39	33.12	35.10	32.74	**33.99**	**1.01**
TiO2	2.10	2.10	2.09	1.91	2.10	**2.06**	**0.08**
Al2O3	17.33	17.80	16.48	17.02	16.22	**16.97**	**0.64**
FeO	25.86	26.42	26.06	24.92	26.05	**25.86**	**0.56**
MnO	0.46	0.37	0.42	0.23	0.43	**0.38**	**0.09**
MgO	3.69	3.79	3.61	3.86	3.58	**3.71**	**0.12**
CaO	0.08	0.09	0.14	0.14	0.19	**0.13**	**0.04**
Na2O	0.07	0.07	0.08	0.10	0.11	**0.09**	**0.02**
K2O	8.25	8.57	8.02	8.35	8.27	**8.29**	**0.20**
F	0.67	1.13	0.82	0.72	0.78	**0.82**	**0.18**
Cl	0.02	0.02	0.00	0.01	0.03	**0.02**	**0.01**
H2O(c)	3.38	3.20	3.19	3.35	3.18	**3.26**	**0.10**
O=F	0.28	0.47	0.34	0.31	0.33	**0.35**	**0.07**
O=Cl	0.00	0.00	0.00	0.00	0.01	**0.00**	**0.00**
Sum Ox%	96.21	97.46	93.69	95.40	93.35	**95.22**	**1.72**
Si	5.60	5.52	5.55	5.70	5.52	**5.58**	**0.08**
Ti	0.26	0.25	0.26	0.23	0.27	**0.25**	**0.01**
Al/Al IV	2.40	2.48	2.45	2.30	2.48	**2.42**	**0.08**
Al VI	0.91	0.89	0.80	0.95	0.75	**0.86**	**0.08**
Fe2+	3.50	3.55	3.65	3.38	3.68	**3.55**	**0.12**
Mn2+	0.06	0.05	0.06	0.03	0.06	**0.05**	**0.01**
Mg	0.89	0.91	0.90	0.93	0.90	**0.91**	**0.02**
Ca	0.02	0.02	0.03	0.02	0.03	**0.02**	**0.01**
Na	0.02	0.02	0.03	0.03	0.04	**0.03**	**0.01**
K	1.70	1.75	1.71	1.73	1.78	**1.74**	**0.03**
F	0.34	0.57	0.43	0.37	0.42	**0.43**	**0.09**
Cl	0.01	0.01	0.00	0.00	0.01	**0.01**	**0.00**
OH	3.65	3.42	3.57	3.62	3.57	**3.57**	**0.09**
Sum Cat#	19.36	19.43	19.43	19.32	19.50	**19.41**	**0.07**
Mg#	20.30	20.40	19.80	21.60	19.70	**20.36**	**0.76**
Oct	5.61	5.64	5.67	5.54	5.66	**5.62**	**0.05**
Int	1.74	1.79	1.76	1.78	1.85	**1.79**	**0.04**
Fe+Mg	4.39	4.45	4.55	4.32	4.58	**4.46**	**0.13**
Ti+Al6	1.16	1.14	1.06	1.19	1.02	**1.11**	**0.10**

Muscovite	MTS70-1	MTS70-2	MTS70-3	MTS70-4	MTS70-5	MTS70-6	MTS70-7	MTS70-8	MTS70-9	Average MTS70	STDEV MTS70
SiO2	48.00	47.73	48.20	46.79	45.66	48.35	47.92	48.33	48.25	**47.69**	**0.90**
TiO2	0.78	0.60	0.46	0.58	0.48	0.57	0.57	0.70	0.50	**0.58**	**0.10**
Al2O3	34.89	34.14	34.61	33.68	33.36	34.47	33.80	34.23	34.15	**34.15**	**0.48**
FeO	1.96	1.84	1.93	1.97	2.01	1.86	1.97	2.14	2.09	**1.97**	**0.10**
MnO	0.08	0.11	0.06	0.08	0.04	0.02	0.00	0.05	0.03	**0.05**	**0.03**
MgO	0.78	0.87	0.93	0.79	0.81	0.73	0.93	0.94	0.87	**0.85**	**0.08**
CaO	0.00	0.01	0.01	0.01	0.00	0.00	0.01	0.00	0.01	**0.01**	**0.01**
Na2O	0.38	0.44	0.44	0.31	0.43	0.37	0.37	0.38	0.37	**0.39**	**0.04**
K2O	10.21	10.25	9.97	9.94	9.85	10.16	10.18	9.98	10.09	**10.07**	**0.14**
F	0.43	0.14	0.52	0.33	0.48	0.46	0.39	0.37	0.29	**0.38**	**0.12**
Cl	0.00	0.01	0.00	0.00	0.04	0.01	0.01	0.00	0.02	**0.01**	**0.01**
H2O(c)	4.39	4.47	4.34	4.30	4.14	4.36	4.35	4.41	4.42	**4.35**	**0.09**
O=F	0.18	0.06	0.22	0.14	0.20	0.20	0.16	0.15	0.12	**0.16**	**0.05**
O=Cl	0.00	0.00	0.00	0.00	0.01	0.00	0.00	0.00	0.00	**0.00**	**0.00**
Sum Ox%	101.71	100.56	101.25	98.65	97.08	101.16	100.32	101.38	100.96	**100.34**	**1.52**
Si	6.26	6.30	6.31	6.29	6.25	6.33	6.34	6.32	6.34	**6.31**	**0.03**
Ti	0.08	0.06	0.05	0.06	0.05	0.06	0.06	0.07	0.05	**0.06**	**0.01**
Al/Al IV	1.74	1.70	1.69	1.71	1.75	1.67	1.66	1.68	1.66	**1.69**	**0.03**
Al VI	3.63	3.62	3.65	3.63	3.64	3.65	3.61	3.60	3.62	**3.63**	**0.02**
Fe2+	0.21	0.20	0.21	0.22	0.23	0.20	0.22	0.23	0.23	**0.22**	**0.01**
Mn2+	0.01	0.01	0.01	0.01	0.00	0.00	0.00	0.01	0.00	**0.01**	**0.00**
Mg	0.15	0.17	0.18	0.16	0.17	0.14	0.18	0.18	0.17	**0.17**	**0.01**
Ca	0.00	0.00	0.00	0.00	0.00	0.00	0.00	0.00	0.00	**0.00**	**0.00**
Na	0.10	0.11	0.11	0.08	0.11	0.09	0.09	0.10	0.09	**0.10**	**0.01**
K	1.70	1.73	1.66	1.71	1.72	1.70	1.72	1.67	1.69	**1.70**	**0.02**
F	0.18	0.06	0.22	0.14	0.21	0.19	0.16	0.15	0.12	**0.16**	**0.05**
Cl	0.00	0.00	0.00	0.00	0.01	0.00	0.00	0.00	0.00	**0.00**	**0.00**
OH	3.82	3.94	3.78	3.86	3.78	3.81	3.84	3.85	3.88	**3.84**	**0.05**
Sum Cat#	17.88	17.90	17.87	17.87	17.92	17.85	17.88	17.85	17.86	**17.88**	**0.02**
Mg#	41.40	45.60	46.10	41.60	41.80	41.00	45.70	44.00	42.50	**43.30**	**2.06**
Oct	4.08	4.06	4.09	4.08	4.09	4.06	4.06	4.09	4.08	**4.08**	**0.01**
Int	1.80	1.84	1.78	1.79	1.83	1.79	1.81	1.76	1.79	**1.80**	**0.03**
Fe+Mg+Mn	0.37	0.39	0.40	0.39	0.40	0.35	0.40	0.42	0.40	**0.39**	**0.02**
Al6+Si	9.89	9.92	9.95	9.93	9.89	9.99	9.95	9.92	9.96	**9.93**	**0.03**
Ti+Al4	1.81	1.76	1.74	1.77	1.80	1.72	1.72	1.75	1.71	**1.75**	**0.03**
Fe+Mg	0.37	0.38	0.39	0.38	0.40	0.35	0.40	0.42	0.40	**0.39**	**0.02**

Muscovite	MTSS71-1	MTSS71-2	MTSS71-3	MTSS71-4	MTSS71-5	MTSS71-6	MTSS71-7	MTSS71-8	MTSS71-9	Average MTS71	STDEV MTS71
SiO2	48.69	49.01	49.02	46.25	48.58	46.54	47.46	49.06	48.15	**48.08**	**1.14**
TiO2	0.83	0.86	0.65	0.51	0.67	0.56	0.79	0.71	0.76	**0.70**	**0.12**
Al2O3	34.65	34.73	34.83	34.50	34.11	32.99	34.20	34.95	34.04	**34.33**	**0.63**
FeO	2.21	2.18	2.07	1.88	2.11	1.94	2.17	2.14	1.98	**2.08**	**0.11**
MnO	0.09	0.00	0.06	0.04	0.07	0.00	0.00	0.00	0.05	**0.03**	**0.03**
MgO	0.79	0.82	0.73	0.59	0.79	0.63	0.79	0.82	0.81	**0.75**	**0.09**
CaO	0.03	0.05	0.02	0.03	0.00	0.04	0.01	0.04	0.01	**0.03**	**0.02**
Na2O	0.23	0.29	0.31	0.36	0.34	0.28	0.32	0.35	0.35	**0.31**	**0.03**
K2O	10.05	10.40	10.23	10.32	10.28	10.41	10.34	9.87	10.31	**10.25**	**0.17**
F	0.36	0.37	0.27	0.33	0.58	0.52	0.39	0.54	0.48	**0.43**	**0.11**
Cl	0.00	0.03	0.04	0.02	0.01	0.02	0.01	0.00	0.03	**0.02**	**0.01**
H2O(c)	4.45	4.47	4.51	4.30	4.31	4.16	4.35	4.40	4.33	**4.36**	**0.11**
O=F	0.15	0.15	0.11	0.14	0.24	0.22	0.16	0.23	0.20	**0.18**	**0.05**
O=Cl	0.00	0.01	0.01	0.00	0.00	0.00	0.00	0.00	0.01	**0.00**	**0.01**
Sum Ox%	102.22	103.05	102.61	98.98	101.61	97.85	100.66	102.65	101.07	**101.19**	**1.85**
Si	6.31	6.32	6.33	6.22	6.35	6.33	6.27	6.33	6.33	**6.31**	**0.04**
Ti	0.08	0.08	0.06	0.05	0.07	0.06	0.08	0.07	0.08	**0.07**	**0.01**
Al/Al IV	1.69	1.68	1.67	1.78	1.65	1.67	1.73	1.68	1.67	**1.69**	**0.04**
Al VI	3.61	3.59	3.63	3.68	3.60	3.62	3.60	3.63	3.60	**3.62**	**0.03**
Fe2+	0.24	0.23	0.22	0.21	0.23	0.22	0.24	0.23	0.22	**0.23**	**0.01**
Mn2+	0.01	0.00	0.01	0.00	0.01	0.00	0.00	0.00	0.01	**0.00**	**0.00**
Mg	0.15	0.16	0.14	0.12	0.15	0.13	0.16	0.16	0.16	**0.15**	**0.02**
Ca	0.00	0.01	0.00	0.00	0.00	0.01	0.00	0.01	0.00	**0.00**	**0.00**
Na	0.06	0.07	0.08	0.09	0.09	0.07	0.08	0.09	0.09	**0.08**	**0.01**
K	1.66	1.71	1.69	1.77	1.71	1.81	1.74	1.62	1.73	**1.72**	**0.05**
F	0.15	0.15	0.11	0.14	0.24	0.23	0.16	0.22	0.20	**0.18**	**0.05**
Cl	0.00	0.01	0.01	0.01	0.00	0.00	0.00	0.00	0.01	**0.00**	**0.00**
OH	3.85	3.85	3.88	3.86	3.76	3.77	3.84	3.78	3.79	**3.82**	**0.05**
Sum Cat#	17.82	17.86	17.84	17.93	17.86	17.91	17.90	17.81	17.87	**17.87**	**0.04**
Mg#	38.90	40.30	38.60	36.00	40.10	36.60	39.30	40.60	42.10	**39.17**	**2.06**
Oct	4.09	4.07	4.07	4.07	4.06	4.02	4.07	4.09	4.05	**4.07**	**0.02**
Int	1.73	1.79	1.77	1.87	1.80	1.89	1.83	1.72	1.82	**1.80**	**0.05**
Fe+Mg+Mn	0.40	0.39	0.37	0.33	0.39	0.35	0.40	0.39	0.38	**0.37**	**0.02**
Al6+Si	9.92	9.91	9.97	9.90	9.95	9.95	9.87	9.96	9.93	**9.93**	**0.03**
Ti+Al4	1.77	1.77	1.73	1.84	1.72	1.73	1.81	1.74	1.75	**1.76**	**0.04**
Fe+Mg	0.39	0.39	0.37	0.33	0.38	0.35	0.40	0.39	0.38	**0.37**	**0.02**

Appendix 2: Precision and accuracy of SEM-EDS quantitative analysis on Albite, Almandine, Clinopyroxene, Orthopyroxene and Pyrope.

Feldspar Analysis	Na2O	Al2O3	SiO2	K2O	CaO	Total	Si	Al	Ca	Na	K	Cat Total
Albite 1	11.14	19.25	68.35	0.18	0.14	98.97	3.01	1.00	0.01	0.95	0.01	4.97
Albite 2	11.13	19.45	68.67	0.18	0.14	99.47	3.01	1.00	0.01	0.94	0.01	4.97
Albite 3	11.21	19.14	68.52	0.17	0.14	99.07	3.01	0.99	0.01	0.96	0.01	4.97
Albite 4	11.41	19.02	68.59	0.15	0.12	99.17	3.01	0.98	0.01	0.97	0.01	4.98
Albite 5	11.45	19.05	68.60	0.23	0.11	99.24	3.01	0.98	0.01	0.97	0.01	4.99
Albite 6	11.33	19.20	69.21	0.16	0.21	100.01	3.01	0.98	0.01	0.96	0.01	4.97
Albite 7	11.21	19.22	68.41	0.22	0.12	98.98	3.01	1.00	0.01	0.96	0.01	4.98
Albite 8	11.48	19.15	68.92	0.15	0.05	99.65	3.01	0.99	0.00	0.97	0.01	4.98
Albite 9	11.35	19.35	68.41	0.19	0.02	99.24	3.00	1.00	0.00	0.97	0.01	4.98
Albite 10	11.34	19.20	68.96	0.16	0.11	99.68	3.01	0.99	0.01	0.96	0.01	4.98
Average (n=10)	**11.30**	**19.20**	**68.66**	**0.18**	**0.11**	**99.35**	**3.01**	**0.99**	**0.01**	**0.96**	**0.01**	**4.98**
Albite Reference	**11.58**	**19.53**	**68.52**	**0.22**	**0.13**	**100.00**	**2.99**	**1.00**	**0.01**	**0.98**	**0.01**	**5.00**
Difference	0.28	0.33	0.14	0.04	0.02	0.65	0.02	0.01	0.00	0.02	0.00	0.02
%Rel Error	0.60	0.42	0.05	5.07	3.12	0.16	0.13	0.34	3.05	0.52	4.99	0.10
Stdev (n=10)	0.13	0.13	0.28	0.03	0.05	0.34	0.00	0.01	0.00	0.01	0.00	0.01

Garnet Analysis	MgO	Al2O3	SiO2	CaO	MnO	FeO	Total	Si	Al	Fe tot	Mn	Mg	Ca	TOT
Almandine1	10.56	21.86	39.08	4.21	0.70	23.34	99.78	2.98	1.95	1.49	0.05	1.20	0.34	8.01
Almandine2	10.47	21.75	39.18	4.21	0.62	23.59	99.88	2.99	1.94	1.51	0.04	1.19	0.34	8.01
Almandine3	10.42	21.78	39.04	4.31	0.67	23.53	99.71	2.98	1.94	1.50	0.04	1.19	0.35	8.02
Almandine4	10.51	21.86	39.11	4.19	0.56	23.62	99.90	2.98	1.95	1.51	0.04	1.20	0.34	8.01
Almandine5	10.52	21.94	39.12	4.27	0.65	23.55	100.15	2.98	1.95	1.50	0.04	1.19	0.35	8.02
Almandine6	10.54	21.85	39.37	4.23	0.66	23.40	100.11	3.00	1.94	1.49	0.04	1.20	0.34	8.01
Almandine7	10.39	21.89	39.29	4.23	0.59	23.95	100.51	2.99	1.94	1.52	0.04	1.18	0.34	8.01
Almandine8	10.32	21.73	39.09	4.29	0.60	23.41	99.52	2.99	1.94	1.50	0.04	1.18	0.35	8.00
Almandine9	10.55	21.80	39.10	4.21	0.64	23.32	99.58	2.99	1.94	1.49	0.04	1.20	0.34	8.01
Almandine10	10.60	21.84	39.48	4.18	0.70	23.56	100.35	3.00	1.93	1.50	0.04	1.20	0.34	8.01
Average (n=10)	**10.49**	**21.83**	**39.18**	**4.23**	**0.64**	**23.53**	**99.95**	**2.99**	**1.94**	**1.50**	**0.04**	**1.19**	**0.35**	**8.01**
Almandine Reference	**10.70**	**22.05**	**39.19**	**4.20**	**0.59**	**23.27**	**100.00**	**2.98**	**1.96**	**1.48**	**0.04**	**1.21**	**0.34**	**8.01**
Difference	0.21	0.22	0.01	0.03	0.05	0.26	0.05	0.01	0.01	0.02	0.00	0.02	0.00	0.00
%Rel Error	0.50	0.25	0.003	0.19	1.96	0.27	0.01	0.06	0.18	0.34	2.03	0.43	0.26	0.00
Stdev (n=10)	0.09	0.06	0.15	0.04	0.04	0.18	0.32	0.01	0.00	0.01	0.00	0.01	0.00	0.00

Pyroxene Analysis	Na2O	MgO	Al2O3	SiO2	CaO	TiO2	Cr2O3	MnO	FeO	NiO	Total
jjg1424-cpx-1	1.78	16.27	1.47	55.87	23.16	0.25	0.67	0.08	1.70	0.002	101.25
jjg1424-cpx-2	1.74	15.99	1.42	55.71	22.87	0.22	0.64	0.04	1.74	0.008	100.39
jjg1424-cpx-3	1.66	15.93	1.40	55.26	22.78	0.23	0.76	0.08	1.78	0.000	99.88
jjg1424-cpx-4	1.79	15.81	1.43	55.31	22.81	0.24	0.70	0.00	1.63	0.002	99.69
jjg1424-cpx-5	1.72	15.86	1.42	55.05	22.77	0.21	0.71	0.12	1.77	0.005	99.62
jjg1424-cpx-6	1.65	15.83	1.44	55.00	22.75	0.23	0.71	0.18	1.78	0.001	99.57
jjg1424-cpx-7	1.69	15.84	1.44	54.88	22.60	0.24	0.68	0.11	1.70	0.008	99.18
jjg1424-cpx-8	1.81	16.06	1.43	55.39	22.84	0.21	0.71	0.03	1.82	0.005	100.31
jjg1424-cpx-9	1.71	16.04	1.46	55.38	22.65	0.19	0.68	0.08	1.69	0.008	99.89
jjg1424-cpx-10	1.61	15.84	1.41	54.69	22.56	0.20	0.75	0.12	1.65	0.001	98.83
Average (n=10)	**1.72**	**15.95**	**1.43**	**55.25**	**22.78**	**0.22**	**0.70**	**0.08**	**1.73**	**0.004**	**99.86**
JJG1424-cpx Reference	**1.55**	**16.61**	**2.99**	**54.57**	**21.54**	**0.25**	**0.81**	**0.06**	**1.64**	**0.002**	**100.02**
Difference	0.17	0.66	1.56	0.68	1.24	0.03	0.11	0.02	0.09	0.002	0.16
%Rel error	2.53	1.02	17.62	0.31	1.40	3.02	3.56	8.10	1.27	16.67	0.04
Stdev	0.06	0.15	0.02	0.36	0.17	0.02	0.04	0.05	0.06	0.00	0.68

Structural formulae	Si	Ti	Al	Fe tot	Mn	Mg	Ca	Na	Cr	Ni	TOT
jjg1424-cpx-1	1.99	0.01	0.06	0.05	0.002	0.86	0.88	0.20	0.02	0.00	4.06
jjg1424-cpx-2	1.99	0.01	0.06	0.05	0.001	0.85	0.88	0.19	0.02	0.00	4.06
jjg1424-cpx-3	1.99	0.01	0.06	0.05	0.002	0.86	0.88	0.18	0.02	0.00	4.05
jjg1424-cpx-4	1.99	0.01	0.06	0.05	0.000	0.85	0.88	0.20	0.02	0.00	4.06
jjg1424-cpx-5	1.99	0.01	0.06	0.05	0.004	0.85	0.88	0.19	0.02	0.00	4.06
jjg1424-cpx-6	1.99	0.01	0.06	0.05	0.006	0.85	0.88	0.18	0.02	0.00	4.05
jjg1424-cpx-7	1.99	0.01	0.06	0.05	0.004	0.86	0.88	0.19	0.02	0.00	4.06
jjg1424-cpx-8	1.99	0.01	0.06	0.05	0.001	0.86	0.88	0.20	0.02	0.00	4.07
jjg1424-cpx-9	1.99	0.01	0.06	0.05	0.002	0.86	0.87	0.19	0.02	0.00	4.06
jjg1424-cpx-10	1.99	0.01	0.06	0.05	0.004	0.86	0.88	0.18	0.02	0.00	4.05
Average (n=10)	**1.99**	**0.01**	**0.06**	**0.05**	**0.003**	**0.86**	**0.88**	**0.19**	**0.02**	**0.00**	**4.06**
JJG1424-cpx Reference	**1.96**	**0.01**	**0.13**	**0.05**	**0.002**	**0.89**	**0.83**	**0.17**	**0.02**	**0.00**	**4.05**
Difference	0.03	0.00	0.06	0.00	0.00	0.03	0.05	0.02	0.00	0.00	0.01
%Rel error	0.44	2.89	17.51	1.40	8.23	0.89	1.53	2.66	3.43	-	0.06
Stdev	0.00	0.00	0.00	0.00	0.00	0.00	0.00	0.01	0.00	0.00	0.00

Pyroxene Analysis	Na2O	MgO	Al2O3	SiO2	CaO	TiO2	Cr2O3	MnO	FeO	Total
jjg1424-opx-1	0.20	35.10	0.66	59.00	0.23	0.11	0.16	0.22	5.22	100.89
jjg1424-opx-2	0.18	34.52	0.67	57.92	0.27	0.06	0.20	0.16	5.30	99.29
jjg1424-opx-3	0.23	34.91	0.64	58.57	0.22	0.11	0.20	0.21	5.17	100.25
jjg1424-opx-4	0.19	34.90	0.67	58.41	0.27	0.11	0.16	0.27	5.10	100.09
jjg1424-opx-5	0.15	34.76	0.68	58.54	0.28	0.04	0.18	0.29	5.24	100.16
jjg1424-opx-6	0.17	34.57	0.64	58.15	0.18	0.06	0.18	0.19	5.31	99.46
jjg1424-opx-7	0.15	34.88	0.64	58.56	0.24	0.07	0.20	0.17	5.29	100.19
jjg1424-opx-8	0.17	34.94	0.66	58.70	0.26	0.04	0.19	0.16	5.44	100.57
jjg1424-opx-9	0.19	35.33	0.69	59.20	0.19	0.06	0.23	0.05	5.29	101.23
jjg1424-opx-10	0.21	35.29	0.69	59.35	0.25	0.07	0.18	0.12	5.10	101.29
Average (n=10)	**0.18**	**34.92**	**0.66**	**58.64**	**0.24**	**0.07**	**0.19**	**0.18**	**5.25**	**100.34**
JJG1424-opx Reference	**0.16**	**35.71**	**1.18**	**57.57**	**0.30**	**0.11**	**0.21**	**0.08**	**4.91**	**100.07**
Difference	0.02	0.79	0.52	1.07	0.06	0.04	0.02	0.10	0.34	0.27
%Rel error	3.46	0.56	13.96	0.46	5.62	9.81	3.13	19.52	1.65	0.07
Stdev	0.02	0.27	0.02	0.45	0.03	0.03	0.02	0.07	0.10	0.67

Structural formulae	Si	Ti	Al	Fe tot	Mn	Mg	Ca	Na	Cr	TOT
jjg1424-opx-1	2.00	0.00	0.03	0.15	0.01	1.77	0.01	0.02	0.00	3.99
jjg1424-opx-2	2.00	0.00	0.03	0.15	0.00	1.78	0.01	0.02	0.01	3.99
jjg1424-opx-3	2.00	0.00	0.03	0.15	0.01	1.78	0.01	0.02	0.01	3.99
jjg1424-opx-4	2.00	0.00	0.03	0.15	0.01	1.78	0.01	0.02	0.00	3.99
jjg1424-opx-5	2.00	0.00	0.03	0.15	0.01	1.77	0.01	0.02	0.00	3.99
jjg1424-opx-6	2.00	0.00	0.03	0.15	0.01	1.77	0.01	0.02	0.00	3.99
jjg1424-opx-7	2.00	0.00	0.03	0.15	0.00	1.78	0.01	0.02	0.01	3.99
jjg1424-opx-8	2.00	0.00	0.03	0.15	0.00	1.77	0.01	0.02	0.01	3.99
jjg1424-opx-9	2.00	0.00	0.03	0.15	0.00	1.78	0.01	0.02	0.01	3.99
jjg1424-opx-10	2.00	0.00	0.03	0.14	0.00	1.78	0.01	0.02	0.00	3.99
Average (n=10)	**2.00**	**0.00**	**0.03**	**0.15**	**0.01**	**1.78**	**0.01**	**0.02**	**0.00**	**3.99**
JJG1424-opx Reference	**1.97**	**0.00**	**0.05**	**0.14**	**0.00**	**1.82**	**0.01**	**0.02**	**0.01**	**4.01**
Difference	0.03	0.00	0.02	0.01	0.00	0.04	0.00	0.00	0.00	0.02
%Rel error	0.42	9.85	14.00	1.61	19.49	0.60	5.66	3.42	3.17	0.12
Stdev	0.00	0.00	0.00	0.00	0.00	0.00	0.00	0.00	0.00	0.00

Pyroxene Analysis	Na2O	MgO	SiO2	CaO	TiO2	Cr2O3	FeO	Total
Cr Diopside-1	0.43	16.69	54.46	26.04	0.06	0.54	1.44	99.84
Cr Diopside-2	0.50	16.70	54.50	25.93	0.06	0.52	1.54	99.93
Cr Diopside-3	0.48	16.67	54.68	26.04	0.09	0.54	1.44	100.06
Cr Diopside-4	0.48	16.60	54.20	26.00	0.11	0.53	1.44	99.42
Cr Diopside-5	0.50	16.62	54.27	25.91	0.09	0.56	1.40	99.65
Cr Diopside-6	0.45	16.41	53.64	25.71	0.09	0.49	1.40	98.45
Cr Diopside-7	0.47	16.79	54.55	25.95	0.04	0.55	1.45	99.98
Cr Diopside-8	0.50	16.54	54.32	25.94	0.09	0.56	1.42	99.60
Cr Diopside-9	0.46	16.58	54.07	25.79	0.09	0.62	1.41	99.20
Cr Diopside-10	0.46	16.59	54.89	26.24	0.09	0.57	1.43	100.50
Average (n=10)	**0.47**	**16.62**	**54.36**	**25.95**	**0.08**	**0.55**	**1.44**	**99.66**
Cr-Diopside Reference	**0.44**	**17.17**	**54.59**	**25.50**	**0.10**	**0.50**	**1.39**	**99.69**
Difference	0.03	0.55	0.23	0.45	0.02	0.05	0.05	0.03
%Rel error	1.83	0.81	0.11	0.44	5.44	2.28	0.82	0.01
Stdev	0.02	0.10	0.35	0.14	0.02	0.03	0.04	0.56

Structural formulae	Si	Ti	Fe tot	Mg	Ca	Na	Cr	TOT
Cr Diopside-1	1.98	0.002	0.04	0.91	1.02	0.05	0.02	4.03
Cr Diopside-2	1.98	0.002	0.05	0.91	1.01	0.06	0.01	4.03
Cr Diopside-3	1.99	0.002	0.04	0.90	1.01	0.05	0.02	4.03
Cr Diopside-4	1.98	0.003	0.04	0.90	1.02	0.05	0.02	4.03
Cr Diopside-5	1.98	0.002	0.04	0.91	1.01	0.06	0.02	4.03
Cr Diopside-6	1.98	0.003	0.04	0.90	1.02	0.05	0.01	4.03
Cr Diopside-7	1.98	0.001	0.04	0.91	1.01	0.05	0.02	4.03
Cr Diopside-8	1.98	0.002	0.04	0.90	1.02	0.06	0.02	4.03
Cr Diopside-9	1.98	0.002	0.04	0.91	1.01	0.05	0.02	4.03
Cr Diopside-10	1.99	0.002	0.04	0.90	1.02	0.05	0.02	4.02
Average (n=10)	**1.98**	**0.002**	**0.04**	**0.90**	**1.02**	**0.05**	**0.02**	**4.03**
Cr-Diopside Reference	**1.99**	**0.003**	**0.04**	**0.93**	**1.00**	**0.05**	**0.01**	**4.03**
Difference	0.00	0.00	0.00	0.03	0.02	0.00	0.00	0.00
%Rel error	0.06	5.39	0.87	0.76	0.49	1.88	2.33	0.01
Stdev	0.00	0.00	0.00	0.00	0.00	0.00	0.00	0.00

Garnet Analysis	MgO	Al2O3	SiO2	CaO	TiO2	Cr2O3	MnO	FeO	Total
mon-32 grt-1	18.11	21.08	41.20	4.99	1.32	0.40	0.27	13.26	100.63
mon-32 grt-2	17.96	20.89	41.02	4.99	1.37	0.37	0.36	13.13	100.09
mon-32 grt-3	17.66	20.84	40.91	5.08	1.41	0.32	0.38	13.06	99.67
mon-32 grt-4	18.18	21.21	41.59	5.11	1.37	0.43	0.40	13.03	101.32
mon-32 grt-5	18.02	21.01	41.44	5.14	1.31	0.29	0.32	13.30	100.84
mon-32 grt-6	18.08	21.31	41.59	5.03	1.27	0.37	0.40	13.24	101.29
mon-32 grt-17	18.08	21.35	41.73	5.03	1.42	0.34	0.41	13.25	101.61
mon-32 grt-8	17.88	20.94	41.19	5.11	1.43	0.33	0.34	13.21	100.41
mon-32 grt-9	18.20	21.26	41.53	5.14	1.29	0.34	0.31	13.24	101.31
mon-32 grt-10	18.06	21.06	41.66	5.12	1.32	0.35	0.45	13.28	101.28
Average (n=10)	**18.02**	**21.10**	**41.39**	**5.07**	**1.35**	**0.35**	**0.36**	**13.20**	**100.84**
MON32-grt Reference	**18.72**	**21.92**	**41.72**	**4.54**	**1.10**	**0.27**	**0.31**	**11.58**	**100.17**
Difference	0.70	0.82	0.33	0.53	0.25	0.08	0.05	1.62	0.67
%Rel error	0.95	0.96	0.20	2.78	5.11	6.70	4.00	3.27	0.17
Stdev	0.16	0.18	0.28	0.06	0.06	0.04	0.06	0.10	0.63

Structural formulae	Si	Ti	Al	Fe tot	Mn	Mg	Ca	Cr	TOT
mon-32 grt-1	2.98	0.07	1.78	0.80	0.02	1.95	0.39	0.02	8.02
mon-32 grt-2	2.99	0.08	1.77	0.80	0.02	1.95	0.39	0.02	8.01
mon-32 grt-3	2.99	0.08	1.78	0.80	0.02	1.92	0.40	0.02	8.01
mon-32 grt-4	2.99	0.07	1.78	0.78	0.02	1.95	0.39	0.02	8.01
mon-32 grt-5	2.99	0.07	1.77	0.80	0.02	1.94	0.40	0.02	8.01
mon-32 grt-6	2.99	0.07	1.79	0.80	0.02	1.94	0.39	0.02	8.01
mon-32 grt-17	2.99	0.08	1.78	0.79	0.02	1.93	0.39	0.02	8.00
mon-32 grt-8	2.99	0.08	1.77	0.80	0.02	1.93	0.40	0.02	8.01
mon-32 grt-9	2.98	0.07	1.78	0.80	0.02	1.95	0.40	0.02	8.02
mon-32 grt-10	3.00	0.07	1.77	0.80	0.03	1.94	0.39	0.02	8.01
Average (n=10)	**2.99**	**0.07**	**1.78**	**0.80**	**0.02**	**1.94**	**0.39**	**0.02**	**8.01**
MON32-grt Reference	3.00	0.06	1.84	0.70	0.02	2.01	0.35	0.02	7.99
Difference	0.01	0.01	0.06	0.10	0.00	0.07	0.04	0.00	0.03
%Rel error	0.09	5.21	0.85	3.38	4.11	0.84	2.88	6.80	0.08
Stdev	0.00	0.00	0.01	0.01	0.00	0.01	0.00	0.00	0.00

Garnet Analysis	MgO	Al2O3	SiO2	CaO	TiO2	Cr2O3	MnO	FeO	Total
rom-33 grt-1	18.07	21.30	41.50	4.68	1.28	0.15	0.32	12.87	100.17
rom-33 grt-2	18.12	21.46	41.62	4.66	1.19	0.16	0.36	12.75	100.30
rom-33 grt-3	18.21	21.52	41.70	4.72	1.26	0.13	0.35	12.71	100.59
rom-33 grt-4	18.06	21.45	41.48	4.77	1.23	0.10	0.43	12.63	100.15
rom-33 grt-5	17.81	21.23	41.57	4.75	1.20	0.12	0.34	12.71	99.73
rom-33 grt-6	18.40	21.69	42.05	4.84	1.23	0.13	0.31	12.68	101.32
rom-33 grt-7	18.03	21.34	41.74	4.82	1.30	0.12	0.39	12.67	100.41
rom-33 grt-8	18.31	21.50	41.98	4.85	1.31	0.14	0.40	12.66	101.16
rom-33 grt-19	18.37	21.60	41.93	4.87	1.34	0.12	0.35	12.87	101.45
rom-33 grt-10	18.24	21.77	41.80	4.78	1.29	0.11	0.44	12.77	101.20
Average (n=10)	**18.16**	**21.49**	**41.74**	**4.77**	**1.26**	**0.13**	**0.37**	**12.73**	**100.65**
ROM33-grt Reference	**18.48**	**21.75**	**41.63**	**4.62**	**1.17**	**0.13**	**0.34**	**12.21**	**100.34**
Difference	0.32	0.26	0.11	0.15	0.09	0.00	0.03	0.52	0.31
%Rel error	0.43	0.30	0.06	0.82	1.92	0.00	2.01	1.05	0.08
Stdev	0.18	0.17	0.20	0.07	0.05	0.02	0.05	0.08	0.59

Structural formulae	Si	Ti	Al	Fe tot	Mn	Mg	Ca	Cr	TOT
rom-33 grt-1	3.00	0.07	1.80	0.78	0.02	1.95	0.36	0.01	7.99
rom-33 grt-2	3.00	0.07	1.81	0.77	0.02	1.95	0.36	0.01	7.99
rom-33 grt-3	3.00	0.07	1.81	0.77	0.02	1.95	0.36	0.01	7.99
rom-33 grt-4	3.00	0.07	1.81	0.76	0.03	1.95	0.37	0.01	8.00
rom-33 grt-5	3.02	0.07	1.80	0.77	0.02	1.93	0.37	0.01	7.98
rom-33 grt-6	3.01	0.06	1.81	0.76	0.02	1.96	0.37	0.01	7.99
rom-33 grt-7	3.01	0.07	1.80	0.76	0.02	1.94	0.37	0.01	7.99
rom-33 grt-8	3.01	0.06	1.80	0.76	0.02	1.96	0.37	0.01	7.99
rom-33 grt-19	3.00	0.07	1.80	0.77	0.02	1.96	0.37	0.01	8.00
rom-33 grt-10	2.99	0.07	1.82	0.76	0.03	1.95	0.37	0.01	8.00
Average (n=10)	**3.00**	**0.07**	**1.81**	**0.77**	**0.02**	**1.95**	**0.37**	**0.01**	**7.99**
ROM33-grt Reference	3.00	0.06	1.83	0.74	0.02	1.98	0.36	0.01	7.99
Difference	0.01	0.01	0.02	0.03	0.00	0.04	0.01	0.00	0.00
%Rel error	0.05	3.05	0.32	1.03	1.99	0.45	0.80	0.02	0.00
Stdev	0.01	0.00	0.01	0.01	0.00	0.01	0.00	0.00	0.01

Garnet Analysis	MgO	Al2O3	SiO2	CaO	TiO2	Cr2O3	MnO	FeO	Total
mon-34 grt-1	19.49	20.97	42.21	4.98	1.27	0.99	0.17	10.55	100.64
mon-34 grt-2	19.29	20.97	41.93	5.02	1.37	0.94	0.28	10.55	100.34
mon-34 grt-3	19.42	21.05	41.70	4.99	1.29	0.88	0.29	10.50	100.12
mon-34 grt-4	19.51	20.89	41.88	4.95	1.24	0.97	0.23	10.40	100.06
mon-34 grt-5	19.28	20.69	41.74	4.96	1.33	0.91	0.39	10.24	99.53
mon-34 grt-6	19.28	21.11	41.92	4.98	1.20	0.91	0.32	10.55	100.28
mon-34 grt-7	19.37	21.07	41.86	4.96	1.27	0.93	0.22	10.48	100.17
mon-34 grt-8	19.32	20.81	41.55	4.95	1.19	0.95	0.28	10.25	99.29
mon-34 grt-9	19.54	21.15	42.09	5.00	1.30	0.94	0.30	10.57	100.90
mon-34 grt-10	19.52	21.18	42.07	4.98	1.32	0.94	0.31	10.54	100.85
Average (n=10)	**19.40**	**20.99**	**41.89**	**4.98**	**1.28**	**0.94**	**0.28**	**10.46**	**100.22**
MON34-grt Reference	**20.15**	**21.92**	**41.95**	**4.64**	**1.13**	**0.79**	**0.24**	**9.85**	**100.25**
Difference	0.75	0.93	0.06	0.34	0.15	0.15	0.04	0.61	0.03
%Rel error	0.94	1.08	0.03	1.75	3.07	4.20	3.60	1.51	0.01
Stdev	0.11	0.15	0.20	0.02	0.06	0.03	0.06	0.13	0.52

Structural formulae	Si	Ti	Al	Fe tot	Mn	Mg	Ca	Cr	TOT
mon-34 grt-1	3.02	0.07	1.75	0.63	0.01	2.08	0.38	0.06	7.99
mon-34 grt-2	3.01	0.07	1.76	0.63	0.02	2.06	0.39	0.05	7.99
mon-34 grt-3	3.00	0.07	1.77	0.63	0.02	2.08	0.38	0.05	8.00
mon-34 grt-4	3.01	0.07	1.75	0.63	0.01	2.09	0.38	0.05	7.99
mon-34 grt-5	3.02	0.07	1.74	0.62	0.02	2.08	0.38	0.05	7.99
mon-34 grt-6	3.01	0.06	1.77	0.63	0.02	2.06	0.38	0.05	7.99
mon-34 grt-7	3.01	0.07	1.77	0.63	0.01	2.07	0.38	0.05	7.99
mon-34 grt-8	3.01	0.06	1.76	0.62	0.02	2.09	0.38	0.05	7.99
mon-34 grt-9	3.00	0.07	1.76	0.63	0.02	2.08	0.38	0.05	7.99
mon-34 grt-10	3.00	0.07	1.76	0.63	0.02	2.08	0.38	0.05	7.99
Average (n=10)	**3.01**	**0.07**	**1.76**	**0.63**	**0.02**	**2.08**	**0.38**	**0.05**	**7.99**
MON34-grt Reference	**2.98**	**0.06**	**1.82**	**0.59**	**0.01**	**2.14**	**0.35**	**0.04**	**8.00**
Difference	0.02	0.01	0.06	0.04	0.00	0.06	0.03	0.01	0.01
%Rel error	0.20	3.31	0.85	1.74	3.83	0.71	1.98	4.44	0.02
Stdev	0.01	0.00	0.01	0.01	0.00	0.01	0.00	0.00	0.00

Garnet Analysis	MgO	Al2O3	SiO2	CaO	TiO2	Cr2O3	MnO	FeO	Total
jjg1424-grt-1	19.63	22.77	42.01	4.97	0.04	1.06	0.42	8.54	99.44
jjg1424-grt-2	19.61	22.86	42.00	4.99	0.11	1.01	0.52	8.60	99.70
jjg1424-grt-3	20.06	23.25	42.84	4.99	0.08	0.99	0.47	8.50	101.19
jjg1424-grt-14	19.49	22.81	42.11	5.28	0.15	1.13	0.52	8.78	100.28
jjg1424-grt-5	19.97	22.99	42.46	4.91	0.13	1.03	0.39	8.44	100.30
jjg1424-grt-6	19.94	23.16	42.29	4.97	0.07	0.99	0.43	8.39	100.25
jjg1424-grt-7	19.71	22.87	41.94	5.50	0.16	1.03	0.34	8.35	99.90
jjg1424-grt-18	19.98	23.31	42.70	5.02	0.14	0.99	0.48	8.67	101.29
jjg1424-grt-9	20.03	23.44	42.62	5.14	0.14	0.98	0.43	8.63	101.42
jjg1424-grt-10	19.97	23.00	42.41	5.00	0.09	1.03	0.44	8.43	100.38
jjg1424-grt-11	19.98	23.13	42.45	5.02	0.11	1.11	0.45	8.46	100.71
Average (n=10)	**19.87**	**23.08**	**42.38**	**5.08**	**0.12**	**1.03**	**0.45**	**8.52**	**100.54**
JJG1424-grt Reference	**20.47**	**23.31**	**42.32**	**4.65**	**0.09**	**1.06**	**0.32**	**7.91**	**100.13**
Difference	0.60	0.23	0.06	0.43	0.03	0.03	0.13	0.61	0.41
%Rel error	0.74	0.25	0.04	2.22	6.98	0.72	8.34	1.87	0.10
Stdev	0.20	0.21	0.30	0.18	0.03	0.05	0.06	0.14	0.59

Structural formulae	Si	Ti	Al	Fe tot	Mn	Mg	Ca	Cr	TOT
jjg1424-grt-1	3.01	0.00	1.90	0.51	0.03	2.09	0.38	0.06	7.98
jjg1424-grt-2	3.00	0.01	1.91	0.51	0.03	2.09	0.38	0.06	7.98
jjg1424-grt-3	3.01	0.00	1.91	0.50	0.03	2.10	0.38	0.05	7.98
jjg1424-grt-14	3.00	0.01	1.89	0.52	0.03	2.07	0.40	0.06	7.99
jjg1424-grt-5	3.01	0.01	1.90	0.50	0.02	2.11	0.37	0.06	7.98
jjg1424-grt-6	3.00	0.00	1.92	0.50	0.03	2.11	0.38	0.06	7.98
jjg1424-grt-7	2.99	0.01	1.90	0.50	0.02	2.09	0.42	0.06	7.99
jjg1424-grt-18	3.00	0.01	1.91	0.51	0.03	2.09	0.38	0.05	7.98
jjg1424-grt-9	2.99	0.01	1.92	0.51	0.03	2.10	0.39	0.05	7.99
jjg1424-grt-10	3.00	0.00	1.90	0.50	0.03	2.11	0.38	0.06	7.98
jjg1424-grt-11	3.00	0.01	1.91	0.50	0.03	2.10	0.38	0.06	7.98
Average (n=10)	**3.00**	**0.01**	**1.91**	**0.50**	**0.03**	**2.10**	**0.39**	**0.06**	**7.98**
JJG1424-grt Reference	**2.99**	**0.00**	**1.92**	**0.47**	**0.02**	**2.16**	**0.35**	**0.06**	**7.98**
Difference	0.01	0.00	0.02	0.04	0.01	0.06	0.03	0.00	0.00
%Rel error	0.05	6.99	0.24	1.88	8.35	0.73	2.23	0.71	0.01
Stdev	0.01	0.00	0.01	0.01	0.00	0.01	0.01	0.00	0.00

Appendix 3: Run product mineral chemistry

Spinel	MTS7 1000-1	MTS7 1000-2	MTS7 1000-3	MTS7 1000-4	MTS7 1000-5	Average MTS7 1000	STDEV MTS7 1000	MTS8 1000-1	MTS8 1000-2	MTS8 1000-3	Average MTS8 1000	STDEV MTS8 1000
Na_2O	0.70	0.74	0.67	0.67	0.76	0.70	0.04	0.77	2.10	0.67	1.17	0.80
MgO	6.76	7.04	6.87	6.54	6.35	6.71	0.38	9.50	9.41	9.31	9.40	0.20
Al_2O_3	52.12	52.16	53.08	52.26	50.27	51.94	0.97	55.20	55.18	56.10	55.48	0.77
SiO_2	2.35	1.21	2.61	1.22	2.31	1.92	0.66	2.01	1.44	1.58	1.66	0.29
K_2O	0.18	0.07	0.11	0.00	0.22	0.12	0.09	0.17	0.13	0.08	0.13	0.05
CaO	0.02	0.00	0.02	0.04	0.02	0.02	0.01	0.00	0.00	0.01	0.00	0.01
TiO_2	0.49	0.67	0.50	0.40	0.78	0.56	0.15	0.45	0.28	0.35	0.36	0.09
MnO	0.22	0.23	0.02	0.18	0.12	0.16	0.09	0.15	0.21	0.27	0.21	0.06
FeO	38.92	38.99	37.98	38.88	39.43	38.84	0.93	31.99	32.70	32.69	32.46	0.11
Total	100.90	100.93	100.90	100.92	100.90	100.91	0.01	100.87	100.87	100.86	100.87	0.01
Si	0.07	0.03	0.07	0.03	0.07	0.05	0.02	0.06	0.04	0.04	0.05	0.01
Ti	0.01	0.01	0.01	0.01	0.02	0.01	0.00	0.01	0.01	0.01	0.01	0.00
Al	1.75	1.76	1.77	1.79	1.72	1.76	0.03	1.81	1.81	1.84	1.82	0.02
Fe tot	0.91	0.92	0.87	0.92	0.95	0.91	0.03	0.73	0.74	0.73	0.74	0.01
Mn	0.01	0.01	0.00	0.00	0.00	0.00	0.00	0.00	0.00	0.01	0.00	0.00
Mg	0.29	0.31	0.29	0.28	0.27	0.29	0.02	0.40	0.39	0.38	0.39	0.01
Ca	0.00	0.00	0.00	0.00	0.00	0.00	0.00	0.00	0.00	0.00	0.00	0.00
Na	0.04	0.04	0.04	0.04	0.04	0.04	0.00	0.04	0.11	0.04	0.06	0.04
K	0.01	0.00	0.00	0.00	0.01	0.00	0.00	0.01	0.00	0.00	0.00	0.00
Mg#	24.02	25.42	24.93	23.18	22.29	23.97	1.27	35.22	34.44	34.30	34.66	0.49
Cat Total	3.07	3.09	3.05	3.08	3.08	3.07	0.01	3.05	3.11	3.05	3.07	0.03
Fe II	0.84	0.83	0.82	0.85	0.87	0.84	0.02	0.68	0.64	0.68	0.67	0.03
Fe III	0.07	0.09	0.05	0.08	0.08	0.07	0.01	0.05	0.11	0.05	0.07	0.03

Spinel	MTS70 1000-1	MTS70 1000-2	MTS70 1000-3	MTS70 1000-4	MTS70 1000-5	Average MTS70 1000	STDEV MTS70 1000	MTS70 950	MTS70 950-2	MTS70 950-3	MTS70 950-4	Average MTS70 950	STDEV MTS70 950
Na_2O	0.71	0.83	0.83	0.93	0.94	0.84	0.09	0.76	0.59	0.70	0.59	0.65	0.09
MgO	6.43	6.33	6.30	6.40	6.36	6.35	0.24	6.77	7.10	7.32	7.31	7.11	0.32
Al_2O_3	53.73	53.06	51.12	53.58	53.43	52.99	1.87	51.09	51.91	52.05	52.06	51.71	0.77
SiO_2	1.34	1.22	1.46	1.46	1.50	1.37	3.17	2.12	1.12	1.20	1.11	1.38	0.49
K_2O	0.00	0.07	0.09	0.04	0.08	0.05	0.24	0.35	0.00	0.05	0.01	0.10	0.17
CaO	0.02	0.00	0.04	0.00	0.00	0.01	0.02	0.07	0.00	0.05	0.06	0.05	0.03
TiO_2	0.41	0.65	0.51	0.54	0.49	0.52	0.08	0.43	0.53	0.21	0.36	0.38	0.13
MnO	0.33	0.45	0.36	0.37	0.39	0.39	0.05	0.55	0.33	0.53	0.52	0.48	0.10
FeO	38.49	38.31	38.43	38.62	38.33	38.44	1.34	39.00	39.98	38.99	38.98	39.24	0.57
Total	100.96	100.92	100.93	100.95	100.93	100.94	0.02	101.07	101.16	101.08	101.10	101.10	0.04
Si	0.04	0.03	0.23	0.04	0.04	0.08	0.09	0.06	0.03	0.03	0.03	0.04	0.01
Ti	0.01	0.01	0.01	0.01	0.01	0.01	0.00	0.01	0.01	0.00	0.01	0.01	0.00
Al	1.80	1.79	1.61	1.79	1.79	1.76	0.08	1.73	1.76	1.78	1.77	1.76	0.02
Fe tot	0.90	0.92	0.81	0.89	0.90	0.88	0.04	0.93	0.94	0.90	0.92	0.92	0.02
Mn	0.01	0.01	0.01	0.01	0.01	0.01	0.00	0.01	0.01	0.01	0.01	0.01	0.00
Mg	0.28	0.27	0.24	0.27	0.27	0.27	0.01	0.29	0.30	0.32	0.32	0.31	0.01
Ca	0.00	0.00	0.00	0.00	0.00	0.00	0.00	0.00	0.00	0.00	0.00	0.00	0.00
Na	0.04	0.05	0.04	0.05	0.05	0.05	0.01	0.04	0.03	0.04	0.03	0.04	0.00
K	0.00	0.00	0.02	0.00	0.00	0.01	0.01	0.01	0.00	0.00	0.00	0.00	0.01
Mg#	23.50	22.74	23.12	23.26	23.14	23.15	0.27	23.72	24.39	26.02	25.60	24.93	1.06
Cat Total	3.07	3.08	2.98	3.07	3.07	3.06	0.04	3.09	3.09	3.09	3.09	3.09	0.00
Fe II	0.83	0.84	0.83	0.82	0.82	0.83	0.01	0.84	0.85	0.81	0.83	0.83	0.02
Fe III	0.07	0.08	-0.02	0.07	0.07	0.06	0.04	0.09	0.09	0.09	0.09	0.09	0.00

Spinel	MTS70 800-1	MTS70 800-2	MTS70 800-3	MTS70 800-4	MTS70 800-5	Average MTS70 800	STDEV MTS70 800	MTS71 950-1	MTS71 950-2	MTS71 950-3	MTS71 950-4	Average MTS71 950	STDEV MTS71 950
Na_2O	0.86	0.72	1.16	0.62	0.69	0.81	0.22	0.97	1.20	1.12	1.28	1.14	0.13
MgO	4.06	3.87	4.39	3.34	2.61	3.65	0.71	1.74	1.71	2.51	1.85	1.95	0.38
Al_2O_3	50.51	50.62	54.36	47.10	30.31	46.58	9.61	45.29	43.68	44.40	43.18	44.14	0.93
SiO_2	1.31	1.51	2.76	2.35	0.93	1.77	0.77	1.06	1.14	1.25	1.93	1.35	0.40
K_2O	0.08	0.13	0.24	0.17	0.07	0.14	0.07	0.00	0.04	0.06	0.10	0.05	0.04
CaO	0.01	0.00	0.04	0.01	0.09	0.03	0.04	0.09	0.02	0.00	0.01	0.03	0.04
TiO_2	0.61	0.38	0.44	0.23	20.74	4.48	9.24	0.54	0.98	0.80	0.89	0.80	0.19
MnO	0.73	0.82	0.37	0.79	0.74	0.69	0.19	0.15	0.18	0.12	0.18	0.16	0.03
FeO	42.73	42.34	36.70	45.88	42.48	42.03	3.32	51.93	52.84	51.49	52.38	52.16	0.57
Total	100.89	100.39	100.54	100.44	98.65	100.18	0.89	101.78	101.77	101.77	101.79	101.78	0.01
Si	0.04	0.04	0.08	0.07	0.03	0.05	0.02	0.03	0.04	0.04	0.06	0.04	0.01
Ti	0.01	0.01	0.01	0.01	0.49	0.10	0.22	0.01	0.02	0.02	0.02	0.02	0.00
Al	1.75	1.76	1.82	1.67	1.12	1.63	0.29	1.66	1.61	1.62	1.59	1.62	0.03
Fe tot	1.04	1.03	0.86	1.14	1.10	1.03	0.11	1.30	1.34	1.29	1.32	1.31	0.02
Mn	0.02	0.02	0.01	0.02	0.02	0.02	0.00	0.00	0.00	0.00	0.00	0.00	0.00
Mg	0.18	0.17	0.19	0.15	0.12	0.16	0.03	0.08	0.08	0.12	0.09	0.09	0.02
Ca	0.00	0.00	0.00	0.00	0.00	0.00	0.00	0.00	0.00	0.00	0.00	0.00	0.00
Na	0.05	0.04	0.06	0.04	0.04	0.05	0.01	0.06	0.07	0.07	0.08	0.07	0.01
K	0.00	0.00	0.01	0.01	0.00	0.01	0.00	0.00	0.00	0.00	0.00	0.00	0.00
Mg#	14.67	14.19	17.80	11.64	10.01	13.60	2.99	5.82	5.63	8.25	6.12	6.46	1.21
Cat Total	3.09	3.09	3.04	3.11	2.94	3.05	0.07	3.15	3.17	3.16	3.16	3.16	0.01
Fe II	0.94	0.95	0.82	1.04	-	0.98	0.09	1.15	1.17	1.13	1.16	1.15	0.02
Fe III	0.09	0.09	0.04	0.11	-	0.05	0.03	0.15	0.17	0.16	0.16	0.16	0.01

Cordierite	MTS7 1000-1	MTS7 1000-2	MTS7 1000-3	MTS7 1000-4	MTS7 1000-5	MTS7 1000-6	MTS7 1000-7	MTS7 1000-8	MTS7 1000-9	MTS7 1000-10	Average MTS7 1000	STDEV MTS7 1000
Na_2O	0.33	0.42	0.44	0.42	0.25	0.33	0.51	0.45	0.32	0.45	0.39	0.12
MgO	10.20	7.24	8.03	9.53	9.93	9.02	8.25	8.90	9.78	9.56	9.05	0.87
Al_2O_3	34.79	27.72	30.24	33.82	34.48	31.74	30.47	31.21	34.09	33.86	32.24	2.11
SiO_2	45.80	54.58	51.69	47.99	47.44	49.22	50.91	50.41	47.29	47.48	49.28	2.78
K_2O	0.71	1.66	1.40	0.72	0.65	0.98	1.27	1.17	0.59	0.85	1.00	0.56
CaO	0.00	0.00	0.00	0.00	0.00	0.00	0.00	0.00	0.00	0.00	0.00	0.00
TiO_2	0.00	0.00	0.00	0.00	0.00	0.00	0.00	0.00	0.00	0.00	0.00	0.00
MnO	0.29	0.20	0.06	0.00	0.17	0.17	0.03	0.00	0.08	0.08	0.11	0.06
FeO	7.89	6.19	6.69	7.21	7.15	7.38	7.06	6.77	7.69	7.39	7.14	0.50
Total	99.18	99.23	99.19	99.19	99.20	99.21	99.19	99.26	99.20	99.21	99.21	0.02
Si	4.72	5.53	5.27	4.90	4.85	5.04	5.20	5.14	4.84	4.87	5.04	0.25
Ti	0.00	0.00	0.00	0.00	0.00	0.00	0.00	0.00	0.00	0.00	0.00	0.00
Al	4.22	3.31	3.63	4.07	4.15	3.82	3.66	3.74	4.11	4.09	3.88	0.29
Fe tot	0.68	0.52	0.57	0.62	0.61	0.63	0.60	0.58	0.66	0.63	0.61	0.05
Mn	0.03	0.02	0.01	0.00	0.01	0.01	0.00	0.00	0.01	0.01	0.01	0.01
Mg	1.57	1.09	1.22	1.45	1.51	1.38	1.26	1.35	1.49	1.46	1.38	0.15
Ca	0.00	0.00	0.00	0.00	0.00	0.00	0.00	0.00	0.00	0.00	0.00	0.00
Na	0.07	0.08	0.09	0.08	0.05	0.07	0.10	0.09	0.06	0.09	0.08	0.02
K	0.09	0.22	0.18	0.09	0.09	0.13	0.17	0.15	0.08	0.11	0.13	0.05
Mg#	69.85	67.53	68.16	70.35	71.45	68.59	67.54	70.22	69.47	69.88	69.30	1.30
Cat Total	11.27	10.93	11.04	11.16	11.16	11.10	11.08	11.10	11.17	11.21	11.12	0.10

Cordierite	MTS7 950 1	MTS7 950 2	MTS7 950 3	MTS7 950 4	MTS7 950 5	Average MTS7 950	STDEV MTS7 950	MTS70 800-1	MTS70 800-2	MTS70 800-3	MTS70 800-4	MTS70 800-5	MTS70 800-6	MTS70 800-7	Average MTS70 800	STDEV MTS70 800
Na_2O	0.35	0.56	0.37	0.47	0.58	0.46	0.09	0.46	0.35	0.46	0.30	0.36	0.51	0.47	0.41	0.11
MgO	9.63	10.09	9.61	9.06	9.00	9.48	0.48	8.03	7.60	8.62	8.58	7.85	7.52	7.99	8.03	0.41
Al_2O_3	33.04	33.45	33.65	33.55	33.58	33.45	0.23	32.85	33.18	33.50	34.71	31.09	31.53	31.74	32.66	1.20
SiO_2	48.42	48.40	48.74	48.08	48.49	48.43	0.25	48.58	48.11	47.69	46.21	48.98	48.44	49.38	48.20	1.08
K_2O	0.19	0.23	0.11	0.14	0.13	0.16	0.06	0.36	0.47	0.24	0.26	0.78	0.64	0.72	0.49	0.43
CaO	0.09	0.00	0.07	0.00	0.03	0.04	0.05	0.05	0.09	0.16	0.14	0.05	0.02	0.12	0.09	0.03
TiO_2	0.00	0.00	0.00	0.00	0.00	0.00	0.00	0.00	0.00	0.00	0.00	0.00	0.00	0.00	0.00	0.00
MnO	0.00	0.00	0.00	0.00	0.00	0.00	0.00	0.44	0.47	0.49	0.58	0.37	0.45	0.74	0.51	0.11
FeO	7.54	6.58	6.97	8.24	7.92	7.45	0.64	8.45	9.02	8.60	8.96	8.89	8.97	8.03	8.70	0.35
Total	99.44	99.43	99.48	99.46	99.55	99.47	0.05	99.05	99.11	99.20	98.94	99.02	98.83	99.49	99.09	0.21
Si	4.93	4.91	4.94	4.91	4.93	4.93	0.01	4.99	4.96	4.90	4.77	5.07	5.02	5.07	4.97	0.10
Ti	0.00	0.00	0.00	0.00	0.00	0.00	0.00	0.00	0.00	0.00	0.00	0.00	0.00	0.00	0.00	0.00
Al	3.96	4.00	4.02	4.03	4.02	4.01	0.03	3.97	4.03	4.05	4.22	3.79	3.85	3.83	3.96	0.15
Fe tot	0.64	0.56	0.59	0.70	0.67	0.63	0.06	0.73	0.78	0.74	0.77	0.77	0.78	0.69	0.75	0.03
Mn	0.00	0.00	0.00	0.00	0.00	0.00	0.00	0.04	0.04	0.04	0.05	0.03	0.04	0.06	0.04	0.01
Mg	1.46	1.53	1.45	1.38	1.37	1.44	0.07	1.23	1.17	1.32	1.32	1.21	1.16	1.22	1.23	0.07
Ca	0.01	0.00	0.01	0.00	0.00	0.00	0.00	0.01	0.01	0.02	0.02	0.01	0.00	0.01	0.01	0.01
Na	0.07	0.11	0.07	0.09	0.11	0.09	0.02	0.09	0.07	0.09	0.06	0.07	0.10	0.09	0.08	0.02
K	0.02	0.03	0.01	0.02	0.02	0.02	0.01	0.05	0.06	0.03	0.03	0.10	0.08	0.09	0.06	0.03
Mg#	69.50	72.93	70.97	66.45	67.16	69.40	2.68	62.93	59.99	64.19	63.11	61.16	59.89	64.01	62.18	1.82
Cat Total	11.12	11.15	11.09	11.13	11.11	11.12	0.02	11.09	11.10	11.13	11.17	11.11	11.11	11.12	11.12	0.03

Cordierite	MTS8 1000-1	MTS8 1000-2	MTS8 1000-3	MTS8 1000-4	MTS8 1000-5	MTS8 1000-6	MTS8 1000-7	MTS8 1000-8	MTS8 1000-9	MTS8 1000-10	Average MTS8 1000	STDEV MTS8 1000
Na_2O	0.64	0.83	0.67	0.99	0.76	0.82	0.59	0.81	0.73	0.97	0.78	0.13
MgO	9.34	10.15	9.20	7.21	8.89	9.81	9.74	8.47	7.58	7.67	8.81	0.90
Al_2O_3	31.86	34.52	32.31	27.73	31.63	33.76	33.81	31.41	28.41	27.95	31.34	2.20
SiO_2	48.58	45.73	48.55	53.11	49.34	46.66	46.97	49.93	52.85	52.28	49.40	2.90
K_2O	1.59	1.22	1.50	2.36	1.45	1.26	1.38	1.70	2.25	2.63	1.74	0.72
CaO	0.00	0.03	0.00	0.00	0.00	0.07	0.00	0.00	0.00	0.00	0.01	0.01
TiO_2	0.08	0.03	0.06	0.08	0.05	0.06	0.11	0.06	0.07	0.18	0.08	0.11
MnO	0.24	0.43	0.43	0.37	0.13	0.15	0.13	0.09	0.00	0.00	0.20	0.08
FeO	7.11	7.62	6.90	5.96	7.08	7.52	7.13	6.53	5.91	5.89	6.76	0.58
Total	99.12	99.07	99.09	99.11	99.11	99.07	99.10	99.12	99.08	99.19	99.11	0.03
Si	5.00	4.74	4.99	5.44	5.06	4.82	4.84	5.12	5.40	5.36	5.08	0.25
Ti	0.01	0.00	0.00	0.01	0.00	0.00	0.01	0.00	0.01	0.01	0.01	0.00
Al	3.86	4.21	3.91	3.34	3.82	4.10	4.10	3.79	3.42	3.38	3.79	0.32
Fe tot	0.61	0.66	0.59	0.51	0.61	0.65	0.61	0.56	0.50	0.50	0.58	0.06
Mn	0.02	0.04	0.04	0.03	0.01	0.01	0.01	0.01	0.00	0.00	0.02	0.01
Mg	1.43	1.57	1.41	1.10	1.36	1.51	1.50	1.29	1.15	1.17	1.35	0.16
Ca	0.00	0.00	0.00	0.00	0.00	0.01	0.00	0.00	0.00	0.00	0.00	0.00
Na	0.13	0.17	0.13	0.20	0.15	0.16	0.12	0.16	0.15	0.19	0.16	0.03
K	0.21	0.16	0.20	0.31	0.19	0.17	0.18	0.22	0.29	0.34	0.23	0.06
Mg#	70.14	70.42	70.44	68.31	69.16	69.98	70.95	69.85	69.62	69.96	69.88	0.74
Cat Total	11.23	11.37	11.22	11.09	11.18	11.32	11.27	11.17	11.06	11.15	11.21	0.10

Cordierite	MTS8 950 1	MTS8 950 2	MTS8 950 3	MTS8 950 4	MTS8 950 5	Average MTS8 950	STDEV MTS8 950	MTS70 950-1	MTS70 950-2	MTS70 950-3	MTS70 950-4	MTS70 950-5	Average MTS70 950	STDEV MTS70 950
Na_2O	0.49	0.63	0.43	0.60	0.48	0.53	0.10	0.35	0.30	0.00	0.21	0.57	0.29	0.28
MgO	7.47	9.07	8.74	8.97	9.81	8.81	0.77	10.36	10.54	7.81	10.72	7.74	9.43	1.35
Al_2O_3	34.29	33.02	31.78	31.49	32.42	32.60	1.06	33.31	33.47	33.56	33.51	32.80	33.33	0.30
SiO_2	48.60	48.46	48.96	48.89	48.79	48.74	0.21	48.03	47.41	50.38	48.12	49.82	48.75	1.32
K_2O	1.22	1.15	1.08	1.47	1.18	1.22	0.16	0.72	0.66	0.54	0.72	0.46	0.62	0.10
CaO	0.00	0.00	0.00	0.00	0.00	0.00	0.00	0.00	0.00	0.09	0.15	0.00	0.05	0.02
TiO_2	0.38	0.13	0.20	0.21	0.46	0.28	0.08	0.00	0.00	0.00	0.00	0.00	0.00	0.00
MnO	0.18	0.14	0.19	0.23	0.20	0.19	0.03	0.24	0.43	0.37	0.30	0.00	0.27	0.15
FeO	6.72	6.67	7.68	7.32	6.19	6.92	0.66	6.92	7.22	6.60	6.44	7.69	6.97	0.55
Total	99.30	99.28	99.26	99.31	99.26	99.28	0.02	99.61	99.62	99.83	99.57	99.90	99.71	0.15
Si	4.96	4.95	5.02	5.02	4.98	4.99	0.03	4.89	4.84	5.07	4.89	5.05	4.95	0.10
Ti	0.03	0.01	0.02	0.02	0.04	0.02	0.01	0.00	0.00	0.00	0.00	0.00	0.00	0.00
Al	4.12	3.97	3.84	3.81	3.89	3.93	0.12	4.00	4.03	3.98	4.01	3.92	3.98	0.04
Fe tot	0.57	0.57	0.66	0.63	0.53	0.59	0.05	0.59	0.62	0.56	0.55	0.65	0.59	0.04
Mn	0.02	0.01	0.02	0.02	0.02	0.02	0.00	0.02	0.04	0.03	0.03	0.00	0.02	0.01
Mg	1.14	1.38	1.34	1.37	1.49	1.34	0.13	1.57	1.60	1.17	1.62	1.17	1.43	0.24
Ca	0.00	0.00	0.00	0.00	0.00	0.00	0.00	0.00	0.00	0.01	0.02	0.00	0.01	0.01
Na	0.10	0.13	0.09	0.12	0.10	0.10	0.02	0.07	0.06	0.00	0.04	0.11	0.06	0.04
K	0.16	0.15	0.14	0.19	0.15	0.16	0.02	0.09	0.09	0.07	0.09	0.06	0.08	0.02
Mg#	66.11	71.12	66.71	68.57	74.68	69.44	3.52	73.39	72.83	67.76	75.81	63.63	70.68	4.91
Cat Total	11.08	11.18	11.14	11.20	11.16	11.15	0.04	11.20	11.24	10.92	11.19	11.05	11.12	0.13

Cordierite	MTS70 1000-1	MTS70 1000-2	MTS70 1000-3	MTS70 1000-4	MTS70 1000-5	MTS70 1000-6	MTS70 1000-7	MTS70 1000-8	MTS70 1000-9	MTS70 1000-10	Average MTS70 1000	STDEV MTS70 1000
Na_2O	0.52	0.61	0.60	0.62	0.62	0.54	0.55	0.65	0.51	0.48	0.57	0.05
MgO	8.69	8.44	8.42	8.65	8.48	8.34	8.17	8.54	8.66	8.62	8.50	0.15
Al_2O_3	33.47	33.04	32.99	33.16	33.92	33.58	33.10	32.63	33.25	33.27	33.24	0.32
SiO_2	47.73	48.15	47.82	47.74	47.61	47.75	48.31	48.48	47.87	47.90	47.94	0.28
K_2O	0.41	0.37	0.48	0.41	0.37	0.56	0.52	0.61	0.40	0.41	0.45	0.10
CaO	0.00	0.05	0.01	0.00	0.02	0.04	0.03	0.01	0.02	0.03	0.02	0.02
TiO_2	0.00	0.00	0.00	0.00	0.00	0.00	0.00	0.00	0.00	0.00	0.00	0.00
MnO	0.34	0.26	0.26	0.27	0.30	0.24	0.23	0.15	0.17	0.25	0.25	0.04
FeO	7.81	7.96	8.26	8.10	7.78	8.03	7.99	7.76	8.14	8.01	7.99	0.16
Total	98.96	98.94	98.91	98.94	98.94	99.03	98.93	98.94	98.96	98.93	98.95	0.03
Si	4.90	4.95	4.93	4.91	4.89	4.91	4.96	4.98	4.92	4.92	4.93	0.03
Ti	0.00	0.00	0.00	0.00	0.00	0.00	0.00	0.00	0.00	0.00	0.00	0.00
Al	4.05	4.00	4.00	4.02	4.10	4.07	4.01	3.95	4.03	4.03	4.02	0.04
Fe tot	0.67	0.68	0.71	0.70	0.67	0.69	0.69	0.67	0.70	0.69	0.69	0.01
Mn	0.03	0.02	0.02	0.02	0.03	0.02	0.02	0.01	0.01	0.02	0.02	0.00
Mg	1.33	1.29	1.29	1.33	1.30	1.28	1.25	1.31	1.33	1.32	1.30	0.02
Ca	0.00	0.01	0.00	0.00	0.00	0.00	0.00	0.00	0.00	0.00	0.00	0.00
Na	0.10	0.12	0.12	0.12	0.12	0.11	0.11	0.13	0.10	0.10	0.11	0.01
K	0.05	0.05	0.06	0.05	0.05	0.07	0.07	0.08	0.05	0.05	0.06	0.01
Mg#	66.48	65.41	64.48	65.55	66.02	64.91	64.56	66.23	65.47	65.72	65.48	0.68
Cat Total	11.14	11.12	11.15	11.16	11.14	11.15	11.12	11.14	11.14	11.13	11.14	0.01

Cordierite	MTS70 900-1	MTS70 900-2	MTS70 900-3	MTS70 900-4	MTS70 900-5	Average MTS70 900	STDEV MTS70 900	MTS70 850-1	MTS70 850-2	MTS70 850-3	MTS70 850-4	MTS70 850-5	Average MTS70 850	STDEV MTS70 850
Na_2O	0.75	0.74	0.69	0.44	0.49	0.62	0.21	0.45	0.40	0.60	0.61	0.49	0.51	0.08
MgO	8.57	8.86	8.64	7.73	8.30	8.42	0.47	6.28	6.50	6.67	6.56	6.84	6.57	0.21
Al_2O_3	32.01	32.67	32.52	33.76	32.17	32.63	0.65	32.66	30.68	31.86	31.56	31.77	31.71	0.68
SiO_2	48.32	48.29	48.11	47.49	49.08	48.26	0.58	47.51	48.76	46.59	48.61	48.13	47.92	0.93
K_2O	0.96	0.71	0.91	0.94	0.68	0.84	0.12	0.44	1.41	0.77	0.73	0.81	0.83	0.39
CaO	0.06	0.06	0.02	0.04	0.02	0.04	0.01	0.12	0.14	0.14	0.00	0.14	0.11	0.05
TiO_2	0.02	0.04	0.03	0.00	0.00	0.02	0.11	0.10	0.13	0.08	0.03	0.00	0.07	0.05
MnO	0.52	0.35	0.13	0.46	0.48	0.39	0.13	0.70	0.59	0.59	0.32	0.26	0.49	0.16
FeO	7.75	7.12	7.75	7.57	7.56	7.55	0.25	11.44	10.91	12.21	10.70	10.86	11.22	0.57
Total	99.05	99.02	98.95	98.17	98.62	98.76	0.37	99.55	99.67	99.33	99.22	99.37	99.43	0.18
Si	4.98	4.96	4.96	4.92	5.05	4.97	0.05	4.94	5.08	4.90	5.05	5.00	4.99	0.07
Ti	0.00	0.00	0.00	0.00	0.00	0.00	0.00	0.01	0.01	0.01	0.00	0.00	0.01	0.00
Al	3.89	3.95	3.95	4.12	3.90	3.96	0.09	4.00	3.76	3.94	3.86	3.89	3.89	0.09
Fe tot	0.67	0.61	0.67	0.66	0.65	0.65	0.02	0.99	0.95	1.07	0.93	0.94	0.98	0.06
Mn	0.05	0.03	0.01	0.04	0.04	0.03	0.01	0.06	0.05	0.05	0.03	0.02	0.04	0.02
Mg	1.32	1.36	1.33	1.19	1.27	1.29	0.06	0.97	1.01	1.04	1.02	1.06	1.02	0.03
Ca	0.01	0.01	0.00	0.00	0.00	0.00	0.00	0.01	0.02	0.02	0.00	0.02	0.01	0.01
Na	0.15	0.15	0.14	0.09	0.10	0.12	0.03	0.09	0.08	0.12	0.12	0.10	0.10	0.02
K	0.13	0.09	0.12	0.12	0.09	0.11	0.02	0.06	0.19	0.10	0.10	0.11	0.11	0.05
Mg#	66.39	68.82	66.57	64.69	66.25	66.55	1.48	49.49	51.46	49.37	52.16	52.80	51.06	1.56
Cat Total	11.20	11.18	11.19	11.12	11.09	11.15	0.05	11.12	11.16	11.24	11.11	11.15	11.16	0.05

Cordierite	MTS71 1000-1	MTS71 1000-2	MTS71 1000-3	MTS71 1000-4	MTS71 1000-5	MTS71 1000-6	MTS71 1000-7	MTS71 1000-8	MTS71 1000-9	MTS71 1000-10	Average MTS71 1000	STDEV MTS71 1000
Na_2O	0.41	0.36	0.66	0.54	0.64	0.35	0.56	0.90	0.69	0.38	0.55	0.28
MgO	11.24	10.55	6.92	9.84	5.66	8.94	8.36	6.19	5.05	9.46	8.22	1.69
Al_2O_3	34.97	35.53	28.42	37.16	32.35	27.99	33.40	42.28	20.53	34.63	32.73	5.29
SiO_2	46.34	44.62	52.68	44.60	50.11	54.73	47.98	33.09	61.62	47.16	48.29	8.27
K_2O	0.34	0.38	1.33	0.56	1.29	0.32	0.74	1.23	1.31	0.45	0.79	0.94
CaO	0.00	0.00	0.02	0.00	0.02	0.00	0.01	0.02	0.03	0.00	0.01	0.10
TiO_2	0.01	0.07	0.20	0.08	0.22	0.02	0.09	0.35	0.19	0.06	0.13	0.19
MnO	0.27	0.17	0.16	0.07	0.15	0.11	0.19	0.23	0.04	0.00	0.14	0.07
FeO	7.48	9.63	6.70	7.94	7.17	6.35	8.18	17.35	5.13	8.35	8.43	2.96
Total	99.29	99.28	99.29	99.28	99.28	99.27	99.29	99.30	99.29	99.32	99.29	0.01
Si	4.75	4.63	5.39	4.60	5.15	5.50	4.94	3.67	6.17	4.84	4.96	0.66
Ti	0.00	0.01	0.02	0.01	0.02	0.00	0.01	0.03	0.01	0.00	0.01	0.01
Al	4.19	4.31	3.40	4.48	3.88	3.29	4.02	5.48	2.40	4.15	3.96	0.82
Fe tot	0.63	0.82	0.57	0.68	0.61	0.53	0.69	1.59	0.42	0.71	0.72	0.32
Mn	0.02	0.01	0.01	0.01	0.01	0.01	0.02	0.02	0.00	0.00	0.01	0.01
Mg	1.71	1.63	1.05	1.51	0.86	1.33	1.28	1.02	0.75	1.44	1.26	0.33
Ca	0.00	0.00	0.00	0.00	0.00	0.00	0.00	0.00	0.00	0.00	0.00	0.00
Na	0.08	0.07	0.13	0.11	0.13	0.07	0.11	0.19	0.13	0.08	0.11	0.04
K	0.04	0.05	0.17	0.07	0.17	0.04	0.10	0.17	0.17	0.06	0.10	0.06
Mg#	73.28	66.03	64.59	68.96	57.84	71.86	64.36	37.62	63.43	66.86	63.49	10.09
Cat Total	11.21	11.28	11.01	11.28	11.05	10.78	11.15	12.00	10.59	11.13	11.15	0.37

Cordierite	MTS71 950-1	MTS71 950-2	MTS71 950-3	MTS71 950-4	MTS71 950-5	Average MTS71 950	STDEV MTS71 950	MTS71 900-1	MTS71 900-2	MTS71 900-3	MTS71 900-4	MTS71 900-5	MTS71 900-6	Average MTS71 900	STDEV MTS71 900
Na_2O	0.69	0.92	0.31	0.36	0.38	0.53	0.40	0.53	0.58	0.50	0.46	0.82	0.48	0.56	0.15
MgO	8.57	7.48	8.72	8.50	7.96	8.25	0.50	7.25	7.17	7.32	7.36	6.97	6.68	7.12	0.25
Al_2O_3	32.25	32.65	33.04	33.16	30.86	32.39	0.88	29.79	33.03	33.48	32.00	30.67	34.77	32.29	1.76
SiO_2	50.24	48.21	48.12	48.86	51.03	49.29	1.32	50.89	47.67	47.12	49.11	49.77	46.23	48.47	1.81
K_2O	0.27	0.33	0.32	0.28	0.72	0.38	0.26	0.56	0.18	0.15	0.25	0.38	0.24	0.29	0.00
CaO	0.12	0.10	0.06	0.04	0.03	0.07	0.07	0.00	0.00	0.00	0.00	0.00	0.00	0.00	0.03
TiO_2	0.00	0.00	0.00	0.00	0.00	0.00	0.00	0.18	0.09	0.04	0.13	0.04	0.05	0.09	0.11
MnO	0.00	0.21	0.02	0.10	0.11	0.09	0.07	0.04	0.09	0.05	0.17	0.04	0.14	0.09	0.09
FeO	7.17	9.52	8.91	8.43	8.24	8.45	0.88	9.20	10.02	10.27	9.27	9.75	10.64	9.86	0.19
Total	99.47	99.52	99.43	99.45	99.45	99.46	0.03	99.03	98.66	98.57	98.79	98.62	98.94	98.77	0.16
Si	5.10	4.97	4.93	4.99	5.20	5.04	0.11	5.24	4.95	4.90	5.06	5.16	4.81	5.02	0.00
Ti	0.00	0.00	0.00	0.00	0.00	0.00	0.00	0.01	0.01	0.00	0.01	0.00	0.00	0.01	0.24
Al	3.85	3.96	3.99	3.99	3.71	3.90	0.12	3.61	4.03	4.10	3.88	3.74	4.25	3.94	0.05
Fe tot	0.61	0.82	0.76	0.72	0.70	0.72	0.08	0.79	0.87	0.89	0.80	0.84	0.92	0.85	0.00
Mn	0.00	0.02	0.00	0.01	0.01	0.01	0.01	0.00	0.01	0.00	0.01	0.00	0.01	0.01	0.04
Mg	1.30	1.15	1.33	1.29	1.21	1.26	0.07	1.11	1.11	1.13	1.13	1.08	1.03	1.10	0.00
Ca	0.01	0.01	0.01	0.00	0.00	0.01	0.00	0.00	0.00	0.00	0.00	0.00	0.00	0.00	0.03
Na	0.14	0.18	0.06	0.07	0.07	0.11	0.05	0.11	0.12	0.10	0.09	0.16	0.10	0.11	0.02
K	0.03	0.04	0.04	0.04	0.09	0.05	0.02	0.07	0.02	0.02	0.03	0.05	0.03	0.04	2.09
Mg#	68.16	58.24	63.55	64.25	63.23	63.49	3.54	58.40	56.05	55.93	58.55	56.04	52.82	56.30	0.04
Cat Total	11.05	11.19	11.10	11.07	11.02	11.09	0.06	11.02	11.09	11.11	11.03	11.07	11.13	11.08	0.04

Cordierite	MTS71 850-1	MTS71 850-2	MTS71 850-3	MTS71 850-4	MTS71 850-5	MTS71 850-6	MTS71 850-7	MTS71 850-8	MTS71 850-9	MTS71 850-10	Average MTS71 850	STDEV MTS71 850
Na_2O	0.65	0.60	0.49	0.52	0.81	0.78	0.68	0.57	0.37	0.43	0.59	0.15
MgO	7.08	7.86	8.12	8.09	7.16	6.46	6.04	7.87	6.76	7.21	7.27	0.66
Al_2O_3	33.75	34.38	33.71	33.18	34.01	31.53	29.15	34.58	34.18	27.91	32.64	2.16
SiO_2	45.83	45.99	47.54	47.83	46.12	49.46	51.25	46.12	46.35	54.17	48.07	2.94
K_2O	0.31	0.13	0.18	0.36	0.47	0.22	1.16	0.26	0.28	0.37	0.37	0.42
CaO	0.09	0.04	0.09	0.10	0.10	0.01	0.10	0.05	0.08	0.03	0.07	0.05
TiO_2	0.00	0.00	0.00	0.00	0.00	0.00	0.00	0.00	0.00	0.00	0.00	0.00
MnO	0.09	0.09	0.10	0.02	0.31	0.00	0.20	0.07	0.10	0.00	0.10	0.13
FeO	11.50	10.64	9.23	9.43	10.20	10.49	9.59	10.04	11.02	8.35	10.05	0.93
Total	99.10	99.31	99.11	99.35	99.05	98.97	99.03	99.09	99.20	99.30	99.15	0.13
Si	4.79	4.77	4.90	4.93	4.81	5.11	5.31	4.78	4.82	5.49	4.97	0.25
Ti	0.00	0.00	0.00	0.00	0.00	0.00	0.00	0.00	0.00	0.00	0.00	0.00
Al	4.15	4.20	4.09	4.02	4.17	3.84	3.55	4.22	4.18	3.33	3.97	0.31
Fe tot	1.01	0.92	0.79	0.81	0.89	0.91	0.83	0.87	0.96	0.71	0.87	0.09
Mn	0.01	0.01	0.01	0.00	0.03	0.00	0.02	0.01	0.01	0.00	0.01	0.01
Mg	1.10	1.22	1.25	1.24	1.11	1.00	0.93	1.22	1.05	1.09	1.12	0.11
Ca	0.01	0.00	0.01	0.01	0.01	0.00	0.01	0.01	0.01	0.00	0.01	0.00
Na	0.13	0.12	0.10	0.10	0.16	0.16	0.14	0.11	0.07	0.09	0.12	0.03
K	0.04	0.02	0.02	0.05	0.06	0.03	0.15	0.03	0.04	0.05	0.05	0.04
Mg#	52.18	56.91	61.34	60.69	55.56	52.20	52.79	58.44	52.09	60.87	56.31	3.87
Cat Total	11.23	11.21	11.12	11.14	11.24	11.04	11.05	11.20	11.13	10.84	11.12	0.12

Cordierite	MTS71 800-1	MTS71 800-2	MTS71 800-3	MTS71 800-4	Average MTS71 800	STDEV MTS71 800
Na_2O	0.94	0.74	0.88	0.78	0.84	0.09
MgO	3.74	3.92	3.88	4.27	3.95	0.23
Al_2O_3	26.02	30.12	29.57	29.36	28.77	1.86
SiO_2	51.13	51.59	52.22	52.14	51.77	0.51
K_2O	1.41	1.16	1.24	1.31	1.28	0.11
CaO	0.14	0.17	0.23	0.17	0.18	0.04
TiO_2	2.77	0.03	0.26	0.02	0.77	1.34
MnO	0.02	0.25	0.30	0.07	0.16	0.14
FeO	13.63	11.89	11.32	11.76	12.15	1.02
Total	99.80	99.87	99.90	99.88	99.86	0.04
Si	5.37	5.33	5.39	5.39	5.37	0.02
Ti	0.22	0.00	0.02	0.00	0.06	0.11
Al	3.22	3.67	3.59	3.57	3.51	0.20
Fe tot	1.20	1.03	0.98	1.02	1.05	0.10
Mn	0.00	0.02	0.03	0.01	0.01	0.01
Mg	0.59	0.60	0.60	0.66	0.61	0.03
Ca	0.02	0.02	0.03	0.02	0.02	0.00
Na	0.19	0.15	0.18	0.16	0.17	0.02
K	0.19	0.15	0.16	0.17	0.17	0.02
Mg#	32.84	37.01	37.92	39.29	36.70	2.78
Cat Total	10.99	10.98	10.96	10.99	10.98	0.01

Biotite	MTS8 900· 1	MTS8 900· 2	MTS8 900· 3	MTS8 900· 4	Avergae MTS8 900	STDEV MTS8 900	MTS7 850· 1	MTS7 850· 2	MTS7 850· 3	MTS7 850· 4	MTS7 850· 5	Average MTS7 850	STDEV MTS7 850
Na_2O	0.17	0.81	0.69	0.45	0.53	0.28	0.67	0.82	0.26	0.65	0.54	0.59	0.21
MgO	12.84	12.27	9.84	13.62	12.14	1.63	9.38	10.09	8.00	9.46	8.22	9.03	0.89
Al_2O_3	16.38	15.38	15.03	15.91	15.67	0.60	17.95	17.68	17.59	17.02	18.23	17.69	0.45
SiO_2	39.80	41.57	40.97	39.66	40.50	0.92	35.30	36.19	35.43	35.37	36.01	35.66	0.41
K_2O	9.41	8.83	8.70	9.21	9.04	0.33	9.62	8.81	9.34	9.37	9.29	9.29	0.30
TiO_2	2.97	2.91	5.19	2.92	3.50	1.13	2.16	1.87	2.50	2.67	1.74	2.19	0.40
MnO	0.00	0.01	0.11	0.08	0.05	0.05	0.09	0.00	0.18	0.04	0.00	0.06	0.12
FeO	13.66	12.83	15.29	14.01	13.95	1.02	20.33	19.79	21.77	20.45	21.73	20.81	0.89
Total	95.23	94.62	95.82	95.85	95.38	0.58	95.53	95.22	95.13	95.04	95.67	95.32	0.27
Si	5.85	6.09	6.01	5.81	5.94	0.13	5.41	5.51	5.48	5.45	5.51	5.47	0.04
Ti	0.33	0.32	0.57	0.32	0.39	0.12	0.25	0.21	0.29	0.31	0.20	0.25	0.05
Al	2.83	2.65	2.59	2.74	2.71	0.11	3.24	3.17	3.20	3.09	3.29	3.20	0.07
Fe tot	1.68	1.57	1.87	1.72	1.71	0.13	2.61	2.52	2.82	2.64	2.78	2.67	0.12
Mn	0.00	0.00	0.01	0.01	0.01	0.01	0.01	0.00	0.02	0.01	0.00	0.01	0.01
Mg	2.81	2.68	2.15	2.97	2.65	0.36	2.15	2.29	1.85	2.17	1.88	2.07	0.20
Na	0.05	0.23	0.20	0.13	0.15	0.08	0.20	0.24	0.08	0.19	0.16	0.17	0.06
K	1.76	1.65	1.63	1.72	1.69	0.06	1.88	1.71	1.84	1.84	1.81	1.82	0.06
Mg#	62.83	63.22	53.58	63.60	60.81	4.83	45.18	47.67	39.63	45.24	40.33	43.61	3.47
Cat Total	15.31	15.20	15.03	15.42	15.24	0.16	15.75	15.66	15.58	15.71	15.63	15.67	0.07

Biotite	MTS8 850 1	MTS8 850 2	MTS8 850 3	MTS8 850 4	MTS8 850 5	MTS8 850 6	Average MTS8 850	STDEV MTS8 850	MTS7 800 1	MTS7 800 2	MTS7 800 3	MTS7 800 4	MTS7 800 5	Average MTS7 800	STDEV MTS7 800
Na_2O	0.62	0.87	0.63	0.32	0.71	0.51	0.61	0.21	0.82	0.90	0.77	0.98	1.28	0.95	0.23
MgO	9.08	9.33	8.40	7.81	9.55	7.44	8.60	0.84	8.94	8.66	8.47	8.85	7.62	8.51	0.52
Al_2O_3	17.57	17.30	18.18	17.68	17.73	17.05	17.59	0.39	17.50	17.74	17.58	18.54	17.46	17.76	0.45
SiO_2	36.23	35.61	35.97	35.32	36.12	35.34	35.76	0.40	37.38	36.09	37.04	36.65	36.18	36.67	0.55
K_2O	9.21	9.26	9.47	9.67	9.22	9.73	9.43	0.24	9.14	8.94	9.20	9.20	9.30	9.16	0.14
TiO_2	2.39	2.61	1.71	1.93	1.87	2.73	2.21	0.46	3.09	2.37	2.24	1.61	2.34	2.33	0.48
MnO	0.02	0.20	0.06	0.39	0.24	0.32	0.21	0.14	0.03	0.02	0.03	0.12	0.13	0.07	0.12
FeO	20.40	20.68	21.46	22.12	20.47	22.41	21.26	0.89	19.81	21.47	20.88	20.65	21.91	20.95	0.81
Total	95.52	95.90	95.86	95.22	95.87	95.59	95.66	0.27	96.54	96.13	96.14	96.74	96.39	96.39	0.26
Si	5.53	5.44	5.50	5.48	5.50	5.48	5.49	0.03	5.61	5.49	5.61	5.52	5.53	5.55	0.05
Ti	0.27	0.30	0.20	0.23	0.21	0.32	0.25	0.05	0.35	0.27	0.25	0.18	0.27	0.27	0.06
Al	3.16	3.11	3.28	3.23	3.18	3.11	3.18	0.06	3.09	3.18	3.14	3.29	3.14	3.17	0.07
Fe tot	2.60	2.64	2.75	2.87	2.61	2.91	2.73	0.13	2.48	2.73	2.65	2.60	2.80	2.65	0.12
Mn	0.00	0.03	0.01	0.05	0.03	0.04	0.03	0.02	0.00	0.00	0.00	0.02	0.02	0.01	0.01
Mg	2.07	2.13	1.92	1.81	2.17	1.72	1.97	0.18	2.00	1.96	1.91	1.99	1.74	1.92	0.11
Na	0.18	0.26	0.19	0.10	0.21	0.15	0.18	0.05	0.24	0.27	0.23	0.29	0.38	0.28	0.06
K	1.79	1.81	1.85	1.92	1.79	1.93	1.85	0.06	1.75	1.74	1.78	1.77	1.81	1.77	0.03
Mg#	44.33	44.66	41.13	38.63	45.53	37.14	41.90	3.48	44.63	41.81	41.96	43.34	38.22	42.00	2.40
Cat Total	15.60	15.73	15.68	15.67	15.70	15.67	15.68	0.04	15.49	15.64	15.56	15.67	15.73	15.62	0.09

Biotite	MTS8 800 1	MTS8 800 2	MTS8 800 3	MTS8 800 4	MTS8 800 5	Average MTS8 800	STDEV MTS8 800	MTS70 800-1	MTS70 800-2	MTS70 800-3	MTS70 800-4	MTS70 800-5	Average MTS70 800	STDEV MTS70 800
Na_2O	0.51	0.62	0.80	0.90	0.97	0.76	0.19	0.34	0.08	0.31	0.50	0.47	0.34	0.17
MgO	9.67	9.36	10.28	10.50	10.68	10.10	0.56	9.17	9.34	11.54	11.93	11.38	10.67	1.31
Al_2O_3	17.78	17.72	18.74	18.15	17.85	18.05	0.42	14.87	15.09	16.89	16.71	16.41	15.99	0.94
SiO_2	37.52	36.78	37.82	38.21	38.19	37.70	0.59	37.06	36.41	37.73	39.90	39.66	38.15	1.56
K_2O	9.43	9.36	8.94	9.17	9.05	9.19	0.21	10.51	10.59	10.13	9.18	9.26	9.93	0.68
TiO_2	2.88	2.60	2.21	2.40	2.70	2.56	0.26	4.55	4.28	1.94	2.55	2.96	3.26	1.12
MnO	0.06	0.11	0.11	0.00	0.00	0.06	0.09	0.22	0.38	0.32	0.15	0.03	0.22	0.14
FeO	19.11	20.00	17.76	17.26	17.40	18.31	1.19	19.40	19.79	17.61	15.05	15.68	17.51	2.13
Total	96.99	96.57	96.69	96.53	96.82	96.72	0.19	96.12	95.95	96.46	95.97	95.85	96.07	0.24
Si	5.59	5.54	5.59	5.65	5.63	5.60	0.04	5.65	5.58	5.64	5.85	5.85	5.71	0.13
Ti	0.32	0.29	0.25	0.27	0.30	0.29	0.03	0.52	0.49	0.22	0.28	0.33	0.37	0.13
Al	3.12	3.14	3.26	3.16	3.10	3.16	0.06	2.67	2.72	2.97	2.89	2.85	2.82	0.12
Fe tot	2.38	2.52	2.19	2.13	2.15	2.27	0.17	2.47	2.53	2.20	1.84	1.93	2.19	0.31
Mn	0.01	0.01	0.01	0.00	0.00	0.01	0.01	0.03	0.05	0.04	0.02	0.00	0.03	0.02
Mg	2.15	2.10	2.27	2.31	2.35	2.24	0.11	2.09	2.14	2.57	2.61	2.50	2.38	0.25
Na	0.15	0.18	0.23	0.26	0.28	0.22	0.05	0.10	0.02	0.09	0.14	0.14	0.10	0.05
K	1.79	1.80	1.68	1.73	1.70	1.74	0.05	2.04	2.07	1.93	1.71	1.74	1.90	0.17
Mg#	47.41	45.48	50.77	52.00	52.23	49.58	2.99	45.74	45.71	53.89	58.59	56.42	52.07	6.03
Cat Total	15.50	15.58	15.49	15.50	15.50	15.51	0.04	15.56	15.61	15.66	15.35	15.33	15.50	0.15

Biotite	MTS71 800-1	MTS71 800-2	MTS71 800-3	MTS71 800-4	MTS71 800-5	Average MTS71 800	STDEV MTS71 800	MTS7 750 1	MTS7 750 2	MTS7 750 3	MTS7 750 4	MTS7 750 5	Average MTS7 750	STDEV MTS7 750
Na_2O	0.30	0.21	0.44	0.67	0.40	0.40	0.27	0.76	1.07	0.72	0.61	0.92	0.82	0.18
MgO	5.31	4.77	4.90	4.48	4.56	4.80	0.31	8.34	8.28	7.55	6.41	6.90	7.50	0.84
Al_2O_3	17.97	17.50	20.25	18.53	17.60	18.37	1.16	17.53	17.59	18.02	17.47	17.69	17.66	0.22
SiO_2	37.00	37.26	40.13	40.38	39.60	38.87	1.69	36.06	35.62	36.31	35.46	36.51	35.99	0.45
K_2O	10.78	10.76	8.16	9.05	10.08	9.76	1.03	9.58	9.16	9.55	8.80	8.98	9.21	0.34
TiO_2	2.97	3.67	2.65	3.10	3.11	3.10	0.34	2.08	2.21	2.62	3.50	3.52	2.79	0.69
MnO	0.01	0.00	0.05	0.00	0.04	0.02	0.17	0.30	0.40	0.35	0.19	0.20	0.29	0.09
FeO	21.89	21.97	18.47	19.45	20.47	20.45	1.41	21.80	22.10	21.19	24.18	21.63	22.18	1.16
Total	95.81	95.56	95.66	95.92	96.00	95.79	0.18	96.45	96.42	96.30	96.62	96.36	96.43	0.12
Si	5.69	5.73	5.93	6.01	5.97	5.87	0.15	5.51	5.45	5.53	5.45	5.55	5.50	0.05
Ti	0.34	0.42	0.29	0.35	0.35	0.35	0.05	0.24	0.25	0.30	0.40	0.40	0.32	0.08
Al	3.25	3.17	3.52	3.25	3.13	3.26	0.15	3.15	3.17	3.23	3.16	3.17	3.18	0.03
Fe tot	2.81	2.82	2.28	2.42	2.58	2.58	0.24	2.78	2.83	2.70	3.11	2.75	2.83	0.16
Mn	0.00	0.00	0.01	0.00	0.01	0.00	0.00	0.04	0.05	0.04	0.03	0.03	0.04	0.01
Mg	1.22	1.09	1.08	0.99	1.03	1.08	0.09	1.90	1.89	1.71	1.47	1.56	1.71	0.19
Na	0.09	0.06	0.13	0.19	0.12	0.12	0.05	0.23	0.32	0.21	0.18	0.27	0.24	0.05
K	2.11	2.11	1.53	1.71	1.94	1.88	0.25	1.87	1.79	1.85	1.72	1.74	1.80	0.06
Mg#	30.16	27.87	32.04	29.09	28.42	29.52	1.65	40.58	40.08	38.89	32.13	36.27	37.59	3.48
Cat Total	15.43	15.32	14.85	14.99	15.13	15.14	0.24	15.72	15.76	15.58	15.52	15.47	15.61	0.13

Biotite	MTS8 750 1	MTS8 750 2	MTS8 750 3	MTS8 750 4	MTS8 750 5	Average MTS8 750	STDEV MTS8 750	MTS70 750-1	MTS70 750-2	MTS70 750-3	MTS70 750-4	MTS70 750-5	Average MTS70 750	STDEV MTS70 750
Na_2O	0.57	0.56	0.66	0.83	0.76	0.68	0.14	0.42	0.59	0.42	0.66	0.38	0.49	0.12
MgO	10.12	9.60	8.58	9.38	8.54	9.24	0.64	5.17	5.36	4.82	5.57	4.01	4.99	0.61
Al_2O_3	17.82	18.27	17.74	18.04	18.23	18.02	0.24	18.40	18.65	17.29	18.66	16.07	17.81	1.12
SiO_2	37.08	36.63	35.95	36.76	36.90	36.66	0.43	40.31	38.57	36.16	37.78	36.60	37.88	1.65
K_2O	9.23	9.21	9.71	9.22	9.23	9.32	0.22	9.04	9.50	9.59	9.47	9.73	9.47	0.26
TiO_2	3.07	2.68	2.78	2.46	2.43	2.68	0.24	1.65	2.08	1.80	2.08	1.64	1.85	0.22
MnO	0.25	0.10	0.24	0.06	0.17	0.16	0.08	0.47	0.13	0.51	0.39	0.82	0.46	0.25
FeO	18.22	19.34	20.50	19.20	19.93	19.44	0.88	20.57	21.35	25.79	21.92	27.24	23.38	2.94
Total	96.21	96.34	96.23	95.99	96.28	96.21	0.13	96.04	96.22	96.38	96.52	96.49	96.33	0.20
Si	5.55	5.50	5.47	5.54	5.56	5.52	0.04	6.03	5.82	5.63	5.72	5.75	5.79	0.15
Ti	0.35	0.30	0.32	0.28	0.28	0.30	0.03	0.19	0.24	0.21	0.24	0.19	0.21	0.02
Al	3.14	3.23	3.18	3.20	3.24	3.20	0.04	3.24	3.31	3.17	3.33	2.97	3.21	0.14
Fe tot	2.28	2.43	2.61	2.42	2.51	2.45	0.12	2.57	2.69	3.35	2.77	3.57	2.99	0.44
Mn	0.03	0.01	0.03	0.01	0.02	0.02	0.01	0.06	0.02	0.07	0.05	0.11	0.06	0.03
Mg	2.26	2.15	1.95	2.11	1.92	2.08	0.14	1.15	1.21	1.12	1.26	0.94	1.14	0.12
Na	0.17	0.16	0.19	0.24	0.22	0.20	0.03	0.12	0.17	0.13	0.19	0.12	0.15	0.04
K	1.76	1.76	1.89	1.77	1.78	1.79	0.05	1.72	1.83	1.90	1.83	1.95	1.85	0.09
Mg#	49.97	47.00	42.61	46.60	43.21	45.88	3.01	30.71	30.66	24.81	30.92	20.63	27.55	4.65
Cat Total	15.50	15.54	15.65	15.58	15.54	15.56	0.06	15.08	15.28	15.58	15.38	15.60	15.38	0.22

Biotite	MTS71 750-1	MTS71 750-2	MTS71 750-3	MTS71 750-4	MTS71 750-5	Average MTS71 750	STDEV MTS71 750	MTS8 950 1	MTS8 950 2	MTS8 950 3	MTS8 950 4	MTS8 950 5	MTS8 950 6	MTS8 950 7	Average MTS8 950	STDEV MTS8 950
Na_2O	0.76	0.70	0.68	0.94	0.86	0.79	0.09	1.08	0.57	0.57	0.68	0.61	1.01	0.75	0.75	0.21
MgO	5.21	4.97	4.80	5.81	5.47	5.25	0.36	9.75	10.37	13.00	11.28	11.05	11.58	11.98	11.29	1.06
Al_2O_3	19.97	18.72	18.31	19.91	19.45	19.27	0.71	15.24	15.47	16.11	15.51	16.16	15.98	16.19	15.81	0.39
SiO_2	40.00	41.74	41.24	40.91	40.86	40.95	0.64	42.96	39.14	38.38	40.33	39.94	39.10	39.52	39.91	1.48
K_2O	8.71	9.18	9.38	9.15	8.90	9.06	0.26	8.71	8.48	9.28	9.16	8.90	8.86	9.09	8.93	0.28
TiO_2	1.82	2.06	2.09	1.53	2.29	1.96	0.37	4.07	4.76	3.51	4.30	4.45	4.21	3.35	4.09	0.50
MnO	0.01	0.48	0.39	0.34	0.08	0.26	0.16	0.10	0.07	0.05	0.00	0.19	0.00	0.00	0.06	0.15
FeO	18.98	17.83	18.51	17.14	17.88	18.07	0.74	13.92	17.00	15.01	14.59	14.42	15.23	15.15	15.04	0.98
Total	95.51	95.71	95.52	95.44	95.88	95.61	3.33	95.90	95.90	95.91	95.84	95.83	95.91	95.87	95.88	5.05
Si	5.95	6.16	6.14	6.04	6.02	6.06	0.09	6.22	5.80	5.67	5.91	5.85	5.76	5.81	5.86	0.18
Ti	0.20	0.23	0.23	0.17	0.25	0.22	0.03	0.44	0.53	0.39	0.47	0.49	0.47	0.37	0.45	0.06
Al	3.50	3.25	3.21	3.46	3.37	3.36	0.13	2.60	2.70	2.80	2.68	2.79	2.77	2.80	2.73	0.08
Fe tot	2.36	2.20	2.30	2.12	2.20	2.24	0.10	1.69	2.11	1.85	1.79	1.77	1.87	1.86	1.85	0.13
Mn	0.00	0.06	0.05	0.04	0.01	0.03	0.03	0.01	0.01	0.01	0.00	0.02	0.00	0.00	0.01	0.01
Mg	1.15	1.09	1.07	1.28	1.20	1.16	0.09	2.11	2.29	2.86	2.46	2.41	2.54	2.62	2.47	0.24
Na	0.22	0.20	0.20	0.27	0.25	0.23	0.03	0.30	0.17	0.16	0.19	0.17	0.29	0.21	0.21	0.06
K	1.65	1.73	1.78	1.72	1.67	1.71	0.05	1.61	1.60	1.75	1.71	1.66	1.67	1.70	1.67	0.05
Mg#	32.77	33.15	31.50	37.86	35.35	34.13	2.51	55.60	52.15	60.77	58.01	57.79	57.63	58.56	57.22	2.70
Cat Total	15.04	14.94	15.00	15.06	14.98	15.00	0.05	14.99	15.20	15.49	15.22	15.18	15.36	15.38	15.26	0.16

Muscovite	MTS70 750-1	MTS70 750-2	MTS70 750-3	MTS70 750-4	MTS70 750-5	Average MTS70 750	STDEV MTS70 750	MTS71 750-1	MTS71 750-2	MTS71 750-3	MTS71 750-4	MTS71 750-5	Average MTS71 750	STDEV MTS71 750
Na_2O	0.76	1.08	0.62	0.75	0.75	0.79	0.18	0.76	0.59	0.76	0.78	0.58	0.69	0.10
MgO	0.30	0.34	0.29	0.28	0.46	0.33	0.07	0.00	0.00	0.00	0.00	0.00	0.00	0.00
Al_2O_3	31.74	32.01	31.58	31.46	31.13	31.58	0.33	30.88	32.71	31.55	31.37	31.64	31.63	0.67
SiO_2	47.97	47.74	47.81	48.27	48.54	48.07	0.33	49.24	47.97	49.16	48.42	48.10	48.58	0.59
K_2O	11.02	10.66	11.44	10.93	10.80	10.97	0.30	11.04	10.91	11.09	10.91	11.25	11.04	0.14
TiO_2	0.80	0.57	0.48	0.63	0.53	0.60	0.11	0.43	0.29	0.41	0.58	0.84	0.51	0.21
MnO	0.09	0.00	0.09	0.00	0.24	0.08	0.08	0.08	0.00	0.04	0.14	0.13	0.08	0.06
FeO	2.03	1.81	2.19	2.23	2.14	2.08	0.16	2.37	2.33	1.72	2.57	2.22	2.24	0.32
Total	94.72	94.24	94.49	94.53	94.56	94.51	0.17	94.79	94.80	94.73	94.78	94.76	94.77	0.03
Si	6.47	6.45	6.48	6.51	6.54	6.49	0.04	6.63	6.45	6.60	6.53	6.48	6.54	0.03
Ti	0.08	0.06	0.05	0.06	0.05	0.06	0.01	0.04	0.03	0.04	0.06	0.08	0.05	0.07
Al	5.04	5.09	5.04	5.00	4.94	5.02	0.06	4.89	5.18	4.99	4.98	5.02	5.01	0.02
Fe tot	0.23	0.20	0.25	0.25	0.24	0.23	0.02	0.27	0.26	0.19	0.29	0.25	0.25	0.10
Mn	0.01	0.00	0.01	0.00	0.03	0.01	0.01	0.01	0.00	0.00	0.02	0.02	0.01	0.04
Mg	0.06	0.07	0.06	0.06	0.09	0.07	0.02	0.00	0.00	0.00	0.00	0.00	0.00	0.00
Na	0.20	0.28	0.16	0.20	0.20	0.21	0.04	0.20	0.15	0.20	0.20	0.15	0.18	0.00
K	1.90	1.84	1.98	1.88	1.86	1.89	0.05	1.89	1.87	1.90	1.88	1.93	1.90	0.03
Mg#	21.09	25.32	18.91	18.05	27.91	22.26	4.23	0.00	0.00	0.00	0.00	0.00	0.00	0.00
Cat Total	13.98	14.00	14.02	13.96	13.95	13.98	0.03	13.92	13.94	13.91	13.95	13.96	13.94	0.00

Tourmaline	MTS71 850O-1	MTS71 850O-2	MTS71 850O-3	MTS71 850O-4	Average MTS71 850O	STDEV MTS71 850O	MTS71 850N-1	MTS71 850N-2	MTS71 850N-3	MTS71 850N-4	MTS71 850N-5	MTS71 850N-6	Average MTS71 850N	STDEV MTS71 850N
Na_2O	2.33	2.65	2.64	2.79	2.60	0.19	2.94	2.81	2.52	2.78	3.14	3.01	2.86	0.22
MgO	3.34	1.87	3.42	2.80	2.85	0.71	5.20	3.89	1.94	4.89	4.74	5.17	4.31	1.25
Al_2O_3	32.71	31.17	32.32	30.41	31.65	1.05	31.59	31.51	30.60	31.85	31.65	31.53	31.45	0.44
SiO_2	36.53	35.04	36.05	35.34	35.74	0.67	35.67	36.06	35.19	36.07	36.19	36.11	35.88	0.39
K_2O	0.20	0.07	0.09	0.13	0.12	0.06	0.17	0.00	0.00	0.22	0.00	0.04	0.07	0.10
CaO	0.24	0.26	0.05	0.12	0.17	0.10	0.20	0.15	0.17	0.10	0.21	0.25	0.18	0.05
TiO_2	0.71	1.63	0.16	1.48	1.00	0.69	0.84	0.91	1.60	1.08	0.71	0.53	0.95	0.37
MnO	0.00	0.06	0.00	0.36	0.10	0.17	0.12	0.00	0.29	0.05	0.10	0.00	0.09	0.11
FeO	9.34	13.14	10.66	12.54	11.42	1.74	9.21	10.45	13.47	9.18	9.04	9.25	10.10	1.73
Total	85.61	85.47	85.81	85.76	85.66	0.15	85.87	85.79	86.00	86.13	85.78	85.82	85.90	0.14
Si	6.06	5.97	6.02	6.00	6.01	0.04	5.94	6.02	5.98	5.97	6.02	6.00	5.99	0.03
Ti	0.09	0.21	0.02	0.19	0.13	0.09	0.11	0.11	0.20	0.13	0.09	0.07	0.12	0.05
Al	6.39	6.25	6.36	6.08	6.27	0.14	6.20	6.20	6.13	6.21	6.19	6.17	6.18	0.03
Fe tot	1.29	1.87	1.49	1.78	1.61	0.26	1.28	1.46	1.91	1.27	1.25	1.28	1.41	0.26
Mn	0.00	0.01	0.00	0.05	0.01	0.02	0.02	0.00	0.04	0.01	0.01	0.00	0.01	0.02
Mg	0.83	0.47	0.85	0.71	0.72	0.17	1.29	0.97	0.49	1.21	1.18	1.28	1.07	0.31
Ca	0.04	0.05	0.01	0.02	0.03	0.02	0.04	0.03	0.03	0.02	0.04	0.04	0.03	0.01
Na	0.75	0.87	0.85	0.92	0.85	0.07	0.95	0.91	0.83	0.89	1.01	0.97	0.93	0.06
K	0.04	0.02	0.02	0.03	0.03	0.01	0.04	0.00	0.00	0.05	0.00	0.01	0.02	0.02
Mg#	19.11	10.29	17.95	14.26	15.41	3.99	25.30	20.02	10.20	24.54	24.33	25.15	21.59	5.91
Cat Total	15.53	15.65	15.68	15.75	15.65	0.09	15.84	15.71	15.66	15.74	15.80	15.83	15.76	0.07
Na+K+Ca (X)	0.84	0.94	0.88	0.97	0.91	0.06	1.02	0.94	0.86	0.96	1.05	1.03	0.97	0.07
Al (Y)	0.39	0.25	0.36	0.08	0.27	0.14	0.20	0.20	0.13	0.21	0.19	0.17	0.18	0.03
Al (Z)	6.00	6.00	6.00	6.00	6.00	0.00	6.00	6.00	6.00	6.00	6.00	6.00	6.00	0.00

Tourmaline	MTS70 800-1	MTS70 800-2	MTS70 800-3	MTS70 800-4	MTS70 800-5	Average MTS70 800	STDEV MTS70 800	MTS71 800-1	MTS71 800-2	MTS71 800-3	MTS71 800-4	MTS71 800-5	Average MTS71 800	STDEV MTS71 800
Na_2O	3.44	3.40	2.97	3.07	4.22	3.42	0.49	3.10	3.07	3.29	2.98	3.42	3.17	0.18
MgO	3.95	4.25	4.41	4.06	4.19	4.17	0.18	2.28	2.53	3.78	2.87	3.54	3.00	0.64
Al_2O_3	29.94	30.03	30.57	30.38	28.38	29.86	0.87	30.46	30.22	29.92	29.96	29.79	30.07	0.27
SiO_2	38.05	38.23	38.15	37.70	38.21	38.07	0.22	36.75	36.50	37.97	37.40	36.58	37.04	0.63
K_2O	0.00	0.06	0.13	0.04	0.07	0.06	0.05	0.13	0.18	0.12	0.03	0.15	0.12	0.06
CaO	0.10	0.10	0.11	0.16	0.04	0.10	0.04	0.02	0.09	0.02	0.02	0.09	0.05	0.04
TiO_2	0.54	0.54	0.93	0.83	1.40	0.85	0.35	0.55	1.29	0.74	0.87	0.91	0.87	0.27
MnO	0.09	0.13	0.02	0.12	0.14	0.10	0.05	0.05	0.08	0.00	0.18	0.14	0.09	0.12
FeO	9.80	9.23	9.00	9.89	9.58	9.50	0.38	12.45	11.70	10.19	11.95	11.16	11.49	0.86
Total	85.90	85.96	86.28	86.22	86.20	86.11	0.17	85.79	85.67	85.94	86.28	85.81	85.90	0.23
Si	6.09	6.10	6.04	6.01	6.12	6.07	0.04	6.01	5.97	6.11	6.06	5.97	6.02	0.06
Ti	0.07	0.07	0.11	0.10	0.17	0.10	0.04	0.07	0.17	0.10	0.11	0.12	0.11	0.04
Al	6.25	6.25	6.32	6.32	5.93	6.21	0.16	6.38	6.33	6.18	6.22	6.23	6.27	0.09
Fe tot	1.33	1.25	1.21	1.34	1.30	1.29	0.06	1.76	1.65	1.42	1.67	1.57	1.62	0.13
Mn	0.01	0.02	0.00	0.01	0.02	0.01	0.01	0.01	0.01	0.00	0.03	0.02	0.01	0.01
Mg	0.95	1.02	1.05	0.97	1.01	1.00	0.04	0.53	0.58	0.86	0.65	0.81	0.69	0.14
Ca	0.04	0.04	0.04	0.06	0.01	0.04	0.02	0.01	0.02	0.01	0.01	0.02	0.01	0.01
Na	0.94	0.93	0.81	0.84	1.16	0.93	0.14	0.92	0.91	0.96	0.88	1.01	0.94	0.05
K	0.00	0.02	0.04	0.01	0.02	0.02	0.01	0.03	0.04	0.02	0.01	0.03	0.02	0.01
Mg#	20.84	22.46	23.25	21.06	21.83	21.89	1.00	11.60	13.10	18.72	14.09	17.00	14.90	2.91
Cat Total	15.69	15.68	15.59	15.64	15.83	15.68	0.09	15.69	15.67	15.68	15.64	15.81	15.70	0.07
Na+K+Ca (X)	0.98	0.98	0.88	0.91	1.19	0.99	0.12	0.95	0.97	0.99	0.89	1.07	0.97	0.07
Al (Y)	0.25	0.25	0.32	0.32	-0.07	0.21	0.16	0.38	0.33	0.18	0.22	0.23	0.27	0.09
Al (Z)	6.00	6.00	6.00	6.00	6.00	6.00	0.00	6.00	6.00	6.00	6.00	6.00	6.00	0.00

Tourmaline	MTS8 800L-1	MTS8 800L-2	MTS8 800L-3	MTS8 800L-4	MTS8 800L-5	Average MTS8 800L	STDEV MTS8 800L	MTS8 800D-1	MTS8 800D-2	MTS8 800D-3	MTS8 800D-4	MTS8 800D-5	Average MTS8 800D	STDEV MTS8 800D
Na2O	3.53	3.69	3.41	3.36	3.62	3.52	0.14	2.62	2.41	2.54	2.61	2.68	2.57	0.11
MgO	2.08	1.98	2.40	1.94	1.95	2.07	0.19	3.90	3.59	3.83	4.41	3.82	3.91	0.31
Al2O3	30.07	29.59	29.97	29.49	29.46	29.72	0.28	32.19	32.16	32.50	31.26	31.22	31.86	0.59
SiO2	37.76	37.99	37.71	37.66	37.27	37.68	0.26	37.97	38.01	37.90	37.90	37.53	37.86	0.19
K2O	0.14	0.09	0.00	0.11	0.03	0.08	0.06	0.02	0.13	0.04	0.15	0.06	0.08	0.06
CaO	0.03	0.01	0.03	0.05	0.08	0.04	0.03	0.17	0.17	0.18	0.18	0.16	0.17	0.01
TiO2	0.27	0.22	0.21	0.19	0.41	0.26	0.09	0.22	0.30	0.26	0.57	0.45	0.36	0.15
MnO	0.23	0.14	0.18	0.30	0.23	0.22	0.06	0.03	0.16	0.00	0.12	0.03	0.07	0.07
FeO	11.98	12.52	12.31	12.93	13.17	12.58	0.48	8.85	9.22	8.97	8.91	9.78	9.15	0.38
Total	86.09	86.23	86.22	86.03	86.22	86.16	0.09	85.97	86.13	86.22	86.11	85.72	86.03	0.19
Si	6.34	6.38	6.32	6.36	6.30	6.34	0.03	6.24	6.25	6.21	6.24	6.23	6.23	0.01
Ti	0.03	0.03	0.03	0.02	0.05	0.03	0.01	0.03	0.04	0.03	0.07	0.06	0.04	0.02
Al	5.94	5.86	5.92	5.86	5.86	5.89	0.04	6.23	6.22	6.27	6.06	6.10	6.18	0.09
Fe tot	1.68	1.76	1.73	1.83	1.86	1.77	0.07	1.22	1.27	1.23	1.23	1.36	1.26	0.06
Mn	0.03	0.02	0.03	0.04	0.03	0.03	0.01	0.00	0.02	0.00	0.02	0.00	0.01	0.01
Mg	0.52	0.50	0.60	0.49	0.49	0.52	0.05	0.95	0.88	0.93	1.08	0.94	0.96	0.08
Ca	0.01	0.00	0.01	0.01	0.01	0.01	0.00	0.03	0.03	0.03	0.03	0.03	0.03	0.00
Na	1.15	1.20	1.11	1.10	1.19	1.15	0.04	0.83	0.77	0.81	0.83	0.86	0.82	0.04
K	0.03	0.02	0.00	0.02	0.01	0.02	0.01	0.00	0.03	0.01	0.03	0.01	0.02	0.01
Mg#	11.80	11.01	12.88	10.55	10.43	11.33	1.02	21.98	20.48	21.61	23.44	20.51	21.60	1.22
Cat Total	15.74	15.76	15.74	15.74	15.81	15.76	0.03	15.53	15.49	15.52	15.59	15.59	15.55	0.04
Na+K+Ca (X)	1.19	1.22	1.12	1.13	1.21	1.17	0.05	0.87	0.82	0.85	0.90	0.90	0.87	0.03
Al (Y)	-0.06	-0.14	-0.08	-0.14	-0.14	-0.11	0.04	0.23	0.22	0.27	0.06	0.10	0.18	0.09
Al (Z)	6.00	6.00	6.00	6.00	6.00	6.00	0.00	6.00	6.00	6.00	6.00	6.00	6.00	0.00

Tourmaline	MTS8 750-1	MTS70 750-1	MTS70 750-2	MTS70 750-3	MTS70 750-4	MTS70 750-5	Average MTS70 750	STDEV MTS70 750	MTS71 750-1	MTS71 750-2	MTS71 750-3	MTS71 750-4	MTS71 750-5	Average MTS71 750	STDEV MTS71 750
Na_2O	2.72	3.10	2.82	2.92	3.11	2.76	2.94	0.23	3.28	3.03	3.10	3.07	3.21	3.14	0.10
MgO	4.13	3.94	3.93	3.66	3.85	3.68	3.81	0.20	3.64	4.31	3.31	4.11	3.18	3.71	0.49
Al_2O_3	32.18	30.35	30.33	30.03	30.27	30.47	30.29	0.93	29.63	29.97	29.50	30.35	29.79	29.85	0.33
SiO_2	37.82	37.63	37.65	38.16	37.47	37.99	37.78	0.27	36.55	36.85	36.57	37.04	36.94	36.79	0.22
K_2O	0.07	0.06	0.00	0.13	0.05	0.36	0.12	0.14	0.11	0.00	0.13	0.00	0.11	0.07	0.07
CaO	0.34	0.14	0.15	0.25	0.13	0.22	0.18	0.09	0.11	0.14	0.16	0.13	0.11	0.13	0.02
TiO_2	0.79	0.74	0.80	0.75	0.91	0.85	0.81	0.07	1.14	0.98	1.30	0.50	0.93	0.97	0.30
MnO	0.00	0.16	0.08	0.13	0.08	0.01	0.09	0.07	0.09	0.05	0.20	0.12	0.09	0.11	0.05
FeO	8.73	10.63	11.00	10.69	11.14	10.48	10.79	1.03	11.40	10.57	11.93	10.49	11.45	11.17	0.62
Total	86.78	86.85	86.85	86.81	87.10	86.90	86.90	0.11	85.94	85.90	86.17	85.79	85.80	85.92	0.15
Si	6.18	5.99	6.00	6.07	5.97	6.03	6.01	0.08	5.94	5.95	5.94	5.97	6.00	5.96	0.03
Ti	0.10	0.11	0.12	0.11	0.13	0.12	0.12	0.01	0.15	0.12	0.17	0.06	0.12	0.12	0.04
Al	6.19	6.25	6.24	6.18	6.23	6.25	6.23	0.03	6.18	6.21	6.16	6.29	6.22	6.21	0.05
Fe tot	1.19	1.47	1.52	1.48	1.54	1.45	1.49	0.13	1.59	1.46	1.66	1.45	1.59	1.55	0.09
Mn	0.00	0.03	0.01	0.02	0.01	0.00	0.01	0.00	0.01	0.01	0.03	0.02	0.01	0.02	0.01
Mg	1.00	0.91	0.91	0.84	0.89	0.85	0.88	0.06	0.91	1.07	0.82	1.02	0.79	0.92	0.12
Ca	0.06	0.02	0.03	0.04	0.02	0.04	0.03	0.01	0.03	0.05	0.05	0.04	0.04	0.04	0.01
Na	0.79	0.97	0.88	0.91	0.97	0.86	0.92	0.07	0.99	0.90	0.93	0.92	0.96	0.94	0.03
K	0.01	0.01	0.00	0.02	0.01	0.06	0.02	0.02	0.02	0.00	0.02	0.00	0.02	0.01	0.01
Mg#	22.86	19.03	18.61	18.12	18.22	18.46	18.49	1.82	18.22	21.14	16.61	20.63	16.63	18.65	2.16
Cat Total	15.53	15.76	15.69	15.68	15.77	15.67	15.71	0.09	15.82	15.76	15.78	15.76	15.76	15.78	0.03
Na+K+Ca (X)	1.19	2.19	3.19	4.19	5.19	6.19	7.19	1.87	9.19	10.19	11.19	12.19	13.19	14.19	1.58
Al (Y)	0.19	0.25	0.24	0.18	0.23	0.25	0.23	0.03	0.18	0.21	0.16	0.29	0.22	0.21	0.05
Al (Z)	6.00	7.00	8.00	9.00	10.00	11.00	12.00	1.87	14.00	15.00	16.00	17.00	18.00	19.00	1.58

K-feldspar	MTS7 850 1	MTS7 850 2	MTS7 850 3	MTS7 850 4	MTS7 850 5	Average MTS7 850	STDEV MTS7 850	MTS7recr 850-1	MTS7recr 850-2	MTS7recr 850-3	MTS7recr 850-4	Average MTS7recr 850	STDEV MTS7recr 850
Na_2O	2.51	2.57	2.42	2.40	2.48	2.48	0.07	2.81	2.54	3.21	2.52	2.77	0.32
Al_2O_3	18.72	18.68	19.00	18.86	18.66	18.78	0.14	19.53	19.38	19.98	19.11	19.50	0.36
SiO_2	64.09	63.73	63.58	64.17	63.82	63.88	0.25	64.33	64.60	64.04	64.99	64.49	0.40
K_2O	13.20	12.96	13.39	12.96	13.40	13.18	0.22	13.35	13.89	12.11	13.41	13.19	0.76
CaO	0.00	0.00	0.00	0.00	0.00	0.00	0.00	0.00	0.00	0.69	0.14	0.21	0.33
TiO_2	0.00	0.00	0.09	0.00	1.04	0.23	0.46	0.34	0.26	0.16	0.23	0.25	0.07
FeO	0.25	0.56	0.39	0.22	0.00	0.29	0.21	0.39	0.16	0.30	0.29	0.29	0.09
Total	99.10	98.73	99.11	98.91	98.99	98.97	0.15	100.75	100.83	100.49	100.69	100.69	0.15
Si	2.97	2.96	2.95	2.97	2.96	2.96	0.01	2.94	2.95	2.92	2.96	2.94	0.02
Ti	0.00	0.00	0.00	0.00	0.04	0.01	0.02	0.01	0.01	0.01	0.01	0.01	0.00
Al	1.02	1.02	1.04	1.03	1.02	1.03	0.01	1.05	1.04	1.07	1.03	1.05	0.02
Fe tot	0.01	0.02	0.02	0.01	0.00	0.01	0.01	0.01	0.01	0.01	0.01	0.01	0.00
Ca	0.00	0.00	0.00	0.00	0.00	0.00	0.00	0.00	0.00	0.03	0.01	0.01	0.02
Na	0.23	0.23	0.22	0.22	0.22	0.22	0.01	0.25	0.22	0.28	0.22	0.24	0.03
K	0.78	0.77	0.79	0.77	0.79	0.78	0.01	0.78	0.81	0.70	0.78	0.77	0.04
Cat Total	5.02	5.02	5.03	5.00	5.02	5.02	0.01	5.04	5.04	5.03	5.02	5.03	0.01

K-feldspar	MTS8 850 1	MTS8 850 2	MTS8 850 3	MTS8 850 4	MTS8 850 5	Average MTS8 850	STDEV MTS8 850	MTS8recr 850-1	MTS8recr 850-2	MTS8recr 850-3	MTS8recr 850-4	MTS8recr 850-5	MTS8recr 850-6	MTS8recr 850-7	Average MTS8recr 850	STDEV MTS8recr 850
Na_2O	2.50	2.48	2.75	2.81	2.53	2.62	0.15	2.76	3.62	3.03	2.64	2.53	2.48	2.60	2.81	0.40
Al_2O_3	17.80	18.07	18.01	17.79	18.08	17.95	0.14	18.83	19.96	19.34	18.12	19.58	19.07	18.78	19.10	0.60
SiO_2	65.34	65.21	65.01	65.04	65.11	65.14	0.13	65.09	63.70	64.07	65.76	63.70	64.78	64.46	64.51	0.76
K_2O	13.35	13.47	13.07	13.41	13.71	13.40	0.23	13.83	11.75	13.37	13.53	13.97	14.20	14.24	13.56	0.86
CaO	0.00	0.00	0.00	0.00	0.00	0.00	0.00	0.00	0.91	0.13	0.00	0.00	0.00	0.00	0.15	0.34
TiO_2	0.00	0.74	0.00	0.00	0.00	0.15	0.33	0.10	0.14	0.21	0.15	0.23	0.11	0.28	0.17	0.07
FeO	0.35	0.05	0.24	0.68	0.11	0.29	0.25	0.18	0.51	0.32	0.29	0.82	0.25	0.32	0.38	0.22
Total	99.46	99.69	99.18	99.59	99.82	99.55	0.24	100.79	100.59	100.47	100.49	100.83	100.89	100.68	100.68	0.17
Si	3.01	3.00	3.00	3.00	3.00	3.00	0.00	2.97	2.91	2.94	3.00	2.92	2.96	2.96	2.95	0.03
Ti	0.00	0.03	0.00	0.00	0.00	0.01	0.01	0.00	0.00	0.01	0.01	0.01	0.00	0.01	0.01	0.00
Al	0.97	0.98	0.98	0.97	0.98	0.97	0.01	1.01	1.07	1.04	0.97	1.06	1.03	1.01	1.03	0.03
Fe tot	0.01	0.00	0.01	0.03	0.00	0.01	0.01	0.01	0.02	0.01	0.01	0.03	0.01	0.01	0.01	0.01
Ca	0.00	0.00	0.00	0.00	0.00	0.00	0.00	0.00	0.04	0.01	0.00	0.00	0.00	0.00	0.01	0.02
Na	0.22	0.22	0.25	0.25	0.23	0.23	0.01	0.24	0.32	0.27	0.23	0.22	0.22	0.23	0.25	0.04
K	0.78	0.79	0.77	0.79	0.81	0.79	0.01	0.81	0.68	0.78	0.79	0.82	0.83	0.83	0.79	0.05
Cat Total	5.01	5.01	5.01	5.03	5.02	5.01	0.01	5.04	5.05	5.06	5.02	5.06	5.05	5.06	5.05	0.02

K-feldspar	MTS7 800 1	MTS7 800 2	MTS7 800 3	MTS7 800 4	MTS7 800 5	Average MTS7 800	STDEV MTS7 800	MTS8 800 1	MTS8 800 2	MTS8 800 3	MTS8 800 4	MTS8 800 5	Average MTS8 800	STDEV MTS8 800	MTS7 750 plag	MTS8 800 plag
Na_2O	2.64	2.04	2.60	2.23	1.87	2.28	0.34	2.42	2.27	2.38	2.40	2.51	2.40	0.09	11.21	10.12
Al_2O_3	17.29	16.77	16.75	17.19	17.16	17.03	0.25	17.32	17.49	17.48	17.36	17.18	17.37	0.12	20.44	22.99
SiO_2	66.04	65.77	66.47	66.25	65.80	66.07	0.30	64.56	62.38	64.58	64.70	64.80	64.21	1.02	65.44	62.95
K_2O	13.12	14.68	13.08	13.59	14.59	13.81	0.78	13.28	12.22	13.11	13.13	12.95	12.94	0.42	0.62	0.30
CaO	0.00	0.00	0.00	0.00	0.00	0.00	0.00	0.00	0.00	0.00	0.00	0.00	0.00	0.00	1.96	3.22
TiO_2	0.00	0.00	0.00	0.00	0.00	0.00	0.00	0.00	2.15	0.00	0.00	0.00	0.43	0.96	0.00	0.00
FeO	0.36	0.51	0.51	0.50	0.00	0.38	0.22	1.15	7.12	0.42	0.35	1.19	2.04	2.86	0.22	0.13
Total	99.45	99.73	99.36	99.71	99.56	99.56	0.16	99.74	98.54	99.48	99.52	99.61	99.38	0.48	99.88	99.71
Si	3.04	3.04	3.06	3.04	3.04	3.04	0.01	2.99	2.93	3.00	3.00	3.00	2.99	0.03	2.90	2.80
Ti	0.00	0.00	0.00	0.00	0.00	0.00	0.00	0.00	0.08	0.00	0.00	0.00	0.02	0.03	0.00	0.00
Al	0.94	0.91	0.91	0.93	0.93	0.92	0.01	0.95	0.97	0.95	0.95	0.94	0.95	0.01	1.07	1.20
Fe tot	0.01	0.02	0.02	0.02	0.00	0.01	0.01	0.04	0.28	0.02	0.01	0.05	0.08	0.11	0.01	0.00
Ca	0.00	0.00	0.00	0.00	0.00	0.00	0.00	0.00	0.00	0.00	0.00	0.00	0.00	0.00	0.09	0.15
Na	0.24	0.18	0.23	0.20	0.17	0.20	0.03	0.22	0.21	0.21	0.22	0.23	0.22	0.01	0.96	0.87
K	0.77	0.87	0.77	0.80	0.86	0.81	0.05	0.79	0.73	0.78	0.78	0.77	0.77	0.02	0.03	0.02
Cat Total	4.99	5.02	4.99	4.99	5.01	5.00	0.02	5.02	5.02	5.01	5.01	5.01	5.01	0.01	5.06	5.05

K-feldspar	MTS7 750 1	MTS7 750 2	MTS7 750 3	MTS7 750 4	MTS7 750 5	Average MTS7 750	STDEV MTS7 750	MTS8 750 1	MTS8 750 2	MTS8 750 3	MTS8 750 4	MTS8 750 5	Average MTS8 750	STDEV MTS8 750
Na_2O	1.93	2.77	2.90	2.51	2.51	2.52	0.37	1.83	1.66	2.29	2.35	2.08	2.04	0.29
Al_2O_3	16.55	16.58	16.50	16.78	16.78	16.64	0.14	17.21	16.79	16.99	17.17	17.13	17.06	0.17
SiO_2	66.04	66.12	66.41	65.95	65.95	66.09	0.19	65.94	65.78	65.54	66.00	66.26	65.90	0.27
K_2O	14.74	13.79	13.31	13.89	13.89	13.92	0.52	14.47	15.26	14.14	13.67	13.90	14.28	0.62
CaO	0.00	0.00	0.00	0.00	0.00	0.00	0.00	0.00	0.00	0.00	0.00	0.00	0.00	0.00
TiO_2	0.00	0.00	0.10	0.00	0.00	0.02	0.04	0.00	0.00	0.00	0.00	0.00	0.00	0.00
FeO	0.00	0.06	0.25	0.27	0.27	0.17	0.13	0.04	0.14	0.15	0.10	0.17	0.12	0.05
Total	99.45	99.34	99.30	99.39	99.39	99.37	0.06	99.58	99.62	99.13	99.24	99.48	99.41	0.22
Si	3.06	3.06	3.06	3.05	3.05	3.05	0.01	3.04	3.05	3.04	3.05	3.05	3.04	0.00
Ti	0.00	0.00	0.00	0.00	0.00	0.00	0.00	0.00	0.00	0.00	0.00	0.00	0.00	0.00
Al	0.90	0.90	0.90	0.91	0.91	0.91	0.01	0.93	0.92	0.93	0.93	0.93	0.93	0.01
Fe tot	0.00	0.00	0.01	0.01	0.01	0.01	0.00	0.00	0.01	0.01	0.00	0.01	0.00	0.00
Ca	0.00	0.00	0.00	0.00	0.00	0.00	0.00	0.00	0.00	0.00	0.00	0.00	0.00	0.00
Na	0.17	0.25	0.26	0.23	0.23	0.23	0.03	0.16	0.15	0.21	0.21	0.19	0.18	0.03
K	0.87	0.81	0.78	0.82	0.82	0.82	0.03	0.85	0.90	0.84	0.80	0.82	0.84	0.04
Cat Total	5.02	5.02	5.01	5.01	5.01	5.01	0.00	5.00	5.02	5.01	4.99	4.98	5.00	0.02

K-feldspar	MTS8 1000-1	MTS8 1000-2	MTS8 1000-3	Average MTS8 1000	STDEV MTS8 1000
Na_2O	1.44	1.55	1.47	1.49	0.06
Al_2O_3	16.77	16.57	16.89	16.74	0.16
SiO_2	65.12	65.02	65.11	65.08	0.05
K_2O	15.02	15.18	14.93	15.04	0.13
CaO	0.00	0.00	0.00	0.00	0.00
TiO_2	0.14	0.20	0.13	0.16	0.04
FeO	0.11	0.11	0.07	0.10	0.02
Total	98.61	98.65	98.58	98.61	0.03
Si	3.04	3.04	3.04	3.04	0.00
Ti	0.01	0.01	0.00	0.01	0.00
Al	0.92	0.91	0.93	0.92	0.01
Fe tot	0.00	0.00	0.00	0.00	0.00
Ca	0.00	0.00	0.00	0.00	0.00
Na	0.13	0.14	0.13	0.13	0.01
K	0.90	0.91	0.89	0.90	0.01
Cat Total	5.00	5.02	5.00	5.01	0.01

Ilmenite	MTS7 950-1	MTS7 950-2	MTS7 950-3	Average MTS7 950	STDEV MTS7 950	MTS8 950-1	MTS70 950-1	MTS70 950-2	MTS70 950-3	Average MTS70 950	STDEV MTS70 950	MTS8 750-1	MTS71 750-1	MTS7 800-1
Na_2O	0.40	0.41	0.44	0.42	0.02	0.49	0.50	0.34	0.42	0.42	0.08	0.37	0.53	0.58
MgO	0.40	0.55	0.54	0.50	0.09	2.49	1.83	1.29	1.97	1.70	0.36	0.50	0.42	0.86
Al_2O_3	1.33	1.13	1.31	1.26	0.11	1.04	0.97	0.64	0.76	0.79	0.17	0.34	0.64	0.52
SiO_2	2.90	3.93	2.43	3.08	0.77	1.70	0.96	0.70	1.07	0.91	0.19	0.83	1.38	0.51
K_2O	0.25	0.34	0.18	0.26	0.08	0.21	0.08	0.02	0.08	0.06	0.03	0.17	0.20	0.00
CaO	0.08	0.07	0.00	0.05	0.04	0.00	0.00	0.00	0.00	0.00	0.00	0.06	0.08	0.09
TiO_2	45.08	72.83	42.11	53.34	16.94	43.79	48.21	54.31	47.69	50.07	3.68	62.89	50.66	64.74
MnO	0.00	0.45	0.00	0.15	0.26	0.45	0.85	0.88	0.73	0.82	0.08	0.64	0.22	0.66
Fe Total	45.32	29.77	47.18	40.75	9.56	49.83	46.65	43.04	47.22	45.64	2.27	34.39	45.92	31.66
FeO	39.90	-	40.86	40.38	-	44.42	40.13	40.08	40.47	40.23	-	34.39	43.09	31.66
Fe2O3	5.42	-	6.31	5.87	-	5.41	6.91	2.12	7.21	5.41	-	-	2.83	-
Total	95.76	109.48	94.19	99.81	8.41	100.00	100.39	100.40	100.40	100.40	0.01	100.18	100.07	99.62
Si	0.06	0.08	0.05	0.06	0.01	0.04	0.03	0.02	0.04	0.03	0.01	0.02	0.03	0.01
Ti	0.69	0.98	0.65	0.77	0.18	0.84	0.85	0.94	0.85	0.88	0.05	1.11	0.95	1.14
Al	0.05	0.04	0.05	0.04	0.01	0.03	0.04	0.02	0.03	0.03	0.01	0.01	0.02	0.01
Fe tot	1.40	0.81	1.48	1.23	0.36	1.06	1.04	0.94	1.06	1.02	0.06	0.68	0.96	0.62
Mn	0.00	0.00	0.00	0.00	0.00	0.01	0.02	0.02	0.01	0.02	0.00	0.01	0.00	0.01
Mg	0.01	0.02	0.02	0.02	0.00	0.09	0.09	0.06	0.10	0.08	0.02	0.02	0.02	0.03
Ca	0.00	0.00	0.00	0.00	0.00	0.00	0.00	0.00	0.00	0.00	0.00	0.00	0.00	0.00
Na	0.02	0.02	0.02	0.02	0.00	0.02	0.03	0.02	0.03	0.03	0.00	0.02	0.03	0.03
K	0.01	0.01	0.01	0.01	0.00	0.01	0.01	0.00	0.01	0.01	0.00	0.01	0.01	0.00
Mg#	0.97	2.02	1.26	1.41	0.54	8.18	8.09	6.33	8.58	7.66	1.00	2.51	1.62	4.64
Cat Total	2.24	1.94	2.28	2.16	0.18	2.12	2.11	2.03	2.12	2.09	0.04	1.87	2.02	1.86
Fe II	1.05	-	1.09	1.07	-	0.95	0.93	0.91	0.94	0.93	-	-	0.94	-
Fe III	0.14	-	0.17	0.16	-	0.12	0.11	0.03	0.12	0.09	-	-	0.02	-

Ilmenite	MTS8 900 1	MTS7 850 1	MTS8 850 1	MTS8 850 2	Average MTS8 850	STDEV MTS8 850	MTS70 800-1	MTS7 750 1	MTS7 750 2	Average MTS7 750	STDEV MTS7 750	MTS7 1000-1	MTS7 1000-2	Average MTS7 1000	STDEV MTS7 1000
Na_2O	0.76	0.39	1.05	0.43	0.74	0.43	0.74	0.35	0.46	0.41	0.08	0.44	0.46	0.45	0.01
MgO	2.99	1.09	1.59	1.40	1.50	0.14	1.25	0.69	0.64	0.67	0.04	2.73	2.30	2.51	0.30
Al_2O_3	1.53	0.50	0.35	0.28	0.32	0.05	0.95	0.60	0.41	0.51	0.13	0.70	0.87	0.79	0.12
SiO_2	3.24	0.85	0.47	0.72	0.59	0.18	2.10	0.76	1.75	1.26	0.70	0.33	0.95	0.64	0.44
K_2O	0.31	0.09	0.15	0.11	0.13	0.03	0.14	0.18	0.21	0.20	0.02	0.06	0.12	0.09	0.04
CaO	0.00	0.11	0.13	0.02	0.07	0.08	0.02	0.01	0.07	0.04	0.04	0.02	0.04	0.03	0.02
TiO_2	41.35	51.40	65.70	65.79	65.74	0.07	42.48	43.25	44.17	43.71	0.65	47.57	46.10	46.84	1.04
MnO	0.13	0.57	0.93	0.53	0.73	0.29	0.64	0.93	0.74	0.84	0.13	0.16	0.22	0.19	0.04
Fe Total	49.67	45.07	29.85	29.68	29.76	0.12	50.69	49.09	48.02	48.56	0.76	48.09	48.32	48.20	0.16
FeO	43.49	44.29	-	-	29.76	-	45.11	44.54	44.37	44.45	-	44.27	44.54	44.40	-
Fe2O3	6.18	0.78	-	-	-	-	5.58	4.55	3.65	4.10	-	3.82	3.78	3.80	-
Total	99.98	100.08	100.02	99.16	99.59	0.60	99.01	95.86	96.47	96.17	0.43	100.10	99.38	99.74	0.51
Si	0.08	0.02	0.01	0.02	0.02	0.03	0.05	0.02	0.05	0.03	0.02	0.02	0.05	0.03	0.02
Ti	0.79	0.97	1.15	1.15	1.15	0.17	0.83	0.88	0.88	0.88	0.03	0.90	0.87	0.89	0.02
Al	0.05	0.01	0.01	0.01	0.01	0.02	0.03	0.02	0.01	0.02	0.01	0.02	0.03	0.03	0.00
Fe tot	1.05	0.94	0.58	0.58	0.58	0.25	1.10	1.11	1.07	1.09	0.02	1.01	1.01	1.01	0.00
Mn	0.00	0.01	0.01	0.01	0.01	0.01	0.01	0.02	0.02	0.02	0.00	0.00	0.01	0.00	0.00
Mg	0.11	0.04	0.05	0.05	0.05	0.03	0.05	0.03	0.03	0.03	0.01	0.10	0.08	0.09	0.01
Ca	0.00	0.00	0.00	0.00	0.00	0.00	0.00	0.00	0.00	0.00	0.00	0.00	0.00	0.00	0.00
Na	0.04	0.02	0.03	0.01	0.02	0.01	0.04	0.02	0.02	0.02	0.01	0.02	0.02	0.02	0.00
K	0.01	0.00	0.00	0.00	0.00	0.00	0.00	0.01	0.01	0.01	0.00	0.00	0.01	0.00	0.00
Mg#	9.69	4.17	8.22	7.34	7.78	2.33	4.21	2.44	2.32	2.38	1.06	8.70	7.40	8.05	0.92
Cat Total	2.13	2.02	1.85	1.83	1.84	0.14	2.12	2.10	2.08	2.09	0.02	2.08	2.08	2.08	0.00
Fe II	0.92	0.92	-	-	-	-	0.98	1.01	0.98	1.00	-	0.93	0.93	0.93	-
Fe III	0.13	0.02	-	-	-	-	0.12	0.10	0.08	0.09	-	0.08	0.08	0.08	-

Glass	MTS7 1000-1	MTS7 1000-2	MTS7 1000-3	MTS7 1000-4	MTS7 1000-5	Average MTS7 1000	STDEV MTS7 1000	MTS8 1000-1	MTS8 1000-2	MTS8 1000-3	Average MTS8 1000	STDEV MTS8 1000
Na_2O	1.69	1.69	1.78	1.68	1.69	1.70	0.04	1.81	1.78	1.86	1.82	0.04
MgO	0.00	0.06	0.06	0.07	0.07	0.05	0.03	0.00	0.00	0.15	0.05	0.09
Al_2O_3	10.95	10.76	10.73	10.60	10.65	10.74	0.13	11.91	11.75	11.90	11.86	0.09
SiO_2	74.29	74.30	74.12	74.79	74.38	74.38	0.25	71.93	72.02	71.67	71.88	0.18
K_2O	6.82	6.86	6.91	6.51	6.64	6.75	0.17	8.08	8.07	7.72	7.96	0.21
CaO	0.05	0.05	0.09	0.06	0.11	0.07	0.03	0.05	0.05	0.05	0.05	0.00
TiO_2	0.40	0.58	0.29	0.40	0.43	0.42	0.10	0.33	0.35	0.62	0.43	0.16
MnO	0.06	0.00	0.10	0.10	0.08	0.07	0.04	0.05	0.10	0.02	0.05	0.04
FeO	2.03	2.13	2.06	1.94	2.17	2.07	0.09	1.91	1.85	2.01	1.92	0.08
Total	96.27	96.42	96.14	96.14	96.22	96.24	0.12	96.07	95.98	96.00	96.01	0.05
Si	4.21	4.21	4.22	4.24	4.22	4.22	0.01	4.13	4.14	4.12	4.13	0.01
Ti	0.02	0.02	0.01	0.02	0.02	0.02	0.00	0.01	0.01	0.03	0.02	0.01
Al	0.73	0.72	0.72	0.71	0.71	0.72	0.01	0.81	0.80	0.81	0.80	0.01
Fe tot	0.10	0.10	0.10	0.09	0.10	0.10	0.00	0.09	0.09	0.10	0.09	0.00
Mn	0.00	0.00	0.00	0.00	0.00	0.00	0.00	0.00	0.00	0.00	0.00	0.00
Mg	0.00	0.00	0.00	0.01	0.01	0.00	0.00	0.00	0.00	0.01	0.00	0.01
Ca	0.00	0.00	0.01	0.00	0.01	0.00	0.00	0.00	0.00	0.00	0.00	0.00
Na	0.19	0.19	0.20	0.18	0.19	0.19	0.01	0.20	0.20	0.21	0.20	0.00
K	0.49	0.50	0.50	0.47	0.48	0.49	0.01	0.59	0.59	0.57	0.58	0.02
Mg#	0.00	4.62	4.76	5.84	5.25	4.15	2.34	0.00	0.00	12.01	4.54	6.93
Cat Total	5.74	5.74	5.76	5.72	5.74	5.74	0.01	5.85	5.84	5.84	5.84	0.00

Glass	MTS70 1000-1	MTS70 1000-2	MTS70 1000-3	MTS70 1000-4	Average MTS70 1000	STDEV MTS70 1000	MTS71 1000-1	MTS71 1000-2	MTS71 1000-3	Average MTS71 1000	STDEV MTS71 1000
Na_2O	1.17	1.13	1.02	1.11	1.11	0.06	2.14	2.14	2.16	2.14	0.01
MgO	0.60	0.49	0.37	0.52	0.50	0.09	0.55	0.72	0.63	0.63	0.08
Al_2O_3	11.95	11.89	11.79	11.99	11.91	0.09	12.87	13.74	13.01	13.21	0.47
SiO_2	73.15	74.12	74.34	74.09	73.92	0.53	67.63	65.48	67.12	66.74	1.12
K_2O	5.90	5.94	6.00	5.88	5.93	0.05	5.58	5.95	5.39	5.64	0.28
CaO	0.14	0.11	0.12	0.14	0.13	0.01	0.51	0.66	0.52	0.56	0.08
TiO_2	0.72	0.72	0.74	0.59	0.69	0.07	0.65	0.79	0.57	0.67	0.11
MnO	0.23	0.06	0.12	0.18	0.15	0.08	0.08	0.10	0.09	0.09	0.01
FeO	3.73	3.36	3.35	3.50	3.49	0.17	3.96	4.29	4.50	4.25	0.28
Total	97.59	97.82	97.84	98.00	97.81	0.17	93.95	93.88	94.00	93.94	0.06
Si	4.11	4.14	4.15	4.14	4.14	0.02	3.99	3.90	3.97	3.96	0.05
Ti	0.03	0.03	0.03	0.02	0.03	0.00	0.03	0.04	0.03	0.03	0.01
Al	0.79	0.78	0.78	0.79	0.78	0.01	0.89	0.96	0.91	0.92	0.04
Fe tot	0.18	0.16	0.16	0.16	0.16	0.01	0.20	0.21	0.22	0.21	0.01
Mn	0.01	0.00	0.01	0.01	0.01	0.00	0.00	0.01	0.00	0.00	0.00
Mg	0.05	0.04	0.03	0.04	0.04	0.01	0.05	0.06	0.06	0.06	0.01
Ca	0.01	0.01	0.01	0.01	0.01	0.00	0.03	0.04	0.03	0.04	0.01
Na	0.13	0.12	0.11	0.12	0.12	0.01	0.24	0.25	0.25	0.25	0.00
K	0.42	0.42	0.43	0.42	0.42	0.00	0.42	0.45	0.41	0.43	0.02
Mg#	22.20	20.62	16.53	20.97	20.20	2.46	19.75	22.90	19.99	20.92	1.75
Cat Total	5.73	5.71	5.70	5.71	5.71	0.02	5.86	5.93	5.88	5.89	0.03

Glass	MTS7 950 1	MTS7 950 2	MTS7 950 3	MTS7 950 4	MTS7 950 5	Average MTS7 950	STDEV MTS7 950	MTS8 950 1	MTS8 950 2	MTS8 950 3	MTS8 950 4	Average MTS8 950	STDEV MTS8 950
Na_2O	1.29	1.26	1.25	1.29	1.32	1.28	0.03	1.95	1.89	2.00	2.07	1.98	0.08
MgO	0.04	0.20	0.15	0.06	0.17	0.13	0.07	0.00	0.00	0.00	0.00	0.00	0.00
Al_2O_3	10.43	10.24	10.23	10.20	10.10	10.24	0.12	10.88	10.93	11.06	11.09	10.99	0.10
SiO_2	76.90	76.84	76.70	77.19	76.99	76.92	0.18	74.50	74.79	74.20	74.31	74.45	0.26
K_2O	4.94	5.07	4.92	5.07	5.04	5.01	0.07	7.15	7.10	7.29	7.39	7.23	0.13
CaO	0.06	0.00	0.13	0.05	0.09	0.06	0.05	0.10	0.07	0.12	0.07	0.09	0.02
TiO_2	0.25	0.47	0.21	0.37	0.30	0.32	0.10	0.40	0.40	0.25	0.27	0.33	0.08
MnO	0.03	0.01	0.02	0.00	0.05	0.02	0.02	0.10	0.00	0.00	0.01	0.03	0.05
FeO	2.44	2.23	2.33	2.34	2.33	2.33	0.07	1.45	1.43	1.51	1.30	1.42	0.09
Total	96.36	96.32	95.94	96.56	96.39	96.32	0.23	96.52	96.61	96.42	96.52	96.51	0.08
Si	4.29	4.29	4.30	4.30	4.30	4.30	0.00	4.22	4.22	4.21	4.21	4.21	0.01
Ti	0.01	0.02	0.01	0.02	0.01	0.01	0.00	0.02	0.02	0.01	0.01	0.01	0.00
Al	0.69	0.67	0.67	0.67	0.66	0.67	0.01	0.73	0.73	0.74	0.74	0.73	0.01
Fe tot	0.11	0.10	0.11	0.11	0.11	0.11	0.00	0.07	0.07	0.07	0.06	0.07	0.00
Mn	0.00	0.00	0.00	0.00	0.00	0.00	0.00	0.00	0.00	0.00	0.00	0.00	0.00
Mg	0.00	0.02	0.01	0.00	0.01	0.01	0.01	0.00	0.00	0.00	0.00	0.00	0.00
Ca	0.00	0.00	0.01	0.00	0.01	0.00	0.00	0.01	0.00	0.01	0.00	0.01	0.00
Na	0.14	0.14	0.14	0.14	0.14	0.14	0.00	0.21	0.21	0.22	0.23	0.22	0.01
K	0.35	0.36	0.35	0.36	0.36	0.36	0.00	0.52	0.51	0.53	0.53	0.52	0.01
Mg#	2.75	13.94	10.54	4.23	11.75	8.75	4.89	0.00	0.00	0.00	0.00	0.00	0.00
Cat Total	5.60	5.60	5.60	5.60	5.61	5.60	0.00	5.77	5.76	5.78	5.79	5.77	0.02

Glass	MTS70 950-1	MTS70 950-2	MTS70 950-3	MTS70 950-4	Average MTS70 950	STDEV MTS70 950	MTS71 950-1	MTS71 950-2	MTS71 950-3	MTS71 950-4	MTS71 950-5	Average MTS71 950	STDEV MTS71 950
Na_2O	1.16	1.15	1.04	1.11	1.11	0.05	1.67	1.75	1.83	1.82	1.72	1.76	0.07
MgO	0.30	0.30	0.18	0.06	0.21	0.12	0.03	0.06	0.14	0.03	0.13	0.08	0.06
Al_2O_3	11.22	11.08	11.16	10.71	11.04	0.23	11.39	11.44	12.31	11.35	11.93	11.68	0.42
SiO_2	72.23	72.42	72.26	72.70	72.40	0.21	71.72	71.32	70.28	72.04	71.00	71.27	0.68
K_2O	6.56	6.55	6.61	6.75	6.62	0.09	4.78	4.95	4.84	4.84	4.92	4.87	0.07
CaO	0.18	0.19	0.21	0.14	0.18	0.03	0.44	0.45	0.37	0.41	0.52	0.44	0.06
TiO_2	0.45	0.16	0.28	0.54	0.36	0.17	0.30	0.51	0.41	0.38	0.31	0.38	0.09
MnO	0.05	0.09	0.16	0.12	0.11	0.05	0.07	0.18	0.13	0.17	0.01	0.11	0.07
FeO	1.83	1.82	1.79	1.77	1.80	0.03	2.79	2.82	3.06	2.72	3.09	2.89	0.17
Total	93.98	93.77	93.70	93.89	93.84	0.13	93.18	93.47	93.38	93.77	93.63	93.49	0.23
Si	4.19	4.21	4.20	4.22	4.20	0.01	4.18	4.16	4.11	4.18	4.13	4.15	0.03
Ti	0.02	0.01	0.01	0.02	0.02	0.01	0.01	0.02	0.02	0.02	0.01	0.02	0.00
Al	0.77	0.76	0.76	0.73	0.75	0.02	0.78	0.79	0.85	0.78	0.82	0.80	0.03
Fe tot	0.09	0.09	0.09	0.09	0.09	0.00	0.14	0.14	0.15	0.13	0.15	0.14	0.01
Mn	0.00	0.00	0.01	0.01	0.01	0.00	0.00	0.01	0.01	0.01	0.00	0.01	0.00
Mg	0.03	0.03	0.02	0.00	0.02	0.01	0.00	0.00	0.01	0.00	0.01	0.01	0.00
Ca	0.01	0.01	0.01	0.01	0.01	0.00	0.03	0.03	0.02	0.03	0.03	0.03	0.00
Na	0.13	0.13	0.12	0.12	0.13	0.01	0.19	0.20	0.21	0.20	0.19	0.20	0.01
K	0.49	0.49	0.49	0.50	0.49	0.01	0.36	0.37	0.36	0.36	0.37	0.36	0.01
Mg#	22.63	22.72	15.06	5.38	17.12	8.20	1.76	3.43	7.56	1.82	7.03	4.51	2.80
Cat Total	5.72	5.72	5.71	5.70	5.71	0.01	5.69	5.71	5.73	5.70	5.72	5.71	0.02

Glass	MTS7 900 1	MTS7 900 2	MTS7 900 3	Average MTS7 900	STDEV MTS7 900	MTS8 900 1	MTS8 900 2	MTS8 900 3	Average MTS8 900	STDEV MTS8 900
Na_2O	2.26	2.07	2.18	2.17	0.10	2.10	2.29	2.22	2.20	0.10
MgO	0.11	0.08	0.08	0.09	0.02	0.09	0.14	0.19	0.14	0.05
Al_2O_3	11.63	11.36	11.12	11.37	0.25	11.53	11.06	11.30	11.29	0.23
SiO_2	72.20	72.87	73.31	72.79	0.56	71.65	72.78	71.95	72.13	0.59
K_2O	7.10	6.83	6.89	6.94	0.14	7.38	6.66	6.96	7.00	0.37
CaO	0.11	0.16	0.10	0.12	0.03	0.10	0.09	0.09	0.09	0.01
TiO_2	0.32	0.38	0.30	0.33	0.04	0.36	0.38	0.40	0.38	0.02
MnO	0.17	0.06	0.00	0.08	0.09	0.02	0.05	0.00	0.02	0.02
FeO	1.30	1.45	1.30	1.35	0.08	1.31	1.10	1.47	1.29	0.19
Total	95.21	95.25	95.28	95.25	0.03	94.55	94.55	94.56	94.55	0.00
Si	4.16	4.18	4.20	4.18	0.02	4.16	4.20	4.17	4.17	0.02
Ti	0.01	0.02	0.01	0.01	0.00	0.02	0.02	0.02	0.02	0.00
Al	0.79	0.77	0.75	0.77	0.02	0.79	0.75	0.77	0.77	0.02
Fe tot	0.06	0.07	0.06	0.06	0.00	0.06	0.05	0.07	0.06	0.01
Mn	0.01	0.00	0.00	0.00	0.00	0.00	0.00	0.00	0.00	0.00
Mg	0.01	0.01	0.01	0.01	0.00	0.01	0.01	0.02	0.01	0.00
Ca	0.01	0.01	0.01	0.01	0.00	0.01	0.01	0.01	0.01	0.00
Na	0.25	0.23	0.24	0.24	0.01	0.24	0.26	0.25	0.25	0.01
K	0.52	0.50	0.50	0.51	0.01	0.55	0.49	0.51	0.52	0.03
Mg#	13.50	8.58	9.43	10.49	2.63	11.37	18.73	18.70	16.36	4.24
Cat Total	5.82	5.78	5.78	5.80	0.02	5.82	5.78	5.81	5.81	0.02

Glass	MTS70 900-1	MTS70 900-2	MTS70 900-3	MTS70 900-4	MTS70 900-5	Average MTS70 900	STDEV MTS70 900
Na_2O	1.11	1.07	1.05	1.11	1.08	1.08	0.02
MgO	0.14	0.18	0.24	0.13	0.22	0.18	0.05
Al_2O_3	10.95	11.64	11.35	11.15	11.03	11.22	0.28
SiO_2	72.57	71.70	72.04	72.11	72.48	72.18	0.35
K_2O	6.97	7.02	6.69	6.96	6.81	6.89	0.13
CaO	0.12	0.22	0.13	0.12	0.16	0.15	0.04
TiO_2	0.42	0.54	0.38	0.53	0.42	0.46	0.07
MnO	0.06	0.06	0.07	0.08	0.14	0.08	0.04
FeO	1.61	1.80	1.94	1.61	1.76	1.74	0.14
Total	93.95	94.21	93.90	93.80	94.10	93.99	0.16
Si	4.21	4.16	4.18	4.19	4.20	4.19	0.02
Ti	0.02	0.02	0.02	0.02	0.02	0.02	0.00
Al	0.75	0.79	0.78	0.76	0.75	0.77	0.02
Fe tot	0.08	0.09	0.09	0.08	0.09	0.08	0.01
Mn	0.00	0.00	0.00	0.00	0.01	0.00	0.00
Mg	0.01	0.02	0.02	0.01	0.02	0.02	0.00
Ca	0.01	0.01	0.01	0.01	0.01	0.01	0.00
Na	0.12	0.12	0.12	0.12	0.12	0.12	0.00
K	0.52	0.52	0.50	0.52	0.50	0.51	0.01
Mg#	13.52	15.06	18.29	12.67	17.98	15.71	2.55
Cat Total	5.72	5.74	5.72	5.72	5.72	5.72	0.01

Glass	MTS7 850 1	MTS7 850 2	MTS7 850 3	MTS7 850 4	Average MTS7 850	STDEV MTS7 850	MTS8 850 1	MTS8 850 2	MTS8 850 3	Average MTS8 850	STDEV MTS8 850
Na_2O	2.23	2.29	2.37	2.48	2.34	0.11	2.52	2.39	2.48	2.47	0.07
MgO	0.02	0.00	0.00	0.00	0.00	0.01	0.00	0.06	0.29	0.12	0.16
Al_2O_3	11.82	11.74	11.92	11.90	11.85	0.08	11.75	12.73	12.93	12.47	0.63
SiO_2	73.84	73.97	73.73	73.82	73.84	0.10	72.32	70.37	69.61	70.77	1.40
K_2O	6.30	6.13	6.30	6.40	6.28	0.11	6.01	7.29	6.54	6.62	0.64
CaO	0.21	0.19	0.24	0.21	0.21	0.02	0.21	0.12	0.15	0.16	0.04
TiO_2	0.11	0.30	0.22	0.13	0.19	0.09	0.15	0.09	0.07	0.10	0.04
MnO	0.12	0.00	0.10	0.05	0.06	0.05	0.05	0.03	0.05	0.04	0.01
FeO	1.50	1.51	1.54	1.39	1.49	0.07	1.38	1.51	2.05	1.65	0.35
Total	96.15	96.14	96.41	96.39	96.27	0.15	94.39	94.59	94.18	94.39	0.21
Si	4.18	4.18	4.17	4.18	4.18	0.01	4.17	4.09	4.07	4.11	0.05
Ti	0.00	0.01	0.01	0.01	0.01	0.00	0.01	0.00	0.00	0.00	0.00
Al	0.79	0.78	0.79	0.79	0.79	0.01	0.80	0.87	0.89	0.85	0.05
Fe tot	0.07	0.07	0.07	0.07	0.07	0.00	0.07	0.07	0.10	0.08	0.02
Mn	0.01	0.00	0.00	0.00	0.00	0.00	0.00	0.00	0.00	0.00	0.00
Mg	0.00	0.00	0.00	0.00	0.00	0.00	0.00	0.00	0.03	0.01	0.01
Ca	0.01	0.01	0.01	0.01	0.01	0.00	0.01	0.01	0.01	0.01	0.00
Na	0.25	0.25	0.26	0.27	0.26	0.01	0.28	0.27	0.28	0.28	0.01
K	0.46	0.44	0.45	0.46	0.45	0.01	0.44	0.54	0.49	0.49	0.05
Mg#	2.23	0.00	0.00	0.00	0.57	1.12	0.00	6.27	20.30	11.19	10.39
Cat Total	5.77	5.76	5.78	5.79	5.77	0.01	5.78	5.87	5.87	5.84	0.05

Glass	MTS70 850-1	MTS70 850-2	MTS70 850-3	Average MTS70 850	STDEV MTS70 850	MTS71 850-1	MTS71 850-2	MTS71 850-3	MTS71 850-4	Average MTS71 850	STDEV MTS71 850
Na_2O	1.16	1.26	1.13	1.18	0.06	1.55	1.41	1.49	1.51	1.49	0.06
MgO	0.00	0.00	0.00	0.00	0.00	0.00	0.00	0.00	0.00	0.00	0.00
Al_2O_3	11.29	11.53	11.46	11.43	0.13	12.12	11.15	11.82	11.71	11.70	0.41
SiO_2	72.26	71.85	71.68	71.93	0.30	66.84	68.15	66.80	66.75	67.14	0.68
K_2O	6.87	6.95	7.02	6.95	0.07	6.30	5.96	6.21	6.22	6.17	0.15
CaO	0.12	0.18	0.12	0.14	0.03	0.39	0.37	0.50	0.38	0.41	0.06
TiO_2	0.24	0.18	0.35	0.26	0.08	0.08	0.23	0.06	0.53	0.23	0.22
MnO	0.06	0.03	0.17	0.08	0.07	0.05	0.08	0.00	0.05	0.05	0.03
FeO	1.66	1.67	1.76	1.70	0.06	2.29	2.39	2.64	2.68	2.50	0.19
Total	93.66	93.63	93.69	93.66	0.03	89.62	89.75	89.53	89.84	89.69	0.14
Si	4.20	4.19	4.18	4.19	0.01	4.10	4.16	4.10	4.09	4.11	0.03
Ti	0.01	0.01	0.02	0.01	0.00	0.00	0.01	0.00	0.02	0.01	0.01
Al	0.77	0.79	0.79	0.78	0.01	0.88	0.80	0.85	0.84	0.84	0.03
Fe tot	0.08	0.08	0.09	0.08	0.00	0.12	0.12	0.14	0.14	0.13	0.01
Mn	0.00	0.00	0.01	0.00	0.00	0.00	0.00	0.00	0.00	0.00	0.00
Mg	0.00	0.00	0.00	0.00	0.00	0.00	0.00	0.00	0.00	0.00	0.00
Ca	0.01	0.01	0.01	0.01	0.00	0.03	0.02	0.03	0.02	0.03	0.00
Na	0.13	0.14	0.13	0.13	0.01	0.18	0.17	0.18	0.18	0.18	0.01
K	0.51	0.52	0.52	0.52	0.01	0.49	0.46	0.49	0.49	0.48	0.01
Mg#	0.00	0.00	0.00	0.00	0.00	0.00	0.00	0.00	0.00	0.00	0.00
Cat Total	5.72	5.74	5.74	5.73	0.01	5.80	5.75	5.80	5.79	5.78	0.02

Glass	MTS8 800-1	MTS8 800-2	Average MTS8 800	STDEV MTS8 800	MTS7 800-1	MTS7 800-2	Average MTS7 800	STDEV MTS7 800	MTS70 800-1	MTS70 800-2	MTS70 800-3	MTS70 800-4	MTS70 800-5	Average MTS70 800	STDEV MTS70 800
Na_2O	2.21	2.40	2.30	0.13	3.04	4.01	3.53	0.68	1.19	1.19	1.22	1.24	1.29	1.23	0.04
MgO	0.18	0.04	0.11	0.10	1.27	0.30	0.78	0.69	0.00	0.00	0.00	0.00	0.00	0.00	0.00
Al_2O_3	12.90	13.60	13.25	0.50	16.59	15.87	16.23	0.51	11.57	11.33	11.47	11.39	11.13	11.38	0.16
SiO_2	73.16	72.25	72.70	0.65	70.74	71.30	71.02	0.40	71.62	71.61	72.10	72.35	71.75	71.89	0.33
K_2O	6.08	7.29	6.69	0.86	3.66	4.44	4.05	0.56	8.02	7.88	7.38	7.54	7.65	7.69	0.26
CaO	0.20	0.26	0.23	0.04	0.65	0.87	0.76	0.15	0.09	0.12	0.08	0.07	0.09	0.09	0.02
TiO_2	0.52	0.21	0.37	0.21	0.07	0.16	0.11	0.06	0.24	0.31	0.23	0.19	0.50	0.29	0.12
MnO	0.03	0.06	0.04	0.02	0.02	0.04	0.03	0.01	0.06	0.17	0.10	0.16	0.02	0.10	0.06
FeO	2.11	1.27	1.69	0.60	2.47	1.55	2.01	0.65	1.34	1.40	1.55	1.39	1.60	1.46	0.11
Total	97.39	97.38	97.38	0.01	98.51	98.53	98.52	0.01	94.12	94.01	94.15	94.33	94.01	94.12	0.13
Si	4.11	4.08	4.09	0.02	3.91	3.95	3.93	0.03	4.17	4.18	4.19	4.19	4.18	4.18	0.01
Ti	0.02	0.01	0.02	0.01	0.00	0.01	0.00	0.00	0.01	0.01	0.01	0.01	0.02	0.01	0.01
Al	0.85	0.90	0.88	0.04	1.08	1.04	1.06	0.03	0.79	0.78	0.78	0.78	0.76	0.78	0.01
Fe tot	0.10	0.06	0.08	0.03	0.11	0.07	0.09	0.03	0.07	0.07	0.08	0.07	0.08	0.07	0.01
Mn	0.00	0.00	0.00	0.00	0.00	0.00	0.00	0.00	0.00	0.01	0.01	0.01	0.00	0.01	0.00
Mg	0.01	0.00	0.01	0.01	0.10	0.02	0.06	0.06	0.00	0.00	0.00	0.00	0.00	0.00	0.00
Ca	0.01	0.02	0.01	0.00	0.04	0.05	0.05	0.01	0.01	0.01	0.01	0.00	0.01	0.01	0.00
Na	0.24	0.26	0.25	0.02	0.33	0.43	0.38	0.07	0.13	0.13	0.14	0.14	0.15	0.14	0.00
K	0.44	0.52	0.48	0.06	0.26	0.31	0.29	0.04	0.60	0.59	0.55	0.56	0.57	0.57	0.02
Mg#	12.88	5.20	10.15	5.43	47.81	25.41	40.99	15.84	0.00	0.00	0.00	0.00	0.00	0.00	0.00
Cat Total	5.78	5.86	5.82	0.05	5.84	5.89	5.86	0.04	5.78	5.78	5.75	5.76	5.77	5.77	0.01

Glass	MTS71 800-1	MTS71 800-2	MTS71 800-3	Average MTS71 800	STDEV MTS71 800
Na_2O	1.07	0.98	1.04	1.03	0.05
MgO	0.00	0.28	0.06	0.12	0.15
Al_2O_3	13.52	14.81	13.64	13.99	0.71
SiO_2	64.24	65.98	67.52	65.91	1.64
K_2O	5.84	6.33	6.59	6.26	0.38
CaO	0.23	0.27	0.30	0.27	0.04
TiO_2	1.87	0.10	0.17	0.71	1.00
MnO	0.06	0.07	0.00	0.05	0.04
FeO	4.46	2.31	1.68	2.81	1.46
Total	91.28	91.13	91.00	91.14	0.14
Si	3.92	3.97	4.06	3.98	0.07
Ti	0.09	0.00	0.01	0.03	0.05
Al	0.97	1.05	0.96	1.00	0.05
Fe tot	0.23	0.12	0.08	0.14	0.07
Mn	0.00	0.00	0.00	0.00	0.00
Mg	0.00	0.03	0.01	0.01	0.01
Ca	0.01	0.02	0.02	0.02	0.00
Na	0.13	0.11	0.12	0.12	0.01
K	0.45	0.49	0.51	0.48	0.03
Mg#	0.00	17.93	6.32	6.81	9.09
Cat Total	5.80	5.79	5.76	5.79	0.02

Appendix 4: Biotite-muscovite pairs for equilibrium evaluation

Electron Microprobe data for the calculation of partition coefficients

Sample	**MTS70 starting material**					**MTS70 750, 3.2 kbar**									
Biotite	Bt1	Bt2	Bt3	Bt4	Bt5	Bt1	Bt2	Bt3	Bt4	Bt5	Bt6	Bt7	Bt8	Bt9	Bt10
SiO_2	36.45	35.85	34.27	36.13	36.53	33.57	34.55	44.63	33.19	35.88	34.68	38.39	37.66	34.75	37.49
Na_2O	0.08	0.12	0.04	0.08	0.16	0.21	0.16	0.28	0.60	0.27	0.23	0.15	0.19	0.06	0.19
Cl	0.07	0.10	0.07	0.11	0.12	0.05	0.04	0.09	0.10	0.10	0.04	0.04	0.05	0.01	0.06
K_2O	6.81	8.48	8.92	8.71	8.74	7.80	7.91	5.76	3.71	8.46	8.00	8.97	7.93	9.03	8.91
Al_2O_3	19.26	18.79	18.08	18.70	18.53	20.37	20.50	18.36	15.49	19.04	20.02	21.62	20.92	18.52	20.43
F	0.50	0.57	0.53	0.33	0.26	0.36	0.43	0.30	0.34	0.50	0.57	0.56	0.45	0.43	0.58
TiO_2	2.02	1.90	2.02	2.15	2.03	2.17	2.28	1.59	1.54	1.88	1.91	1.92	2.00	1.73	2.48
CaO	0.07	0.07	0.03	0.06	0.07	0.01	0.03	0.17	0.24	0.05	0.04	0.02	0.08	0.01	0.03
MgO	4.07	4.04	3.94	3.94	3.81	4.97	5.08	2.95	1.80	4.68	5.71	5.75	4.92	4.90	5.71
MnO	0.53	0.55	0.49	0.58	0.46	0.48	0.43	0.49	0.58	0.41	0.46	0.37	0.46	0.54	0.44
FeO	26.50	27.21	25.91	26.98	25.90	25.20	23.81	19.96	38.38	23.09	26.55	19.88	22.10	27.16	19.46
Cr_2O_3	0.03	-	0.04	0.03	0.03	0.04	-	-	0.02	0.04	0.07	0.02	0.04	0.06	-
Total	96.40	97.68	94.35	97.80	96.65	95.23	95.22	94.58	95.98	94.40	98.28	97.70	96.79	97.20	95.78
Muscovite	Mu1	Mu2	Mu3	Mu4	Mu5	Mu1	Mu2	Mu3	Mu4	Mu5	Mu6	Mu7	Mu8	Mu9	Mu10
SiO_2	46.55	46.52	45.99	45.91	46.05	45.40	45.03	45.56	45.22	46.48	45.31	46.12	46.65	45.52	45.93
Na_2O	0.45	0.49	0.44	0.43	0.46	0.29	0.31	0.32	0.34	0.20	0.43	0.29	0.36	0.21	0.21
Cl	0.06	0.01	0.05	0.04	0.02	0.02	0.03	0.01		0.03	0.03	-	-	0.03	0.02
K_2O	10.45	10.36	10.51	10.53	10.34	10.11	10.11	10.21	10.31	8.22	10.34	10.44	10.41	10.50	10.44
Al_2O_3	35.39	35.73	35.69	35.61	35.95	34.50	34.60	34.46	34.63	35.28	34.76	35.45	35.62	35.00	35.17
F	0.18	0.04	0.22	0.32	0.28	0.21	0.24	0.17	0.30	0.27	0.27	0.22	0.31	0.40	0.22
TiO_2	0.65	0.68	0.71	0.68	0.64	0.48	0.59	0.57	0.55	0.56	0.55	0.50	0.50	0.57	0.82
CaO	0.00	-	-	0.00	-	-	-	-	-	-	-	-	-	-	-
MgO	0.80	0.69	0.69	0.81	0.69	0.87	0.86	0.86	0.85	0.83	0.94	0.84	0.85	0.81	0.83
MnO	0.13	0.05	0.07	0.10	0.10	0.02	0.09	0.07	0.07	0.04	0.08	0.06	0.08	0.08	0.04
FeO	2.29	2.12	2.51	2.11	2.06	1.99	2.01	1.97	1.94	2.10	2.11	2.11	2.09	2.45	2.19
Cr_2O_3	0.04	0.01	0.04	0.04	0.02	0.03	0.04	-	0.00	-	0.02	-	-	0.05	0.03
Total	96.99	96.71	96.94	96.56	96.60	93.92	93.90	94.20	94.22	94.02	94.84	96.02	96.86	95.62	95.90

Distribution coefficients D(M)bt/mu

Mt Stafford: 750 C and 3.2 kbar

Pairs	Bt/Mu1	Bt/Mu2	Bt/Mu3	Bt/Mu4	Bt/Mu5	Bt/Mu6	Bt/Mu7	Bt/Mu8	Bt/Mu9	Bt/Mu10	**Average**	**Stdev**
D (F)	1.68	1.76	1.80	1.12	1.83	2.12	2.53	1.44	1.06	2.59	**1.79**	**0.52**
D (Cl)	3.13	1.56	6.05		3.76	1.18			0.45	3.52	**2.81**	**1.91**
D (Si)	0.85	0.88	1.06	0.89	0.90	0.77	0.83	0.81	0.76	0.82	**0.86**	**0.09**
D (Ti)	5.20	4.43	3.03	3.35	3.92	3.47	3.87	4.02	3.04	3.03	**3.74**	**0.70**
D (Al)	0.68	0.68	0.58	0.54	0.63	0.58	0.61	0.59	0.53	0.58	**0.60**	**0.05**
D (Fe)	14.62	13.52	11.01		12.88	4.45			1.17		**9.61**	**5.50**
D (Mn)		5.27	7.77	9.99	11.33	12.58	9.42	10.57	11.09	8.89	**9.66**	**2.17**
D (Mg)	6.62	6.76	3.72	2.56	6.60	5.96	6.50	5.91	6.82	11.63	**6.31**	**2.36**
D (Ca)						6.09	6.86	5.78	6.04	6.85	**6.33**	**0.50**
D (Na)	0.82	0.61	0.95	2.10	1.56	0.53	0.54	0.53	0.27	0.89	**0.88**	**0.55**
D (K)	0.89	0.89	0.61	0.43	1.21	0.77	0.86	0.76	0.86	0.85	**0.81**	**0.20**
D (Cr)	1.38					0.87	0.92	0.92	0.89	0.92	**0.98**	**0.20**

Distribution coefficients D(M)bt/mu

Mt Stafford starting material

Pairs	Bt/Mu pr1	Bt/Mu pr2	Bt/Mu pr3	Bt/Mu pr4	**Average**	**Stdev**
D (F)	2.81	2.38	1.03	0.95	**1.80**	**0.94**
D (Cl)	1.18	1.29	3.20	6.97	**3.16**	**2.70**
D (Si)	0.78	0.75	0.79	0.79	**0.78**	**0.02**
D (Ti)	3.12	2.85	3.18	3.16	**3.08**	**0.16**
D (Al)	0.54	0.51	0.53	0.52	**0.52**	**0.02**
D (Fe)	0.70	0.96	0.75	1.71	**1.03**	**0.47**
D (Mn)	11.57	10.32	12.79	12.57	**11.81**	**1.13**
D (Mg)	4.19	7.07	6.03	4.72	**5.50**	**1.30**
D (Ca)	5.08	5.69	4.88	5.53	**5.29**	**0.38**
D (Na)	0.18	0.09	0.20	0.34	**0.20**	**0.10**
D (K)	0.65	0.85	0.83	0.85	**0.79**	**0.09**
D (Cr)	0.91	0.90	0.91	0.93	**0.91**	**0.01**

- End of document -